University of Puerto Rico

Assessing the Impact of Coastal Processes on Archaeological Sites in Loíza Puerto Rico: Integrating Geographic Information System (GIS), Remote Sensing, and Numerical Modeling Techniques

by

Loderay I. M. Bracero Marrero

A dissertation submitted to the Environmental Sciences Department, College of Natural Sciences, Río Piedras Campus in partial fulfillment of the requirements for the degree of

DOCTOR IN PHILOSOPHY

Graduate Supervisory Committee:

Qiong Gao, Ph.D., Committee Chair

Maritza Barreto Orta, Ph.D., Co-Chair

Reniel Rodríguez Ramos, Ph.D.

Nick Brokaw, Ph.D.

Xiaoming Zou, Ph.D.

May 9, 2022

ASSESSING THE IMPACT OF COASTAL PROCESSES ON ARCHAEOLOGICAL SITES IN LOÍZA PUERTO RICO: INTEGRATING GEOGRAPHIC INFORMATION SYSTEM (GIS), REMOTE SENSING, AND NUMERICAL MODELING TECHNIQUES

Approved by the Faculty of the Doctoral Program in Environmental Sciences, Natural Sciences Faculty, University of Puerto Rico in partial fulfillment of the requirement for the degree of

Doctor of Philosophy

Qiong Gao, Ph.D., Environmental Sciences Department

Thesis Advisor

Maritza Barreto Orta, Ph.D., Graduate School of Planning

Co-Advisor

Reniel Rodríguez Ramos, Ph.D, Social Sciences & Pedagogy

Thesis Committee Member

Nick Brokaw, Ph.D.., Environmental Sciences Department

Thesis Committee Member

Xiaoming Zou, Ph.D., Environmental Sciences Department

Thesis Committee Member

May 9, 2022

DEDICATION

¡Río Grande de Loíza!... Río grande. Llanto grande.

El más grande de todos nuestros llantos isleños,

si no fuera más grande el que de mi se sale

por los ojos del alma para mi esclavo pueblo […]

Extract from "Río Grande de Loíza" poem by Julia de Burgos

I am deeply honored and grateful for life and the Universe

To my family

To motherhood

To science

To accessible public education

ACKNOWLEDGMENTS

This journey would not have been possible without the support of my family: my husband and my daughter, my parents, my siblings, my aunts, my cousins, and my extended family. I am deeply indebted to my committee members, especially to my mentor, my co-advisor, and my archaeology professor. I also want to express my gratitude to my labmates, who supported me through this process.

Words cannot express my gratitude to all the University programs and agencies that funded and supported my graduate studies: (1) National Aeronautics and Space Administration Land Cover and Land Use Program (NNX12AE98G), (2) National Aeronautics and Space Administration (HICE-PR Project Grant), (3) Decanato de Estudios Graduados e Investigación (Teaching Assistant, Travel Grant, and Dissertation and Project Grant), and (4) Coastal Research and Planning Institute from the Graduate School of Planning, Coastal and Marine Science Center, Wood Hole Institute (United States Geological Survey Grant # G19AC00148) and Federal Emergency Management Agency (sub-award 4339-0007P).

Many thanks to the Coastal Engineering Branch of the Coastal Hydraulics Laboratory, Engineering Research and Development Center for their knowledgeable help with the software, scientific guidance, and moral support. I would like to thank my colleagues: Institute of Electrical and Electronics Engineers colleagues, professors, and friends, especially Juan Rivera Fontán, who showed me the research potential at Loíza. I would also like to thank the Natural Sciences and Environmental Sciences Department administrative personnel and professors for their personal and professional support.

Special thanks also go to the Loíza Community and the University programs and libraries: Centro de Competencias Lingüísticas, Red Graduada, CITEC, Rafael Picó Library, Proyecto el Mundo, and Colección Puertorriqueña. I wish to thank also offices and professionals who helped with data, result interpretation, and more: Geographic Mapping Technologies, ESRI, Consejo para la Protección del Patrimonio Arqueológico Terrestre de Puerto Rico, Office of Management and Budget of Puerto Rico, Office of Coastal Management (NOAA), and UPR-Mayagüez professors and Caribbean Coastal Ocean Observing System (CARICOSS).

I also would like to acknowledge all the musicians and music for making this journey more colorful. Thanks to those students and professors who post online resources for graduate students. Finally, thanks to every student and worker who crossed my path defending our Alma Mater, the University of Puerto Rico.

To all, I want to express my gratitude and respect.

ABOUT THE AUTHOR

Loderay I.M. Bracero Marrero finished a bachelor's degree in Anthropology and Geography at the University of Puerto Rico, Río Piedras campus. Also, she has a Master of Science in GIS at the University of Redlands, California. She has been an IEEE member for five years in the International Geoscience and Remote Sensing Society, where she is currently an active volunteer in the Puerto Rico and Caribbean Section. She works as the Mobile Outreach Program (MOVE) coordinator in the Puerto Rico chapter and volunteers with the Red Cross Puerto Rico chapter.

Loderay was a research assistant in projects to evaluate the shoreline changes in Puerto Rico before and after Hurricanes Irma and Maria in 2017 with the Coastal Research and Planning Institute of Puerto Rico, Graduate School of Planning of the University of Puerto Rico. She also has worked as a teacher assistant in geographic information systems (GIS), Remote Sensing, and Statistics courses.

Loderay is currently a physical science student trainee at the Coastal Engineering Branch of the Coastal Hydraulics Laboratory, Engineering Research Development Center, USACE. She has also worked as a GIS Analyst for the Consejo para la Protección del Patrimonio Arqueológico Terrestre de Puerto Rico, Instituto de Cultura Puertorriqueña. Her main interests are spatial analysis, geoscience, archaeology, and modeling using remote sensing, GIS, and numerical simulation.

TABLE OF CONTENTS

LIST OF FIGURES

LIST OF TABLES

ABSTRACT

Assessing the Impact of Coastal Processes on Archaeological Sites in Loíza Puerto Rico: Integrating Geographic Information System (GIS), Remote Sensing, and Numerical Modeling Techniques

by

Loderay I. M. Bracero Marrero

Archaeological sites are a part of cultural heritage that is threatened by accelerated climate change. This research evaluated climate hazard impacts on archaeological sites in Loíza, Puerto Rico. The main methods applied to understand these threats to archaeological sites were fieldwork, data collection, geographic information systems, remote sensing, statistics, and numerical modeling. Using the Digital Shoreline Analysis System, an analysis of shoreline changes was conducted from 1902 to 2108 to establish the proximity of archaeological sites to erosional areas and to estimate when these sites may be impacted in the future by shoreline recession. The archaeological sites' spatial intersections with threats such as sea-level rise projections (1-ft to 3-ft), storm surges, high tide flooding, and FEMA zones were evaluated. A total physical vulnerability value was then calculated using these threats, and a prioritization ranking value, using the Scottish Coastal Archaeology and the Problem of Erosion approach, was assigned to each archaeological site based on its significance and physical vulnerability value. Due to the complexity of the coast of Puerto Rico and Loíza, the numerical models CMS-Wave and Flow were used to understand morphological changes due to wave energy, wind, and bathymetry.

Findings indicated that eight Loíza sites are vulnerable to shoreline recession within 100 years, and 15 sites could be vulnerable within 100 to 500 years. The majority of the sites (16) are vulnerable to four hazards: FEMA V Zones (1%) and A Zones (1% and 0.2%), and tsunami run up zones. Four sites are vulnerable to 10 hazards: FEMA A Zones (1% and 0.2%), shallow coastal flooding, sea level rise (1-ft, 2-ft, and 3-ft), storm surges (Hurricane Categories 1, 2, and 3), and tsunami run up zones. For sea level rise scenarios, 13 sites will be vulnerable by 2050, 2070, or 2090. Furthermore, the results regarding morphological changes showed that archaeological sites such as LO-27 Playa Berwind in Punta Uvero were near erosional areas in the nearshore area.

The final prioritization value for management purposes showed that most of the sites obtained a high priority (45%), followed by medium priority (40%), and low priority (15%). Cueva de los Indios and Parroquia Espíritu Santo y San Patricio, archaeological sites registered in the National Register of Historic Places, obtained high and medium priority values, respectively. These priority values indicate the urgency that should be given to archaeological sites for management purposes.

This research is significant because it presents new methods for evaluating possible accelerated climate change hazards to archaeological sites in Loíza, Puerto Rico. In addition, it provides new data regarding shoreline changes and morphological changes for the sites, which may also be used for coastal management and planning processes.

Chapter 1 – INTRODUCTION

Archaeology is a science that investigates past societies through the material remains left in ancient sites. An archaeological site is a spatially and temporally confined context that preserves remnants of previous human activity (Society for American Archaeology, 2018). An undisturbed archaeological stratigraphy within each site allows the interpretation of changes that took place over time based on the excavated vestiges of structures, elements, ecofacts, and artifacts that are found in specific layers of the sites, which are then interpreted using different theoretical frameworks (Harris, 1981). Thus, the stratigraphic integrity of each site is of utmost importance, as it allows researchers to understand the processes that took place in each location from a diachronic perspective (Ochoa et al., 2019). The stratigraphic layers—formed by natural processes and/or anthropogenic activities—reveal important chronological information; however, these same processes, in addition to site formation and transformation, can disturb or impact the stratigraphy of each analyzed context.

In this dissertation, I analyzed one set of processes that has been determined to constitute a major hazard for preserving the integrity of archaeological sites: coastal erosion, flooding due to rises in sea levels, high tide flooding, tsunami, FEMA zones, and storm surges. After evaluating the physical vulnerability, I established a prioritization value for each site for management purposes. In addition, I analyzed the proximity of the archaeological sites to nearshore and insular morphological change (erosion or accretion).

1.1 Integrity of Archaeological Sites

Anthropogenic activities (e.g., artifact movement, looting, sand extraction, urban construction) or natural processes (e.g., erosion, soil mixing, rainfall, flooding, landslides) can impact the integrity of archaeological sites. Wildesen (1982) comprehensively defines the term “impact” by type and importance when analyzing the integrity of an archaeological site and its potential for conservation and management. Consequently, it is essential for archaeologists to analyze these impacts while conducting archaeological work (reconnaissance visits, surveys, or excavations). By analyzing these threats, archaeologists can recognize current threats or envision future impacts on archaeological sites, especially in the context of accelerated climate change.

Other anthropogenic activities such as construction (Williams & Corfield, 2013), land use (RESEARCH, 2021), looting (Barker, 2018), sand extraction (Agency for Cultural Resource Management & Leap Sustainable Development, 2016), and agricultural activities (Meylemans et al., 2014) may impact a site’s integrity. For example, according to Barker (2018), $7.8 billion were generated from the trade of antiques that were extracted by looting without a scientific approach. The project Remote Sensing Techniques for Archaeology (RESEARCH) studies how land-use changes can damage the integrity of archaeological sites if these activities are conducted without proper management tools. Although anthropogenic impacts are considered one of the biggest threats to archaeology, natural processes can also have similar effects on site integrity.

Other natural processes such as landslides, flooding, rainfall, sea-level rise (SLR), shoreline changes, coastal erosion, swells, and storm surges may also impact the

archaeological record. As recognized by the archaeological community in both early and recent research (Wainwright, 1994; Rapp & Hill, 1998; Howard et al., 2005; Marzeion & Levermann, 2014), the archaeological record globally has been and is being impacted by each of these threats. This reality, combined with decades of poor management practices for archaeological sites, is detrimental. Consequently, it is crucial to address the impact of natural processes, such as coastal erosion, which can disturb the archaeological integrity of each archaeological context. Indeed, the loss of archaeological information is perpetual when sites are disturbed.

An undisturbed stratigraphy is of utmost importance for chronologically placing archaeological contexts by both relative and absolute dating methods. Stratigraphy is used as a relative dating method to obtain chronological information on the order of different elements in an archaeological site (i.e., artifacts or ecofacts). Absolute dating methods, such as radiocarbon and dendrochronology, are used to provide chronological information (Renfrew & Bahn, 2004a). The difference between relative and absolute dating methods is that the former (e.g., stratigraphy, seriation) relies on an artifact's location in particular strata or characteristics to assign dating, whereas the latter relies on examining the timeframe of specific materials (Barone, 2021). If artifacts are found in a stratum where absolute dating is possible, chronological information could be correlated using the stratigraphy. Erosional processes affect the integrity of archaeological sites, however, making it more challenging to study these sites.

The effects of erosion on archaeological sites could be compared to looting: when a site is dug up for looting/larceny without recording vertical profiles or associations, this impact is permanent (Renfrew & Bahn, 2004b). The archaeological stratigraphy of the

site is further affected by the dynamism of shoreline changes, erosion driven by water, wind, sediment composition, and geology, among other issues. As explained by Enevold et al. (2019) and Zhurbin et al. (2019), in some cases, chronological information challenges can be tackled through the use of new technology, such as 3D scanning and geographic information systems (GIS).

Archaeological excavations are considered a process of destruction (Evis et al., 2016), but when an excavation is conducted scientifically, the chronological information (Berggren, 2009) that is gathered adds new data and information to historical knowledge. Thus, the main problem is losing archaeological strata since, without it, it is not possible to properly analyze and study the archaeological site. This could happen when sites on the coast are affected by erosion and vestiges or artifacts are eventually returned to land by waves, now lacking the contextual information necessary to conduct temporal analysis.

The analysis of possible climate change threats to archaeological sites becomes urgent in the context of rapid climate change (Hil, 2020). Although more research has been conducted regarding direct anthropogenic impacts, research concerning how accelerated climate change impacts past, current, and future archaeological sites is growing in the scientific community and in popularity.

1.2 Climate Change Scenarios

Accelerated climate change is one of the biggest problems and challenges faced by humanity. According to the Intergovernmental Panel on Climate Change (IPCC), “it is unequivocal that human influence has warmed the atmosphere, ocean, and land” (2021).

Anthropogenic-induced changes that generate the greenhouse effect are causing accelerated global climate change. The greenhouse effect, responsible for making life possible on Earth by regulating its temperature (Sagan, 1985) causes the atmosphere to heat when gases (e.g., water vapor and carbon dioxide) absorb emitted surface longwave radiation. Increasing levels of greenhouse gas emissions (e.g., carbon dioxide and methane) from anthropogenic activities block the longwave energy from being emitted to space, however, increasing the temperature of the Earth's surface (NASA, 2022). In summary, the greenhouse effect is induced by a group of gases in the atmosphere that blocks the longwave emissions from the Earth's surface, but this process is being altered by anthropogenic activities linked to the current global economic system.

The abovementioned physicochemical processes were in balance before the Industrial Revolution and the "success" of industrial capitalist cities (Marques, 2020). Since then, especially over the last three decades, the massive quantities of gases such as carbon dioxide, nitrous oxide, methane, and water vapor that have been emitted due to economic activities (e.g., fossil fuel burning and deforestation) have increased the Earth's temperature at faster rates. In 20 to 30 years, the Earth will be different than it is today (IPCC, 2022) because of the changes provoked by natural processes. For example, mean surface temperature, extreme heat, cold spells, heavy precipitation, coastal flooding, erosion, ocean acidity, and more are likely to increase due to accelerated climate change (IPCC, 2022). This will be exacerbated by variations in the rain, drought, and wind patterns, decreases in pH; and melting glaciers (NASA, 2019). As the Earth has a "global climate," these effects affect all regions of the world, but they could have other consequences in the Caribbean and the United States.

In the United States and the Caribbean, increases in storm intensity and temperatures; reductions in fresh water supplies, sea-level rise jeopardizing coastal communities and critical infrastructure; and coral bleaching due to warming of the coral reefs are expected (Díaz, E.L.; Gould et al., 2018). Climate patterns in Puerto Rico have been changing. For example, according to the National Integrated Drought Information Systems (NIDIS), over a 90-day period, Puerto Rico's southern and central-eastern cities experienced rainfall deficits (2 – 4 inches), and 35% of the area has been classified as "Abnormally Dry (D0)".

In this climate change scenario, archaeological sites, which are part of our cultural heritage, are also being threatened. In the following section, a general state of the art will be presented, discussing this problem.

1.3 State of the Art

In recent years, the study of how climate change may impact archaeological sites has started to increase in popularity, despite being long recognized by the scientific community. The topic has captured interest worldwide (Williams, 2017; Radio Televisón Española & Agencias EFE, 2022). The archaeological community has discussed this issue in both early and recent research (Wainwright, 1994; Rapp & Hill, 1998; Howard et al., 2005; Marzeion & Levermann, 2014; Reeder-Myers, 2015), and a diverse archaeological record around the globe has been and is being impacted by natural threats due to accelerated climate change. This reality, combined with decades of poor management practices of archaeological sites, is detrimental to their preservation. As a result, global efforts to address and tackle these threats have been put in place.

World heritage sites (WHS), including archaeological sites, will be affected by the effects of accelerated climate change. According to the Climate Change and World Heritage Report (World Heritage Centre, 2007), climate change risks will affect cultural heritage in different ways. For example, sea-level rise (SLR) could cause coastal flooding and seawater incursion, provoking population movements, coastal erosion, or loss of activities by the communities in these areas. This interaction of communities and ecosystems may vary depending on the WHS type.

Types of WHS include glaciers, marine biodiversity, terrestrial biodiversity, archaeological sites, and historic sites (World Heritage Convention, UNESCO, 2007). Sagarmatha National Park (Nepal), Sundarbans (India/Bangladesh), Cape Floral Region (South Africa), Chan (Perú), and the city of London are examples of each cultural heritage type respectively. This global view illustrates the complexity of WHS and how to evaluate the threats to each individual site in a climate change scenario. Sea-level rise is one of the most common concerns for archaeological sites near coastal areas.

According to Cooper and Peros (2010), SLR is one of the primary hazards to archaeological sites in the Caribbean. SLR is one of the impacts of accelerated climate change and can be the result of melting ice sheets, thermal expansion, changes in wind and currents (eustatic), and land elevation changes, which are caused by tectonic movement (isostatic; Davidson-Arnott, 2010). Eustatic changes refer to changes in the volume, density, or mass of water (Church et al., 2013), whereas isostatic processes refer to the uplift of tectonic plates or land movement. The study of eustatic changes and isostatic levels is complex (Carter, 1988) because these processes work together, making it difficult to differentiate which one is causing the SLR in a specific area (Davidson-

Arnott, 2010). Due to its complexity, since the 1990s, there have been debates about eustatic changes in sea level (Tooley, 1993). For example, advances in technology have tackled debates about the uncertainty of surface of the earth calculations (Pirazzoli, 2005), but one of the effects of SLR is shoreline changes.

SLR effects on shoreline changes are not uniform but depend on the coastal type, river inflows, constructions on the coastline, and more. Shoreline diversity and classification (Finkl, 2004) are therefore vital in understanding SLR contributions to shoreline changes in specific locations. For example, when the sea reaches the land at the shoreline, the environment encountered by the tide—vegetation, rocks, structures, bays, lagoons, or sand—should be considered. These and other factors will determine how SLR affects specific coastal types, so evaluating shoreline changes is of fundamental importance to evaluating the SLR impact on archaeological sites.

Shoreline changes can affect present communities and ecosystems, but also archaeological sites. Commonly, shoreline changes have been studied to analyze threats to ecosystems and individual populations (Hsu et al., 2007; Kermani et al., 2016; Vu et al., 2018; Shayegh et al., 2021). Shoreline retreat could also impact archaeological sites on or near the shoreline (Erlandson, 2012; Reimann et al., 2018). The focus of shoreline change analysis is to analyze the positional change of the shoreline through the years (Boak & Turner, 2005; Shayegh et al., 2021). The processes of erosion/accretion also lead to shoreline changes, which may vary for various archaeological sites, including rock art sites, middens, and structures.

The presence of archaeological sites on coastlines increases the need to assess shoreline changes and their impacts on these contexts. As previously mentioned, more

research and an interdisciplinary approach are needed to address the impacts on archaeological heritage in shoreline areas. This problem worsens when archaeological sites along the shoreline are abandoned or not surveyed. Some authors have asserted that this is most common when a site does not have a fixed or concrete structure to "evidence" the site's archaeological value (Erlandson, 2012). For example, while we have the success story of the Cape Hatteras Lighthouse in North Carolina, where the lighthouse was moved inland to protect it from coastal erosion, the same attention is not given to other archaeological sites, such as the ancient Indigenous communities of Native Americans in the United States. As noted by Erlandson (2012, p.1):

> I do not regret the move or the money spent, but I wonder how many significant Native American sites were lost to coastal erosion in the Outer Banks area during the same time period, with little or no public notice or mitigation.

Several authors have established this need and have mentioned how engineering, GIS, geology, remote sensing, and other disciplines can give broader perspectives to explain how these forces impact archaeological sites. For instance, Meylemans et al. (2014, p.10):

> One of the main points emerging from conference discussions has been the need for inter-disciplinary dialogue and cooperation. Combining a broad spectrum of approaches from a multitude of research disciplines (geomorphology, soil science, geography, geology, archaeology, etc.) could lead to true advances. Although this seems to be a logical, obvious conclusion—especially in heritage management circles—this practice is rarely employed. For example, a wide gap exists between users and developers of GIS-based models and field researchers

In this regard, Erlandson also establishes (2012, p.141):

> We need a wider and more public dialog about the nature of the threats that rising seas and coastal erosion pose to the human and ecological histories we study and benefit from. We need a concerted, collaborative, and global effort to bring the problem to the attention of government leaders and the general public […]
> In coastal regions around the world, archaeologists, historic preservationists, and land managers need to significantly increase their efforts to inventory, investigate, and interpret the history of endangered coastal sites before they are lost forever. As the world warms, we are racing a rising tide.

Furthermore, shoreline change analysis can supply erosion and accretion statistics to enhance the understanding of how archaeological sites can be affected by these two processes. Knowledge of these processes along the shoreline can help explain which archaeological sites' management agencies should be prioritized for their protection and study. In addition, analyzing these shoreline changes can guide archeologists in understanding past and future processes. Most importantly, this analysis will complement the more commonly addressed impacts of anthropogenic activities on archaeological sites: construction, looting, sand extraction, extraction of the Earth's crust, and other forces.

Analysis of shoreline changes, SLR, or other climate hazards has been addressed by several authors. Other research has addressed the possible impacts of climate change on archaeological sites (Dawson, 2013; Reeder-Myers, 2015). In Australia, Taçon et al. (2021) studied how the rock art at the Djarrng archaeological site was degraded after the tropical cyclone Monica in 2006. In the Caribbean, Ezcurra and Rivera-Collazo (2018) correlated SLR map projections and site locations to evaluate which sites could be impacted. Additionally, Rivera-Collazo is currently working on a project to update archaeological site inventories to create a Coastal Vulnerability Index for archaeological sites in Puerto Rico (Figueroa Cancel, 2021a; I.C. Rivera Collazo, personal communication, March 3, 2019).

Recently, Hofman et al. (2021) integrated paleoenvironmental data, shoreline change data, and archaeological excavations to evaluate how climate drivers have impacted archaeological sites in the Lesser Antilles. Anderson et al. (2017) conducted similar work in the United States, both along shorelines and inland. Most importantly, actual

communities could apply past practices to assess climate change in the present, affecting landscape integrity, identification, preservation, and the conservation of cultural heritage. To examine how SLR impacts archaeological sites, however, the variation in coastal areas should be considered.

In summary, several investigations have focused on evaluating the impacts of these erosion processes on archaeological sites. However, these processes can affect each type of archaeology site differently. For example, earthen sites are more vulnerable to rain than to wind in Suoyang City in, China (Richards et al., 2019). The application of methods can enhance our understanding of how erosion affects archaeological sites, including the loss of a site's archaeological record. Past studies have focused on studying the erosion processes both along shorelines and in other locations, such as basins, riverine areas, agricultural lands, and landslide-prone areas, but the methods applied should depend on a site's location. For example, some authors have used computer modeling to understand how soil erosion affects archaeological sites. Others have used modeling methods and shoreline changes to understand erosion processes. These different methods do not invalidate each other; instead, method selection highly depends on a site's location and the importance of an interdisciplinary approach.

An interdisciplinary approach is necessary to understand how different climate changes may impact archaeological sites. Present advances in data availability and production of climate change hazards offer possibilities to analyze which threats can alter and affect the world's cultural heritage, including archaeological sites. In recognition of the broad climate change subject and its coastal implications, however, this research

focused on specific threats to archaeological sites in the coastal municipality of Loíza, Puerto Rico.

1.4 Scope of this Project

Loíza is a coastal municipality located in the northeast region of Puerto Rico. This municipality reflects the reality of other Puerto Rico coastal areas where coastal processes threaten communities, ecosystems, infrastructure, and cultural heritage. The importance of this is highlighted by the fact that, according to the 2020 census, 67% of the total population of Puerto Rico lives in coastal municipalities (M. Barreto-Orta, personal communication, March 2021). Moreover, 24% of the 799 linear miles of Puerto Rico's coast is constructed (Programa de Manejo de la Zona Costanera, 2017), a reality that has enhanced coastal erosion, endangering communities, socioeconomic activities, ecological areas, and cultural heritage. Moreover, Puerto Rico and Climate Change Council (PRCC) (2013) have studied other social and ecological impacts beyond the coastal areas. In this scenario, the cultural heritage, including archaeological sites, is also vulnerable.

Loíza cultural heritage has been and continues to be affected by several natural and anthropogenic hazards (Meléndez Maíz, 1997). The Oficina Estatal de Conservación Histórica, or State Historic Preservation Office (SHPO), has recorded 72 archaeological sites (2018). The Consejo para la Protección del Patrimonio Arqueológico Terrestre de Puerto Rico, or Council for the Protection of the Terrestrial Archaeological Patrimony of Puerto Rico (shortened as Consejo de Arqueología Terrestre or CAT), has recorded 49 in their GIS point layer (2015). Loíza has two sites recognized in the National Register of

Historical Places: Cueva de los Indios and Parroquia Espíritu Santo (OECH, 2010). The current study conducted an evaluation of climate change hazards to these archaeological sites.

Firstly, I evaluated threats to all the archaeological sites in the study area, not only the ones near the coast of Loíza municipality. Secondly, I integrated quantitative data from shoreline change rates, instead of collecting the proximity from field trips. Furthermore, I estimated how long (in years) it would be before shoreline retreat would affect archaeological sites. In this study, I integrated coastal erosion rates, SLR projections, and coastal flooding (tsunami, storm surge, FEMA Zones, and high tide flooding) to evaluate the physical vulnerability of archaeological sites. The following sections will briefly describe the conceptual model used to evaluate the physical vulnerability and the models used to establish a prioritization ranking for each archaeological site.

1.4.1 Conceptual Model of the Physical Vulnerability

The way in which this research evaluated the physical vulnerability of archaeological sites to erosion processes is summarized in Figure 1.1. The central concept is climate change and all the possible effects that can worsen due to its acceleration (shoreline changes, flooding, SLR), with an additional threat from abrupt disturbances (tsunami). These impacts or threats to archaeological sites were considered to establish a final value of physical vulnerability to each archaeological site. A detailed explanation of this concept and the other parameters used to establish a final prioritization value for each archaeological site will be given in the next section.

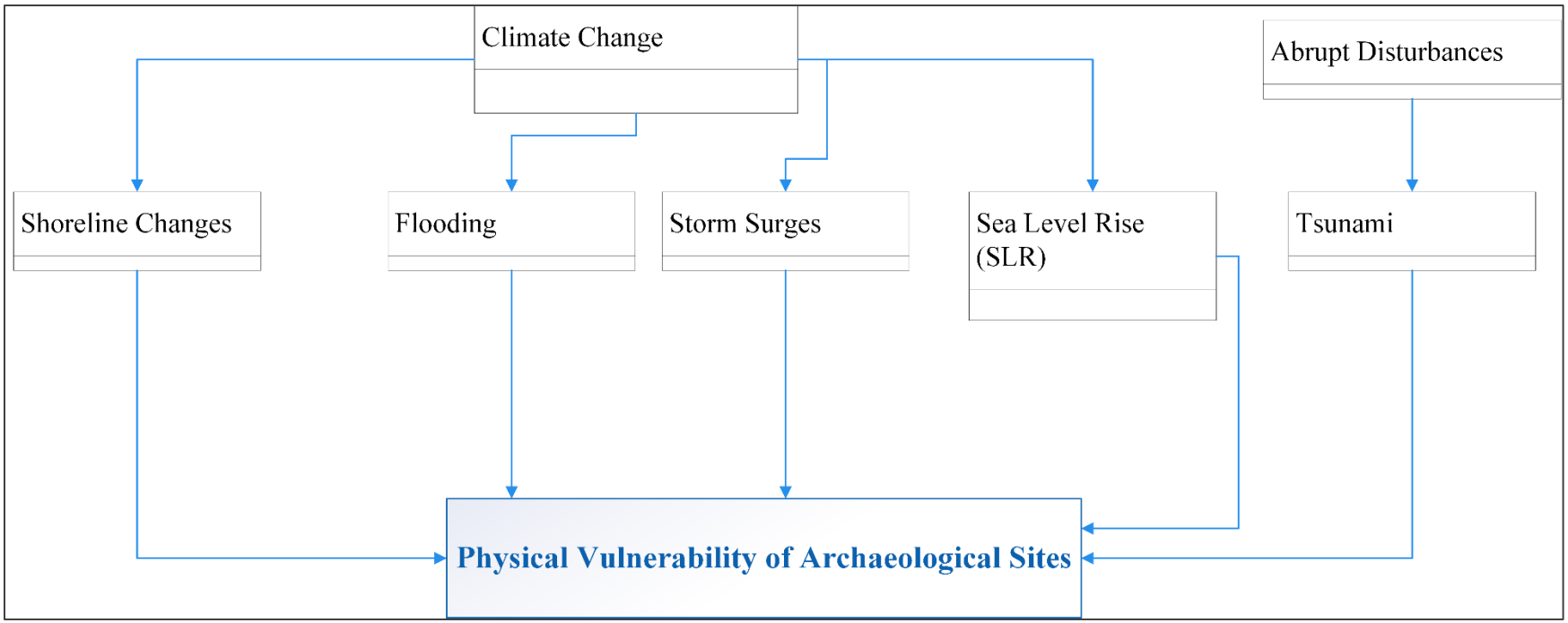

Figure 1.1: Conceptual Model for Evaluating the Physical Vulnerability of Archaeological Sites

1.4.2 Physical Vulnerability and Prioritization of Archaeological Sites

In this research, the following impacts of coastal processes on archaeological sites in Loíza, Puerto Rico, will be evaluated: shoreline changes (erosion and accretion) from 1902 to 2018, shoreline recession, tsunami, flooding, storm surges, and sea-level rise. A preliminary analysis of the archaeological sites in Loíza showed that 44% percent were located within 100 to 300 meters of the coast (Bracero Marrero, 2019). Ezcurra and Rivera-Collazo (2018) also established that different SLR scenarios threaten some archaeological sites in Loíza, concluding that their research "did not model coastal erosion following inundation, nor did it assess the potential impact of any other climate change impacts over Puerto Rico's tangible and intangible heritage" (p.11). It is, therefore, crucial to understand how different coastal processes, such as shoreline changes and coastal flooding events, may have "direct impacts" on the integrity of archaeological sites in the study area.

"Direct impacts," as defined by Wildesen (1982), are those events that happened or occurred at the "same time and place" as archaeological sites (p.54). This definition was used to evaluate the estimated locations of the threats and compared to the archaeological locations. For example, if an archaeological site was proximate to or within a specific coastal hazard, this threat was considered a direct impact on the archaeological site. By including several threats to archaeological sites in this investigation (shoreline changes from 1902 to 2018, shoreline recession, tsunami, flooding, storm surges, high tide flooding, and SLR), this research introduced a novel approach to evaluating a "physical vulnerability" and prioritizing archaeological sites for management purposes.

The following definitions were used for the physical vulnerability and prioritization values of archaeological sites. Recognizing the vast and multiple debates concerning vulnerability, I assumed the physical vulnerability concept to be the level of exposition (Fuchs et al., 2018) to the direct threats. The prioritization used in this project is based on the scoring system from the Scottish Coastal Archaeology and the Problem of Erosion (SCAPE) model, as described by Dawson (2013). This model is divided into stages to evaluate final prioritization based on vulnerability to coastal erosion (proximity) and the significance value of the archaeological sites (archaeological potential for investigation). The SCAPE model was not modified by Rivera-Collazo (2019), who instead used the Reeder-Myers approach (2015). In the current research, sites beyond the coastal area were also considered, several stages of the SCAPE model were used, variables to establish physical vulnerability were expanded, and quantitative data were used to establish the proximity of sites to coastal erosion.

Each site's final priority level score was gathered from the physical vulnerability and site significance (integrity, density, size, cultural components). The total physical vulnerability (total of threats) and archaeological significance were therefore summed to determine the final archaeological prioritization value. After evaluating the final prioritization value, the priority levels were divided into low, medium, and high priority. Moreover, morphological change analysis was also conducted for some archaeological sites with high priority values near the coast.

In summary, first, changes in shoreline position were studied in Loíza. Next, the location of the archaeological sites where flooding was estimated was analyzed. Finally, a vulnerability assessment of the archaeological sites was conducted, adding other

variables, such as storm surges. Hence, each archaeological site's total threat rank and significance value were summed to establish a final priority level.

1.4.3 Methodological Glimpse

Several methods and approaches were applied to assess the physical vulnerability of archaeological sites. Shoreline changes were addressed by deriving the shoreline contours from topographic maps, aerial images, and orthographic images from 1902 to 2018. The Digital Shoreline Analysis System (DSAS) was then used to calculate rates of change and other statistics to estimate shoreline recession rates (Himmelstoss et al., 2018a). Shoreline changes are based on calculating erosional rates and estimating shoreline recession rates. The shorelines from 1902, 1931, 1951, 1977, 1990, 2010, and 2018 were extracted from topographic maps, aerial images, and orthographic images.

Previously developed GIS layers such as the SLR, tsunami reaches, storm surges, high tide flooding, and flooding zones from the Federal Emergency Management Agency (FEMA) were intersected with the locations of the archaeological sites. These data were extracted from Coastal Flood Exposure maps developed by the Office for Coastal Management of the National Oceanic and Atmospheric Administration (NOAA, 2021a).

The proximity of specific archaeological sites to some regions of morphological change or shifts in the sea bottom, which indicate erosion or accretion, was evaluated. The hydrodynamics and morphological change along the coast of Loíza for 2018 were evaluated using numerical modeling (Passeri et al., 2015), integrating the Coastal Modeling Systems (CMS) Flow and CMS-Wave models (Beck, 2019; Li et al., 2019). The CMS-Flow model can calculate the sediment movement according to wave parameters and others assigned in CMS-Wave (USACE, 2020).

Fieldwork visits were conducted to specific archeological sites inside the inventory, and information such as photos and audio files was collected using Survey 123 apps (ESRI, n.d.-i, 2019). A survey was created using the known locations of archaeological sites, and a reconnaissance of some of the archaeological sites was conducted. Uncrewed Aircraft Systems (UAS) were also used to evaluate the actual status of individual archaeological sites.

In summary, the archaeological significance of each archaeological site was gathered from the available literature. The physical vulnerability value was established based on several indicators: erosion rates, shoreline recession, and flooding events (SLR, FEMA flooding zones, high tide flooding, storm surges, and tsunami). The archaeological significance and physical vulnerability values were summed to assign a priority value for each archaeological site. Finally, proximity to morphological changes such as erosion or accretion was evaluated for high priority sites.

1.5 Dissertation Structure

The current dissertation is divided into five chapters (see Figure 1.2). Chapter 1 states the problem of archaeological record loss due to different climate change hazards and addresses the current research on these topics. Chapter 2 addresses shoreline changes in the Loíza coastline from 1902 to 2018, presenting maps, graphs, and statistical analyses to understand which areas present higher rates of erosion or accretion and any correlation between periods and rates of erosion and accretion. In addition, Chapter 2 also shows the results of forecasted shoreline changes in 2032 and 2042 using DSAS forecasting tools. Chapter 3 presents an evaluation of coastal sediment transport patterns caused by

hydrodynamics along the coastline of Loíza. Morphological change data were used to evaluate the proximity of archaeological sites to areas of erosion or accretion, yielding information that is valuable to decision-making and management processes for the area. Overall, Chapter 3 offers valuable information for understanding the sites' coastal shoreline changes and sediment transport due to wave-induced currents and wave heights.

Chapter 4 shows the results of ranking physical vulnerability and prioritization for the archaeological sites. The data produced in Chapter 2 was used to estimate the effect of shoreline movement on archaeological sites, especially near erosional coastal sites. The total physical vulnerability was then evaluated by including coastal hazards (storm surges, tsunami, flooding, high tide flooding, and SLR projections) at the sites. This chapter explains the archaeological data depuration that was conducted to establish an archaeological significance, and the final prioritization values are presented as low, medium, or high levels.

Chapter 5 presents conclusions for the different chapters, discusses limitations of the investigation, and suggests future work scenarios. A detailed literature review and explanation of methodology are included in each dissertation chapter, which are titled as follows:

- Chapter 1: Introduction
- Chapter 2: Shoreline Change Trends in Loíza Puerto Rico from 1902 to 2018
- Chapter 3: Analyzing Coastal Sediment Transport Patterns Using Numerical Modeling at Loíza, Puerto Rico

- Chapter 4: Physical Vulnerability Assessment of Archaeological Sites and Prioritization Ranking for Management in Loíza, Puerto Rico in Response to Accelerated Climate Change Threats
- Chapter 5: Conclusions

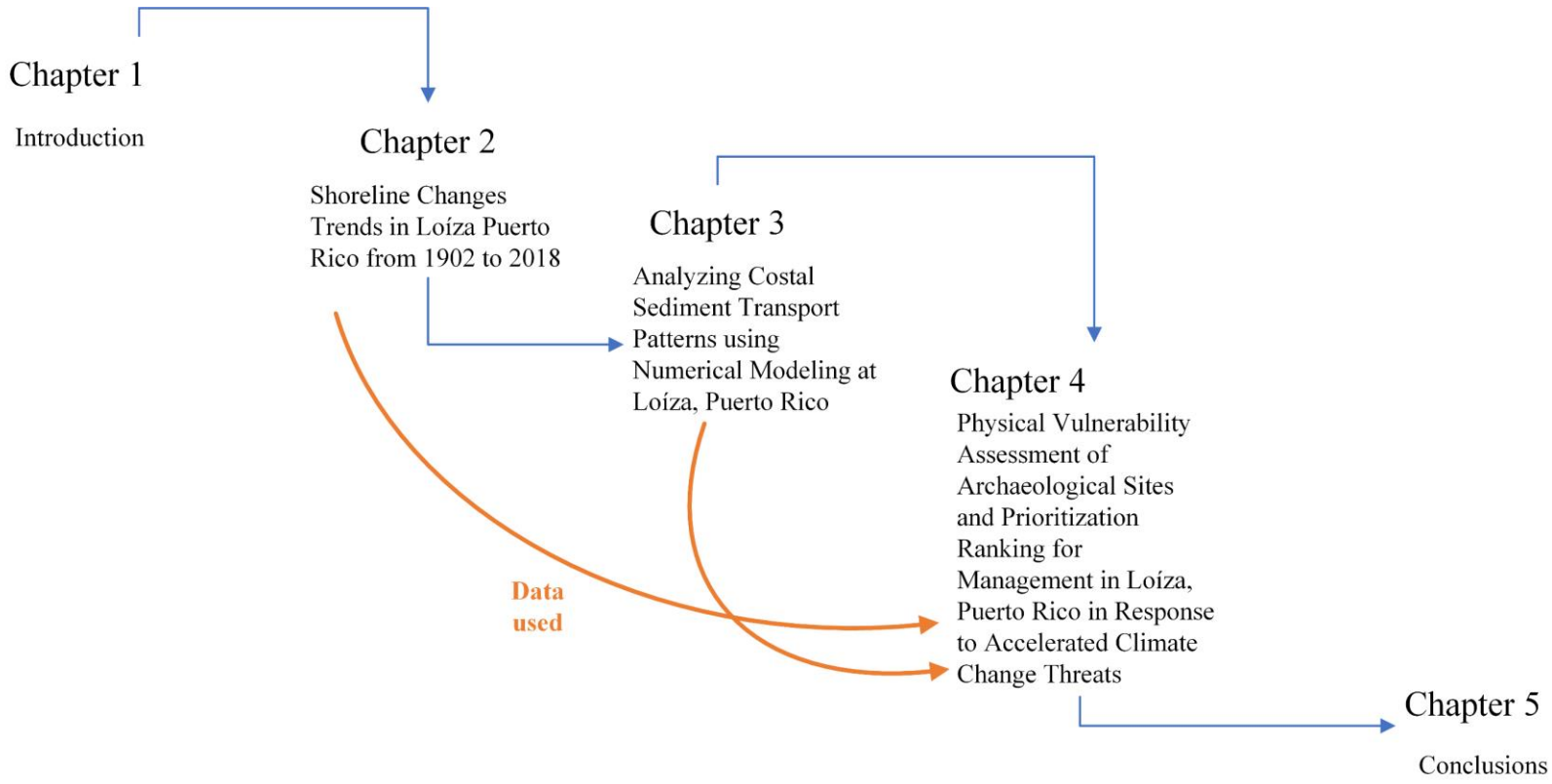

Figure 1.2: Dissertation Structure and Relationships between Chapters

Chapter 2 – SHORELINE CHANGE TRENDS IN LOÍZA PUERTO RICO FROM 1902 TO 2018

2.1 Abstract

Shoreline change analysis is one of the most common methods used to analyze the possible accretional or erosional areas along a coast due to sea-level rise, flooding, and anthropogenic activities. This method is highly viable when historical images are used to extract the shoreline. This investigation evaluated shoreline change trends in Loíza, Puerto. The high-water line was used as a proxy to analyze shoreline change, extracted from topographic sheets, aerial images, and orthophotos. Shorelines from six years were used for the long- and short-term analysis: 1902, 1931, 1951, 1977, 1990, 2010, and 2018. Using the shoreline data, I also forecasted the possible rates of change in 10 years and 20 years. The forecasting, rates of change, and both linear regression and weighted linear regression of those rates were calculated using the Digital Shoreline Analysis System. R Studio was used to run parametric and non-parametric tests (t-tests, paired t-tests, and Wilcoxon) to find other trends and correlations between accretion and erosion rates among the different time periods.

The main results of this investigation indicated increasing erosional rates as time passed. Moreover, periods with higher erosional rates corresponded to sand extraction events, droughts, and dam construction. For the periods 1951 – 1977, 1977 – 1977, and 1990 – 2010, statistics supported the hypothesis that erosional rates were dominant, whereas the periods 1902 – 1931, 1931 – 1951, and 2010 – 2018 were dominated by accretional rates of change. Despite observing a continuous pattern of erosional rates as time passed, the most recent period, 2010 – 2018, was dominated by accretional rates.

The forecasted shorelines for 2032 and 2042 showed a high inclination to erosional rates, and the uncertainty increased. The linear regression rates supported the establishment of general trends in certain areas. For example, in Punta Uvero, despite the latest period showing accretional rates, the linear regression indicated erosion.

Overall, this study showed how statistical analysis, linear regression, and non-parametric and parametric tests can be applied to understand more information about shoreline rates of change. Moreover, it provided previously unrecorded rate change data for 116 years in Loíza, Puerto Rico.

2.2 Introduction

For this research, I conducted shoreline change analysis (SCA) assessment in Loíza, Puerto Rico, from 1902 to 2018. The study's primary goal was to understand the trends in shoreline changes in Loíza, Puerto Rico, during this 116-year period. The main questions of the study were:

1. What is the SCA assessment (erosion, accretion, or stable) for the entire coastline of Loíza for the period of 1902 to 2018?
2. Do accretion or erosion rates dominate a specific period?
3. Is there a significant difference between the period's rates?
4. What are the erosion/accretion projections for the Loíza area in 2032 and 2042?

SCA has been broadly applied in earlier years and has been a comprehensive method of assessing different climate change threats, such as sea-level rise and shoreline erosion (Pacific Coastal and Marine Science Center, USGS, 2021). This method has been applied

globally to measure how shorelines worldwide are retreating due to erosion or advancing seaward due to accretional processes (Miller & Dean, 2004; Hsu et al., 2007; Prasita, 2015; Donadio et al., 2018; Jayanthi et al., 2018; Bagheri et al., 2019). Applications and development methods to create and improve shoreline changes have been broadly discussed globally (Pajak & Leatherman, 2002; Boak & Turner 2005; Thieler et al., 2007; Addo et al., 2008; Manno et al., 2017; Foti et al., 2019). For example, a homogenized process to extract the shoreline is one of the most discussed issues. Moreover, because the coast has many features, shoreline definitions, mapping methods, and uncertainties have been discussed and addressed in previous and recent investigations (Moore, 2000; Le Cozannet et al., 2016; Manno et al., 2017; Le Cozannet et al., 2019). For example, Moore et al. (2006) analyzed differences in digitization positions when using the same definition of the shoreline digitized by different scientists. The scientific community uses several geographic sources to collect shoreline positions in this scenario.

Shorelines can be extracted using diverse sources such as topographic maps, aerial photos, orthophotos, satellite images, and elevation or bathymetry data. After collecting shorelines, positional differences over the years are measured through SCA (Kabuth et al., 2014; Kermani et al., 2016; Do et al., 2019; Sabour et al., 2020). When several shorelines from different years are extracted, the distances between them can be measured (Himmelstoss et al., 2018), allowing scientists to analyze differences in meters between years, rates per year, beach width, erosional hotspots, and more. When measuring distances between shorelines, however, it is essential to keep the same proxy or indicator of the shoreline.

Several indicators or proxies can be used for shorelines. According to Boak and Turner (2005), an indicator is "a feature that is used as a proxy to represent the 'true' shoreline position" (p. 689). Furthermore, an indicator should be consistent and repeatable over different years (Pajak & Leatherman, 2002). Each scientist chooses the best indicator for their research based on investigation questions and data availability. These indicators can be extracted by photo interpretation, satellite image classification methods, or a tidal datum. Boak and Turner (2005) mentioned a vast list of different physically extracted indicators, such as the high-water line (HWL), the wet/dry line, and the groundwater exit point. In general, some proxies or indicators are used more often than others, depending on several factors.

Two of the most common indicators are the HWL and the wet/dry line (Kabuth et al., 2014). As high-resolution data increases, however, other datum reference shorelines are extracted using the mean high-water line (MHW) proxy. The chosen shoreline indicators highly rely on data availability and scientific questions. For example, the HWL is selected as an indicator when topographic sheets (T-Sheets) are used as a data source (Anders & Byrnes, 1990; Crowell et al., 1990). If aerial images or orthophotos are used, other indicators such as the wet/dry line and the instantaneous line can be identified. If Lidar Digital Elevation Models or other models are available, the MHW indicator could be used with other tidal data and buoy data. Moreover, other studies may use satellite images to analyze shoreline changes.

Studies that use satellite images to extract the shoreline perform classification methods based on spectral information, with the goal of classifying the satellite images into land and sea to extract the shoreline position (Wu et al., 2018). Hence, shoreline

extraction relies heavily on the difference between the instantaneous line and the land, or water and land classification. Some authors explain that using satellite images such as LANDSAT can increase the long-term shoreline analysis, but the spatial resolution is limited (Bishop-Taylor et al., 2021). The satellite shoreline is a limitation when other historical shorelines are available. For example, historical shorelines are available in Italy (Donadio et al., 2018) and the United States (Ruggiero et al., 2013), reaching back over 100 years. In this regard, new advances in the Digital Shoreline Analysis System (DSAS) allow for the comparison of shoreline changes using two different indicators: MHW and HWL (Himmelstoss et al., 2018). Thus, when using satellite images for shoreline change analysis, differences between indicators should be addressed. New research has yet to be conducted to calculate these differences between indicators and measure if there are significant differences when conducting SCA.

In summary, when conducting SCA, scientists must account for two things: (1) using the same indicator throughout the years and (2) application of a homogenized method to extract the shoreline proxy. Examples of physical indicators according to Boak and Turner (2005) are presented in Figure 2.1. For example, the instantaneous line is oceanside and the ground water exit proxies are below the wet/dry line, the HWL, and the extreme event line (e.g., storm surge, swells, high tide flooding). Of the proxies visible in this image, however, the ground water exit point and instantaneous line vary due to local conditions (e.g., wave direction and height), which is one of the reasons why HWL is a more commonly used proxy.

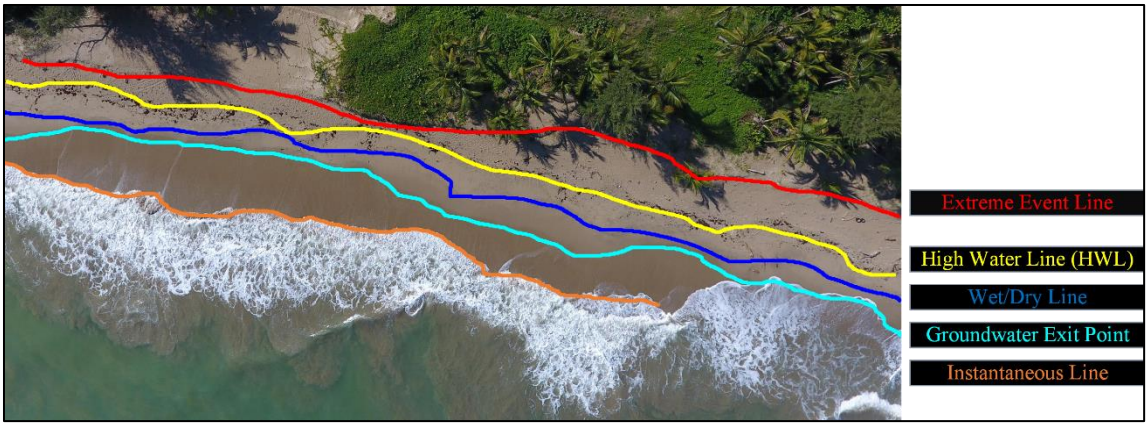

Figure 2.1: Examples of Physical Indicators or Proxies for Analyzing Shoreline Changes

The HWL is one of the most common physical indicators used (Pajak & Leatherman, 2002). As with other indicators, however, the existence of several definitions for the HWL may present a challenge. The complexity of extracting the HWL can result in different interpretations by different scientists when identifying the HWL in images. For example, in a review by Boak and Turner (2005), eleven different definitions were included because different authors used different features to identify the HWL. For example, some authors used (1) pixel brightness (Shoshany & Degani, 1992, as cited in Boak and Turner, 2005), (2) the line where seaweed lined up (Gorman, Morang & Larson, 1998, as cited in Boak and Turner 2005) or (3) the boundary on a beach, recognized by an abrupt or subtle change (Byrnes, Mcbride & Hiland, 1991, as cited in Boak and Turner 2005). These differences were measured by Moore et al. (2006) when they compared the three different HWLs with the MHW digitization differences among scientists between Maryland and Virginia. The average horizontal offset was 18.8 meters between these two shorelines, when using 2002 data, highlighting those variations in individual researchers' interpretations of the shoreline.

This variation highly relies on the photo interpreter, bringing uncertainty to the shoreline extracted. Nevertheless, a critical aspect of evaluating shoreline changes is maintaining the same definition while digitizing different years. For this reason, after the methodology is chosen for extracting the shoreline, the scientist should consistently compare the same indicator over the years to minimize the error. Uncertainty will remain present, however, despite choosing the same definitions and methods to extract the shoreline. Previous research has shown ways to address this issue (Ruggiero et al., 2013; Long & Plant, 2012; Manno et al., 2017; Do et al., 2019). Some of the variables considered to address shoreline error include the spatial resolution of the image, the horizontal accuracy of the image, and local tides. Because change rates and other statistics are derived from the digitized shoreline, an evaluation of the uncertainty is essential to understanding which rates should be considered with more precaution than others. For example, if a rate is below the uncertainty level, this rate should be taken with caution in the uncertainty range. In contrast, if a rate surpasses the uncertainty range, scientists can have more confidence in the measured statistic.

2.2.1 Previous Shoreline Change Analyses in Loíza

Studies involving SCA have been conducted in Puerto Rico since 1978. Jack Morelock conducted one of the first mostly complete studies on the shoreline of Puerto Rico, including Loíza. In this report, “Shoreline of Puerto Rico” (Morelock, 1978), different areas along the shoreline were identified as erosion/accretion/stable. For example, in Loíza, east of Punta Maldonado, erosion was recorded due to sand extraction occurring to construct the airport. Erosional rates were also documented to the east of Vacía Talega and the east of Río Grande de Loíza. Morelock’s study captured the different

anthropogenic activities that affect the shoreline of Puerto Rico, such as sand extraction. In the years following that primary work, further research has also been conducted on the shoreline of Loíza and other areas of Puerto Rico (Crespo Jones, 2013). Moreover, some of the following investigations in Loíza have also covered other areas of Puerto Rico.

The study areas in Loíza in other investigations have varied because some have focused on specific areas, while others showed all municipality shorelines of Loíza. Investigations previously conducted in the study area (Thieler and Danforth, 1994; Barreto-Orta, 1997; Morelock & Barreto, 2000; Barreto-Orta et al. 2017) are summarized in Figure 2.2. For example, Thieler and Danforth (1994) conducted one of the first SCA assessments in Puerto Rico using the Digital Shoreline Mapping System, an earlier version of the current DSAS. They focused on analyzing the changes in Punta Uvero Parcelas Vieques (east sandpit) in Loíza using the following sources to extract the shoreline: (a) National Topographic Sheets, 1959 and 1964; (b) topographic maps (1982); and (c) aerial photos for 1936, 1951, and 1987. A total of 25 transects were analyzed, of which four were accretional and the rest were erosional.

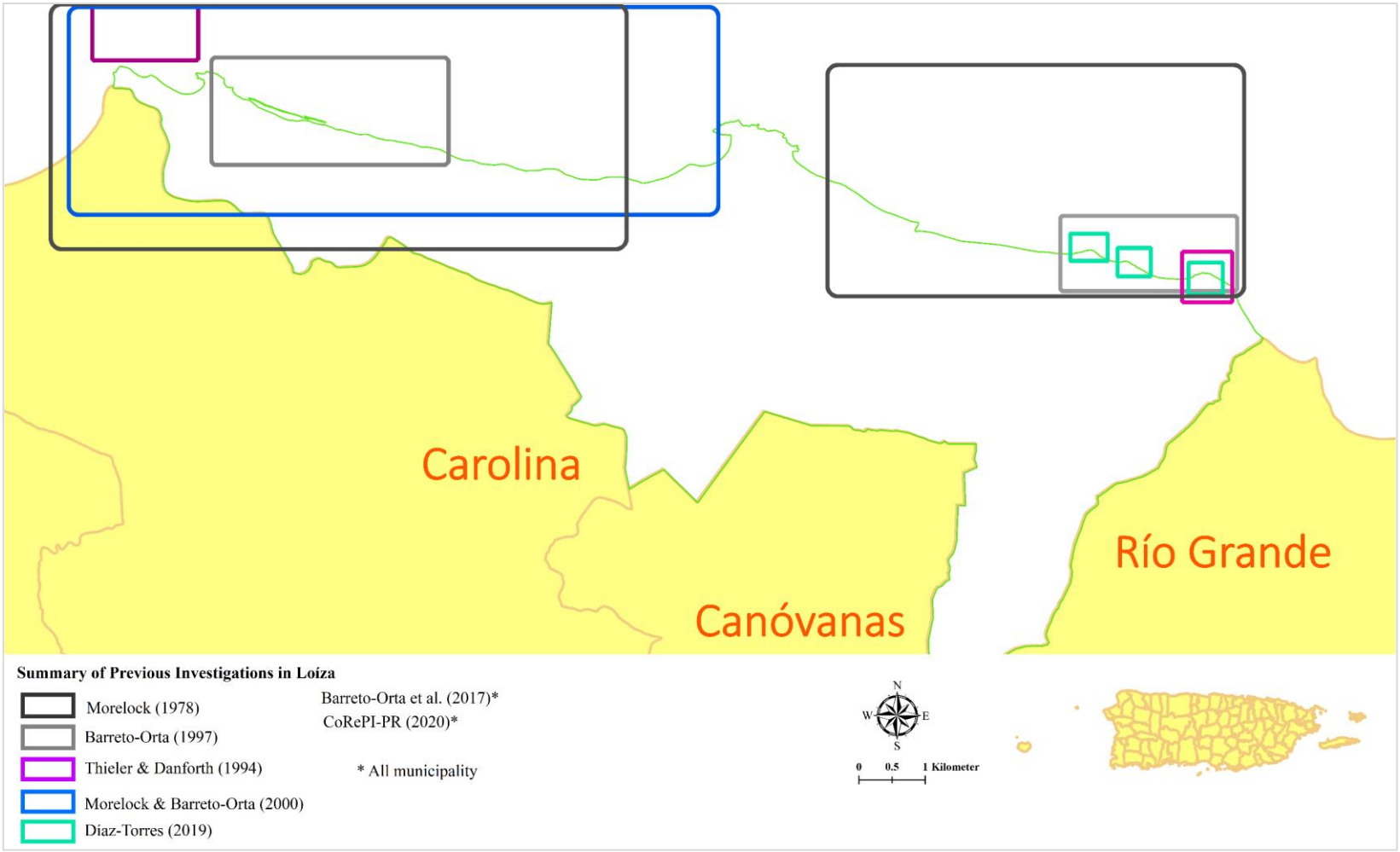

Figure 2.2: Study Area and Previous SCA Investigations: Loíza is located in the northeast of Puerto Rico. Several investigations have been conducted in this location

Barreto-Orta (1997) conducted a shoreline change study in the municipality of Loíza that combined aerial images, multispectral images, and field stations to assess shoreline changes and identify possible variables associated with these changes. The results showed a diverse erosion/accretion behavior along the shoreline at the site. An accretion event was shown to have occurred in Boca Cangrejos (western part of Loíza) between 1964 and 1987. At Piñones Beach (La Pocita), erosional rates were documented from 1936 to 1951, severe erosion occurred from 1964 to 1971, and then from 1971 to 1977, erosion rates dominated the stations. At Punta Iglesias, from 1968 to 1984, accretion rates were observed, but between 1984 and 1987, erosion occurred. Finally, erosion was also observed at Punta Uvero from 1968 to 1987. In 2000, Morelock & Barreto, 2000 published new data on coastal erosion. In their report, Loíza showed moderate (-0.62 m/yr) and stable (-0.12 m/yr) rates. Additionally, a project was conducted to evaluate SCA using the wet/dry line as the indicator (Barreto-Orta et al., 2017). The investigators used aerial images from the 1970s, orthophotos from 2010, and field station data to extract the shoreline. The report identified Loíza as one of the areas with the highest erosion rates (-1.93 m/yr) from 1970 to 2010.

Finally, one of the most recent works involving SCA in Loíza was conducted by Díaz-Torres (2019), who studied the communities of Parcelas Suárez, Villas del Mar, and Villa Cristiana. The author combined different methodologies to analyze shoreline changes using aerial images: fieldwork, field stations, and shoreline extraction. The results showed a sharp contrast between accretion and erosion rates over a short period (2016 – 2017) in Villa Cristiana when compared to Parcelas Suárez and Villas del Mar. In Villa Cristiana, a consistent erosion pattern was observed from 1970 – 2010, 2010 –

2016, and 2016 – 2017. The last period, 2017 – 2018, showed a switch to accretion in some areas. Moreover, in 2020, the Instituto de Investigación y Planificación Costera de Puerto Rico, or Coastal Research and Planning Institute of Puerto Rico (CoRePI-PR), measured beach width using 2017 and 2018 orthophotos to evaluate the impact of Hurricane Maria. In Loíza, preliminary results showed that in 2017 and 2018, shorelines showed 42% and 28% erosion, respectively.

Currently, Loíza is the target of different projects and investigations due to its known risks to climate change threats. For example, to manage erosion, the United States Army Corps of Engineers (USACE) is conducted the "Emergency Streambank and Shoreline Protection Project" (n.d.-b). One of the goals of this project is to construct a revetment along the Parcelas Suárez beach area. Additionally, in 2018, the Marine Awareness Research & Education Society (MARES; 2018) wrote a plan to manage different climate changes, risks, and adaptation methods. This report evaluated different risks and vulnerabilities by integrating communities. In addition, Martínez Martínez, (2008) and Díaz-Torres (2019) have studied and applied different mitigation and action plans to tackle different hazards at Loíza.

In summary, changes in the Loíza shoreline have been studied in previous years using different methodologies. In my research, DSAS will be used to extract the primary rate of shoreline changes, and R Studio will be used to run parametric and non-parametric tests on the data concerning rates of change in Loíza. The following section will explain the different methodologies applied in this chapter.

2.3 Methodology

Various research tools were integrated to perform SCA in this study, including DSAS, remote sensing, GIS, and statistics. In this section, data sources used to extract the shoreline, DSAS parameters, error assessment, and more will be explained. Fieldwork data collection methods will be discussed, and the statistical tests conducted, and hypotheses will be explained in this section.

2.3.1 Data to Extract the Shoreline

Several sources were used for digitizing or extracting the shoreline: T-Sheets, aerial images, photomosaics, and orthophotos (see Table 2.1). Most of the images were geometrically corrected or rectified using ArcGIS 10.6.1 (ESRI, 2016) and ArcGIS Pro (ESRI, 2021) . Geometric correction (image-to-map method) was applied to convert the aerial images to planimetric and assign projections (Jensen, 2005), which was necessary in order for measurements to be feasible using the images. After collecting the unrectified aerial images, the Puerto Rico 2009 – 2010 Orthophotos (National Oceanic and Atmospheric Administration (NOAA); National Centers for Environmental Information; OCM Partners, 2022) were used as the map data. Ground control points between the unrectified and rectified aerial images were identified for each image. Each image was rectified with the following parameters: less than 5 meters of root mean squared error (RMSE), a minimum of four ground control points, and a first polynomial transformation. NAD83 State Plane Puerto Rico and the Virgin Islands, Lambert Conformal Conic in meters was used to project all the images.

Table 2.1: Data Sources Used to Extract the Shoreline in the Current Project

SOURCE	GEOMETRIC CORRECTION AUTHOR	YEAR	MONTH	DAY	Resolution (dot per point)	Scale	Camera/ Sensor
Topographic Sheets	Current Project	1902	--	--	1,200	1:20,000	n/a
Aerial Images	Current Project	1930-1931	November - Unknown	--	800	1:10,000	Fairchild K3
Aerial Images	UPR-RP: NASA-Roses	1951	February	4	600	1:20,000	--
Aerial Images	UPR-RP: NASA-Roses	1977	February	12	600	1:20,000	--
Aerial Images	Current Project	1990	April	--	--		--
Orthophotos	N/A	2009 – 2010	Oct., Jan.	31, 27	--	0.3 meter	Leica ADS40 digital senso
Aerial Images	N/A	2018	July – Aug.	--	--	0.5 meter	PhaseOne iXU1000RS

The T-Sheets were accessed from the Shoreline Data Explorer (National Geodetic Survey, NOAA, 2019). Loíza's area was divided into two different T-sheets. After rectifying these sheets, I proceeded to digitize the shoreline. One digitized section of the shoreline was already available, however, so I reprojected it to Puerto Rico's projection. The 1931 aerial photos were from the first flight attempt in Puerto Rico by the United States Marines, which started in December 1930 (Vicente, 1931). Although that dataset was not completed due to a lack of funding (Sepúlveda Rivera, 2004), the photos were published in the digital journal "Revista TP" (Vélez, 2019). I conducted a geometric correction of 26 images for this study but only used 15 due to their quality for the study area. A small section (Punta Maldonado-Torrecilla) was extracted from the raster mosaics created by (López Marrero et al., 2017) as it was not available on the Revista TP website. The average RMSE for these aerial images was 1.71 m. The shoreline digitization was conducted at scales from 1:500 to 1:1000.

The majority of aerial images for Puerto Rico were generated by la Autoridad de Carreteras de Puerto Rico, Departamento de Transportación y Obras Públicas, Puerto Rico (Oficina de Fotogrametría, n.d.), but I was able to access these images from different projects or agencies. The 1951 and 1977 aerial images were provided geometrically corrected by the Spatial Analysis Laboratory of the Environmental Sciences Department, University of Puerto Rico, Río Piedras (UPR-RP) on a base scale of 1:20,000 (Yu et al., 2015). The 1951 aerial images were taken on February 4, 1951. For this study, the shoreline was extracted at scales of 1:500 to 1:1000. A total of 11 images were used for the study area. For the 1977 aerial images, a total of seven images

were used. Four of these images were geometrically corrected, and the remaining images had been previously rectified.

The Office of Management and Budget of Puerto Rico provided the 1990 aerial images, which were taken in April at a 1:20,000 scale. The HWL was digitized in this study on a scale from 1:300 to 1:500. Ten images were geometrically corrected and used for digitization purposes. The 2010 shoreline was digitized and provided by the Geomorphological Laboratory, Graduate School of Planning, UPR-RP [1]. The Puerto Rico 2009 – 20010 Orthophotos, with a ground sample distance of 0.3 meters, were used to rectify the aerial images, but because the digitized proxy was the wet/dry line, we re-edited the shoreline to HWL in scales from 1:500 to 1:1000. Lastly, the 2018 orthophotos were used for digitizing the post-Hurricane Maria shoreline at scales from 1:300 to 1:500. Eleven images were used for digitizing the HWL. All aerial images and orthophotos used for 1930, 1951, 1977,1990, and 2018 are summarized in Table 2.2.

Table 2.2: Individual Image Sources: Aerial Images and Orthophotos Used for Digitization of the High-water Line

	1931: JPG
1	A-02-W-031
2	A-02-W-021
3	B-03-W-281
4	B-03-W-271
5	B-03-W-25
6	B-03-W-23
7	B-02-W-011
8	B-02-W-03
9	B-02-W-04
10	B-02-W-051
11	B-04-E-13
12	B-04-E-15
13	B-04-E-16
14	B-04-E-17
15	B-04-E-18

	1951: TIF
1	GS-LR-12-59
2	GS-LR-12-94
3	GS-LR-12-111
4	GS-LR-12-110
5	GS-LR-12-59
6	GS-LR-12-91
7	GS-LR-12-61
8	GS-LR-12-93
9	GS-LR-12-58
10	GS-LR-12-63
11	GS-L-12-64

	1977: TIF
1	Rio_Grande_1977_4_6
2	Carolina_1977_4_9
3	Rio_Grande_1977_4_7
4	Carolina_1977_3_4
5	Carolina_1977_4_13
6	Carolina_1977_146
7	Carolina_1977_3_5

	1991: SID
1	c9002_0130_03_caroli_20
2	90-02_0128_03_loizax_20
3	90-02_0129_03_loizax_20
4	90-02_0127_03_loizax_20
5	90-02_0126_03_loizax_20
6	c9002_0125_03_loizax_20
7	90-02_0124_03_loizax_20
8	90-02_0116_04_loizax_20
9	90-02_0117_04_loizax_20_Pueblo
10	c9002_0119_04_loizax

2018: TIF (Militar Grids)			
1	20QJF8343	16	20QJF8841
2	20QJF8443	17	20QJF8941
3	20QJF8543	18	20QJF9041
4	20QJF8643	19	20QJF9141
5	20QJF8342	20	20QJF9241
6	20QJF8442	21	20QJF9441
7	20QJF8542	22	20QJF9541
8	20QJF8642	23	20QJF9540
9	20QJF8742	24	20QJF9640
10	20QJF8842	25	20QJF9740
11	20QJF8942	26	20QJF9840
12	20QJF9042	27	20QJF9940
13	20QJF9242	28	20QKF0040
14	20QJF9342	29	20QKF0039
15	20QJF9442	30	20QKF0139

2.3.2 Extracting the High-water Line as a Shoreline Indicator or Proxy

The investigation described in this chapter expanded on the previous analysis in Loíza, Puerto Rico by analyzing the entire shoreline (21 km) at Loíza and expanding the timeframe. A total of seven shorelines were collected or extracted: 1902, 1931, 1951, 1977, 1990, 2010, and 2018. T-sheets, aerial images, and orthophotos were used to

extract the shoreline positions at the site. The HWL indicator was used to analyze shoreline changes at Loíza's coast because data were already available using this indicator (1902 and 2010), and it is one of the most common indicators used (Pajak & Leatherman, 2002). In addition, the HWL matches the definition of historical topographic map surveys (Crowell et al., 1990).

I defined the HWL as the highest point where the water reached and avoided digitizing storm-induced lines. With these shorelines, six periods were compared over the short- and long-term. The six shorelines also allowed me to forecast and project future shoreline positions for 2032 and 2042. DSAS, which is an add-in or extension inside ArcGIS Desktop (ESRI, 2016), is the primary tool used to calculate rates and other statistics and forecast new shorelines (Himmelstoss et al., 2018). An example of the data imported by the user (shoreline and baseline) and the transects generated by the tool is given in Figure 2.3.

Figure 2.3: Data Inputs and Outputs When Forecasting New Shorelines Using the Digital Shoreline Analysis System

This project extracted the shoreline based on HWL as a physical indicator by using photo interpretation. My project combined other physical characteristics to

homogenize the extraction. The extraction depended on the remote sensing data used: aerial photos (panchromatic) or orthophotos (RGB). Due to image quality variation per source, not all indicators were identified during the digitization process, especially in the aerial images from 1931 to 1977.

For panchromatic images, the HWL was identified as the highest contrast in color between dry and wet, or the gray variation. Boak and Turner (2005) defined the HWL in panchromatic images by combining definitions from several authors: “A change in color or gray tone caused by differences in water content of the sand on either side of the high-water line” (p.693). Careful attention was given to avoid digitizing the instantaneous line or near the shore break, however, as this area can create more contrast in the aerial image (black/gray and white). Identifying the HWL in panchromatic images was one of the most challenging tasks because it heavily relied on image quality and resolution.

For RGB images, I identified the HWL as the highest contrast in color between wet and dry. Boak and Turner (2005) defined the HWL in RGB images as a “change in color or shade of the beach sand, or a line of seaweed and debris” (p.694). Because the RGB images possess more detail and resolution, however, other characteristics were analyzed, including the sargasso, the seafoam, and the shell lines drawn by waves as evidence of the last water line, but careful analysis was applied to avoid digitizing other HWL lines due to extreme events. Finally, I drew the contrast between dry and wet algae as the HWL in areas covered by sargasso.

Image brightness was modified to find the highest contrast in color, especially in areas where an image was primarily white due to spectral distortion. I applied this

method using the Contrast, Brightness, and Gamma tools offered in ArcGIS Pro (ESRI, n.d.-e), which helped me identify the highest landward contrast in the image.

The digitization process was conducted inside a geographic database using a Wacom Bamboo tablet. For each period, a feature dataset was created (Figure 2.4).

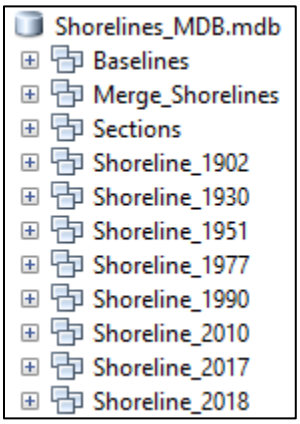

Figure 2.4: Geographic Database Developed for Digitization in the Current Research

The geographical database design and features created before running DSAS are shown in Figure 2.5. I created a features class (type: lines) to digitize the shoreline indicators for different years, as well as creating the baseline manually, assigning each line a DSAS_Group ID for areas. For each shoreline indicator, I created a subtype for classification purposes. For example, I used the classification subtype in areas where the HWL was not visible due to river mouths or rocky areas.

Additionally, I created topology rules for each feature dataset (Baseline and Shorelines). These rules helped increase the digitization quality (ArcGIS Pro Documentation, ESRI, n.d-a). The rules inside the topology were: Must Not Have Dangles, Must Not Self-Overlap, Must Not Overlap, Must Be Single Part, and Must Not Intersect or Touch Interior with Errors.

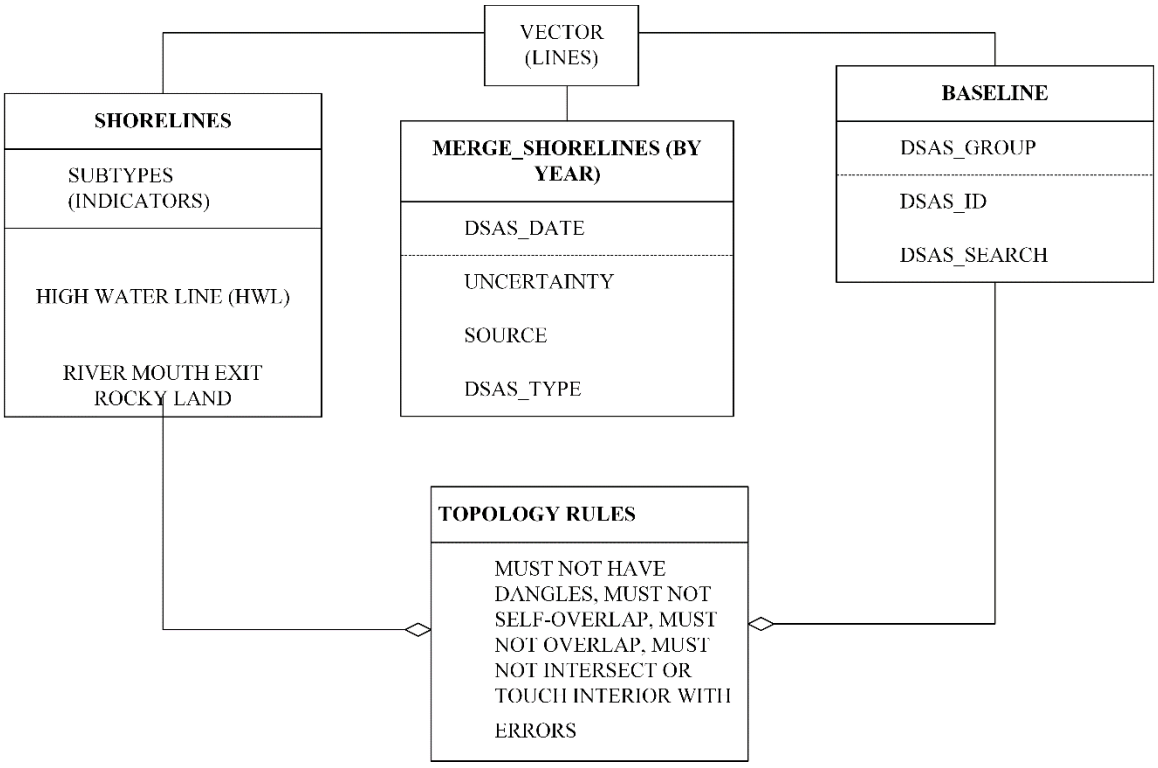

Figure 2.5: Geodatabase Design Delineated in this Research. Main feature classes were created (shorelines, merge shorelines, and baseline), and the topology rules were applied.

After each shoreline was digitized, I conducted a quality control process. First, I applied the ArcGIS Topology Rules for each line and verified the digitized line with the sources used (aerial images or orthophotos). Next, I merged all the shorelines into a single feature class. Finally, I converted the geographic database (.gdb) into a personal database (.mdb), as that is the format required by the DSAS add-in.

2.3.3 Shoreline Errors and Uncertainty

The error in shoreline data is measured from diverse sources. Several authors have discussed and applied different methods to address errors present in shoreline digitization (Anders & Byrnes, 1990; Moore, 2000; Ruggiero et al., 2013; Moussaid et al., 2015). According to Manno et al. (2017), shoreline data have an accumulative error because each source is different (image quality, scale, geometric correction), and local conditions

vary (tides, wind). Thus, shoreline data extraction carries errors due to image, scale, spatial resolution, ground sampling distances, tide variation, and other variables. The selection of the types of errors used in a project will depend on the scientists.

Source errors can be measured by analyzing the spatial resolution, tide variation, and other factors. The selection of the errors depends on the user and the data used. In this project, I calculated the uncertainty using five errors in meters: (a) georeferencing (RMSE); (b) digitizing error; (c) T-sheet error; (d) horizontal accuracy; and I uncertainty of the HWL. When all these errors are analyzed, the uncertainty for each shoreline could be calculated. I used Equation 2.1 to determine the uncertainty using my chosen errors (Ruggiero et al., 2013):

Equation 2.1 Uncertainty of the Shoreline

$$U_t = \sqrt{E_s^2 + E_d^2 + E_{qd}^2}$$

where U_t is the total uncertainty for each shoreline, E_s is the spatial error (aerial photos used for the georeferencing error [RMSE] and horizontal accuracy), E_d is the digitizing human error, and E_{qd} is the MHW error. Each error, description, value, and uncertainty total is summarized in Table 2.3. The MHW for Puerto Rico is 3 meters, which was calculated for Puerto Rico by the Woods Hole DSAS Team.

Table 2.3: Shoreline Error Sources in the Digitization Process (-- not applicable). A total of five (5) errors were considered for each shoreline, if applicable.

Error Source	Description	1902	1931	1951	1977	1990	2010	2018
Georeferencing (Root Mean Square Error)	Average RMSE of the rectified images (1931, 1990). The maximum RMSE value (4) divided by the total images used (1950 and 1970)	0.00	1.71	0.36	4.00	1.73	--	--
Digitizing Error	Human error while digitizing the coast	1.00	1.00	1.00	1.00	1.00	1	1
Topographic Sheet Survey	Error documented on T-Sheets Survey 1:20,000 Scale (Anders & Byrnes, 1990)	10.00	--	--	--	--	--	--
Orthophoto (Horizontal Accuracy)	Position error documented on the metadata	--	--	--	--	--	0.62	1.00
Uncertainty High-water line	The average of the mean high-water line according to buoy data. For 1902, the average of these data was taken.	3	3	3	3	3	3	3
TOTAL UNCERTAINTY U_t		**10.49**	**3.60**	**3.18**	**3.92**	**3.60**	**3.22**	**3.32**

Equation 2.2 was used to calculate the period uncertainty, U_p, which was automated by DSAS using each shoreline uncertainty, U_t (Himmelstoss et al., 2018).

Equation 2.2: Period Uncertainty

$$U_P = \frac{\sqrt{U_n^2 + U_{n+1}^2}}{yr}$$

where U_P is the total period uncertainty, and $U^2{}_n$ and $U^2{}_{n+1}$ are the respective U_t values of two shorelines. The time elapsed between the two shorelines was measured in years (yr). I used the uncertainty range to understand the error present on specific shorelines. The following section explains how DSAS used this uncertainty calculation to indicate statistical significance among rates.

2.3.4 Digital Shoreline Analysis System Parameters and Statistics

We used the DSAS Version 5.0 in ArcMap 10.5 to calculate different statistics, including shoreline change rates or endpoint rate (EPR), the net shoreline movement (NSM), the period uncertainty (EPRunc), linear regression rates (LRR), weighted linear regression rates (WLR), and confidence intervals for LRR and WLR (LCI and WCI, respectively; Himmelstoss et al., 2018). Some statistics required more than four shorelines (LRR, WLR, LCI, and WCI), so I ran DSAS seven times to calculate the rates per period and calculate the rates using the seven shorelines to find the trends. The first six runs were used to calculate the EPR, NSM, shoreline change envelope (SCE), and EPRUnc from Period 1 to Period 6 between two shorelines. I conducted one run with all seven shorelines for the regression statistics and confidence intervals. Because I inserted more than two shorelines, DSAS automatically calculated the EPR for the earliest and latest

parts of the period, 1902 – 2018. Statistics were therefore calculated for the study area for each period, as follows:

- Period 1: 1902 – 1931
- Period 2: 1931 – 1951
- Period 3: 1951 – 1977
- Period 4: 1977 – 1990
- Period 5: 1990 – 2010
- Period 6: 2010 – 2018
- Period 7: 1902 – 2018

The DSAS tool requires three primary datasets: shorelines, baseline, and transects. The latter is generated by the tool after the baseline is inserted. All these datasets should be in the same personal geodatabase (.mdb) format, and the shorelines should include the date and the uncertainty value. The main windows of DSAS parameters are: (1) Baseline, (2) Shorelines, and (3) Transects (Figure 2.6). The baseline was created manually along the shore to ensure transects were drawn perpendicularly, then divided into areas or groups of interest. I assigned dates and uncertainty fields for the shoreline input and chose Seaward Intersection. The transects were generated with a 50-m distance gap (or spacing) and a length of 2500 meters, but the option of clipping the transects to shoreline extent was selected. Once DSAS created the transects, I edited if needed and chose 362 transects (or samples). For example, I eliminated transects along with rocky areas. Although there were 362 transects, the number per period varied, as the HWL was not homogeneously visible in all the shoreline sections. For each transect, statistics were calculated for that specific area.

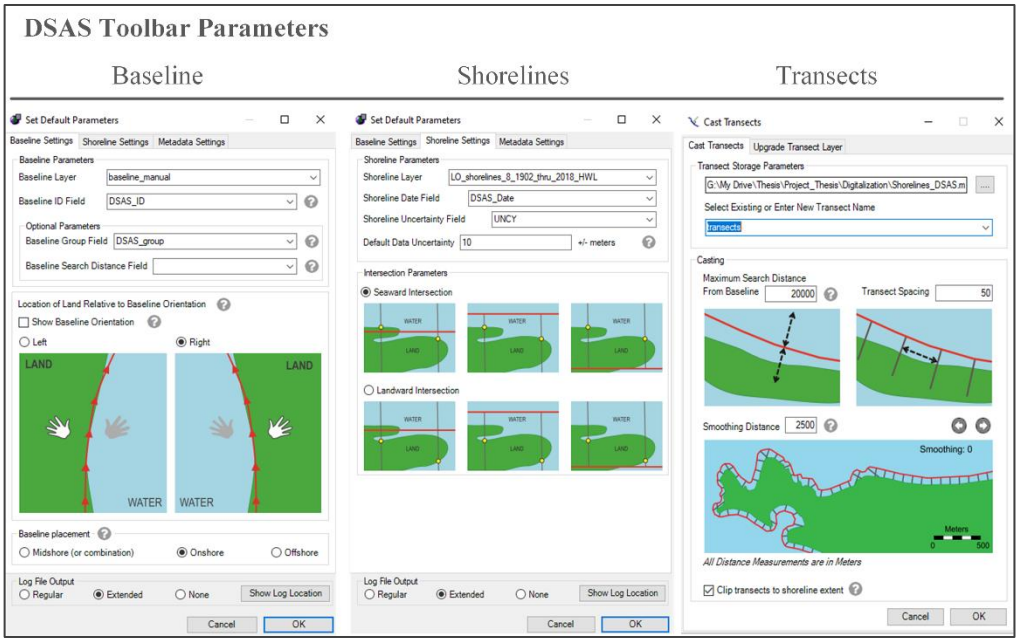

Figure 2.6: Parameters Assigned in the Digital Shoreline Analysis System (DSAS): Baseline, Shorelines, and Transects

As mentioned in the baseline parameters, I divided the shoreline using the baseline groups in DSAS. This feature assigns a Group ID to each transect, allowing the identification of transects by area of interest. DSAS then uses the Group ID to calculate the average and highest erosion or accretion rates and significance transects per area of interest. The groups used as areas of interest assigned a Group ID, as shown in Table 2.4. The results omitted two groups—rocky areas and river mouths—because the current study was focused on sandy beaches. Another reason that I omitted the rocky areas was because they presented high errors and variations in the shoreline data. Hence, I used only the beach areas that were assigned a GroupID.

By assigning a Group ID for each area, the final rates were presented by areas of interest. For example, I divided the shoreline by erosional lagoons (GroupID:13) created due to sand extraction and sandpit areas known for fast erosional processes (GroupID:14 and GroupID:17).

Table 2.4: Areas of Interest along the Shoreline of Loíza

Group ID	Length (meters)	Description	General Area
1	542.7	Rocky Land Boca de Cangrejos	Piñones
2	308.1	Beach Boca de Cangrejos	Piñones
3	945.9	Beach Punta Maldonado	Piñones
5	1,237.9	Beach La Pocita	Piñones
6	3,757.8	Beach Tres Palmitas	Tres Palmitas
7	2,340.0	Beach Torrecilla	Torrecilla
8	943.9	Beach Vacía Talega	Vacía Talega
10	2,124.1	Beach West Río Grande de Loíza	Río Grande de Loíza
12	1,393.9	Beach Río Grande de Loíza East Loíza Aldea	Loíza Aldea
13	772.9	Beach Parcelas Suárez (erosion lagoons)	Parcelas Suárez
14	618.9	Punta Iglesia sandpit	Parcelas Suárez
15	382.4	Beach Parcelas Suárez	Parcelas Suárez
16	1,059.1	Beach between Parcelas Suárez/Parcelas Vieques	Parcelas Suárez & Parcelas Vieques
17	649.6	Punta Uvero sandpit	Parcelas Vieques
18	886.1	Beach Punta Uvero East	Parcelas Vieques

After inserting all required data (shorelines, baseline, and transects) into DSAS, I ran the different statistics, each of which I will now explain in detail. First, the main three statistics used were (a) shoreline change envelope (SCE), (b) net shoreline movement (NSM), and (c) and end point rate (EPR). The SCE is the largest distance observed between two shorelines. This parameter aids in understanding which period in a transect showed the largest distance. The NSM is the total distance, in meters, between two shorelines—hence, the total movement inland or oceanward. The EPR is the NSM divided by the time elapsed, indicating the rate of change in a period. In this project, I

calculated this statistic for each period, resulting in the total change rate in meters per year (m/yr). The EPR, also referred to in this project as the shoreline change rate, was calculated as shown in Equation 2.3:

Equation 2.3: Shoreline Change Rate or End Point Rate (EPR)

$$EPR = \frac{NSM}{T}$$

where NSM is the total distance between two shorelines, and T is the time elapsed between the oldest and newest shorelines.

The shoreline change rate results were presented using the Stewart and Pope (1993) scheme, which divides the different rates into several categories (Table 2.5). Based on these categories, SCA was defined as the following: 1) values greater than or equal to 1 m/yr (> 0.1) were classified as accretional and values less than -2 m/yr were classified as erosional. DSAS calculates the percentages of accretional and erosional transects per Group ID and in total and categorizes rates lower than zero as erosional and more than zero as accretional. Hence, the lowest and highest rates within all the rates will be equivalent to the highest erosion and accretion rates, respectively.

Table 2.5: Classification of Rates of Shoreline Change Type Based on Stewart and Pope's (1993) Scheme

Classification	**Classes (myr^{-1})**
Severe Erosion	< -2.0
Very High Erosion	-1.21 to -2.0
High Erosion	0.71 to -1.2
Moderate Erosion	-0.31 to -0.7
Low Erosion	-0.11 to -0.3
Stable	0.1 to -0.1
Accretion	>0.1

To calculate other shoreline, change statistics, DSAS required more than two shorelines to have meaningful results: LRR and WLR. The LRR is the total distance between shorelines and the baseline (when compared to the dates (x). With the LRR, the user can determine if the overall rates are negative or positive through time by calculating the line's slope, allowing for the determination of a positive or negative relationship between the rates and the time elapsed. The WLR is similar, but it weights the shoreline distances (x) according to the uncertainty value, giving greater emphasis to those shorelines with smaller uncertainty values, e (Equation 2.4).

Equation 2.4: Weight Definition for Weighted Linear Regression

$$w = \frac{1}{e^2}$$

For the LRR and the WLR, additional statistics were calculated to understand the accuracy of the predictions: (a) the standard error, (b) the confidence interval for the linear (LCI) or weighted linear regression (WCI), and (c) the correlation coefficient. The standard error (Equation 2.5) determined the accuracy of the linear regression line by

calculating the distances between the baselines (y) and the predicted distances (y') in relation to the number of shorelines (n):

Equation 2.5: Standard Error

$$Standard\ Error = \sqrt{\frac{\sum(y - y')^2}{n - 2}}$$

Furthermore, for LRR and WLR, DSAS calculates confidence intervals referred to as LCI and WCI, respectively. The user chooses the confidence interval (CI) value beforehand. For my analysis, I preferred a CI of 95.5% (Figure 2.7), so the LCI and WCI were calculated for each sample by multiplying the standard error of the slope by the two-tailed test statistic (using the assigned CI). For example, if there were a LRR of 1.2 m/yr and a LCI of 0.5, the CI range would be 1.2 ± 0.5, resulting in a 95.5 % confidence that the actual rate falls between 0.7 m/yr and 1.4 m/yr.

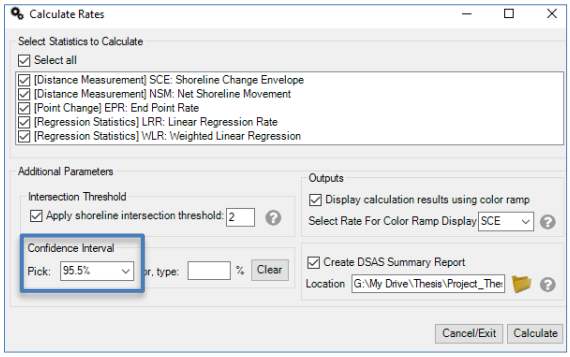

Figure 2.7: Confidence Interval in the Digital Shoreline Analysis System

Finally, the correlation (R^2) was calculated for the LRR and WRR. The R^2 (Equation 2.6) accounts for how the variability in the dependent variable (y) is "explained by the regression line through the independent value x" (Himmelstoss et al., 2018, p.54). If the resulting variability of the residual values between $(y - \overline{y})$ and the predicted $(y - y')$ is small, a better prediction is assumed. An R^2 value close to 1

indicates a perfect correlation because the fit of the linear regression line can explain the variation in the dependent variable. In contrast, if the R^2 value is close to zero, the fit of the linear regression line cannot explain the dependent variable's variability. Because these statistics are "purely computational" (Himmelstoss et al., 2018, p.49), precaution is advised due to outliers highly impacting the linear regression values.

Equation 2.6: Correlation R^2

$$R^2 = 1 - \frac{\sum(y - \hat{y})^2}{\sum(y - \bar{y})^2}$$

DSAS also forecasts or predicts the shoreline position for the next 10 or 20 years using the LRR model and the Kalmar filter. Long and Plant (2012) used the extended Kamar filter but with a "first-order linearization of the forecast equations at each time step" (p.2). In this way, they considered the change through time at the shoreline position. DSAS integrates this equation into the forecasting, allowing the user to predict shorelines 10 years and 20 years in the future. Because this filter uses linear regression to predict the future shoreline, however, this assumption should be taken with precaution due to shoreline variability and other variables. In summary, the Kalmar filter is used to better predict new shoreline positions, and the uncertainty is based on the uncertainty values per shoreline.

DSAS also calculates a "reduced n" and the "uncertainty of the average rate using reduced n." The "reduced n" is based on the "effective sample size" and is represented by the symbol n^*. The effective sample size is calculated from a "spatially lagged autocorrelation of each measure of the rate of uncertainty" (Himmelstoss et al., 2018, p.1), a formula based on the work of Garret and Toulany (1980). For the total number of transects (n) , a n^* is computed, where $n^* < n$. The "uncertainty of the average rate using

reduced n" is a new uncertainty value calculated using the n^* of independent transects (Equation 2.7).

Equation 2.7: Uncertainty using the reduced n

$$U_{R_{q^*}} = \frac{1}{\sqrt{n^*}} \bar{U}_R$$

Where $U_{R_{q^*}}$ is the uncertainty average using n^* , $\bar{U}_R$ is the average uncertainty using n, and n^* is the number of independent samples. The $U_{R_{q^*}}$ is calculated for whole transects and the user's regional areas (Group ID).

Finally, DSAS also reports the "percent of all transects that have statistical significance" for the EPR, the LRR, and WLR. To calculate the statistically significant transects (SSTs) for the EPR, however, DSAS uses the uncertainty per period (Equation 2.2). In contrast, for the linear regression (LRR and WLR), the CI for each one (LCI and WLR) are used. Equation 2.8 shows the calculation of the statistical significance range (SSR):

Equation 2.8: Statistical Significance Range (SSR)

$$SSR = R \pm UCI$$

where R is the rate of change and UCI is the total uncertainty per period (U_P) or the confidence levels reported on the LCI and WCI, respectively. This calculation helps to increase the confidence to determine that a transect is either erosional or accretional once the errors are considered. If the SSR minimum and maximum values are the same sign as the rate, the transect is a SST (Figure 2.8). Moreover, if there is an erosional rate (negative) and both maximum and minimum values are negative, I can be confident that the rate is erosional and, therefore, this transect will be considered a SST. Conversely, if one or both SSR values are positive, there is no confidence that "the rate is either

erosional or accretional" (Himmelstoss et al., 2018, p.63). The same applies to accretional rates.

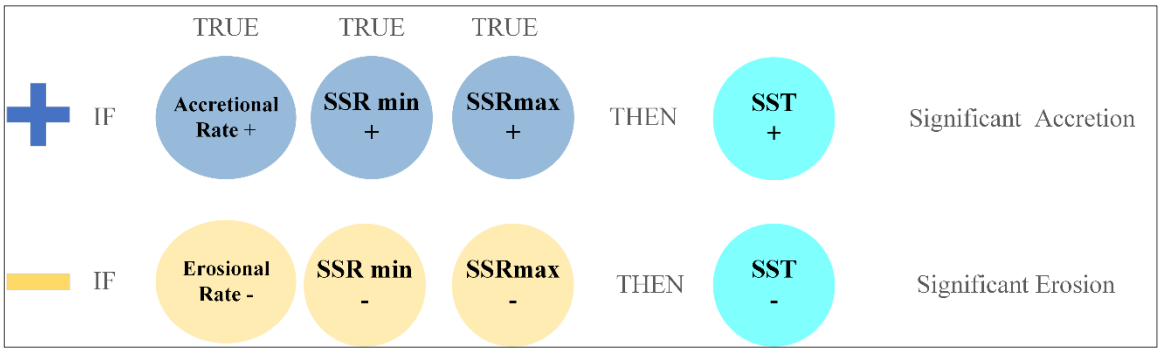

Figure 2.8: Boolean Conditions for Determining a Statistically Significant Transect (SST) for Accretional or Erosional Rates; SSR = Statistical Significance Range

For example, suppose there is a rate of -0.77 m/yr with a U_P of 0.38 m/yr, and the SSR minimum value is -1.15 m/yr and maximum value is -0.39 m/yr. Because both values are negative, this rate is a SST. In contrast, a rate of -0.07 m/yr with the same U_P would have a minimum value of -0.45 m/yr and a maximum value of 0.31 m/yr. As one of the range values is not negative, this transect rate would not be considered a SST.

2.3.5 Paired Comparison and T-Test

By coupling DSAS and other statistics run in RStudio (PBC, 2021), I aimed to understand the trends in shoreline changes in Loíza. To this end, I ran additional statistics to answer the following questions:

1. Do erosion or accretion rates dominate a specific period?
2. By comparing two periods, are they statistically different?
3. By comparing two periods, which one presents higher erosion or accretional rates?

I ran three main tests, two parametric and one non-parametric, using R and RStudio (PBC, 2021). Parametric tests assume that the data has a normal distribution, whereas non-parametric tests do not make this assumption. I used two parametric tests: a t-test and a paired comparison, also known as a paired t-test. For the non-parametric test, I ran a Wilcoxon or Mann-Whitney test (Ross, 2010).

The t-test and the paired comparison assume that the data is normally distributed and analyze the mean values. Specifically, the t-test compares the mean of the sample to a chosen value, whereas the paired comparison compares the difference in means between the samples (Kent State University, 2021). Additionally, the paired comparison assumes that observations are independent and is often used to compare data before and after an event (Statistics Solutions, 2021). Despite the large sample for most of the periods, I also decided to run non-parametric tests because my data had outliers. For this, a Wilcoxon test was used, which is based on the rank-sum to compare two sample medians instead of the means (Ross, 2010).

2.3.6 Fieldwork

Ten fieldwork visits were conducted for recognition and validation in Loíza between 2018 and 2020. Combining fieldwork with remote sensing (Gómez et al., 2017) strengthens results and allows a scientist to have a contextual perspective of the study area (Boas et al., 2020), aiding in understanding the dynamics of a particular coast and analyzing the shoreline results qualitatively. This is particularly important when digitizing the shoreline, as it helps with interpretation and drawing the chosen indicator.

The techniques used and areas visited on each field trip to Loíza are summarized in Table 2.6. UAS, field photos, and the Survey Connect App for Android (ESRI, 2019)

were used to collect fieldwork information (photos, status of the areas). The UAS images and videos were used for reference and interpretation purposes, but no shorelines were extracted. I used UAS images taken in 2018, 2019, and 2020. Flights conducted in October 2018 covered the area from Río Grande de Loíza to Río Herrera, whereas the 2019 and 2020 flights were flown in regions with already high interest and high erosion rates: Punta Iglesias and Punta Uvero. These videos and images proved helpful in understanding the different areas when digitizing the shoreline over the years. In summary, the fieldwork started with two exploratory visits. These visits were followed by a formal visit organized with the Oficina de Manejo de Emergencias, or the Emergency Office, from Loíza on October 12, 2018. Afterward, trips were conducted with local community leaders and alone.

Table 2.6: Fieldwork Visits to Loíza, Puerto Rico

Date	Method	Area Covered	Date	Method	Area Covered
October 8, 2018	Field photos	Vacía Talega	October 24, 2018	UAS	Parcelas Suárez, Loíza Aldea
October 12, 2018	Field photos	Piñones, Vacía Talega, Río Grande de Loíza	October 26, 2018	UAS	Loíza Aldea, Río Grande de Loíza
October 18, 2018	Field photos	Piñones	October 27, 2018	UAS	Río Grande de Loíza, Vacía Talega
October 20, 2018	ff aircraft systems (UAS)	Río Herrera, Villas del Mar	October 20, 2019	UAS	Parcelas Suárez
October 23, 2018	UAS	Villas del Mar, Parcelas Suárez	October 9, 2020	Field photos and UAS	Vacía Talega, Villa Cristiana

2.4 Results

This section presents the results of SCA over a 116-year period (1902 – 2018), followed by SCA results for shorter periods of time: 1902 – 1931, 1931 – 1951, 1951 – 1977, 1977 – 1990, 1990 – 2010, and 2010 – 2018. The short-term SCA showed accretion for the first two periods, 1902 – 1931 and 1931 – 1951. These periods were then followed by high erosion rates from 1951 – 1977, 1977 – 1990, and 1990 – 2010. A switch from erosion to accretion was identified for 2010 – 2018, which exhibited the highest accretional rates among all the periods. The long-term analysis showed erosional rates in areas such as Punta Uvero.

Both LRR and WLR showed the highest erosional rates along Loíza's shoreline, and the highest statistical significance rates for studied timeframe were observed 1951– 1977 and 2010 – 2018. Each subsection in this section will present frequencies using the erosional categories, with graphs showing the distribution by categories and Group ID, and a table summarizing the statistics. A detailed description of rates for each period is given at the end of each section. Finally, by comparing the rates for each period, most periods showed outliers and a tendency toward negative values (erosion).

2.4.1 Shoreline Change Rates (m/yr) by Period

2.4.1.1 Shoreline Change Rates (m/yr): 1902 – 2018 (Overall Long-term Analysis)

The evaluation of overall long-term shoreline changes showed erosion and accretion rates along Loíza's shoreline for the period 1902 – 2018. Moderate and low erosion events were identified along the shoreline during this time (Figure 2.9), with 64% of the transects (n = 223) showing erosion and 36% showing accretion (n = 124). The highest

frequency was observed for accretion (28%, n = 96). The next two highest frequencies were observed for moderate (27%, n = 94) and low erosion (26%, n = 90), with a further 14% (n = 49) being stable, 5% (n = 17) being high erosion, and 0.28% (n = 1) being very high erosion.

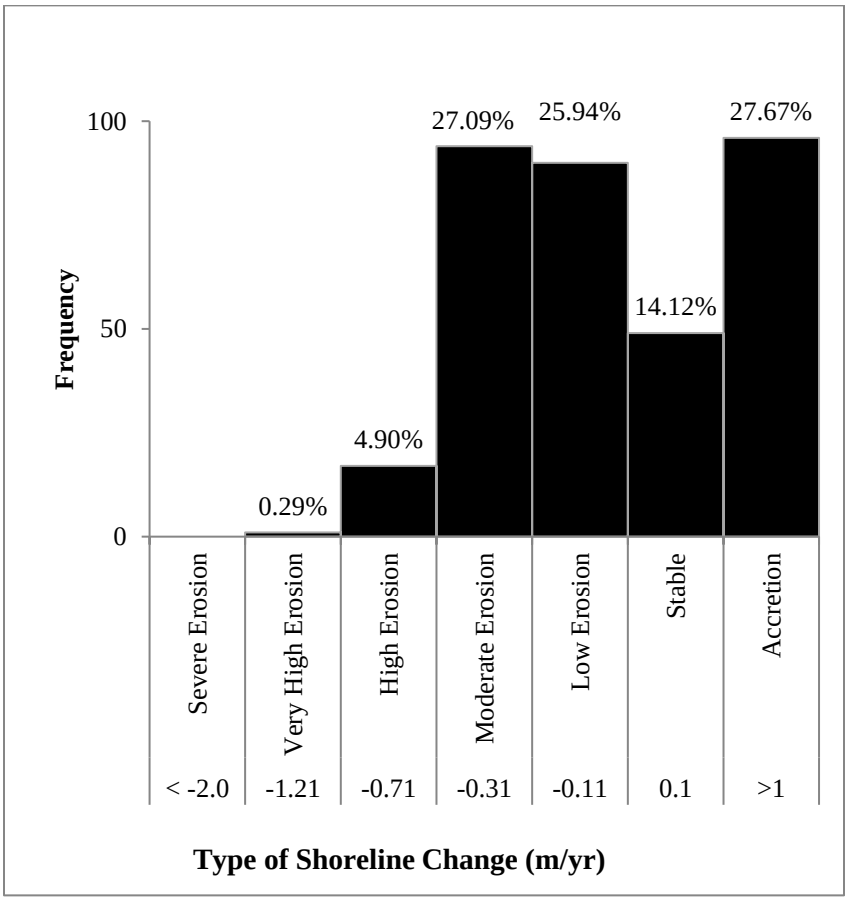

Figure 2.9: Frequencies of Different Types of Shoreline Change Rates (m/yr) from 1902 to 2018

In the long-term analysis (116 years), from 1902 to 2018, 347 transects were analyzed (Figure 2.10). Overall, the maximum rate of change was 1.83 m/yr (84.87 m), the minimum rate was -1.52 m/yr (-117.62 m), and the average rate was -0.09 m/yr. The maximum accretional rates at the Río Grande de Loíza East beach (GroupID:12), the beach between Parcelas Suárez and Vieques (GroupID:16), and the Río Grande de Loíza West beach (GroupID:10) were 1.83, 0.89, and 0.58 m/yr, respectively.

Figure 2.10: Frequencies of Shoreline Change Rates (m/yr) from 1902 to 2018, by Classification (Stewart and Pope, 1993) and GroupID

Geographically (Figure 2.11), in the west, 89% of transects (n = 170) were erosional and 11% (n = 20) were accretional. In the east, 66% of transects (n = 103) were accretional and 34% (n = 54) were erosional. Overall, higher erosion rates were measured in the western section of Loíza). Stable rates were observed in eight areas: Beach Punta Maldonado (GroupID:3), Beach Tres Palmitas (GroupID:6), Beach Torrecilla (GroupID:7), Beach Vacía Talega (GroupID:8), Beach West Río Grande de Loíza (GroupID:10), Beach Parcelas Suárez (GroupID:13), Beach Punta Iglesias (GroupID:14), and Beach Parcelas Suárez (GroupID:15). Mainly low and high erosion rates were observed in the western section, whereas continuous accretion rates were observed in the eastern section. Punta Iglesia and Punta Uvero sandpits showed the highest concentration of erosion rates. Torrecilla (GroupID:7) exhibited the highest erosional rate (-1.52 m/yr) and the eastern section of Río Grande de Loíza and Loíza Aldea (GroupID:12) showed the highest accretional rate (1.83 m/yr).

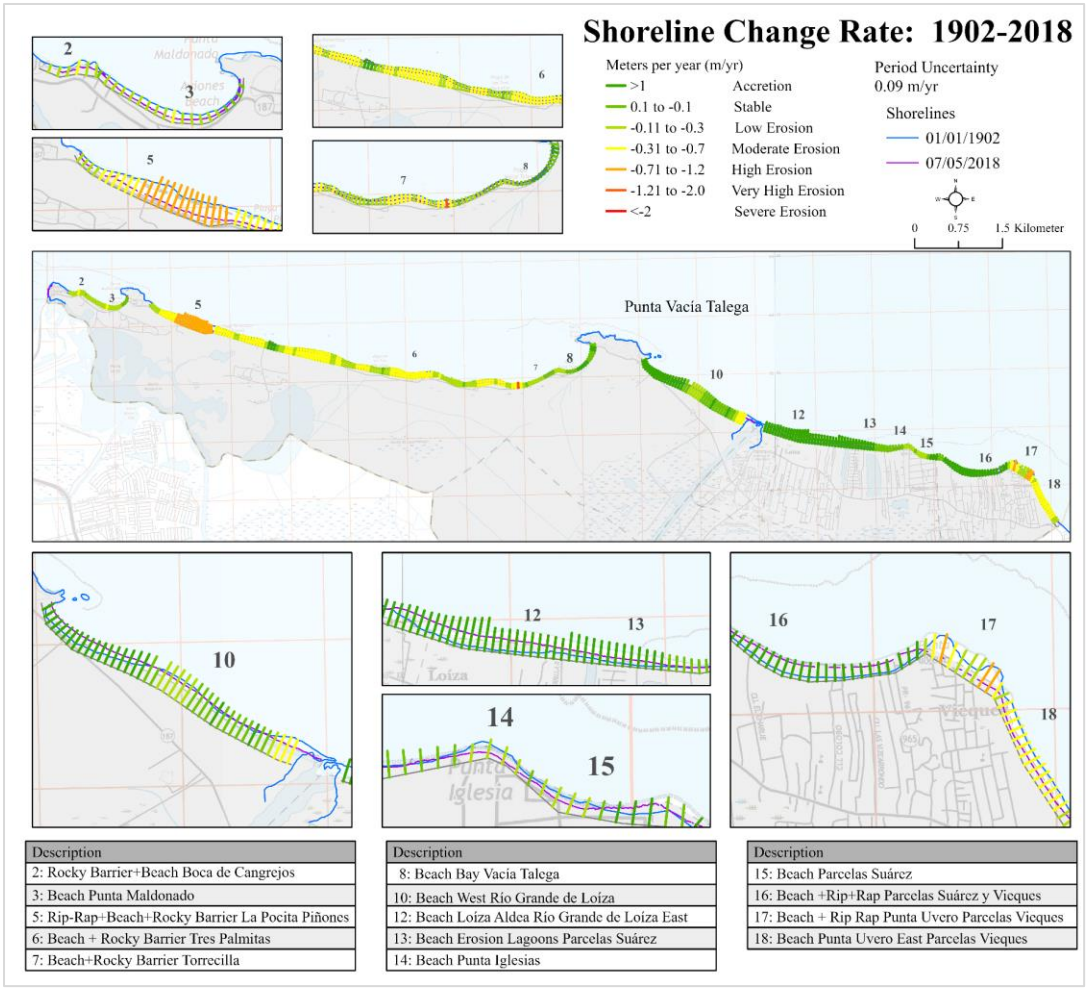

Figure 2.11: Shoreline Change Rates (m/yr) at Loíza: 1902 – 2018

All statistics for the period 1902 – 2018 are summarized in Table 2.7. Two groups showed 100% accretional rates: Beach Río Grande de Loíza East (GroupID:12) and Beach Between Parcelas Suárez and Vieques (GroupID:16). Four different groups showed 100% erosional rates: Beach Boca de Cangrejos (GroupID:2), Beach Punta Maldonado (GroupID:3), Beach La Pocita (GroupID:5), and Beach Punta Uvero East (GroupID:18). On average, eight areas (57%) showed erosional rates and six (43%) showed accretional rates.

Table 2.7: Summary of Statistics: 1902 – 201

Description		Total Transects	Total positive rates	Total negative rates	% Transects Positive	% Transects Negative	Maximum Positive Rate (meters per year)	Maximum Negative Rate (meters per year)
Period 1902-2018		347	123	224	36	64	1.83	-1.52
By Group ID								
2	Beach Boca de Cangrejos	6	0	6	0	100	--	-0.35
3	Beach Punta Maldonado	19	0	19	0	100	--	-0.32
5	Beach La Pocita	24	0	24	0	100	--	-1.01
6	Beach Tres Palmitas	75	3	72	4	96	0.35	-0.7
7	Beach Torrecilla	47	2	45	4	96	0.06	-1.52
8	Beach Vacía Talega	19	15	4	79	21	0.19	-0.25
10	Beach West Río Grande de Loíza	42	29	13	69	31	0.58	-0.52
12	Beach Río Grande de Loíza East Loíza	28	28	0	100	0	1.83	--
13	Beach Parcelas Suárez (erosion lagoons	16	15	1	94	6	0.28	-0.02
14	Punta Iglesia sand pit	12	1	11	8	92	0.03	-0.23
15	Beach Parcelas Suárez	8	6	2	75	25	0.24	-0.16
16	Beach between Parcelas Suárez/Parcel	21	21	0	100	0	0.89	--
17	Punta Uvero sand pit	13	3	10	23	77	0.64	-0.98
18	Beach Punta Uvero East	17	0	17	0	100	--	-0.48

Description		Average Positive Rates	Average Negative Rates	Average Rate	Maximum Positive Distance (meters)	Maximum Negative Distance (meters)	Average Positive Distance	Average Negative Distance	Average Distance
Period 1902-2018		0.35	-0.33	-0.09	84.87	-117.62	37.66	37.88	-11.1
By Group ID									
2	Beach Boca de Cangrejos	--	-0.23	-0.2	--	-40.82	--	-25.69	-25.69
3	Beach Punta Maldonado	--	-0.18	-0.18	--	-36.75	--	-21.2	-21.2
5	Beach La Pocita	--	-0.66	-0.66	--	-117.62	--	-75.55	-75.55
6	Beach Tres Palmitas	0.28	-0.35	-0.32	41.31	-81.64	32.79	-40.79	-37.84
7	Beach Torrecilla	0.04	-0.28	-0.27	6.46	-58.22	4.52	-29.53	-28.08
8	Beach Vacía Talega	0.1	-0.16	0.05	22.41	-29	12.05	-19.11	5.49
10	Beach West Río Grande de Loíza	0.28	-0.2	0.13	67.03	-60.31	32.8	-23.33	15.42
12	Beach Río Grande de Loíza East Loíza	0.62	--	0.62	84.87	--	61.08	--	61.08
13	Beach Parcelas Suárez (erosion lagoons	0.19	-0.02	0.18	32.11	-2.77	21.94	-2.77	20.4
14	Punta Iglesia sand pit	0.03	-0.12	-0.1	3.26	-27.34	3.26	-13.56	-12.16
15	Beach Parcelas Suárez	0.11	-0.16	0.04	27.88	-19.07	13.17	-18.97	5.14
16	Beach between Parcelas Suárez/Parcel	0.49	--	0.49	78.31	--	53.38	--	53.38
17	Punta Uvero sand pit	0.45	0.5	-0.28	68.99	-114.64	50.06	-56.98	-32.28
18	Beach Punta Uvero East	--	-0.36	-0.36	--	-56.46	--	-41.85	-41.85

2.4.1.2 Shoreline Change Rates (m/yr): 1902 – 1931

For the 1902 – 1931 period, descriptive statistics showed that 214 transects were analyzed (see Figure 2.12). Accretion (> 0.1 m/yr) was the major occurring event identified (71%, n = 151 transects). The other two highest frequencies were low erosion (10%, n = 21) and moderate erosion (8%, n = 18). Stable shoreline changes were observed at a frequency of 6% (n = 13). High erosion (4%, n = 8) and very high erosion (1%, n = 3) were the least common.

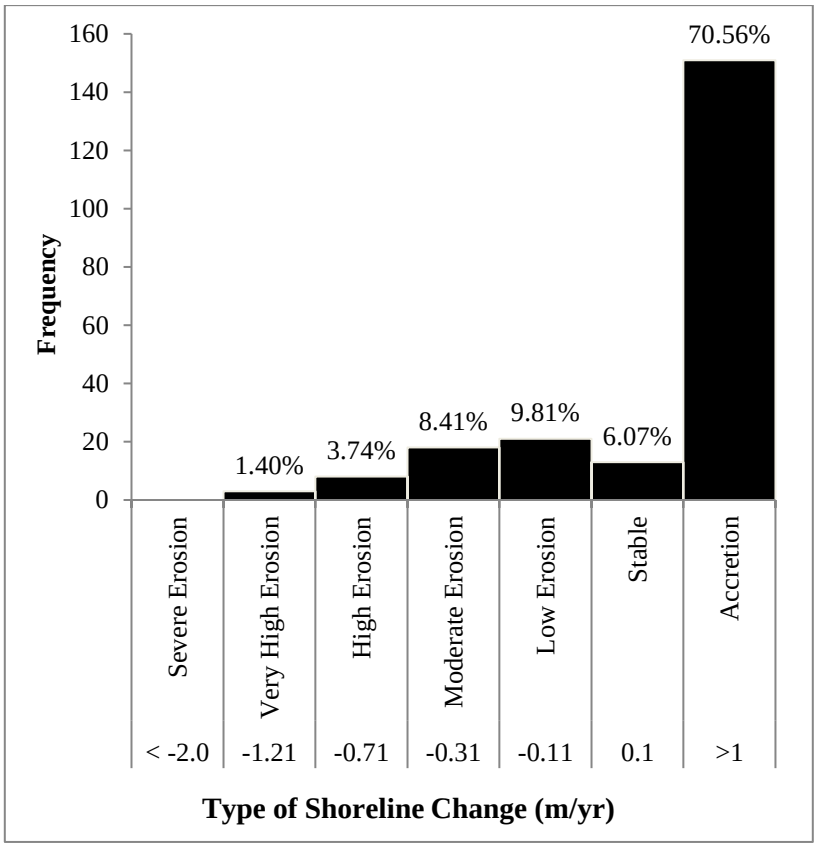

Figure 2.12: Frequencies of Different Types of Shoreline Change Rates (m/yr) from 1902 to 1931

Shoreline change rates per transect are shown in Figure 2.13. A total of 158 transects were accretional (74%) and 56 were erosional (35%). The maximum rate of accretion recorded was 4.93 m/yr (143.03 m). This accretion event was identified at Río Grande de

Loíza east (GroupID: 12). The maximum erosion rate was -1.52 m/yr (-44.19 m), which occurred in Torrecilla (GroupID: 7). The average rate was 1.14 m/yr. The maximum accretion rates were observed at the east and west sections of Río Grande de Loíza (GroupID:11 and 12), and were 4.93 and 3.25 m/yr, respectively. The maximum erosion rates were observed at Beach of Torrecilla (GroupID:7) and Beach of Vacía Talega (GroupID:8), and were -1.52 and -1.21 m/yr, respectively. On average, all areas showed accretional rates, with the exceptions of Beach Boca de Cangrejos (GroupID:2), Beach Torrecilla (GroupID:7), and Punta Iglesia Sandpit (GroupID:14). Hence, on average, 75% of the areas exhibited accretional rates and 25% showed erosional rates.

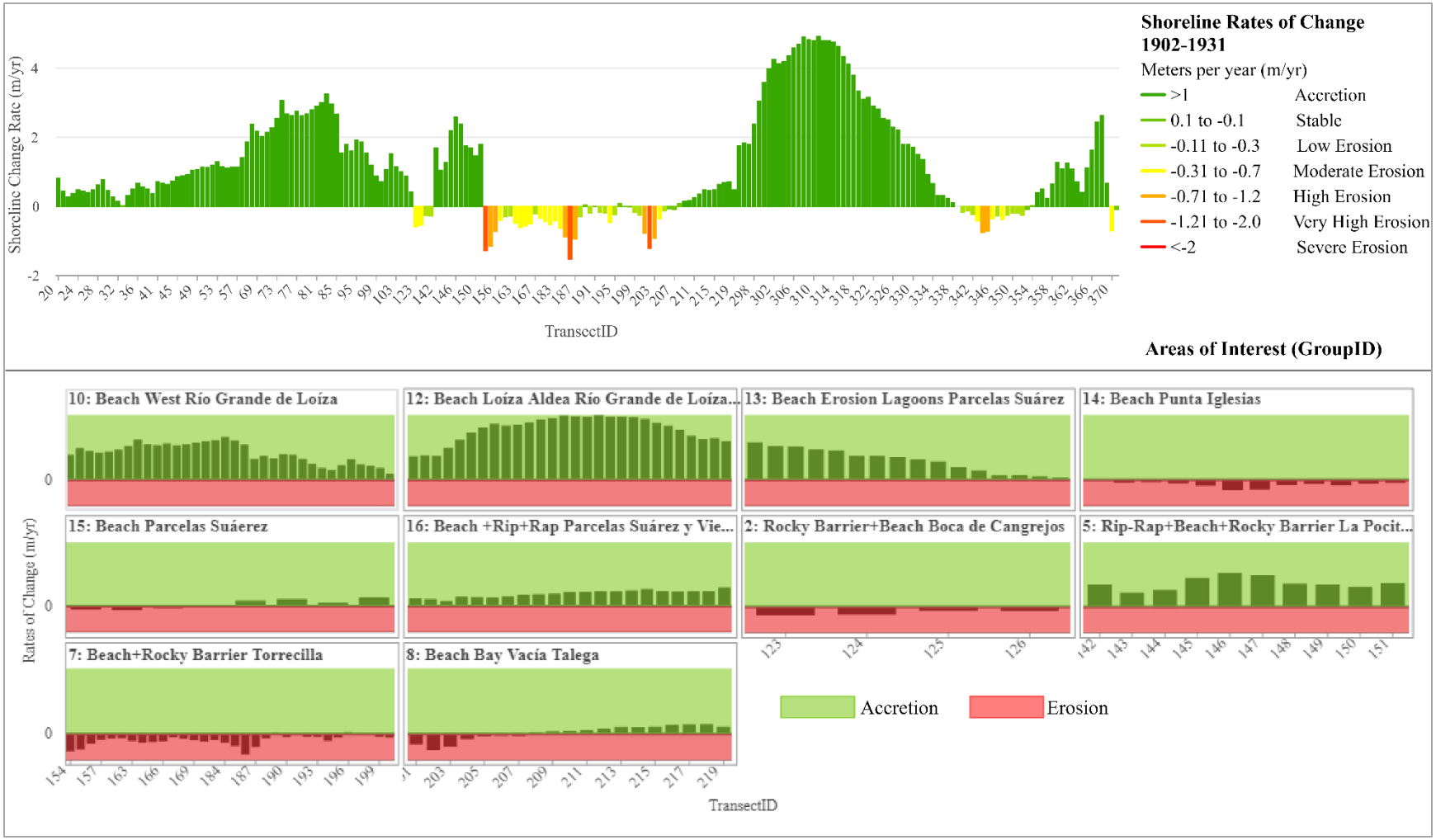

Figure 2.13: Frequencies of Shoreline Change Rates (m/yr) from 1902 to 1931, by Classification (Stewart and Pope, 1993) and GroupID

The rate of change along the shoreline of Loíza is shown in Figure 2.14. The Beach of Torrecilla (GroupID: 7) showed the maximum erosion rate from east to west. Significant accretion was identified at Río Grande de Loíza east and Loíza Aldea (GroupID:12). On the eastern end of the Loíza shoreline (east of Punta Vacía Talega), 133 transects were accretional (89%) and 16 were erosional (11%), showing the highest rate of accretion (4.93 m/yr). On the west side of Punta Vacía Talega, 39 transects were erosional (60%) and 26 were accretional (40%), showing the highest erosion rate (-1.52 m/yr).

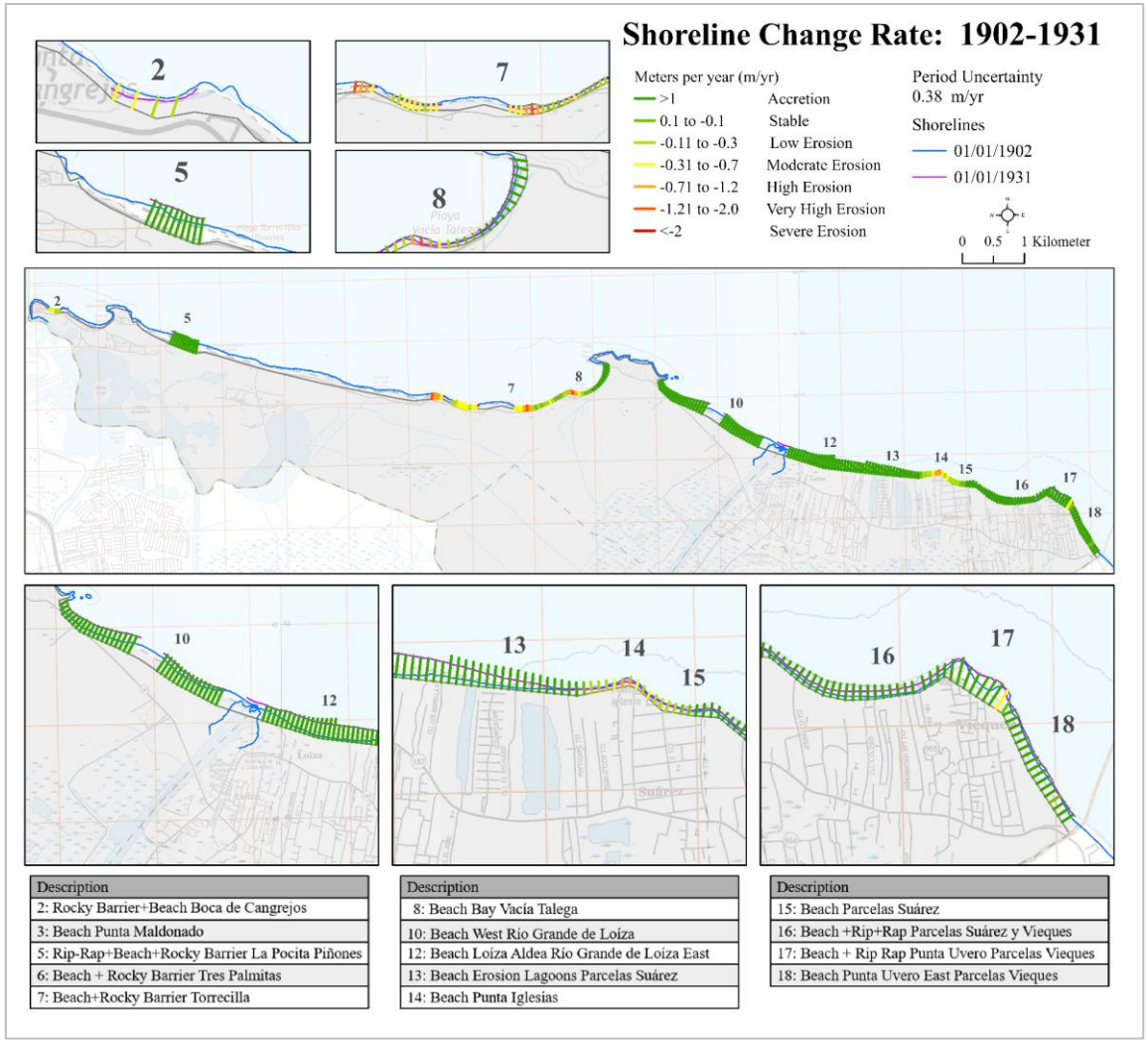

Figure 2.14: Shoreline Change Rates (m/yr) at Loíza: 1902 – 1931

The statistics and percentages for each Group ID are presented in Table 2.8. The areas with 100% accretion rates were the Boca de Cangrejos Beach (GroupID:2), Beach La Pocita (GroupID:5), Beach West Río Grande de Loíza (Group ID: 10), Beach Parcelas Suárez (GroupID:13), Beach between Parcelas Suarez and Vieques (GroupID:16), and the Beach Punta Uvero East (GroupID:18). Conversely, the areas with the highest erosion rates were Beach Torrecilla (GroupID:7) with 88% and Punta Iglesia Sandpit (GroupID:14) with 85%. Of the 12 areas, nine showed accretion rates, with seven of those exhibiting 100% accretion rates. Stable rates (0.1 to -0.1 m/yr) were present in Torrecilla (GroupID:7), Beach Bay Vacía Talega (GroupID:8), Beach Parcelas Suárez, Punta Uvero Sandpit (GroupID:17), and Punta Uvero east area (GroupID:18).

Table 2.8: Summary of Statistics: 1902 – 1931

Description		Total Transects	Total positive rates	Total negative rates	% Transects Positive	% Transects Negative	Maximum Positive Rate (meters per year)	Maximum Negative Rate (meters per year)
Period 1902-1931		214	158	56	74	26	4.93	-1.52
By Group ID								
2	Beach Boca de Cangrejos	4	0	4	100	0	--	-0.59
5	Beach La Pocita	10	10	0	100	0	2.59	--
7	Beach Torrecilla	32	4	28	12	88	0.09	-1.52
8	Beach Vacía Talega	19	12	7	63	37	0.71	-1.21
10	Beach West Río Grande de Loíza	34	34	0	100	0	3.25	--
12	Beach Río Grande de Loíza East Loíza Aldea	28	28	0	100	0	4.93	--
13	Beach Parcelas Suárez (erosion lagoons)	16	16	0	100	0	2.82	--
14	Punta Iglesia sand pit	12	0	12	0	100	--	-0.75
15	Beach Parcelas Suárez	8	5	3	63	38	0.65	-0.25
16	Beach between Parcelas Suárez/Parcelas Vieques	21	21	0	100	0	1.41	--
17	Punta Uvero sand pit	13	11	2	85	15	2.64	-0.7
18	Beach Punta Uvero East	17	17	0	100	0	0.81	--

Description		Average Positive Rates	Average Negative Rates	Average Rate	Maximum Positive Distance (meters)	Maximum Negative Distance (meters)	Average Positive Distance	Average Negative Distance	Average Distance
Period 1902-1931		1.67	-0.44	1.14	143.03	-44.19	48.78	-12.67	32.71
By Group ID									
2	Beach Boca de Cangrejos	--	-0.42	-0.42	--	-17.09	--	-10.36	-10.36
5	Beach La Pocita	1.79	--	1.79	52	--	51.84	--	51.84
7	Beach Torrecilla	0.04	-0.5	-0.44	2.67	-44.19	2.67	-44.19	-12.65
8	Beach Vacía Talega	0.41	-0.51	0.08	20.5	-35.14	20.47	-14.65	2.2
10	Beach West Río Grande de Loíza	2.02	--	2.02	94.1	--	58.46	--	58.46
12	Beach Río Grande de Loíza East Loíza Aldea	3.85	--	3.85	143.03	--	111.68	--	111.68
13	Beach Parcelas Suárez (erosion lagoons)	2.82	--	1.44	81.8	--	41.89	--	41.89
14	Punta Iglesia sand pit	--	-0.32	-0.32	--	-21.24	--	-9.31	-9.31
15	Beach Parcelas Suárez	0.37	-0.17	0.38	18.84	-7.27	10.63	-4.96	4.79
16	Beach between Parcelas Suárez/Parcelas Vieques	0.94	--	0.94	40.76	--	27.22	--	40.76
17	Punta Uvero sand pit	1.3	-0.39	1.04	76.48	-20.26	37.7	-11.43	30.14
18	Beach Punta Uvero East	0.44	--	0.44	23.58	--	12.84	--	12.84

2.4.1.3 Shoreline Change Rates (m/yr): 1931 – 1951

Beach accretion was the most frequent event identified along the Loíza municipality shoreline (143 transects) during the 1931 – 1951 period (Figure 2.15). The highest frequencies were observed in the accretion (72%, n = 103), stable (7%, n = 9), and moderate erosion (11 %, n = 15) categories. The lowest frequencies were observed for high erosion (6%, n = 9), very high erosion (2%, n = 3), and low erosion (2%, n = 3), indicating that major erosion events were not identified on the shoreline for this period.

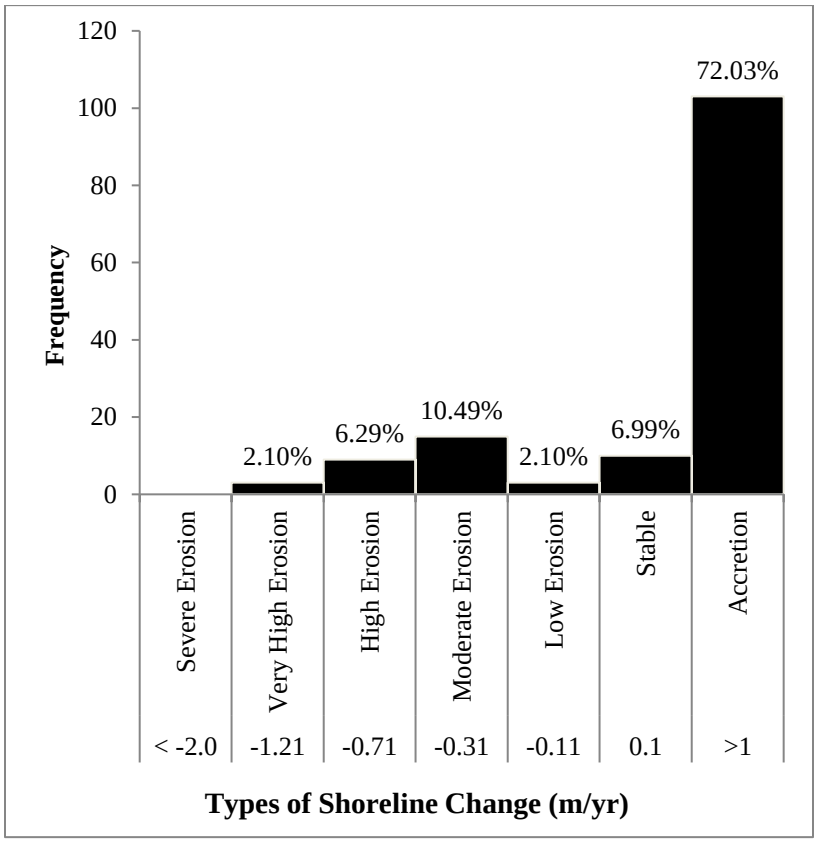

Figure 2.15: Frequencies of Different Types of Shoreline Change Rates from 1931 to 1951

For this period, the maximum accretion rate was 3.5 m/yr and the maximum erosion rate was -1.52 m/yr (Figure 2.16). These rates were measured at Beach Parcelas Suárez

(GroupID:13) and Punta Uvero Sandpit (GroupID:17), respectively. The average rate for this period was 0.9 m/yr. Of the 143 transects, 76% (n = 109) showed accretion and 24% (n = 34) showed erosion. The average accretion rate was 1.38 m/yr and the average erosion rate was -0.62 myr^{-1}, with a maximum positive rate of 3.52 m/yr (70.5 m) and a maximum negative rate of -1.52 m/yr (-30.61 m).

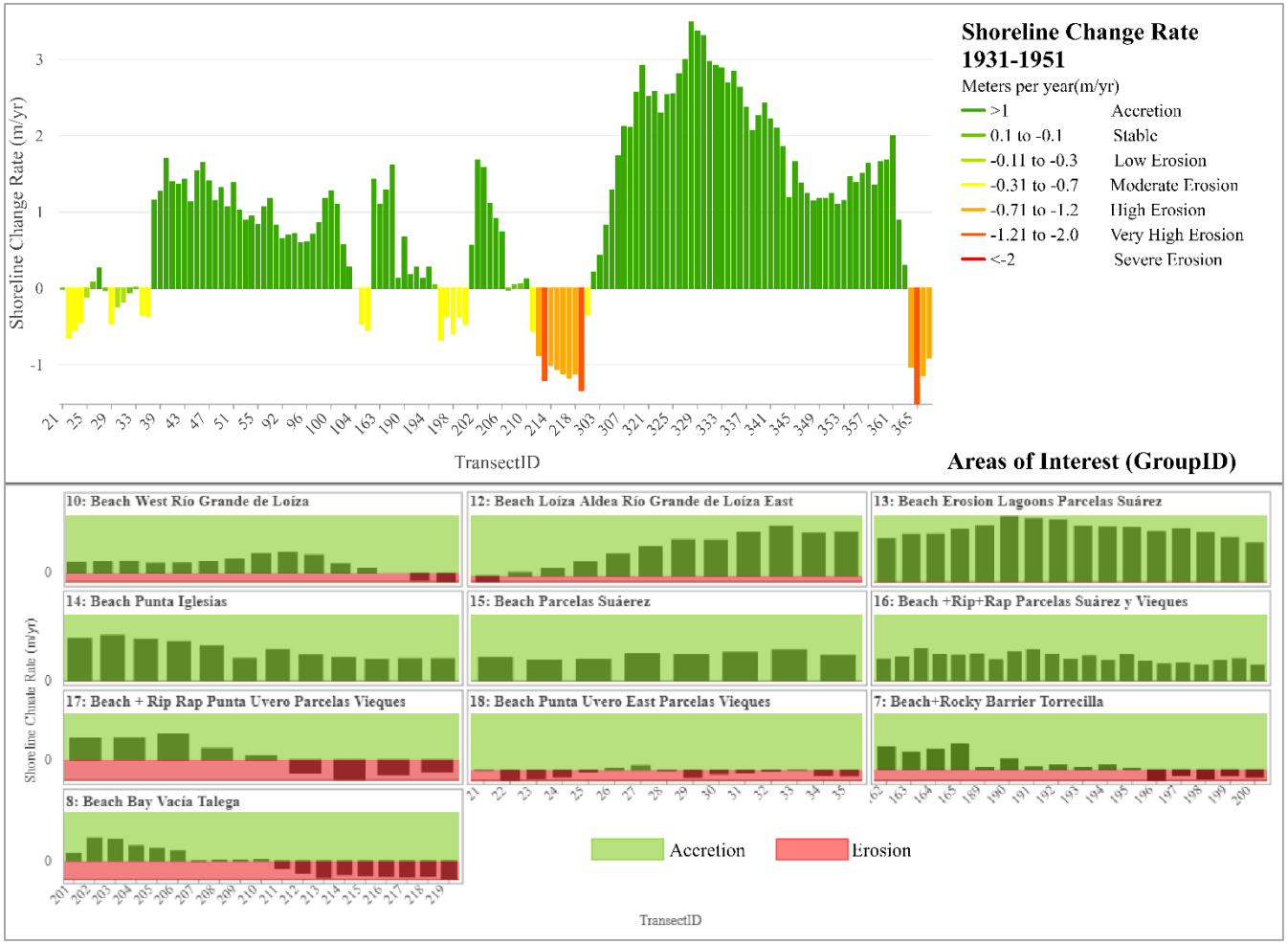

Figure 2.16: Frequencies of Shoreline Change Rates (m/yr) from 1931 to 1951, by Classification (Stewart and Pope, 1993) and GroupID

A map of the transects per area is shown in Figure 2.17. The maximum accretion rates were measured at the Beach Parcelas Suárez (GroupID:13) and the east Río Grande de Loíza (GroupID:12), whereas the maximum erosion rates (-1.52, -1.34, and -0.68 m/yr) were found at the Punta Uvero Sandpit (GroupID:17), Beach Vacía Talega (GroupID:8), and Beach Torrecilla (GroupID:7), respectively. Stable rates (-0.1 to -0.1 m/yr) were observed in three areas: Beach Torrecilla (GroupID:7), Beach Vacía Talega (GroupID:8), and Beach Punta Uvero East (GroupID:18). On the west side of Vacía Talega, 43% of transects were erosional (n = 15) and 57% were accretional (n = 20). On the east, 88 transects (81%) were accretional and 20 (19%) were erosional.

From west to east, in Torrecilla (GroupID:7), 16 transects were analyzed. The average rate was 0.29 m/yr, the maximum erosion rate was -0.68 m/yr (-13.75 m), and the maximum accretion rate was 1.62 m/yr (32.45 m). Five transects were erosional (31%) and 11 were accretional (69%), with average positive and negative rates of 0.62 and -0.5 m/yr, respectively.

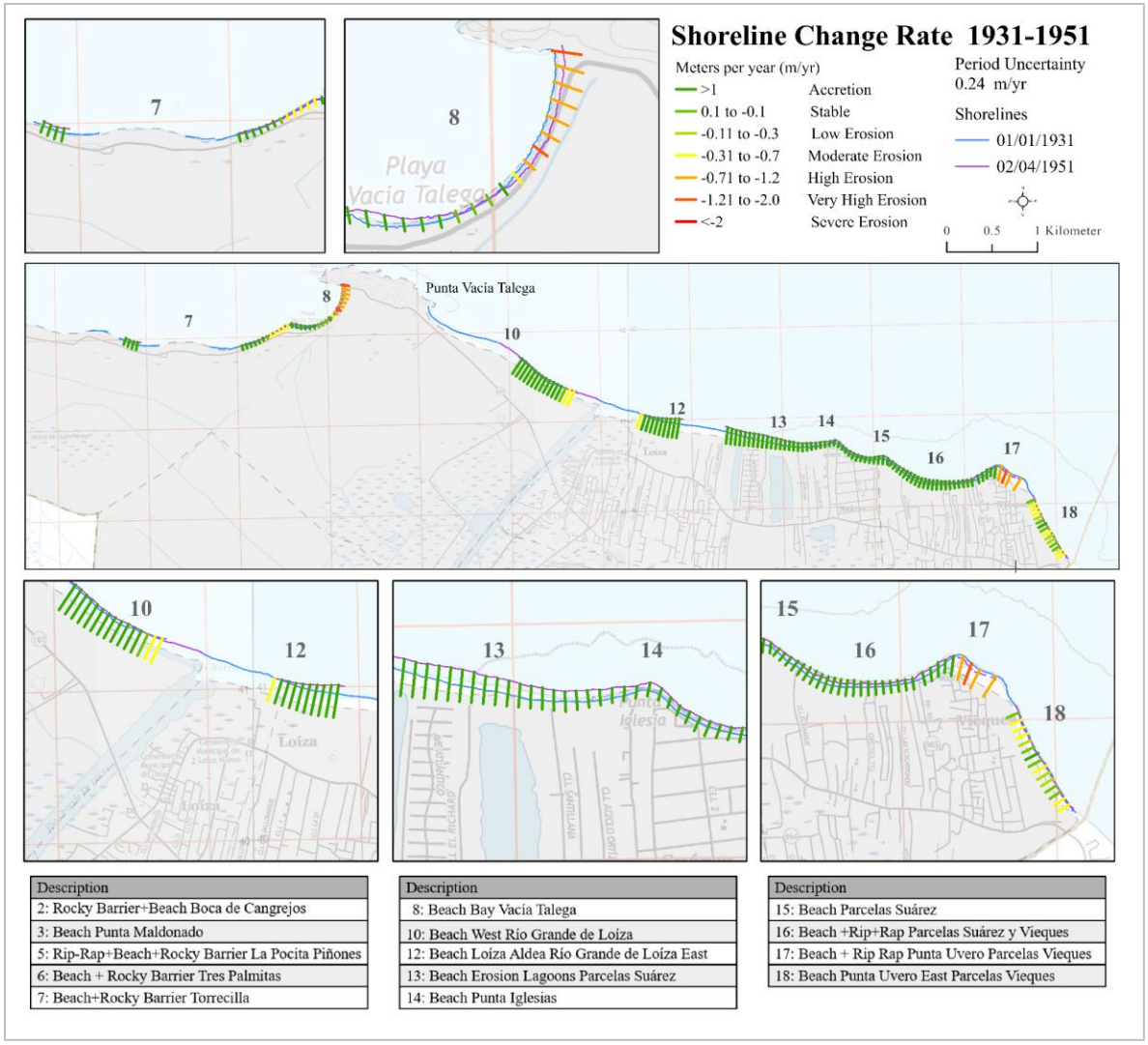

Figure 2.17: Shoreline Change Rates (m/yr) at Loíza: 1931 – 1951

The statistics for each Group ID are summarized in Table 2.9. The areas that presented 100% accretion rates were Beach Parcelas Suárez (GroupID:13), Beach Punta Iglesia Sandpit (GroupID:14), Beach Parcelas Suarez (GroupID:15), and Beach between Parcelas Suarez y Vieques (GroupID:16). In contrast, the areas with the highest erosion rates were Beach Vacía Talega (GroupID:8) and Punta Uvero San pit (GroupID:17). On average, eight out of 10 areas showed accretional rates.

Table 2.9: Summary of Statistics: 1931 – 1951

	Description	Total Transects	Total positive rates	Total negative rates	% Transects Positive	% Transects Negative	Maximum Positive Rate (meters per year)	Maximum Negative Rate (meters per year)
	Period 1931-1951	143	109	34	76	23	3.5	-1.52
	Group ID							
7	Beach Torrecilla	16	11	5	69	31	1.62	-0.68
8	Beach Vacía Talega	19	9	10	47	53	1.68	-1.34
10	Beach West Río Grande de Loíza	15	12	3	80	20	1.28	-0.55
12	Beach Río Grande de Loíza East & Loíza Aldea	12	11	1	92	8	2.92	-0.34
13	Beach Parcelas Suárez (erosion lagoons)	16	16	0	100	0	3.49	--
14	Punta Iglesia sand pit	12	12	0	100	0	2.43	--
15	Beach Parcelas Suárez	8	8	0	100	0	1.64	--
16	Beach between Parcelas Suárez/Parcelas Vieques	21	21	0	100	0	1.7	--
17	Punta Uvero sand pit	9	5	4	56	44	2	-1.52
18	Beach Punta Uvero East	15	3	12	80	20	0.27	-0.65

	Description	Average Positive Rates	Average Negative Rates	Average Rate	Maximum Positive Distance (meters)	Maximum Negative Distance (meters)	Average Positive Distance	Average Negative Distance	Average Distance
	Period 1931-1951	1.38	-0.63	0.9	70.05	-30.61	28.02	-12.31	18.15
	Group ID								
7	Beach Torrecilla	0.65	-0.5	11	32.45	-13.75	32.45	-10.09	5.83
8	Beach Vacía Talega	0.76	-0.95	-0.14	33.84	-27			
10	Beach West Río Grande de Loíza	1.28	-0.34	0.55	25.64	-11	15.49	-6.86	11.02
12	Beach Río Grande de Loíza East & Loíza Aldea	1.76	-0.34	1.58	58.66	-6.83	35.27	-6.83	31.76
13	Beach Parcelas Suárez (erosion lagoons)	2.8	--	2.8	70.05	--	56.21	--	56.21
14	Punta Iglesia sand pit	1.65	--	1.65	48.89	--	48.89	--	48.89
15	Beach Parcelas Suárez	1.35	--	1.35	32.87	--	27.2	--	27.2
16	Beach between Parcelas Suárez/Parcelas Vieques	1.23	--	1.23	34.08	--	24.64	--	24.64
17	Punta Uvero sand pit	1.31	-1.15	0.21	40.19	-30.6	26.23	-23.12	4.3
18	Beach Punta Uvero East	0.12	-0.29	-0.21	5.39	-13.05	2.42	-5.77	-4.14

2.4.1.4 Shoreline Change Rates (m/yr): 1951 – 1977

For Period 3, 1951 – 1977 (Figure 2.18), transects exhibiting very high erosion were observed with the highest frequency (59%, n = 48). Other categories that also represented more than 10% were accretion (12%, n = 10) and moderate erosion (11%, n = 9). The lowest frequencies were observed in the high erosion (9%, n = 7), low erosion (6%, n = 5), and stable (4%, n = 3) categories. Transects with severe erosion were not observed in this period. Of the 82 transects, 84% were erosional (n = 69) and 15% were accretional (n = 13). The average rate was -2.55 m/yr, with a maximum erosion rate of -6.15 m/yr (-160.09 m) at Beach Grande de Loíza West (GroupID:10) and a maximum accretion rate of 0.58 m/yr (14.97 m) at Beach Vacía Talega (GroupID:8).

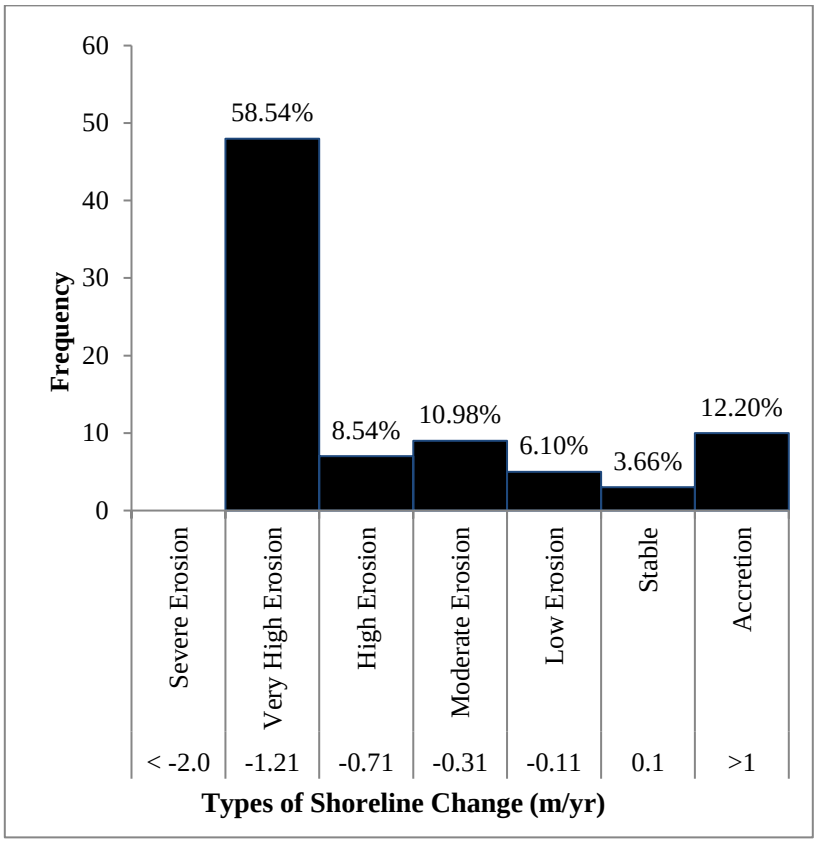

Figure 2.18: Frequencies of Different Types of Shoreline Change Rates (m/yr) from 1951 to 1977

Figure 2.19 shows the rates per area. The maximum accretion rates were found in Beach Vacía Talega (GroupID:8) and the Beach between Parcelas Suárez and Vieques (GroupID:6), which were the only groups with positive rate values. In contrast, the maximum erosion rates were observed at Beach West and East Río Grande de Loíza (GroupID:10, 12), and at Beach Parcelas Suárez (GroupID:13). Stable rates (-0.1 to-0.1 m/yr) were measured at Beach Pocita (GroupID:5, n = 5), Beach Vacía Talega (GroupID:8, n = 2), and Beach Parcelas Suárez (GroupID:13, n = 2).

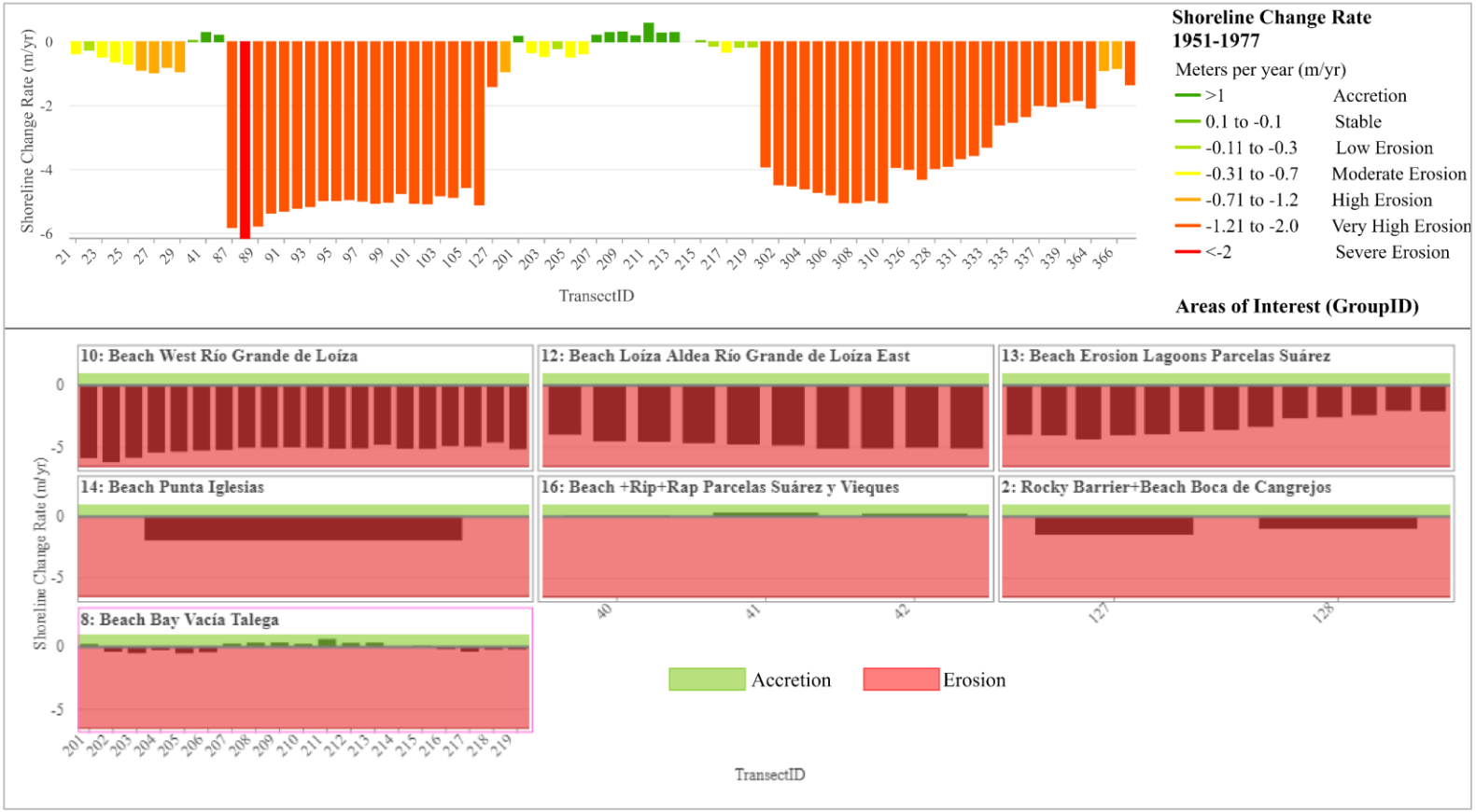

Figure 2.19: Frequencies of Shoreline Change Rates (m/yr) from 1951 to 1977, by Classification (Stewart and Pope, 1993) and GroupID

Along the shoreline of Loíza (

Figure 2.20

Figure 2.19), a high concentration of erosion rates was observed at west of Río Grande de Loíza (GroupID:10), east of the River and Loíza Aldea (GroupID:12), Parcelas Suárez (erosional lagoons; GroupID:13), Punta Uvero (GroupID:17), and Punta Uvero east (GroupID:18). Accretion was observed at Vacía Talega (GroupID:8) and at the beach between Parcelas Suárez and Vieques (GroupID:16).

On the west side of Vacía Talega, 52% (n = 11) were erosional transects and 48% (n = 10) were accretional. On the east side of Vacía Talega, 97% (n = 59) were erosional transects and 3% (n = 2) were accretional.

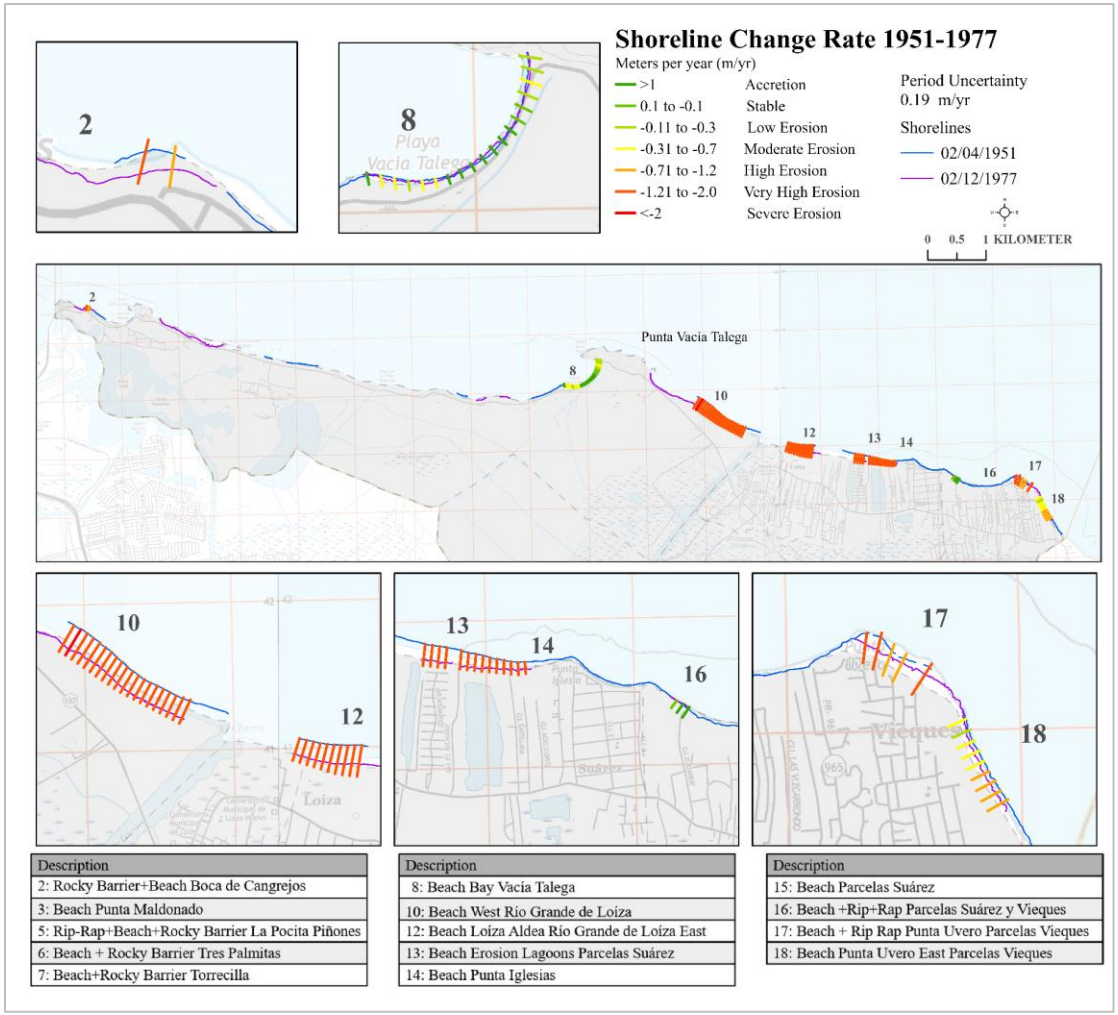

Figure 2.20: Shoreline Change Rates (m/yr) at Loíza: 1951 – 1977

The statistics for each Group ID are summarized in Table 2.10. Only the Beach between Parcelas Suárez and Vieques (GroupID:16) showed 100% accretional rates in this period. Conversely, seven of the nine areas analyzed showed 100% erosional rates. Beach Vacía Talega (GroupID:8) showed a combination of accretional (53%) and erosional (47%). On average, eight out of the nine areas showed erosional rates.

Table 2.10: Summary of Statistics: 1951 – 1977

Description		Total Transects	Total positive rates	Total negative rates	% Transects Positive	% Transects Negative	Maximum Positive Rate (meters per year)	Maximum Negative Rate (meters per year)
Period 1951-1977		82	13	69	15	84	0.58	-6.15
By Group ID								
2	Beach Boca de Cangrejos	2	0	2	0	100	--	-1.4
8	Beach Vacía Talega	19	10	9	53	47	0.58	-0.47
10	Beach West Río Grande de Loíza	20	0	20	0	100	--	-6.15
12	Beach Río Grande de Loíza East Loíza Aldea	10	0	10	0	100	--	-5.04
13	Beach Parcelas Suárez (erosion lagoons)	13	0	13	0	100	--	-4.31
14	Punta Iglesia sand pit	1	0	1	0	100	--	-1.89
16	Beach between Parcelas Suárez/Parcelas Vieques	3	3	0	100	0	0.29	--
17	Punta Uvero sand pit	5	0	5	0	100	--	-2.07
18	Beach Punta Uvero East	9	0	9	0	100	--	-0.97

Description		Average Positive Rates	Average Negative Rates	Average Rate	Maximum Positive Distance (meters)	Maximum Negative Distance (meters)	Average Positive Distance	Average Negative Distance	Average Distance
Period 1951-1977		0.22	-3.07	-2.55	14.97	-160.09	5.68	-79.89	-66.33
By Group ID									
2	Beach Boca de Cangrejos	--	-1.17	-1.17	--	-35.5	--	-30.34	-30.34
8	Beach Vacía Talega	0.23	-0.29	-0.02	14.97	-12.26	6	-7.61	-0.45
10	Beach West Río Grande de Loíza	--	-5.14	-5.14	--	-160.09	--	-133.88	-133.88
12	Beach Río Grande de Loíza East Loíza Aldea	--	-4.7	-4.7	--	-131.08	--	-122.42	-122.42
13	Beach Parcelas Suárez (erosion lagoons)	--	-3.23	-3.23	--	-112.16	--	-84.14	-84.14
14	Punta Iglesia sand pit	--	-1.89	-1.89	--	-49.08	--	-49.08	-49.08
16	Beach between Parcelas Suárez/Parcelas Vieques	0.18	--	0.18	7.53	--	4.62	--	4.62
17	Punta Uvero sand pit	--	-1.4	-1.4	--	-53.98	--	-36.39	-36.39
18	Beach Punta Uvero East	--	-0.67	-0.67	--	-25.31	--	-17.41	-17.41

2.4.1.5 Shoreline Change Rates (m/yr): 1977 – 1990

For Period 4, 1977 – 1990, 71 transects were analyzed (Figure 2.21). This period exhibited rates in all categories except for the severe erosion category. The highest frequency was observed for very high erosion (31%, n = 22) and the second-highest frequency was observed for high erosion (18%, n = 13). The moderate erosion and low erosion categories were found in the same number of transects (13%, n = 9). The accretion category was represented by 17% (n = 12) of transects and the stable category was present at the lowest frequency (8%, n = 6).

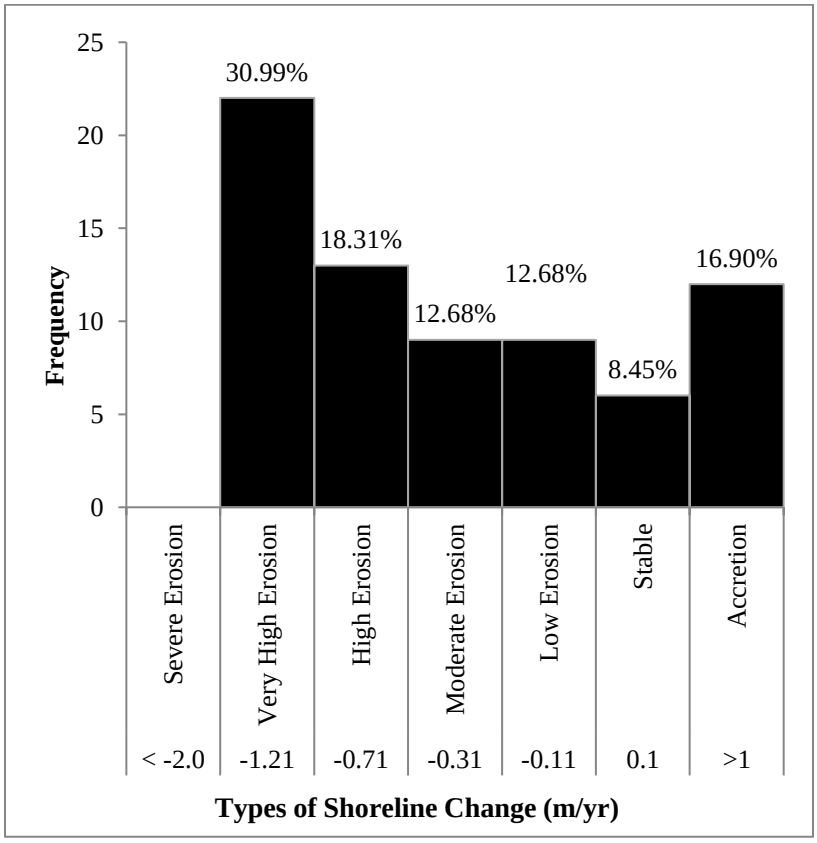

Figure 2.21: Frequencies of Different Types of Shoreline Change Rates (m/yr) from 1977 to 1990

Most of the transects were erosional (79%, n = 56), with less than 25% being accretional (21%, n = 15). The maximum accretion and erosion rates were 1.4 m/yr

(18.42 m) and -4.93 myr^{-1} (-17.86 m), which were found at Beach La Pocita (GroupID:5) and Punta Uvero Sandpit (GroupID:17), respectively. The average rate was -0.99 m/yr.

Graphs showing the transects per area is shown in Figure 2.22.The maximum accretion rates were measured in the Beach Parcelas Suárez (GroupID:13) and Beach Vacía Talega (GroupID:8), whereas the maximum erosion rates were found at the Punta Uvero Sandpit (GroupID:17), Beach Vacía Talega (GroupID:8), and Beach La Pocita (GroupID:5). Stable rates (0.1 to -1.1m/yr) were observed in three areas: Beach la Pocita (GroupID:5), Beach Vacía Talega (GroupID:8), and Beach Parcelas Suárez (GroupID:13).

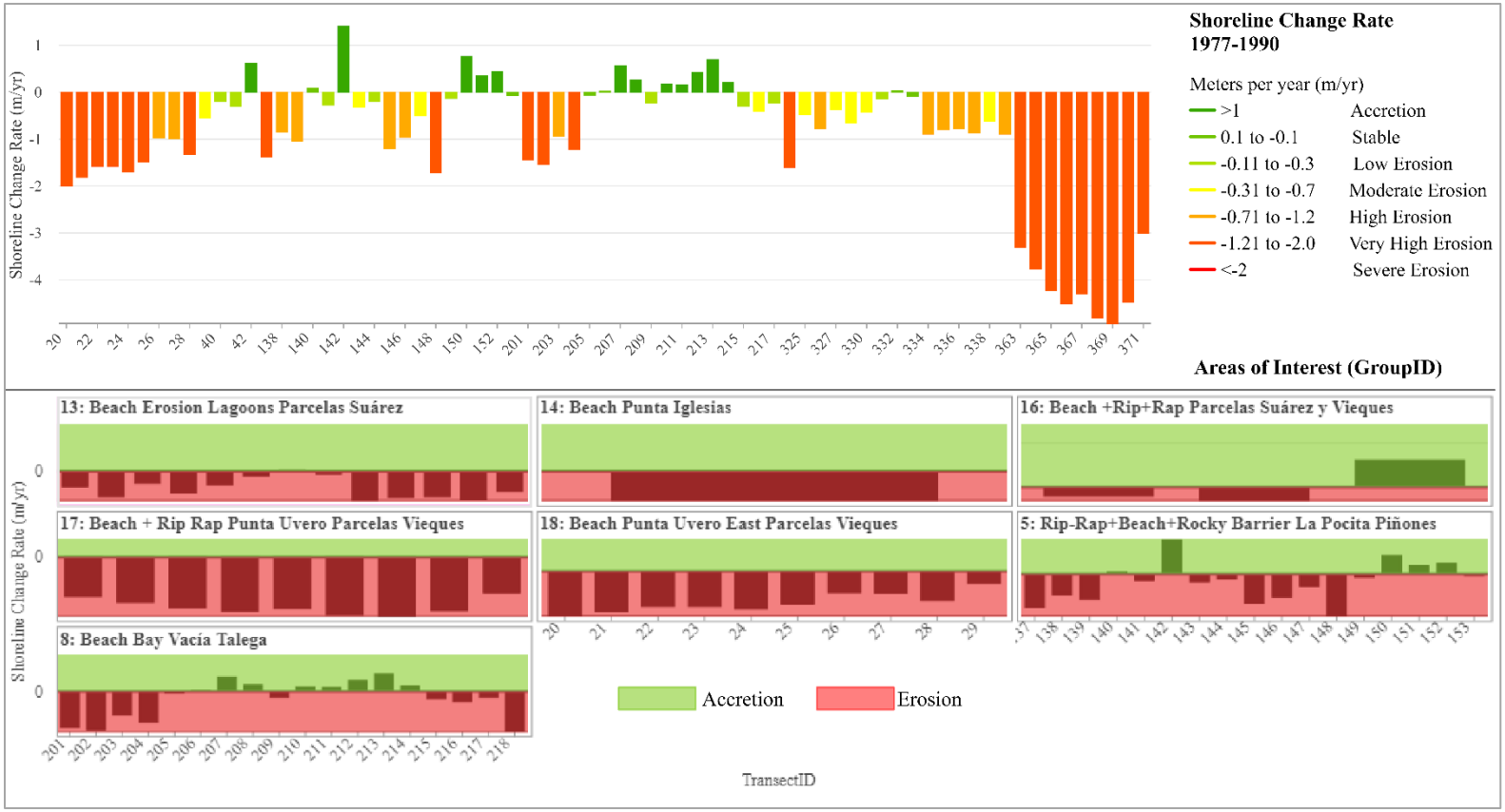

Figure 2.22: Frequencies of Shoreline Change Rates (m/yr) from 1977 to 1990, by Classification (Stewart and Pope, 1993) and GroupID

On the west side of Vacía Talega, 37% of transects were accretional (n = 13) and 63% (n = 22) were erosional (Figure 2.23). On the east side of Vacía Talega, 94% of transects were erosional (n = 34), with only 6% (n = 2) being accretional. The highest erosion rates were found in the Punta Uvero area (GroupID:17 and 18). At La Pocita (GroupID:5), severe and high erosion was also observed. Accretion rates were observed on the Beach of Parcelas Suárez (GroupID:13) and Vacía Talega (GroupID:8). The latter showed also showed erosion rates.

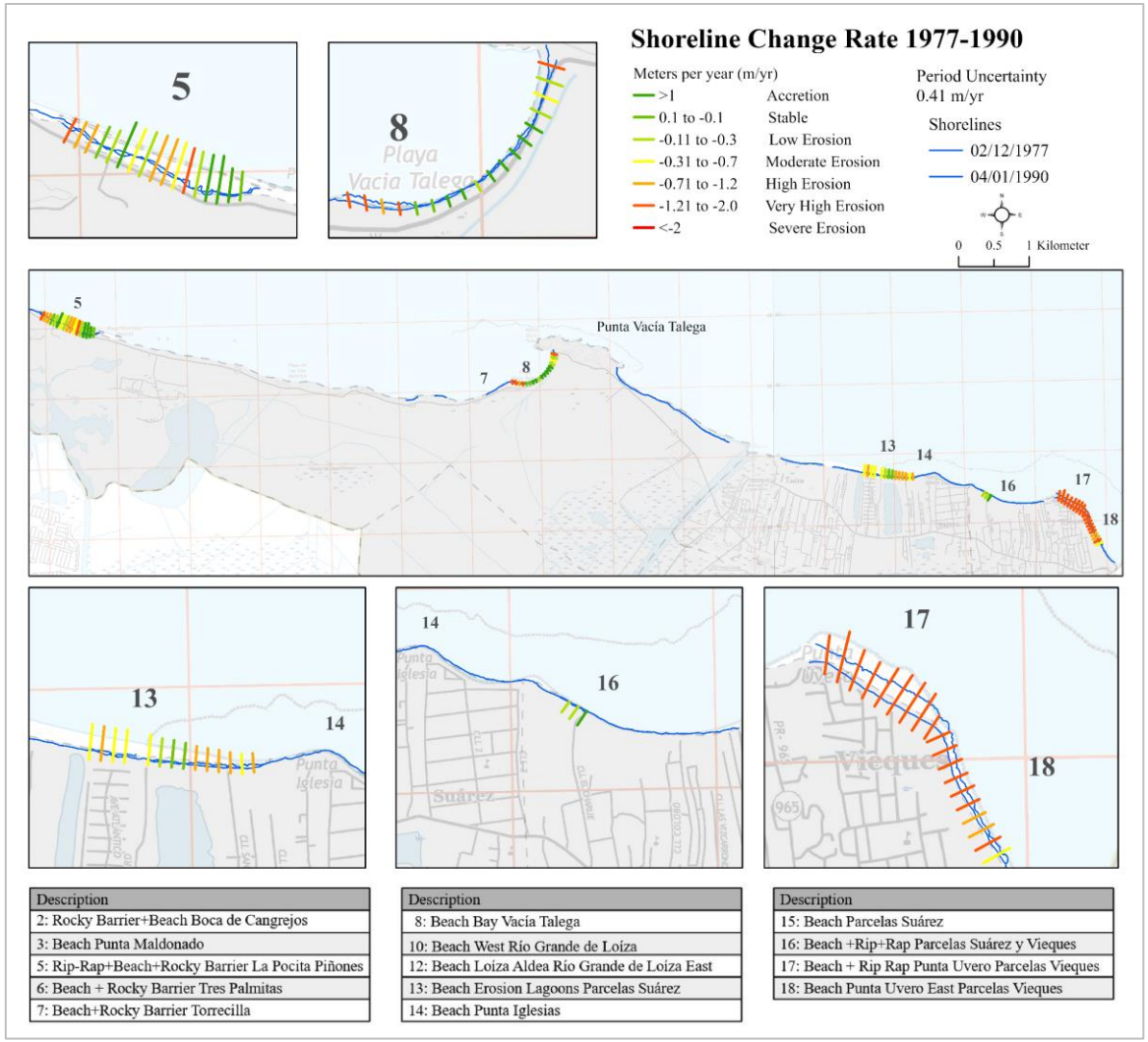

Figure 2.23: Shoreline Change Rates (m/yr) at Loíza: 1977 – 1990

The statistics for each Group ID are summarized in Table 2.11. The three areas that showed accretional rates represented less than 50% of the transects: Beach Vacía Talega (GroupID:8, 44%), Beach Between Parcelas Suárez and Parcelas Vieques (GroupID:16, 33%), and Beach La Pocita (GroupID:5, 29%). The areas with the highest percentage of erosion rates were Punta Iglesia Sandpit (GroupID:14), Punta Uvero Sandpit (GroupID:17), and Beach East Punta Uvero (GroupID:18). On average, all seven areas analyzed for this period presented erosional rates.

Table 2.11: Summary of Statistics: 1977 – 1990

	Description	Total Transects	Total positive rates	Total negative rates	% Transects Positive	% Transects Negative	Maximum Positive Rate (meters per year)	Maximum Negative Rate (meters per year)
Period 1977-1990		71	15	56	21	79	1.4	-4.93
By Group ID								
5	Beach La Pocita	17	5	12	29	71	1.4	-1.72
8	Beach Vacía Talega	18	8	10	44	56	0.69	-1.6
13	Beach Parcelas Suárez (erosion lagoons)	13	1	12	8	92	0.03	-0.89
14	Punta Iglesia sand pit	1	0	1	0	100	--	-0.89
16	Beach between Parcelas Suárez/Parcelas Vieques	3	1	2	33	66	0.61	-0.3
17	Punta Uvero sand pit	9	0	9	0	100	--	-4.93
18	Beach Punta Uvero East	10	0	10	0	100	--	-2

	Description	Average Positive Rates	Average Negative Rates	Average Rate	Maximum Positive Distance (meters)	Maximum Negative Distance (meters)	Average Positive Distance	Average Negative Distance	Average Distance
Period 1977-1990		0.41	-1.36	-0.99	18.42	-17.86	5.37	-17.86	-12.95
By Group ID									
5	Beach La Pocita	0.6	-0.72	-0.33	18.42	-22.56	7.92	-9.44	-4.34
8	Beach Vacía Talega	0.31	-0.79	-0.3	9.1	-21.02	4.05	-10.43	-4
13	Beach Parcelas Suárez (erosion lagoons)	0.03	-0.57	-0.53	0.41	-11.69	0.41	-7.54	-6.92
14	Punta Iglesia sand pit	--	-0.89	-0.89	--	-11.66	--	-11.66	-11.66
16	Beach between Parcelas Suárez/Parcelas Vieques	0.61	-0.25	-0.04	8.07	-3.89	8.07	-3.24	0.53
17	Punta Uvero sand pit	--	-4.15	-4.15	--	-64.8	--	-54.46	-54.46
18	Beach Punta Uvero East	--	-1.4	-1.4	--	-26.22	--	-18.37	-18.37

2.4.1.6 Shoreline Change Rates (m/yr): 1990 – 2010

For the period 1990 – 2010, I analyzed a total of 82 transects. Accretion was observed at the highest frequency (22%, n = 18), followed closely by high and moderate erosion (21%, n = 8; Figure 2.24). Low erosion was observed at a frequency of 17% (n = 14), and both stable and very high erosion showed the lowest frequency, with 10% each (n = 8).

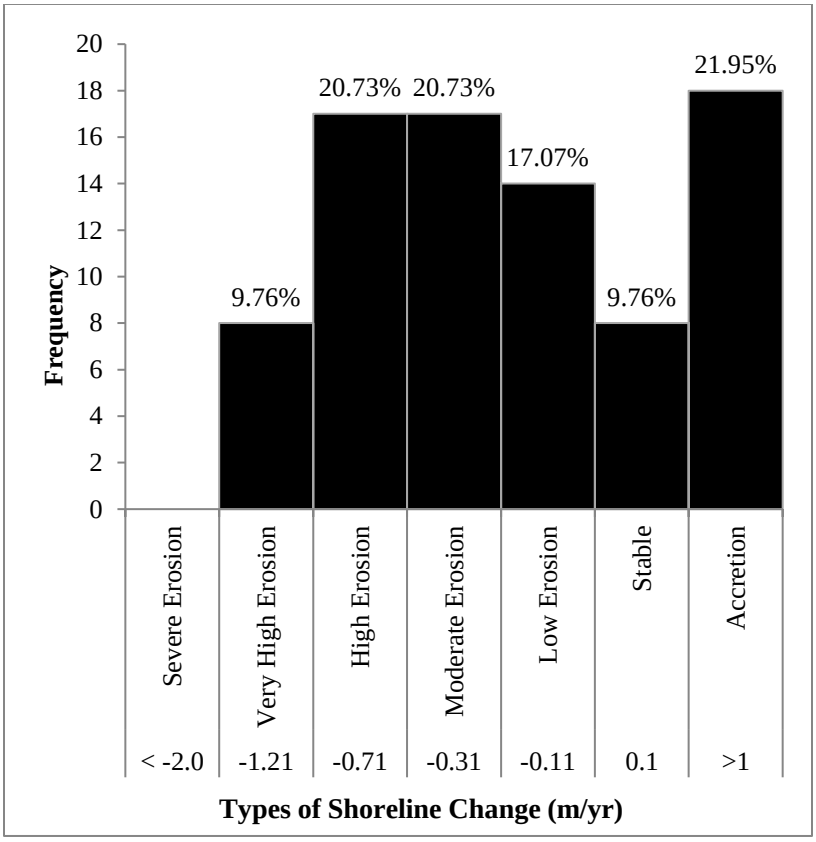

Figure 2.24: Frequencies of Different Types of Shoreline Change Rates (m/yr) from 1990 to 2010

The distribution of shoreline change rates, in general and by Group ID, is presented in Figure 2.25. The maximum accretion rates were observed at Beach Vacía Talega (GroupID:8) and Punta Uvero Sandpit (GroupID:17), with m/yr and 1.45 m/yr, respectively. The maximum erosion rates were observed at Beach La Pocita (GroupID:5),

Punta Iglesia Sandpit (GroupID:14), and the Punta Uvero East (GroupID:17), with measurements of -1.95, -1.45, and -1.25 m/yr, respectively.

On the west side of Vacía Talega, 76% of the transects were erosional (n = 22) and 28% were accretional (n = 8). At the east of Vacía Talega, 72% of the transects were erosional (n = 53) and 28% were accretional (n = 15), and the average rate was -0.33 m/yr. The maximum erosion rate was -1.98 m/yr (-38.95 m) at Beach La Pocita (GroupID:5), and the maximum accretion rate was 1.82 m/yr (35.91 m) at Beach Vacía Talega (GroupID:8).

Figure 2.25: Frequencies of Shoreline Change Rates (m/yr) from 1990 to 2010, by Classification (Stewart and Pope, 1993) and GroupID

The change rates on different sections of the shoreline are shown in Figure 2.26. The highest erosion rates were observed at La Pocita (GroupID:5), Punta Iglesia sandpit (GroupID:14), the beach between Parcelas Suárez and Parcelas Vieques (GroupID:16), and Punta Uvero east (GroupID:18). Higher accretion rates were observed at Vacía Talega (GroupID:8), Beach of Parcelas Suárez (GroupID:13), and Punta Uvero sandpit (GroupID:17). The maximum erosion rate was recorded at La Pocita (GroupID:5), with -1.98 m/yr (-38.95 m). The maximum accretion rate was recorded at Vacía Talega (GroupID:8), with 1.82 m/yr (35.91 m). Stable rates were observed at the Beach Torrecilla (GroupID:7), Beach Parcelas Suárez (GroupID:13), and Punta Uvero Sandpit (GroupID:17).

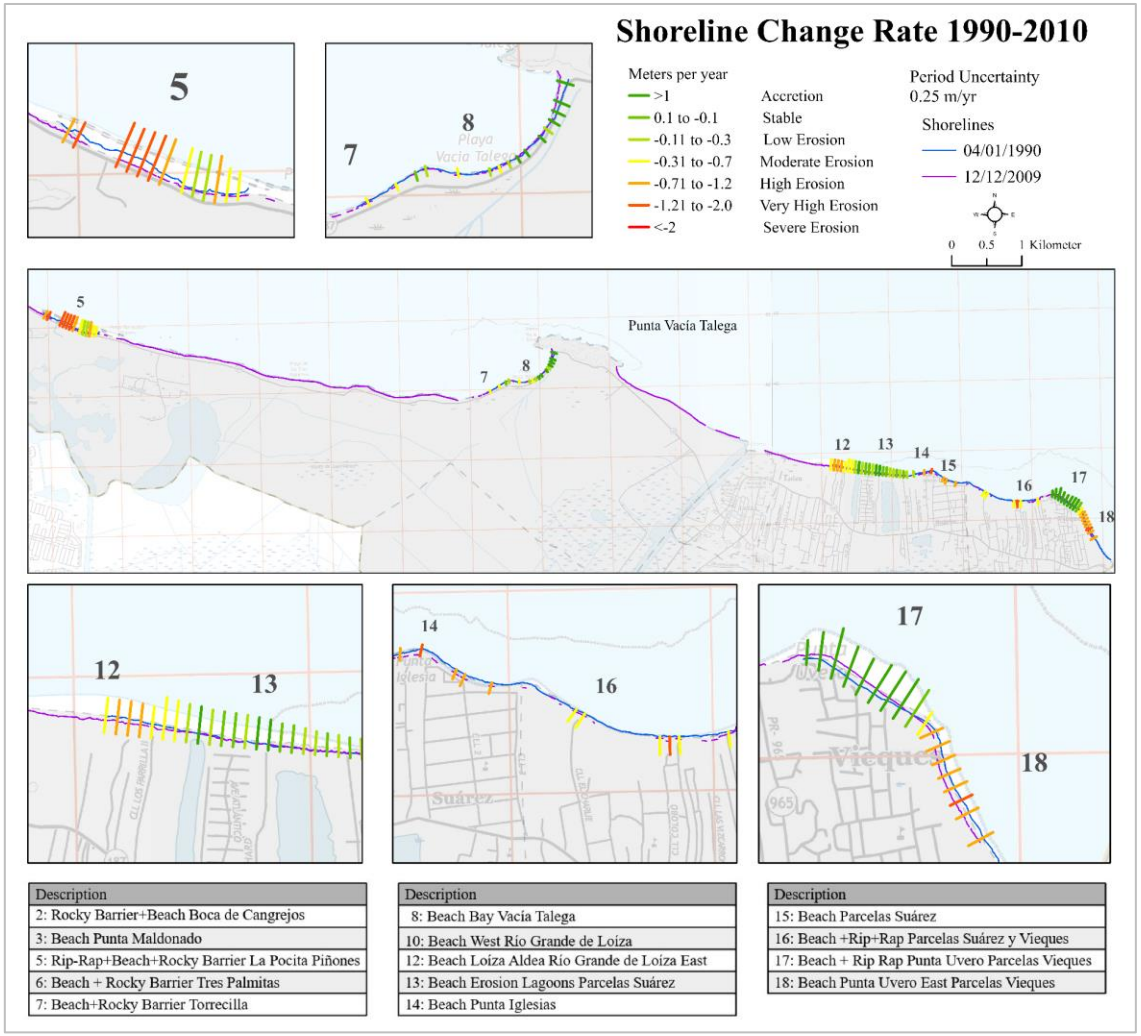

Figure 2.26: Shoreline Change Rates (m/yr) at Loíza: 1990 – 2010

The change rates and statistics for the period 1990 – 2010 are summarized in Table 2.12. Six areas showed 100% erosion rates: Beach La Pocita (GroupID:5), Beach Río Grande de Loíza East-Loíza Aldea (GroupID:12), Punta Iglesia San pit (GroupID:14), Beach Parcelas Suárez (GroupID:15), Beach between Parcelas Suárez and Vieques (GroupID:16), and Beach Punta Uvero East (GroupID:18). Only four areas showed accretional rates: Punta Uvero Sandpit (GroupID:17), Beach Parcelas Suárez (erosion lagoons; GroupID:13), Beach Vacía Talega (GroupID:8), and Beach Torrecilla (GroupID:7). On average, eight out of 10 areas showed erosion rates and two showed accretion rates.

Table 2.12: Summary of Statistics: 1990 – 2010

	Description	Total Transects	Total positive rates	Total negative rates	% Transects Positive	% Transects Negative	Maximum Positive Rate (meters per year)	Maximum Negative Rate (meters per year)
Period 1990-2010		82	23	59	28	72	1.82	-1.98
By Group ID								
5	Beach La Pocita	13	0	13	0	100	--	-1.98
7	Beach Torrecilla	4	1	3	25	75	0.07	-0.48
8	Beach Vacía Talega	12	7	5	58	42	1.82	-0.53
12	Beach Río Grande de Loíza East Loíza Aldea	7	0	7	0	100	--	-0.99
13	Beach Parcelas Suárez (erosion lagoons)	16	7	9	44	56	0.31	-0.2
14	Punta Iglesia sand pit	5	0	5	0	100	--	-1.45
15	Beach Parcelas Suárez	1	0	1	0	100	--	-0.09
16	Beach between Parcelas Suárez/Parcelas Vieques	6	0	6	0	100	--	-1.24
17	Punta Uvero sand pit	10	8	2	80	20	1.45	-0.46
18	Beach Punta Uvero East	8	0	8	0	100	--	-1.25

	Description	Average Positive Rates	Average Negative Rates	Average Rate	Maximum Positive Distance (meters)	Maximum Negative Distance (meters)	Average Positive Distance	Average Negative Distance	Average Distance
Period 1990-2010		0.57	-0.69	-0.33	35.91	-38.95	11.22	-13.52	-6.58
By Group ID									
5	Beach La Pocita	--	-1.02	-1.02	--	-38.95	--	-20.12	-20.12
7	Beach Torrecilla	0.07	-0.39	-0.28	1.33	-9.45	1.33	-7.68	-5.42
8	Beach Vacía Talega	0.71	-0.29	0.29	35.91	-10.52	13.94	-5.66	5.77
12	Beach Río Grande de Loíza East Loíza Aldea	--	-0.69	-0.69	--	-19.58	--	-13.51	-13.51
13	Beach Parcelas Suárez (erosion lagoons)	0.11	-0.15	-0.04	6.17	-3.95	2.12	-2.89	-0.7
14	Punta Iglesia sand pit	--	-0.95	-0.95	--	-28.51	--	-18.69	-18.69
15	Beach Parcelas Suárez	--	-0.09	-0.09	--	-17.76	--	-17.76	-17.76
16	Beach between Parcelas Suárez/Parcelas Vieques	--	-0.65	-0.65	--	-24.46	--	-12.76	-12.76
17	Punta Uvero sand pit	0.92	-0.26	0.68	28.6	-9.13	18.03	-5.08	13.41
18	Beach Punta Uvero East	--	-1.05	-1.05	--	-24.68	--	-20.77	-20.77

2.4.1.7 Shoreline Change Rates (m/yr): 2010 – 2018

For Period 6, 2010 – 2018, I analyzed 254 transects, of which 88% (n = 223) were accretional and 12% were erosional (n = 31). The accretion category was observed with the highest frequency (86%, n = 218; Figure 2.27). All other categories were observed less than 4% of the time, and severe erosion was not observed in any transect.

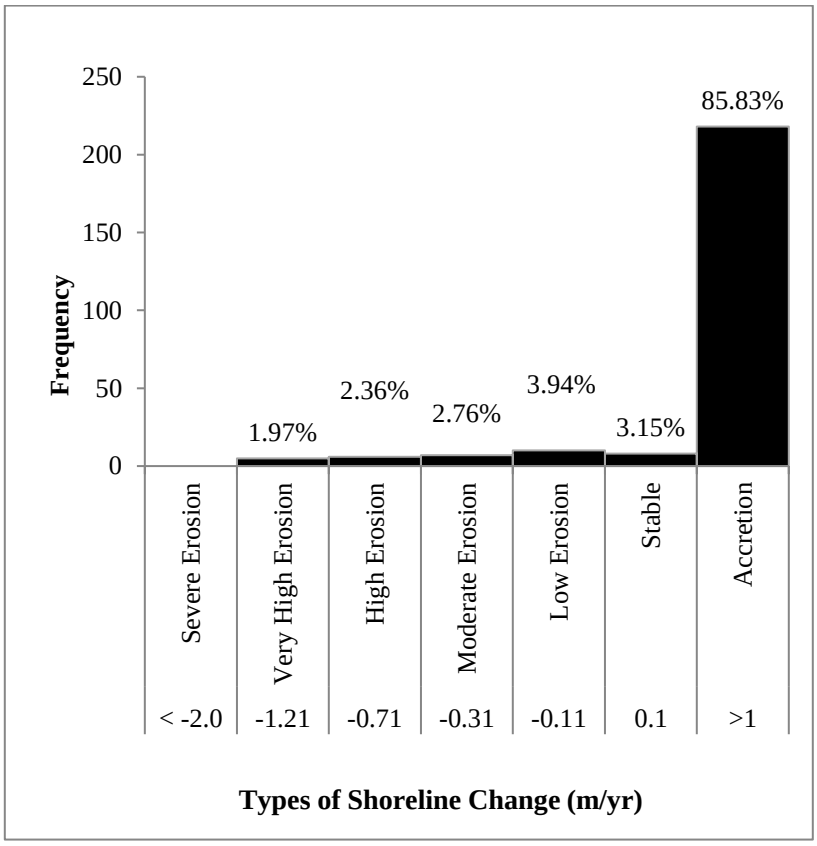

Figure 2.27: Frequencies of Different Types of Shoreline Change Rates (m/yr) from 2010 to 2018

Graphs representing shoreline change in general and by Group ID are shown in Figure 2.28. The maximum accretion rates—7.95, 7.51, and 4.94 m/yr —were observed at Beach Tres Palmitas (GroupID:7), and the west and east sides of Río Grande de Loíza (GroupID:11, 12), respectively. In contrast, the maximum erosion rates were observed at

Punta Uvero sandpit (GroupID:17), Beach Torrecilla (GroupID:7), and Punta Iglesia San pit (GroupID:14), with values of -3.56, -1.86, and -1.63 m/yr, respectively.

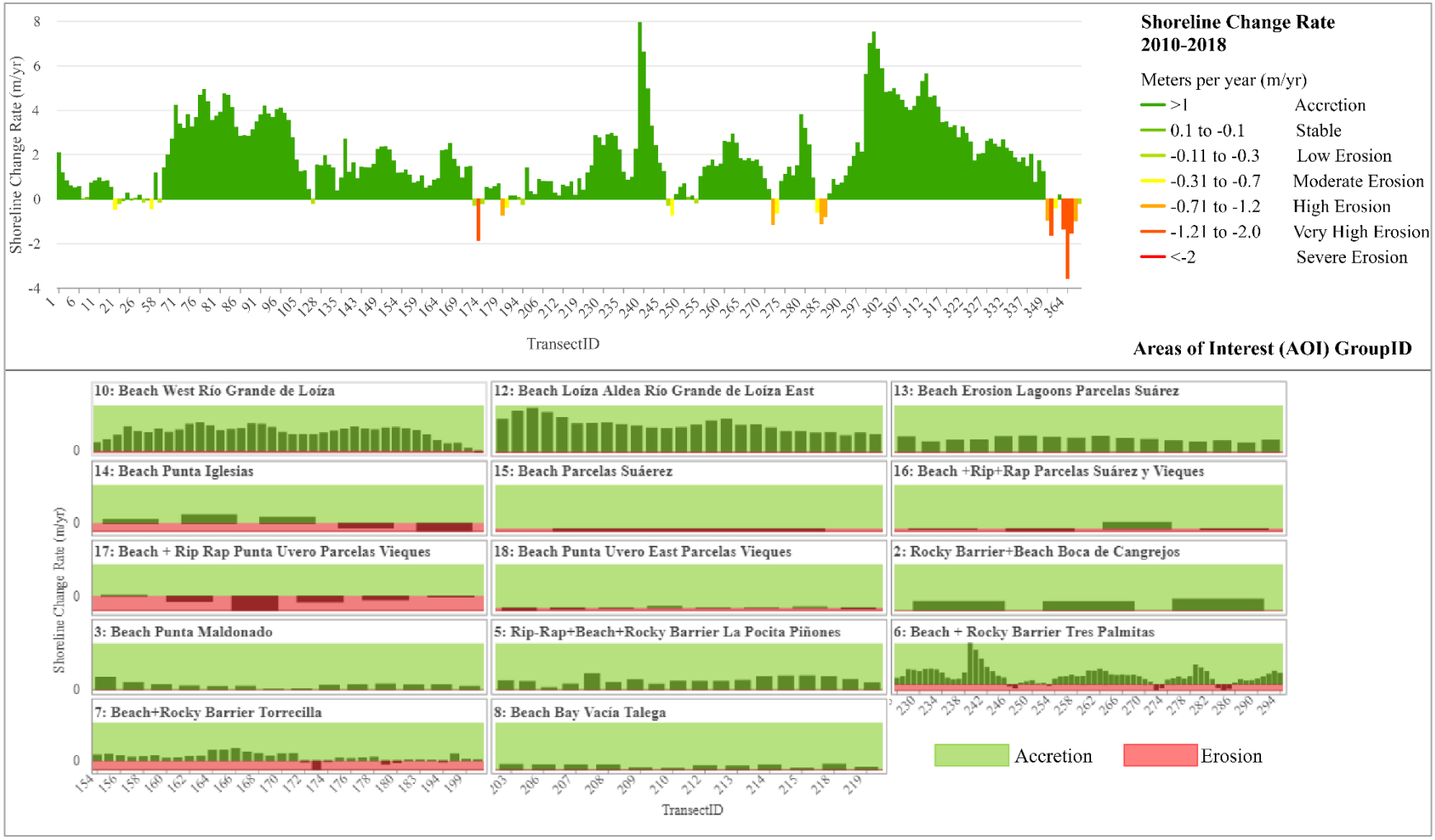

Figure 2.28: Frequencies of Shoreline Change Rates (m/yr) from 2010 to 2018, by Classification (Stewart and Pope, 1993) and GroupID

Along the shoreline (Figure 2.29), on the west side of Vacía Talega, 84% of the measured rates were accretional (n = 87) and 16% were erosional (n = 17). On the east side of Vacía Talega, 91% were accretional (n = 131) and 9% were accretional (n = 14). Indeed, accretion rates were observed along most of the shoreline. Punta Iglesia sandpit (GroupID:14) and Punta Uvero sandpit (GroupID:17) showed the highest erosion rates, with the latter exhibiting the maximum erosion rate of -3.56 m/yr. Tres Palmitas (GroupID:7) showed the maximum accretion rate, with 7.95 m/yr. Less than 3% of the transects (n = 8) showed stable rates. These rates were measured at Beach Punta Maldonado (GroupID:3, n = 2), Beach Tres Palmitas (GroupID:6, n = 1), Beach Torrecilla (GroupID:7, n = 1), Beach between Parcelas Suárez and Parcelas Vieques (GroupID:16, n = 1), and Beach Punta Uvero east (GroupID:18, n = 3).

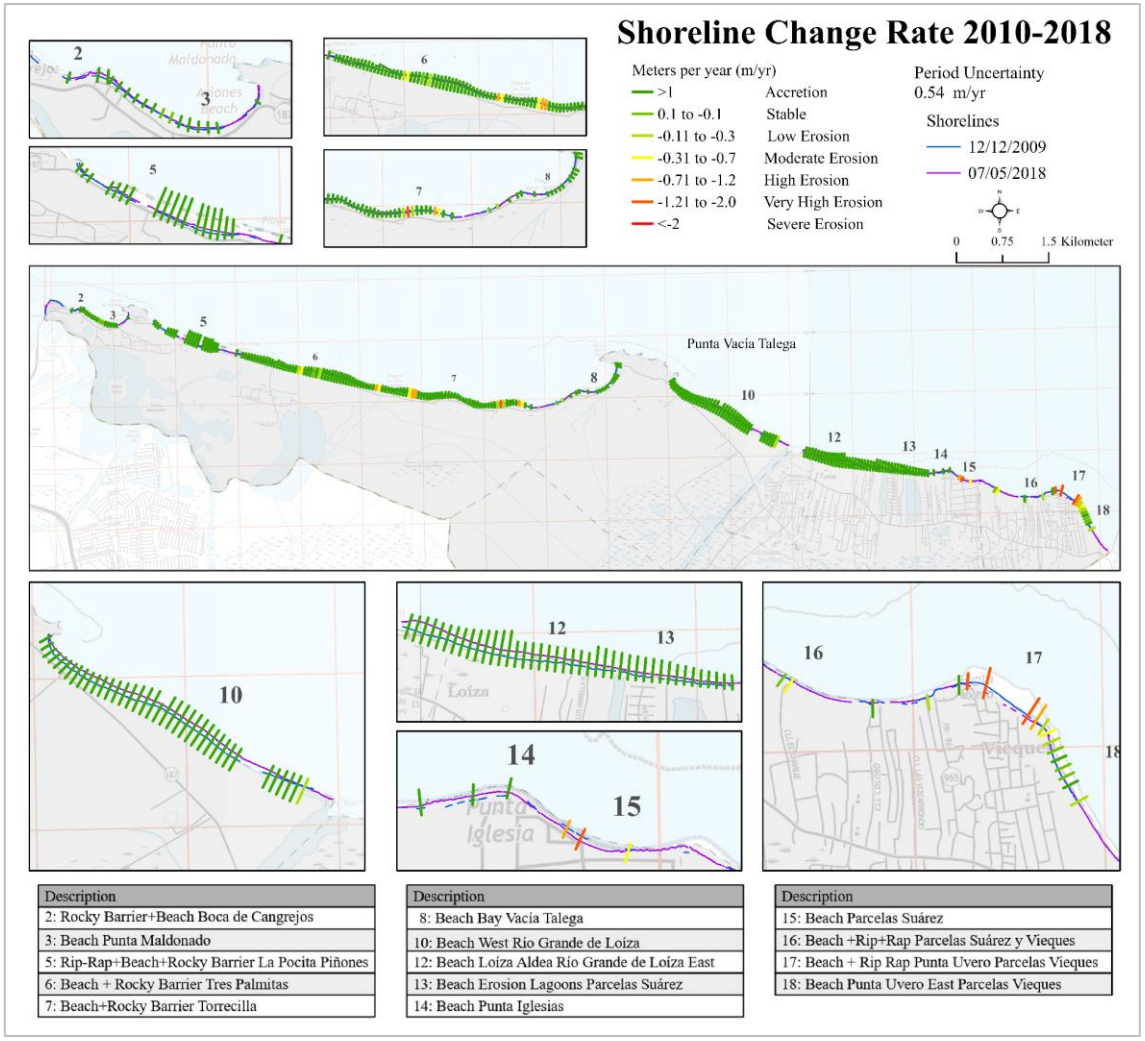

Figure 2.29: Shoreline Change Rates (m/yr) at Loíza: 2010 – 2018

The shoreline change rates and statistics for this period are summarized in Table 2.13. The average rate was 1.79 m/yr, the maximum accretion rate was 7.95 m/yr (68.04 m), and the maximum erosion rate was -3.56 m/yr (-30.46 m). Six areas showed 100% accretional rates: Beach Boca Cangrejos (GroupID:2), Beach Punta Maldonado (GroupID:3), Beach La Pocita (GroupID:5), Beach Vacía Talega (GroupID:8), and Beach West Río Grande de Loíza (GroupID:10) and Loíza Aldea (GroupID:12). Only Beach Parcelas Suárez exhibited 100% erosional rates. On average, of the 14 groups, 79% (n = 11) showed accretion rates and 21% (n = 3) had erosion rates.

Table 2.13: Summary of Statistics: 2010 – 2018

	Description	Total Transects	Total positive rates	Total negative rates	% Transects Positive	% Transects Negative	Maximum Positive Rate (meters per year)	Maximum Negative Rate (meters per year)
	Period 2010-2018	254	223	31	88	12	7.95	-3.56
	By Group ID							
2	Beach Boca de Cangrejos	3	3	0	100	0	1.95	--
3	Beach Punta Maldonado	14	14	0	100	0	2.08	--
5	Beach La Pocita	18	18	0	100	0	2.7	--
6	Beach Tres Palmitas	69	61	8	88	12	7.95	-1.14
7	Beach Torrecilla	34	28	6	82	18	2.49	-1.86
8	Beach Vacía Talega	12	12	0	100	0	0.91	--
10	Beach West Río Grande de Loíza	38	37	1	97	3	4.94	-0.18
12	Beach Río Grande de Loíza East Loíza Aldea	26	26	0	100	0	7.51	--
13	Beach Parcelas Suárez (erosion lagoons)	16	16	0	100	0	2.71	--
14	Punta Iglesia sand pit	5	3	2	60	40	1.73	-1.63
15	Beach Parcelas Suárez	1	0	1	0	100		-0.39
16	Beach between Parcelas Suárez/Parcelas Vieques	4	1	3	25	75	1.17	-0.41
17	Punta Uvero sand pit	6	1	5	17	83	0.19	-3.56
18	Beach Punta Uvero East	8	3	5	37.5	62.5	0.26	-0.44

	Description	Average Positive Rates	Average Negative Rates	Average Rate	Maximum Positive Distance (meters)	Maximum Negative Distance (meters)	Average Positive Distance	Average Negative Distance	Average Distance
	Period 2010-2018	2.13	-0.68	1.79	68.04	-30.46	18.25	-5.85	15.32
	By Group ID								
2	Beach Boca de Cangrejos	1.66	--	1.66	16.68	--	14.24	--	14.24
3	Beach Punta Maldonado	0.75	--	0.75	17.78	--	6.39	--	6.39
5	Beach La Pocita	1.59		1.59	23.12	--	13.58	--	13.58
6	Beach Tres Palmitas	1.89	-0.67	1.6	68.04	-9.76	16.21	-5.76	13.66
7	Beach Torrecilla	0.98	-0.61	0.7	21.31	-15.89	8.42	-5.22	6.01
8	Beach Vacía Talega	0.59		0.59	7.81	--	5.07	--	5.07
10	Beach West Río Grande de Loíza	3.33	-0.18	3.23	42.29	-1.5	28.48	-1.5	27.69
12	Beach Río Grande de Loíza East Loíza Aldea	4.62	--	4.62	64.26	--	39.54	--	39.54
13	Beach Parcelas Suárez (erosion lagoons)	2.15	--	2.15	23.17	--	18.42	--	18.42
14	Punta Iglesia sand pit	1.24	-1.29	0.23	14.77	-13.98	10.6	-11.06	1.94
15	Beach Parcelas Suárez		-0.39	-0.39		-3.37		-3.37	-3.37
16	Beach between Parcelas Suárez/Parcelas Vieques	1.17	-0.2	0.14	9.98	-3.53	9.98	-1.68	1.23
17	Punta Uvero sand pit	0.19	-1.51	-1.23	1.58	-30.46	1.58	-12.92	-10.5
18	Beach Punta Uvero East	0.16	-0.17	-0.05	2.22	-3.74	1.33	-1.46	-0.42

2.4.2 Linear Regression Results

This section presents the results of the two linear regression models calculated by DSAS. The LRR and WLR represent the trends in shoreline change rates from 1902 to 2018 using all shorelines inserted, with a minimum of four shorelines per transect. The difference between the LRR and WLR was that the latter established a weighted regression based on the uncertainty values, giving more weight to those points with less uncertainty.

2.4.2.1 Linear Regression Rate (LRR)

The LRR model was used to analyze all historical shorelines (1902, 1931, 1951, 1977, 1990, 2010, and 2018) for the Loíza municipality. Because this analysis required a minimum of four shorelines, the calculations were conducted for 334 transects. The highest frequency was observed in the moderate erosion category (37%, n = 123), followed by low erosion (28%, n = 93; Figure 2.30). The stable and accretion categories were observed at frequencies of 17% (n = 58) and 12% (n = 41), respectively. The lowest frequencies were observed for very high erosion and high erosion (both 3%, n = 9 and 10, respectively). Accretional trends were observed in 20% of transects (n = 67), with the remaining 79% of transects showing erosional trends (n = 267). Overall, the LRR model suggested that erosional rates dominated the shoreline of Loíza.

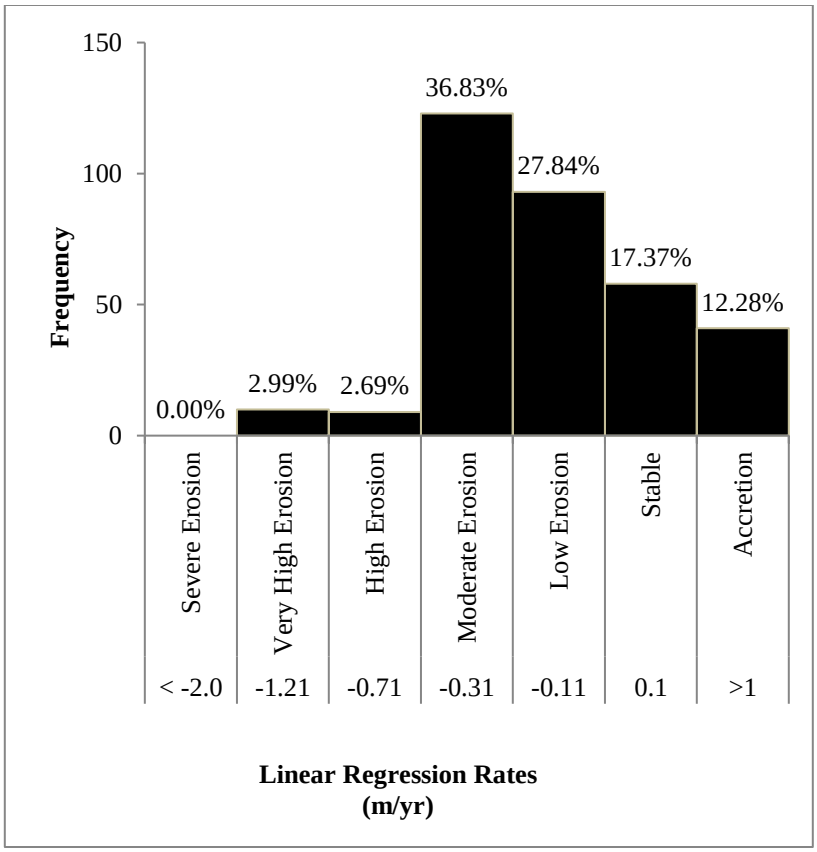

Figure 2.30: Frequencies of Linear Regression Rates for Different Types of Shoreline Change in Loíza, Puerto Rico

LRR values for shoreline change are presented by transect and GroupID in Figure 2.31. Some areas only showed erosion rates, such as Beach Punta Uvero (GroupID:18) and Beach Boca de Cangrejos (GroupID: 2). None of the areas showed 100% accretion rates.

Figure 2.31: Frequencies of Linear Regression Rates (LRR) of Shoreline Change (m/yr) by Classification (Stewart and Pope, 1993) and GroupID

Geographically (Figure 2.32), accretion and stable rates were observed in the eastern region, with the western area showing moderate erosion combined with stable and accretion rates. The maximum erosion rates were observed at La Pocita (GroupID:5), with -1.34 m/yr, and Punta Uvero sandpit (GroupID:17), with -1.15 m/yr. The maximum accretion rate, 0.89 m/yr, was observed at the beach between Parcelas Suárez and Parcelas Vieques (GroupID:16).

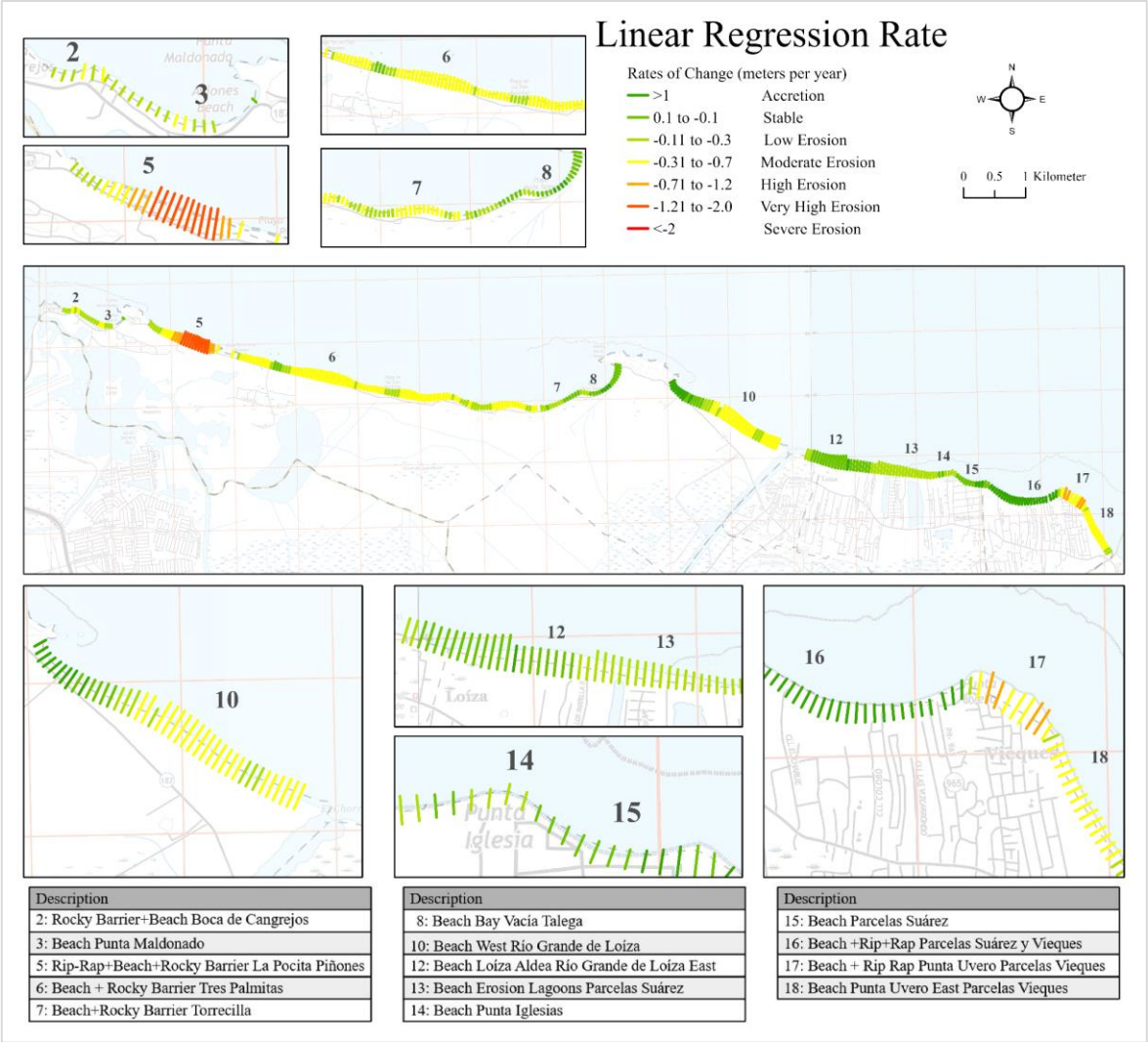

Figure 2.32: Shoreline Linear Regression Rates (m/yr) at Loíza, Puerto Rico

Statistics for the LRR are summarized in Table 2.14. The maximum erosion and accretion rates were -1.34 m/yr and 0.89 m/yr, respectively, with an average of -0.24 m/yr. At the beach of Boca de Cangrejos (GroupID:2), all six transects were erosional, with a maximum rate of -0.41 m/yr and an average rate of -0.28 m/yr. At the beach of Punta Maldonado (GroupID:3), all 14 transects were erosional, with a maximum rate of -0.35 m/yr and an average of -0.23 m/yr.

Table 2.14: Summary of Statistics for Linear Regression Rates (LRR)

Description		Total Transects	Total positive rates	Total negative rates	% Transects Positive	% Transects Negative	Maximum Positive Rate (meters per year)	Maximum Negative Rate (meters per year)	Average Positive Rates	Average Negative Rates
LRR 1902-2018		334	67	267	20	80	0.89	-1.34	0.24	-0.36
By Group ID										
2	Beach Boca de Cangrejos	6	0	6	0	100	--	-0.41	--	-0.28
3	Beach Punta Maldonado	14	0	14	0	100	--	-0.35	--	-0.23
5	Beach La Pocita	24	0	24	0	100	--	-1.34	--	-0.86
6	Beach Tres Palmitas	70	3	67	4	96	0.01	-0.7	0.07	-0.39
7	Beach Torrecilla	46	1	45	98	2	0.05	-0.46	0.05	-0.26
8	Beach Vacía Talega	19	11	8	58	42	0.19	-0.18	0.08	-0.08
10	Beach West Río Grande de Loíza	42	11	31	26	73	0.28	-0.64	0.16	-0.36
12	Beach Río Grande de Loíza East Loíza Aldea	26	10	16	38	62	0.12	-0.29	0.04	-0.11
13	Beach Parcelas Suárez (erosion lagoons)	16	0	16	0	100	--	-0.25	--	-0.18
14	Punta Iglesia sand pit	12	2	10	17	83	0.02	-0.25	0.02	-0.11
15	Beach Parcelas Suárez	8	5	3	62.5	37.5	0.24	-0.07	0.14	-0.05
16	Beach between Parcelas Suárez/Parcelas Vieques	21	21	0	100	0	0.89	--	0.51	--
17	Punta Uvero sand pit	13	3	10	23	76	0.6	-1.15	0.37	-0.71
18	Beach Punta Uvero East	17	0	17	0	100	--	-0.6	--	-0.44

2.4.2.2 Weighted Linear Regression Rate (WLR)

SCA with a WLR model was used to evaluate a total of 334 transects. As previously mentioned, the WLR model differed from the LRR model in that it gave more importance to transects with less uncertainty. The frequencies of different shoreline changes determined using the WLR are shown in Figure 2.33. Moderate erosion events were observed with the highest occurrence along the shoreline (39%, n = 129), followed by low erosion (23%, n = 76). High erosion and stable shorelines were both identified 13% of the time along the coastline, whereas accretion (9%, n = 30) and very high erosion (4%, n = 13) were observed less frequently.

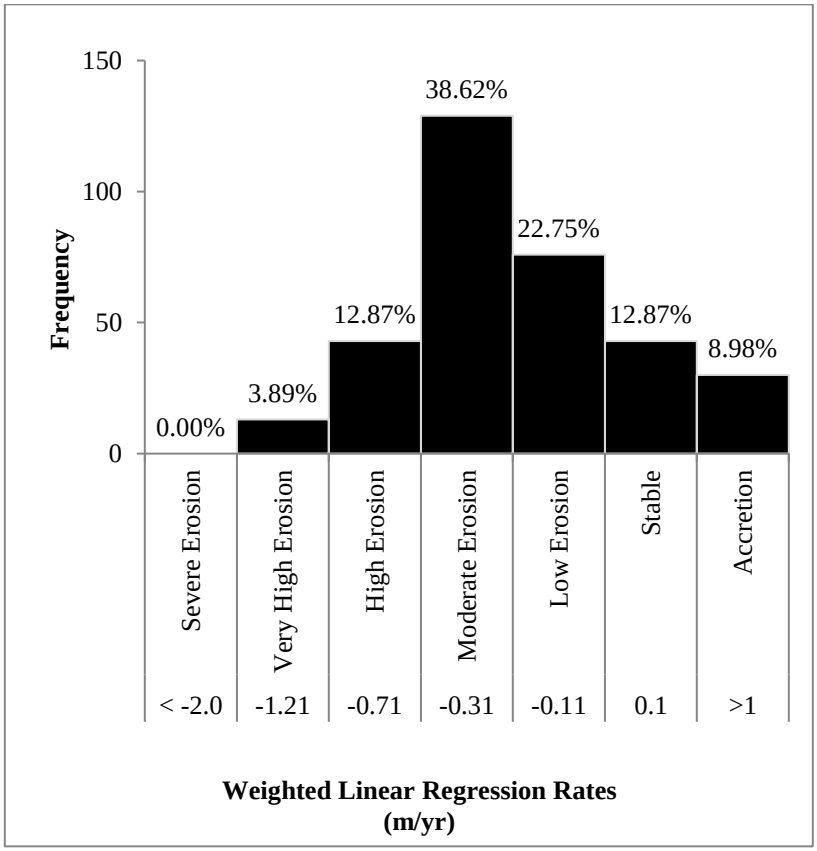

Figure 2.33: Frequencies of Weighted Linear Regression Rates for Different Types of Shoreline Change in Loíza, Puerto Rico

The WLR transects are presented by area in Figure 2.34. The majority of the areas showed more erosional rates, except for Beach Parcelas Suárez and Vieques (GroupID:16), which showed 100% accretional rates.

Figure 2.34: Frequencies of Weighted Linear Regression Rates (WLR) of Shoreline Change (m/yr) by Classification (Stewart and Pope, 1993) and GroupID

Along the shoreline of Loíza (Figure 2.35), moderate erosion, low erosion, and very high erosion were more frequent in the western region. In the east, accretion and high erosion were combined. The maximum rate of accretion was observed at the beach between Parcelas Suárez and Parcelas Vieques (GroupID:16), with 1.81 m/yr, and the maximum rate of erosion was observed at Beach La Pocita (GroupID:5), with -1.77 m/yr.

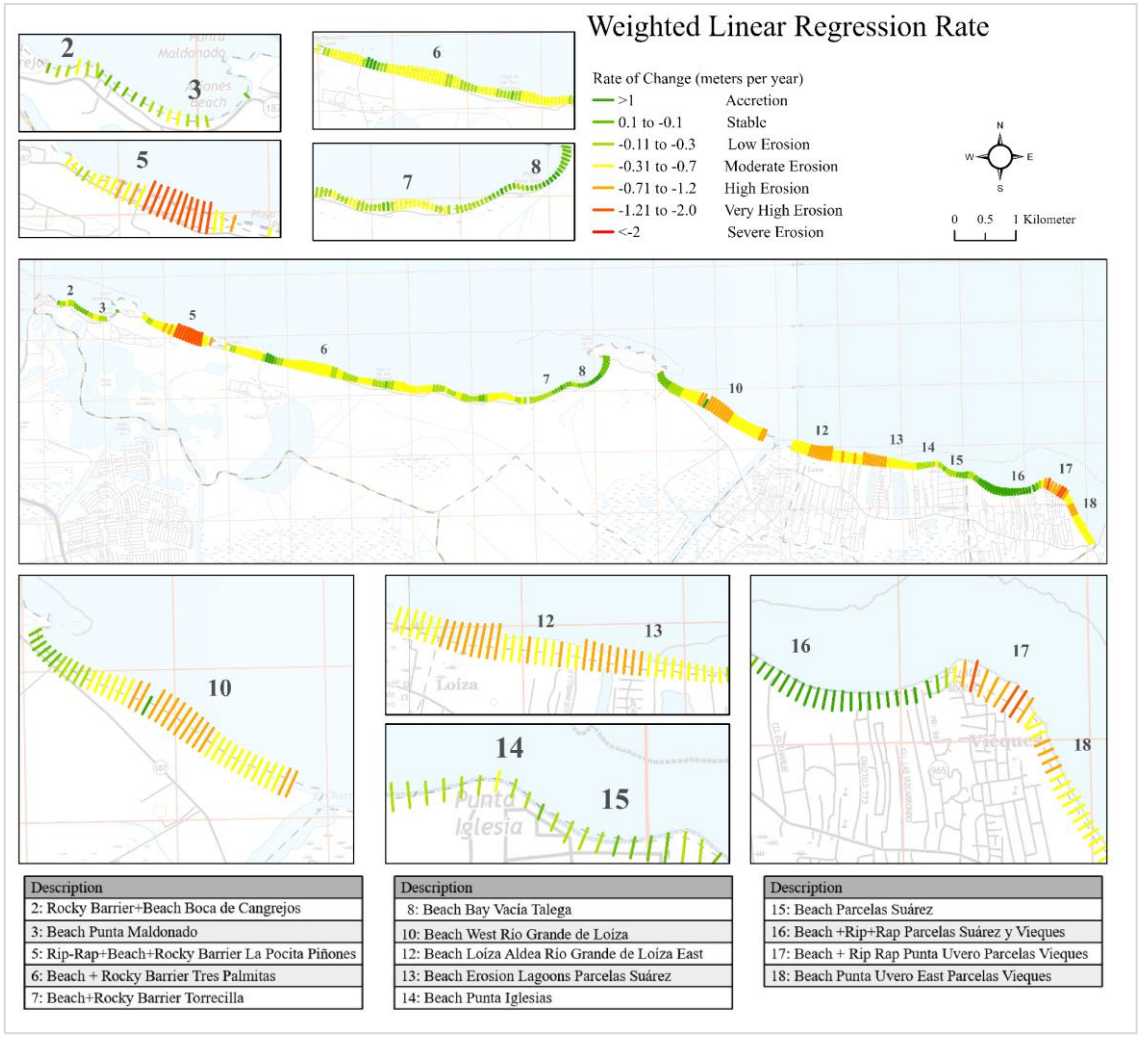

Figure 2.35: Shoreline Weighted Linear Regression Rates (m/yr) at Loíza, Puerto Rico

Statistics for the WLR are summarized in Table 2.15. The maximum erosion and accretion rates were -1.77 m/yr and 0.81 m/yr, respectively, with an average of -0.38 m/yr.

Table 2.15: Summary of Statistics for Weighted Linear Regression Rates (WLR)

Description		Total Transects	Total positive rates	Total negative rates	% Transects Positive	% Transects Negative	Maximum Positive Rate (meters per year)	Maximum Negative Rate (meters per year)	Average Positive Rates	Average Negative Rates	Average Rate
WLR 1902-2018		334	46	288	14	86	0.81	-1.77	0.21	-0.48	-0.38
By Group ID											
2	Beach Boca de Cangrejos	6	0	6	0	100	--	-0.32	--	-0.2	-0.2
3	Beach Punta Maldonado	14	1	13	7	93	0.01	-0.32	0.01	-0.16	-0.15
5	Beach La Pocita	24	0	24	0	100	--	-1.77	--	-1.01	-1.01
6	Beach Tres Palmitas	70	3	67	4	96	0.3	-0.71	0.23	-0.34	-0.32
7	Beach Torrecilla	46	5	41	11	89	0.12	-0.58	0.05	-0.26	-0.23
8	Beach Vacía Talega	19	10	9	53	47	0.2	-0.14	0.1	-0.06	0.02
10	Beach West Río Grande de Loíza	42	1	41	2	98	0.36	-1.01	0.36	-0.52	-0.5
12	Beach Río Grande de Loíza East Loíza	26	0	26	0	100	--	-1.14	--	-0.76	-0.76
13	Beach Parcelas Suárez (erosion lagoons	16	0	16	0	100	--	-0.94	--	-0.64	-0.64
14	Punta Iglesia sand pit	12	0	12	0	100	--	-0.31	--	-0.18	-0.18
15	Beach Parcelas Suárez	8	3	5	37.5	62.5	0.08	-0.24	0.07	-0.14	-0.06
16	Beach between Parcelas Suárez/Parcel	21	21	0	100	0	0.81	--	0.34	--	0.34
17	Punta Uvero sand pit	13	2	11	15	85	0.35	-1.38	0.23	-0.97	-0.79
18	Beach Punta Uvero East	17	0	17	0	100	--	-0.83	--	-0.63	-0.63

2.4.3 Forecasted Shoreline Change Rates (m/yr)

This section describes future shoreline change (m/yr) scenarios for the years 2032 and 2042 using the DSAS forecast model for Loíza municipality. DSAS forecasted two future shoreline positions for 2032 and 2042, which were used to calculate the end point rates from 2018 to 2032, and from 2018 and 2042. Evaluation of forecasting scenarios clarifies future shoreline change for an area and its implications for the coastal management process in the area. Forecasting future changes is key to understanding the shoreline's possible erosional and accretion rates, but as explained by the DSAS tool, forecasting analysis should be addressed with caution by understanding the errors associated with these projections. In Puerto Rico, this analysis will bring a novel approach to understanding or estimating future shoreline changes. I used the forecasted shorelines 2032 and 2042, and the shoreline from 2018, to estimate future changes.

2.4.3.1 Forecasted Shoreline Changes for 2018 – 2032

Forecasting shoreline change (m/yr) scenarios indicated that erosion will be the more frequent event at the study site for the period 2018 – 2032 (85%, 119 transects). The very high erosion category had the highest frequency (37%, n = 85), followed by moderate erosion (20%, n = 45; Figure 2.36). Low erosion (8%, n = 19) and stable (7%, n = 15) were the least frequent events. Accretion was present at a frequency of 12% (n = 28). In general, 80% of transects showed erosion rates (n = 194) and 15% showed accretion rates (n = 34). The average rate was -0.94 m/yr, with maximum rates of erosion and accretion of -3.73 m/yr (-50.35 m) and 1.01 m/yr (13.57 m), respectively. This scenario suggested

that erosional rates will continue to increase in Loíza, Puerto Rico, while accretional rates will reduce.

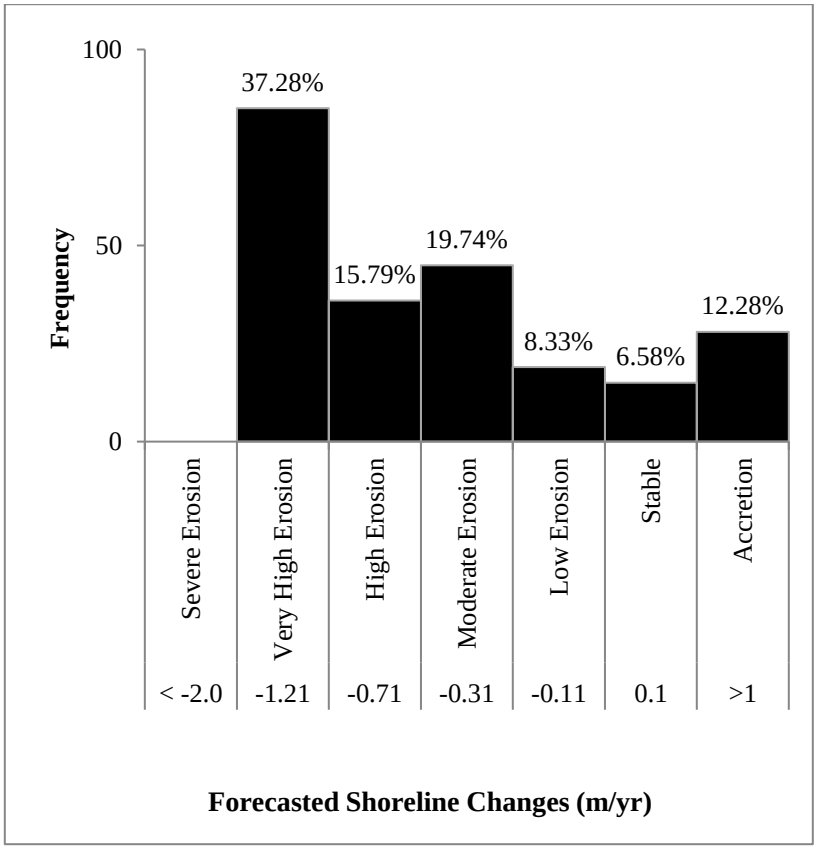

Figure 2.36: Frequencies of Different Types of Shoreline Change Rates (m/yr), Forecasted for 2018 – 2032

Graphs presenting rate distributions and rates by Group ID are shown in Figure 2.37. The maximum accretion rates were found in three areas: Beach between Parcelas Suárez and Parcelas Vieques (GroupID:16), Punta Uvero sandpit (GroupID:17), and Beach Parcelas Suárez (GroupID:15). The Beach between Parcelas Suárez and Parcelas Vieques (GroupID:16) showed the maximum accretion rate, which was 1.01 m/yr (13.57 m). At Punta Uvero Sandpit, 71% of the seven transects were erosional and 29% were accretional. Transects of the west side of the sandpit showed accretional rates, whereas those on the east showed erosional rates.

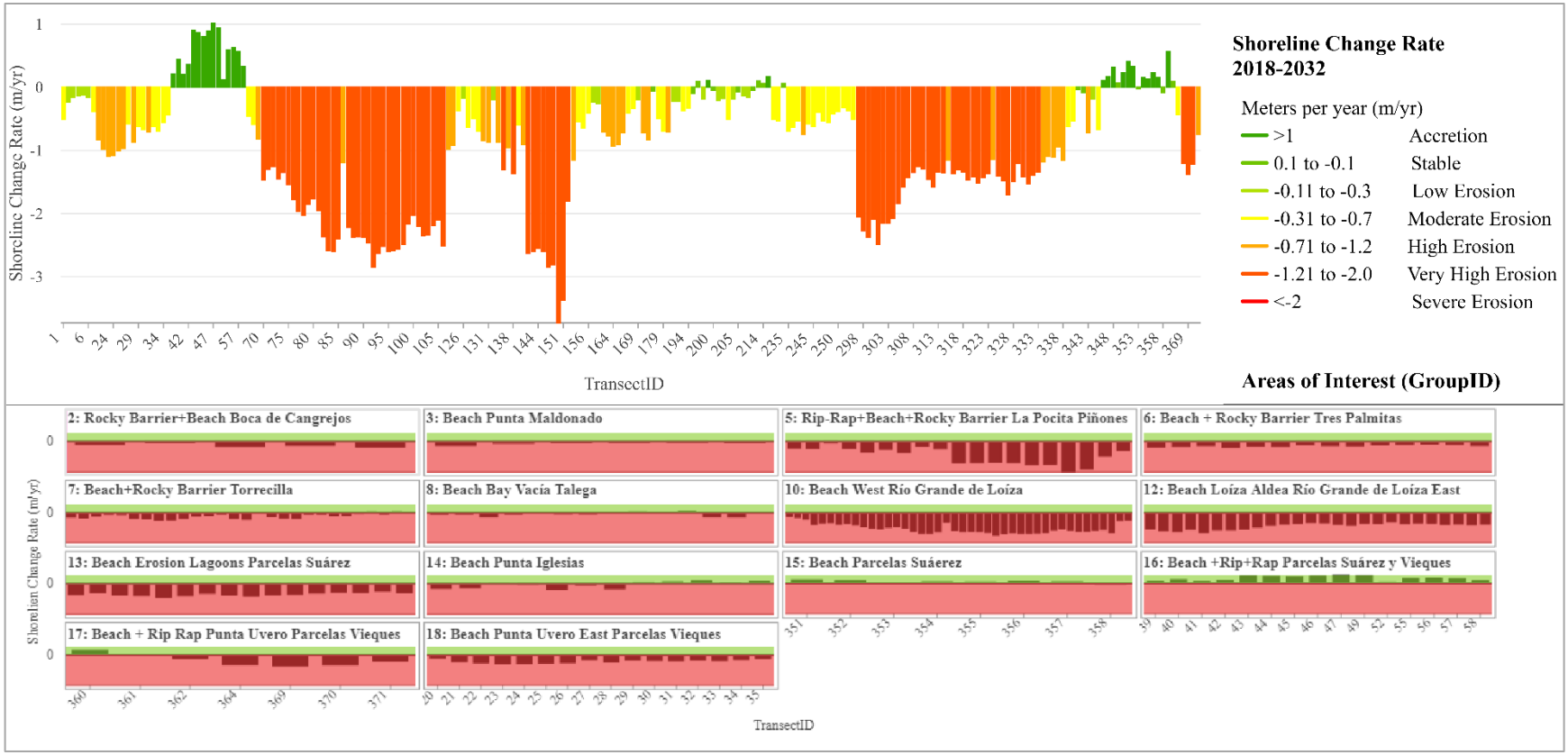

Figure 2.37: Frequencies of Forecasted Shoreline Change Rates (m/yr) from 2018 to 2032, by Classification (Stewart and Pope, 1993) and GroupID

The maximum erosion rates were found at Beach La Pocita (GroupID:5), Beach West Rio Grande de Loíza (GroupID: 10), and Beach East Río Grande de Loíza and Loíza Aldea (GroupID:12). Beach La Pocita (GroupID:5) showed the maximum erosion rate, which was -3.73 m/yr (-50.35 m). Because erosion rates are often observed in areas that have already undergone erosion, this could suggest more shoreline recession in these areas.

Along the shoreline of Loíza (Figure 2.38), the west and east sides of the coast showed accretional rates. In the west, 93% of the transects were accretional (n = 80) and 7% (n = 6) were erosional. In the east, 80% of the transects were erosional (n = 114) and 20% were accretional (n = 28). Sandpits showed mostly erosional rates. Maximum erosion rates surpassed maximum accretion rates in most of the areas, except for Beach Parcelas Suárez (Group ID:15).

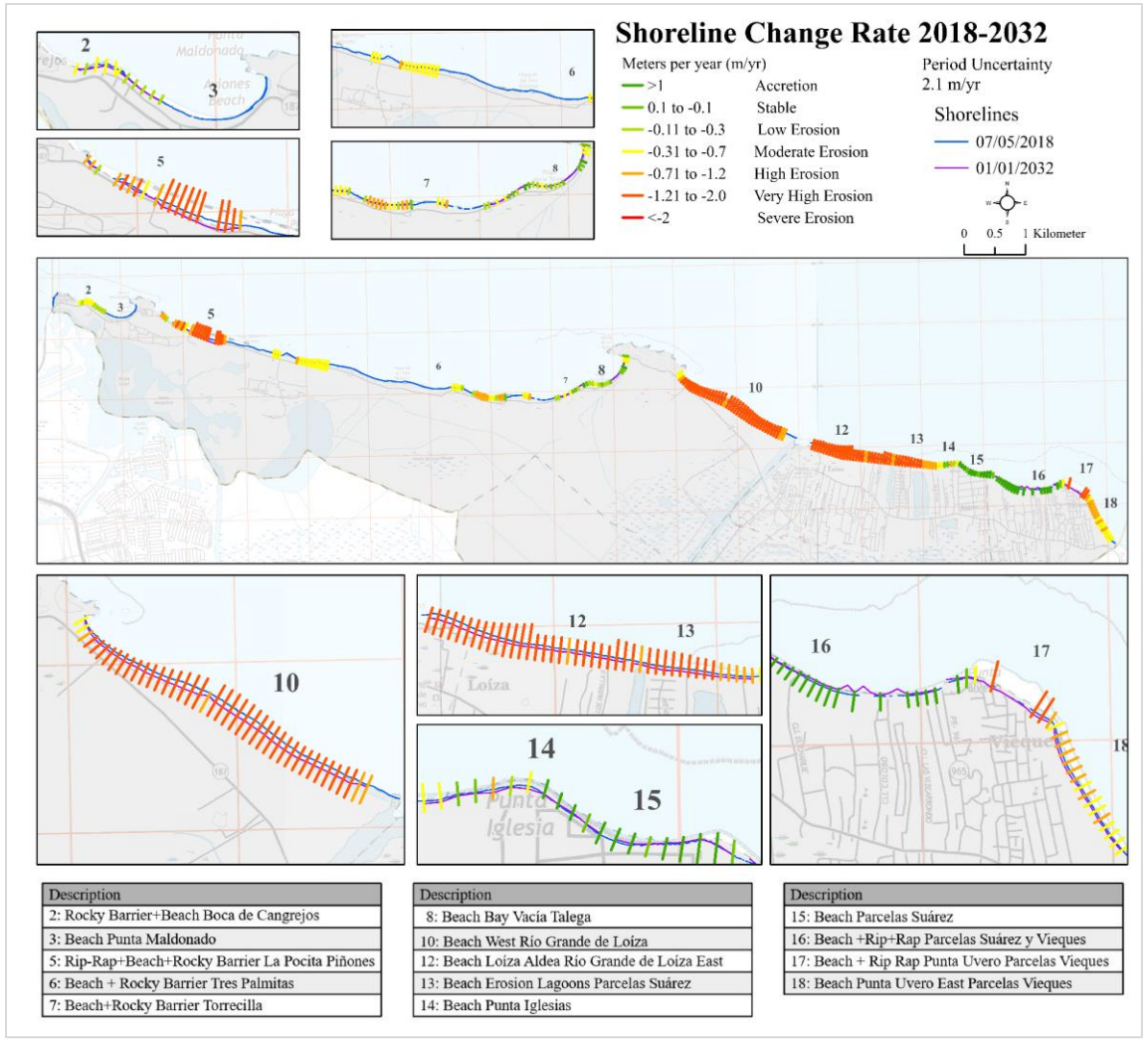

Figure 2.38: Forecasted Shoreline Change Rates (m/yr) at Loíza: 2018 – 2032

The rates forecasted for this period are summarized in Table 2.16. Most of the periods showed 100% erosional rates, with only one showing 100% accretional rates, at Beach between Parcelas Suárez and Vieques (GroupID:16). On average, 12 out of 14 areas (86%) showed erosion rates and two were accretional (14%).

Table 2.16: Summary of Statistics: 2018 – 2032

	Description	Average Positive Rates	Average Negative Rates	Average Rate	Maximum Positive Distance (meters)	Maximum Negative Distance (meters)	Average Positive Distance	Average Negative Distance	Average Distance
Period 2018-2032		0.36	-1.17	-0.94	13.57	-5035	4.91	-15.75	-12.67
By Group ID									
2	Beach Boca de Cangrejos	--	-0.48	-0.48	--	-9.48	--	-6.42	-6.42
3	Beach Punta Maldonado	--	-0.22	-0.18	--	-6.89	--	-3	-3
5	Beach La Pocita	--	-1.79	-1.79	--	-50.35	--	-24.16	-24.16
6	Beach Tres Palmitas	--	-0.52	-0.52	--	-10.14	--	-7.03	-37.84
7	Beach Torrecilla	0.1	-0.47	-0.42	1.49	-12.56	1.32	-6.28	-5.73
8	Beach Vacía Talega	0.1	-0.25	-0.15	2.25	-7.09	1.31	-3.41	-2.06
10	Beach West Río Grande de Loíza	--	-1.97	-1.97	--	-38.46	--	-26.52	-26.52
12	Beach Río Grande de Loíza East Loíza Aldea	--	-1.66	-1.66	--	-33.56	--	-22.38	-22.38
13	Beach Parcelas Suárez (erosion lagoons)	--	-1.31	-1.31	--	-22.91	--	-17.69	-17.69
14	Punta Iglesia sand pit	0.18	-0.41	-0.16	4.25	-9.74	2.4	-5.52	-2.22
15	Beach Parcelas Suárez	0.24	-0.05	0.16	5.5	-1.16	3.18	-0.7	2.21
16	Beach between Parcelas Suárez/Parcelas Vieques	0.59	--	0.59	13.57	--	7.95	--	7.95
17	Punta Uvero sand pit	0.33	-1	-0.62	7.59	-18.67	4.42	-13.46	-8.35
18	Beach Punta Uvero East	--	-0.76	-0.76	--	-14.8	--	-10.22	-10.22

	Description	Total Transects	Total positive rates	Total negative rates	% Transects Positive	% Transects Negative	Maximum Positive Rate (meters per year)	Maximum Negative Rate (meters per year)
Period 2018-2032		228	34	194	15	85	1.01	-3.73
By Group ID								
2	Beach Boca de Cangrejos	5	0	5	0	100	--	-0.7
3	Beach Punta Maldonado	6	0	6	0	100	--	-0.51
5	Beach La Pocita	19	0	19	0	100	--	-3.73
6	Beach Tres Palmitas	14	0	14	0	100	--	-0.75
7	Beach Torrecilla	28	2	26	7	93	0.11	-0.93
8	Beach Vacía Talega	14	4	10	29	71	0.17	-0.53
10	Beach West Río Grande de Loíza	42	0	42	0	100	--	-2.85
12	Beach Río Grande de Loíza East Loíza Aldea	26	0	26	0	100	--	-2.49
13	Beach Parcelas Suárez (erosion lagoons)	16	0	16	0	100	--	-1.7
14	Punta Iglesia sand pit	12	5	7	42	58	0.32	-0.72
15	Beach Parcelas Suárez	8	6	2	75	25	0.41	-0.09
16	Beach between Parcelas Suárez/Parcelas Vieques	15	15	0	100	0	1.01	--
17	Punta Uvero sand pit	7	2	5	29	71	0.56	-1.38
18	Beach Punta Uvero East	16	0	16	0	100	--	-1.1

2.4.3.2 Forecasted Shoreline Changes for 2018 – 2042

To forecast shoreline changes that might occur by 2040, 212 transects were analyzed. The highest frequency was observed in the high erosion category (26%, n = 56), followed by moderate erosion (23%, n = 48; Figure 2.39). The lowest frequency was observed for the accretion category, with 8% (n = 16). The categories for very high erosion, stable, and low erosion were present at frequencies of 18% (n = 38), 13% (n = 28), and 12% (n = 26), respectively. This scenario also suggests that more erosion will occur than accretion, although in comparison with the changes forecasted for 2032, very high erosion rates were decreased.

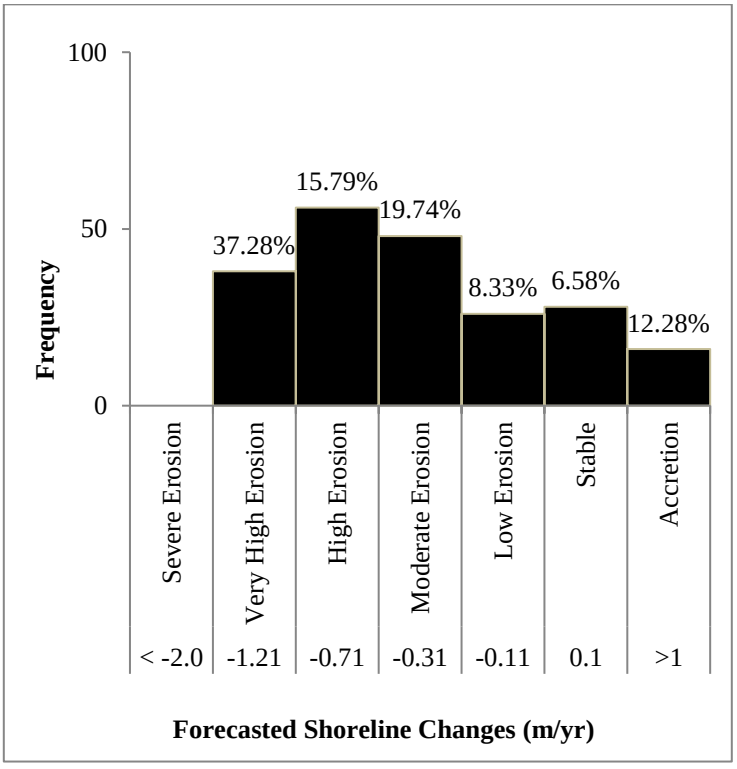

Figure 2.39: Frequencies of Different Types of Shoreline Change Rates (m/yr), Forecasted for 2018 – 2042

The forecasted rates of change are presented per Group ID in Figure 2.40. The maximum erosional rates were measured in the east and west of Río Grande de Loíza (Group ID:10, 12): -1.92 m/yr and -1.57, respectively. Most areas did not exhibit accretion rates, except for Beach Vacía Talega (Group ID:8), Punta Iglesia Sandpit (Group ID:17), Beach Parcelas Suárez erosional lagoons (Group ID: 15), and Beach between Parcelas Suárez and Vieques (Group ID: 16). Indeed, the latter showed 100% accretion rates. Overall, of the total 212 transects, 25 (12%) were accretional and 187 (88%) were erosional. The maximum erosion and accretion rates were -1.92 m/yr (-45.2 m) and 0.65 m/yr (15.3 m), respectively.

Figure 2.40: Frequencies of Forecasted Shoreline Change Rates (m/yr) from 2018 to 2042, by Classification (Stewart and Pope, 1993) and GroupID

Along the shoreline, I observed a combination of accretion and moderate erosion (Figure 2.41). Parcelas Suárez and Parcelas Vieques (GroupID:16) and Río Grande de Loíza west (GroupID:10) showed the maximum rates of accretion and erosion, with 0.65 myr^{-1} (15.3 m) and -1.92 myr^{-1} (-45.2 m), respectively.

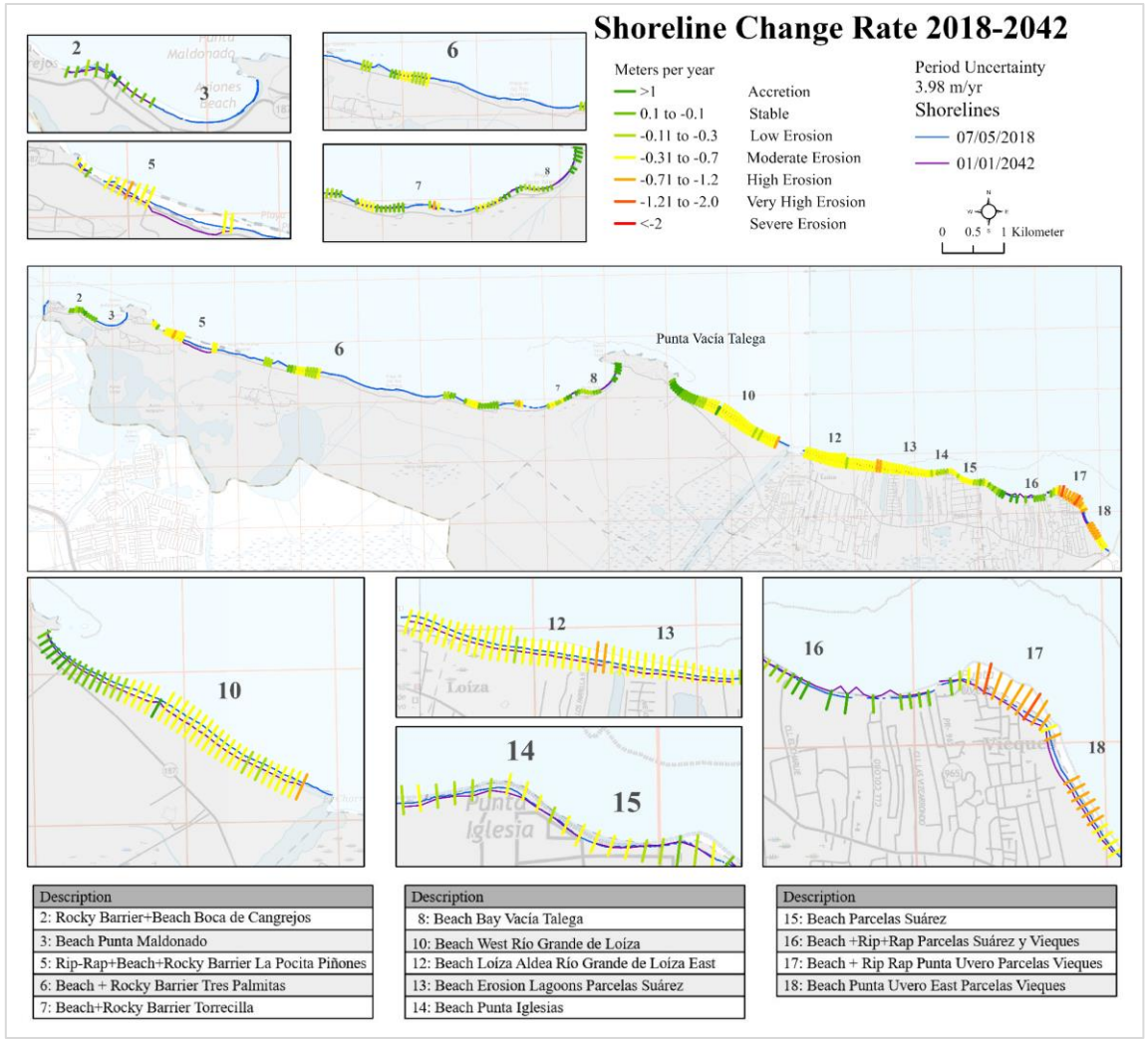

Figure 2.41: Forecasted Shoreline Change Rates (m/yr) at Loíza: 2018 – 2042

The rates of change for this forecasted period are summarized in Table 2.17. Eight areas showed 100% erosion rates and only one showed 100% accretional rates (Beach between Parcelas Suárez and Vieques, GroupID:16). On average, 12 out of the 14 Group IDs showed erosion rates (86%) and two were accretional (14%).

Table 2.17: Summary of Statistics: 2018 – 2042

	Description	Total Transects	Total positive rates	Total negative rates	% Transects Positive	% Transects Negative	Maximum Positive Rate (meters per year)	Maximum Negative Rate (meters per year)
Period 2018-2042		212	25	187	88	12	0.65	-1.92
By Group ID								
2	Beach Boca de Cangrejos	5	0	5	0	100	--	-0.43
3	Beach Punta Maldonado	6	0	6	0	100	--	-0.25
5	Beach La Pocita	11	0	11	0	100	--	-1.25
6	Beach Tres Palmitas	14	0	14	0	100	--	-0.55
7	Beach Torrecilla	28	2	26	7	93	0.13	-0.71
8	Beach Vacía Talega	12	3	9	25	75	0.18	-0.4
10	Beach West Río Grande de Loíza	42	0	42	0	100	--	-1.92
12	Beach Río Grande de Loíza East Loíza Aldea	26	0	26	0	100	--	-1.57
13	Beach Parcelas Suárez (erosion lagoons)	16	0	16	0	100	--	-1.22
14	Punta Iglesia sand pit	12	1	11	8	92	0.06	-0.58
15	Beach Parcelas Suárez	8	5	3	63	38	0.1	-0.18
16	Beach between Parcelas Suárez/Parcelas Vieques	13	13	0	100	0	0.65	--
17	Punta Uvero sand pit	7	1	6	14	86	0.35	-1.34
18	Beach Punta Uvero East	12	0	12	0	100	--	-0.9

	Description	Average Positive Rates	Average Negative Rates	Average Rate	Maximum Positive Distance (meters)	Maximum Negative Distance (meters)	Average Positive Distance	Average Negative Distance	Average Distance
Period 2018-2042		0.22	-0.75	-0.64	15.3	-45.2	5.23	-17.64	-14.95
By Group ID									
2	Beach Boca de Cangrejos	--	-0.27	-0.27	--	-10.06	--	-6.32	-6.32
3	Beach Punta Maldonado	--	-0.09	-0.09	--	-5.8	--	-2.13	-2.13
5	Beach La Pocita	--	-0.77	-0.77	--	-29.32	--	-18.03	-18.03
6	Beach Tres Palmitas	--	-0.41	-0.41	--	-12.97	--	-9.53	-9.53
7	Beach Torrecilla	0.13	-0.34	-0.31	3.15	-16.66	3.03	-7.97	-7.18
8	Beach Vacía Talega	0.16	-0.16	-0.08	4.21	-9.31	3.82	-3.86	-1.94
10	Beach West Río Grande de Loíza	--	-1.25	-1.25	--	-45.2	--	-29.47	-29.47
12	Beach Río Grande de Loíza East Loíza Aldea	--	-1.14	-1.14	--	-36.92	--	-26.81	-26.81
13	Beach Parcelas Suárez (erosion lagoons)	--	-0.96	-0.96	--	-28.7	--	-22.44	-22.44
14	Punta Iglesia sand pit	0.06	-0.27	-0.24	1.32	-13.73	1.32	-6.28	-5.65
15	Beach Parcelas Suárez	0.04	-0.12	-0.02	2.23	-4.28	0.98	-2.76	-0.42
16	Beach between Parcelas Suárez/Parcelas Vieques	0.32	--	0.32	15.3	--	7.6	--	7.6
17	Punta Uvero sand pit	0.35	-0.83	-0.66	8.18	-31.44	8.18	-19.57	-15.61
18	Beach Punta Uvero East	--	-0.68	-0.68	--	-21.25	--	-16.07	-16.07

2.4.3.3 Comparison of Forecasted Periods

The rates forecasted by 2032 and 2042 showed scenarios for different areas in Loíza. Seven of the sites showed the same proportions of erosion rates in both forecasted years. Four areas differed in terms of erosional rates, however, showing higher erosion rates by 2042: Beach Vacía Talega (GroupID: 8), Punta Iglesias sandpit (Group ID: 14), Beach Parcelas Suarez (Group ID:15), and Punta Uvero sandpit (Group ID: 17).

Most areas showed no accretion rates for either forecasted scenario. Only six areas showed accretion rates, and Beach between Parcelas Suárez and Parcelas Vieques (GroupID: 16) showed 100% accretion rates in both projections. In most cases, however, accretional rates decreased by 2042.

2.4.4 Statistically Significant Transects (SSTs) by Period According to Uncertainty

In this section, I will present the statistically significant transects (SSTs) for each period. As explained Section 1.2.4, each shoreline was assigned an uncertainty value (see Equation 2.1and Equation 2.2).

The total SSTs per period are shown in Figure 2.42, including the linear regression rates (LRR and WLR) and forecasted periods. The period that showed the highest percentage of SST accretion rates was 1951 – 1977 (84%), followed by 2010 – 2018 (77%). In contrast, the highest percentage of SST erosion rates was observed during 1977 – 1990 (58%) and 1990 – 2010 (56%). The periods with the lowest percentage of SST accretion rates were 1977 – 1990 (1%) and 1990 – 2010 (28%), and the lowest percentage of SST erosion rates were in 2010 – 2018 (5%), 1902 – 1931 (12%), and 1951 – 1977 (12%).

The forecasted periods (2018 – 2032, 2018 – 2042) showed 0% accretion rates, but showed 15% SST erosion rates for 2018 – 2032 and 18% SST erosion rates for 2018 – 2042. The linear regression showed a similar pattern, where the highest percentage of SSTs was observed in erosion rates: LRR with 16% and WLR with 14%.

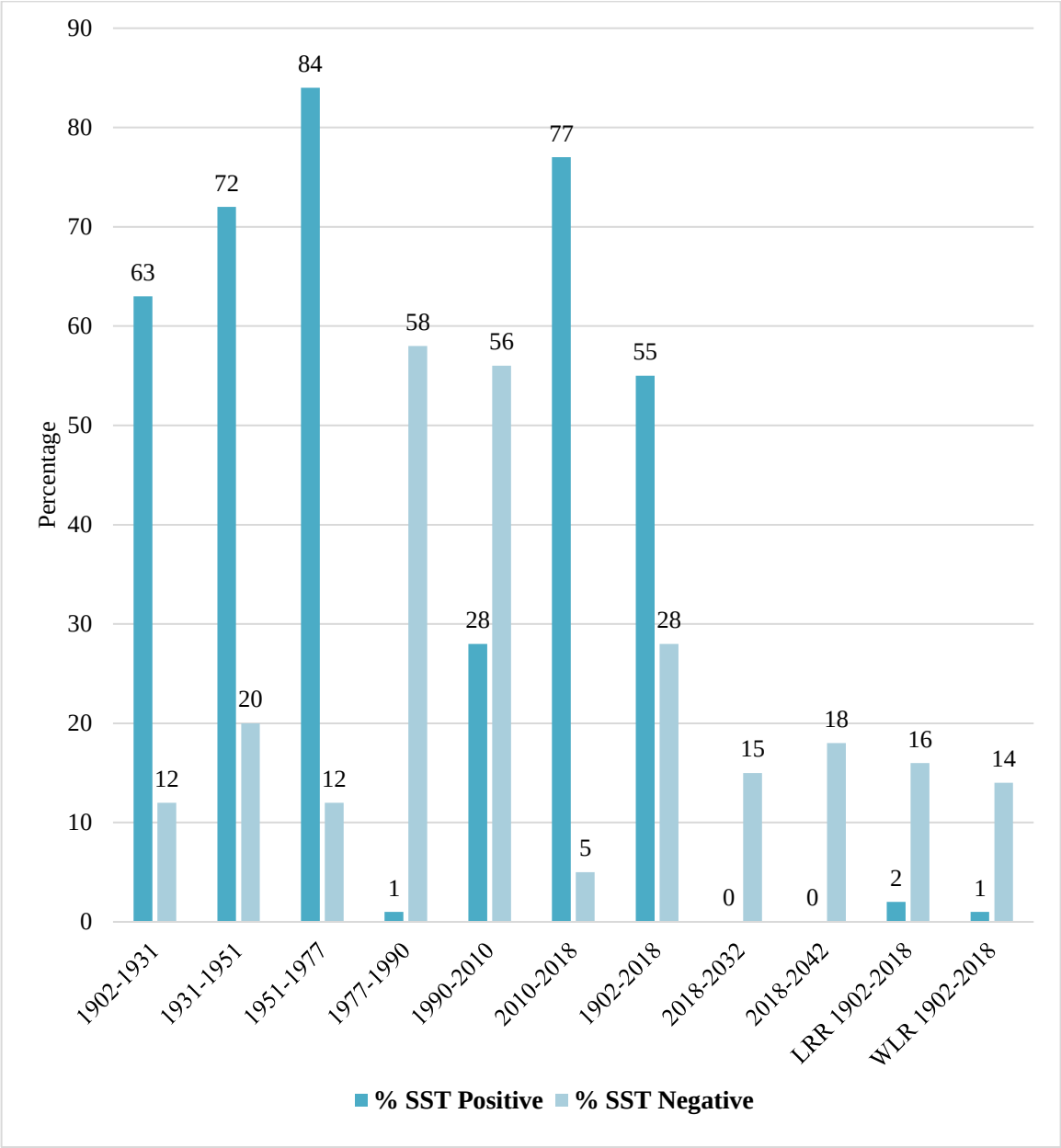

Figure 2.42: Percentage of Statistically Significant Transects (SST) per Period

The following tables present SSTs by Group ID. Some areas showed 100% accretion or erosion rates, indicating greater certainty that the measured rates in those areas were indeed either accretional or erosional, respectively. For example, during the period 1902 – 1931 (Table 2.18), areas such as La Pocita (Group ID:5), West and East Río Grande de Loíza (GroupID: 10, 12), and Beach Parcelas Suárez erosional lagoons (GroupID: 13) showed 100% SSTs in accretion rates.

Other areas showed that 100% of the erosion rates were SSTs. For example, for the period 1977 – 1990 (Table 2.19), areas such as East Río Grande de Loíza (GroupID:12), Punta Iglesia Sandpit (GroupID:14), and Punta Uvero sandpit (GroupID: 7) showed this pattern. Moreover, for 1977 – 1990, Beach Parcelas Suárez with the erosional lagoons (Group ID: 13) showed that 67% of transects were SSTs. Forecasted periods (2018-2032 and 2018-2042) showed less SST (Table 2.20), Río Grande de Loíza West (GroupID:10) being the highest for both periods (52 and 60%, respectively).

The LRR showed 2% SSTs for accretion and 16% for erosion rates (Table 2.21). For accretion rates, Vacía Talega (GroupID:8) and Beach between Parcelas Suárez and Vieques (GroupID:16) showed 16% and 24% STTs. For erosion rates, La Pocita (GroupID:5) and Punta Uvero east (GroupID:17) showed the highest percentages of SSTs, with 67% and 65%, respectively.

The WLR (Table 2.21) showed 1% STTs for accretion and 14% SSTs for erosion rates. Punta Uvero sandpit and east (GroupID:17, 18) showed the highest values for erosion rates, with 62% and 88% SSTs, respectively. For accretion rates, Vacía Talega (GroupID:8) showed 16% SSTs.

The SST calculation for the LRR and WLR used the LCI with a 95.5% confidence level. In summary, the LRR showed 2% SST for accretion and 16% for erosion rates. For erosion rates (Table 2.21), La Pocita (GroupID:5) and Punta Uvero east (GroupID:17) showed the highest percentages of SSTs, with 67% and 65%, respectively. Tres Palmitas (GroupID:6) and Torrecilla (GroupID:7) each presented 20% SSTs. For accretion rates, Vacía Talega (GroupID:8) and Beach between Parcelas Suárez and Vieques (GroupID:16) showed 16% and 24% STTs, respectively.

The WLR SST results (Table 2.21) showed 1% STTs for accretion and 14% SSTs for erosion rates. Punta Uvero sandpit and east (GroupID:17, 18) showed the highest values for erosion rates, with 62% and 88% SSTs, respectively. For accretion, Vacía Talega (GroupID:8) showed 16% SSTs, and Tres Palmitas (GroupID:6) and Torrecilla (GroupID:7) showed 11% and 13% SSTs, respectively.

Table 2.18: Statistically Significant Transects (Percentages) by Group ID: 1902 – 1931, 1931 – 1951, 1951 – 1977

Group ID	Description	General Area	1902-1931		1931-1951		1951-1977	
			+	-	+	-	+	-
2	Beach Boca de Cangrejos	Piñones	--	33	--	--	--	100
3	Beach Punta Maldonado	Piñones	--	--	--	--	--	--
5	Beach La Pocita	Piñones	100	--	--	--	--	--
6	Beach Tres Palmitas	Tres Palmitas	--	--	--	--	--	--
7	Beach Torrecilla	Torrecilla	0	50	63	31	--	--
8	Beach Vacía Talega	Vacía Talega	37	16	37	47	42	47
10	Beach West Río Grande de Loíza	Río Grande de Loíza	100	--	80	13	--	100
12	Beach Río Grande de Loíza East Loíza Aldea	Loíza Aldea	100	--	92	1	--	100
13	Beach Parcelas Suárez (erosion lagoons)	Parcelas Suárez	100	--	100	--	--	100
14	Punta Iglesia sand pit	Parcelas Suárez	--	--	100	--	--	100
15	Beach Parcelas Suárez	Parcelas Suárez	38	0	100	--	67	
16	Beach between Parcelas Suárez/Parcelas Vieques	Parcelas Suárez & Parcelas Vieques	95	--	100	--	--	100
17	Punta Uvero sand pit	Parcelas Vieques	85	1	44	56	--	100
18	Beach Punta Uvero East	Parcelas Vieques	--	65	7	53	--	--

Table 2.19: Statistically Significant Transects (Percentages) by Group ID: 1977 – 1990, 1990 – 2010, 2010 – 2018

Group ID	Description	General Area	1977-1991		1991-2010		2010-2018		1902-2018	
			+	-	+	-	+	-	+	-
2	Beach Boca de Cangrejos	Piñones	--	--	--	--	100	--	--	100
3	Beach Punta Maldonado	Piñones	--	--	--	--	--	71	--	79
5	Beach La Pocita	Piñones	18	41	--	100	--	94	--	100
6	Beach Tres Palmitas	Tres Palmitas	--	--	--	--	80	9	4	93
7	Beach Torrecilla	Torrecilla	0	50	0	50	62	6	0	87
8	Beach Vacía Talega	Vacía Talega	17	28	58	25	67	--	37	16
10	Beach West Río Grande de Loíza	Río Grande de Loíza	--	--	--	--	95	0	48	21
12	Beach Río Grande de Loíza East Loíza Aldea	Loíza Aldea	--	100	--	100	100	--	100	--
13	Beach Parcelas Suárez (erosion lagoons)	Parcelas Suárez	0	69	1	0	100	--	69	0
14	Punta Iglesia sand pit	Parcelas Suárez	--	100	--	100	60	40	0	50
15	Beach Parcelas Suárez	Parcelas Suárez	--	100	--	100	--	0	38	25
16	Beach between Parcelas Suárez/Parcelas Vieques	Parcelas Suárez & Parcelas Vieques	33	0	--	100	25	0	100	--
17	Punta Uvero sand pit	Parcelas Vieques	--	100	80	10	0	67	23	77
18	Beach Punta Uvero East	Parcelas Vieques	--	100	--	100	0	0	--	100

Table 2.20: Statistically Significant Transects (Percentages) by Group ID: 1902 – 2018, 2018 – 2032, 2018 – 2042

Group ID	Description	General Area	1902-2018		2018-2032		2018-2042	
			+	-	+	-	+	-
2	Beach Boca de Cangrejos	Piñones	--	100	0	0	0	0
3	Beach Punta Maldonado	Piñones	--	79	0	0	0	0
5	Beach La Pocita	Piñones	--	100	0	42	0	5
6	Beach Tres Palmitas	Tres Palmitas	4	93	0	0	0	0
7	Beach Torrecilla	Torrecilla	0	87	0	0	0	0
8	Beach Vacía Talega	Vacía Talega	37	16	0	0	0	0
10	Beach West Río Grande de Loíza	Río Grande de Loíza	48	21	0	52	0	60
12	Beach Río Grande de Loíza East Loíza Aldea	Loíza Aldea	100	--	0	19	0	35
13	Beach Parcelas Suárez (erosion lagoons)	Parcelas Suárez	69	0	0	0	0	6
14	Punta Iglesia sand pit	Parcelas Suárez	0	50	0	0	0	0
15	Beach Parcelas Suárez	Parcelas Suárez	38	25	0	0	0	0
16	Beach between Parcelas Suárez/Parcelas Vieques	Parcelas Suárez & Parcelas Vieques	100	--	0	0	0	0
17	Punta Uvero sand pit	Parcelas Vieques	23	77	0	0	0	29
18	Beach Punta Uvero East	Parcelas Vieques	--	100	0	0	0	0

Table 2.21: Statistically Significant Transects (Percentages) by Group ID: Linear Regression Rates (LRR) and Weighted Linear Regression Rates (WLR)

Group ID	Description	General Area	LRR		WLR	
			+	-	+	-
2	Beach Boca de Cangrejos	Piñones	--	0	--	0
3	Beach Punta Maldonado	Piñones	--	7	0	0
5	Beach La Pocita	Piñones	--	67	--	38
6	Beach Tres Palmitas	Tres Palmitas	4	20	13	0
7	Beach Torrecilla	Torrecilla	0	20	11	13
8	Beach Vacía Talega	Vacía Talega	16	0	16	0
10	Beach West Río Grande de Loíza	Río Grande de Loíza	0	2	0	5
12	Beach Río Grande de Loíza East Loíza Aldea	Loíza Aldea	0	0	--	0
13	Beach Parcelas Suárez (erosion lagoons)	Parcelas Suárez	--	0	--	0
14	Punta Iglesia sand pit	Parcelas Suárez	0	0	--	0
15	Beach Parcelas Suárez	Parcelas Suárez	0	0	0	0
16	Beach between Parcelas Suárez/Parcelas Vieques	Parcelas Suárez & Parcelas Vieques	24	--	10	--
17	Punta Uvero sand pit	Parcelas Vieques	0	31	0	62
18	Beach Punta Uvero East	Parcelas Vieques	--	65	--	88

2.4.5 Shoreline Change Rate Comparisons and Statistical Testing

The previous sections presented the results by periods. This section will compare shoreline change rates among the historical periods and the LRR. Descriptive statistics will be used to describe the differences broadly. In addition, the results of comparisons using the one-sample t-test, two-sample paired t-test, and Wilcoxon test will be described.

2.4.5.1 Descriptive Statistics for Shoreline Change Comparisons

The shoreline change rates of all the historical periods are presented in Figure 2.43. I compared rates of change per period and the linear regressions. After analyzing the rate categories, none of the periods showed severe erosion.

The very high erosion category showed a steep increase from Period 2 to Period 3 (2% to 59%), but then showed a decrease in Period 4 (59% to 31%) and was not present in Period 5. In Periods 6 and 7, it was present less than 5% of the time, but Periods 8 and 9 forecasted that very high erosion would increase.

High erosion showed a consistent increase from Period 1 to Period 4 (from 4% to 6% to 8% to 18%), followed by uninterrupted decreases in Periods 5 and 6 (10% to 2%). Periods 8 and 9 forecasted an increase from 16% to 26% in this category. Moderate erosion showed a continuous increase until Period 5 (8% to 11% to 13% to 21%), but then dropped to 3% in P6. Periods 8 and 9 forecasted an increase from 20% to 23%.

The low erosion category showed a reduction in Period 2, from 10% to 2%, followed by a consistent increase from Period 3 to Period 5 (6% to 13% to 21%), and then a steep decrease in Period 6 (4%). Periods 8 and 9 forecasted an increase from 8% to

12%. The stable category showed a 1% increase from Period 1 to Period 2 (6% to 7%), and then a decrease in Period 3 (4%). Afterward, Periods 4 and 5 showed an increase from 8% to 17%, followed by another drop in Period 6 (3%). Periods 8 and 9 forecasted a steep increase from 13% to 17%.

The accretion category slightly increased from Period 1 to Period 2 (71% to 72%), steeply decreased in Period 3 to 12%, increased slightly to 17% in Period 4, and a then decreased again in Period 5 (10%), followed by a significant increase of 86% in Period 6, the highest accretion rate among all the periods. Periods 8 and 9 projected a decrease from 12% to 8%.

In summary, Period 6 showed the highest percentage in accretion, and Period 3 showed the highest percentage in very high erosion. The period with the highest percentage of high erosion was Period 4, and the period with the highest percentage of stable, low erosion, and moderate erosion was Period 5.

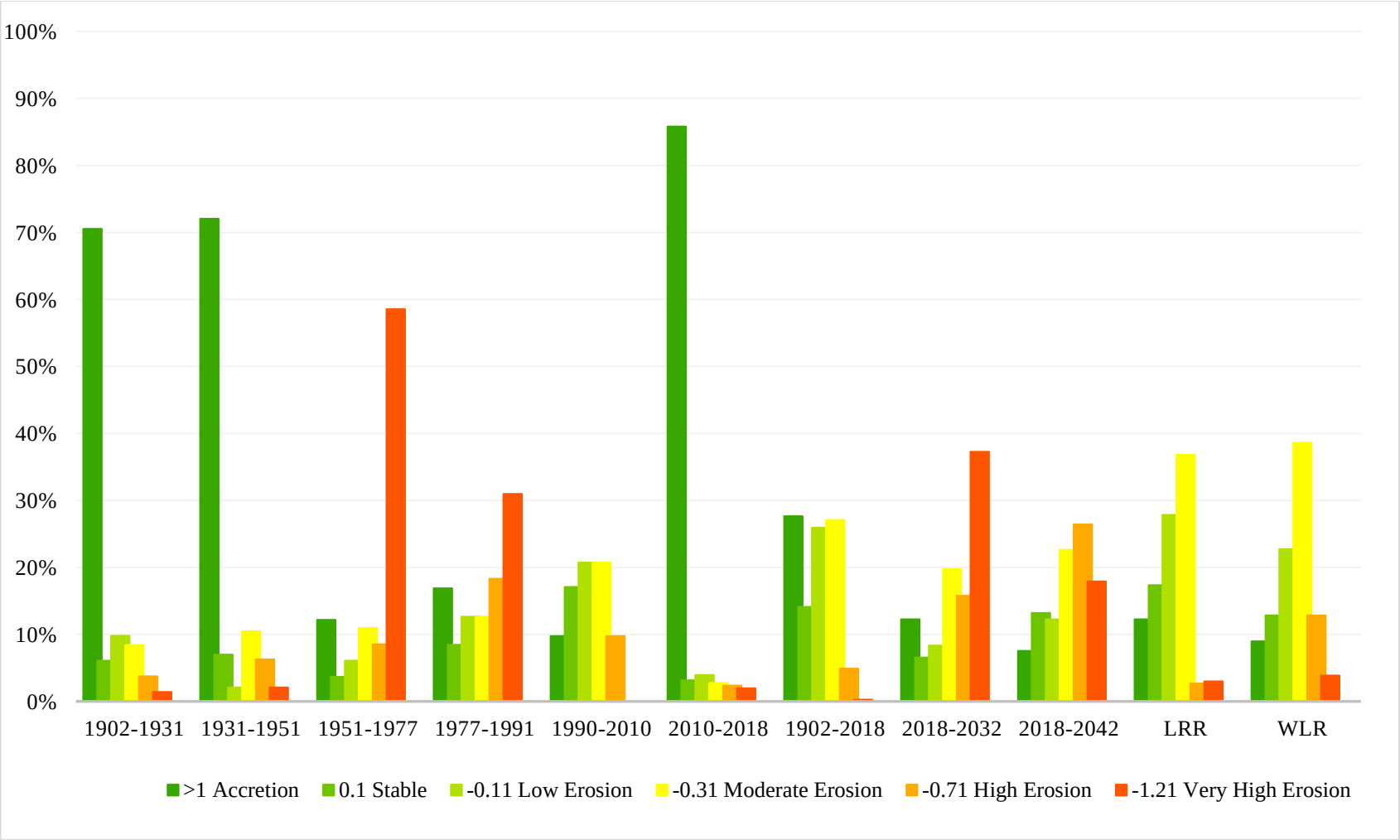

Figure 2.43: Comparison of Shoreline Change Rates (m/yr) by Period, Including Two Forecasted Periods and Both Linear Regression Rates (LRR) and Weighted Linear Regression Rates (WLR)

In both the linear regression model (LRR) and the weighted linear regression model (WLR), none of the projections surpassed 50% per category (Figure 2.44). For the categories of very high erosion, high erosion, and moderate erosion, the WLR showed more percentages. In contrast, for the low erosion, stable, and accretion categories, the LRR exceeded the WLR. Regardless, the highest frequencies in each projection were for moderate erosion, followed by low erosion, stable, and accretion. High erosion and very high erosion showed the lowest frequencies. The greatest difference between the WLR and LRR projections was observed for the high erosion category, with a variation from 3% (LRR) to 13% (WLR).

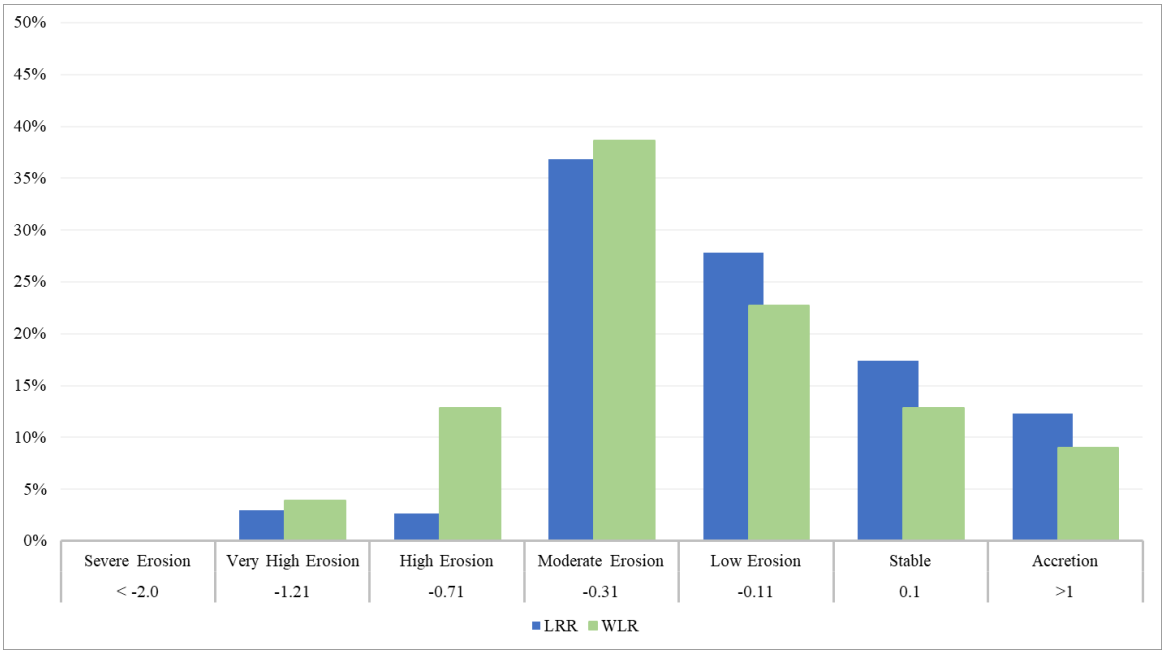

Figure 2.44: Comparison between Linear Regression Rates (LRR) and Weighted Linear Regression Rates (WLR) for Different Types of Shoreline Change

Maps showing the differences in rate categories for each period, long-term, projection, and WLR and LRR along Loíza's shoreline are presented in Figure 2.45. These maps indicate, for example, increases or decreases in patterns of erosion or accretion rates through time.

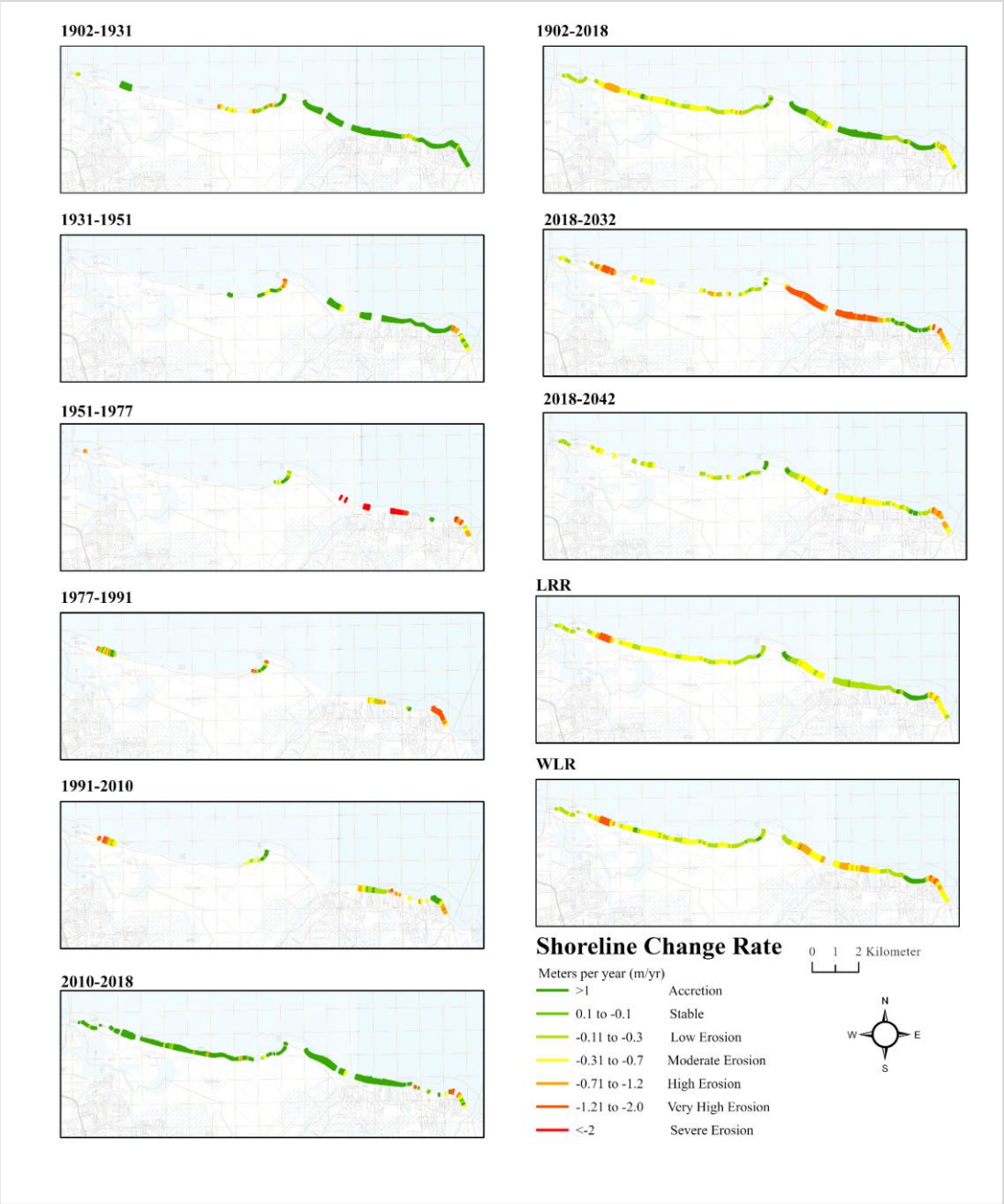

Figure 2.45: Comparison of Shoreline Change Rates (m/yr) by Period, Including Two Forecasted Periods and Both Linear Regression Rates (LRR) and Weighted Linear Regression Rates (WLR)

The western section of the shoreline showed fewer samples, in areas such as La Pocita and Vacía Talega, some patterns can be described. For example, at La Pocita (GroupID:6), accretion rates were measured in Period 1, but in Period 5, erosion rates started to rise and continued to rise in the last period (2010 – 2018). At Vacía Talega

(GroupID:8), accretion rates dominated most of periods, but in Period 4, erosion rates were documented at the bay area sides.

On the east side of Loíza, from Period 1 to Period 5, a constant increase in erosion rates was observed. In Period 6, however, most areas showed accretion rates except in the eastern section (Punta Iglesias, GroupID:14) and Punta Uvero sandpit (GroupID:14). At Punta Uvero (GroupID:17, 18), erosion rates rose from Period 1 until Period 5, when accretion rates were measured north of the sandpit. In Period 6, erosion rates were measured again. In the long-term, from 1902 to 2018, a combination of very high, high, and moderate erosion was measured. Areas like the beach between Parcelas Suárez and Vieques (GroupID:16) and Tres Palmitas (GroupID:6) mainly showed accretion rates, although Period 8 forecasted mostly moderate erosion in the same areas.

Lastly, the LRR showed areas like the Beach of Parcelas Suárez (GroupID:13) to be stable, whereas the WLR showed this area to have high and moderate erosion. In the most recent period (Period 6), mainly accretion rates were documented at the western section of Loíza's shoreline.

2.4.5.2 One-Sample T-Test and Wilcoxon: Shoreline Changes (m/yr)

I explored the rates per period using different statistical analyses and plots. A boxplot presenting the outliers and data skewness by each period is shown in Figure 2.46. Analyzing these characteristics can aid in determining if data have a normal distribution or are inclined to negative or positive values. To this end, I used these plots to understand the outliers for each period and understand if certain periods were more inclined to have positive (accretion) or negative (erosion) rates.

For Periods 1 and 2, the median was positive and close to zero, whereas Periods 4 and 5 showed negative medians, also close to zero. In Period 3, the median was negative and closer to -2, and Period 6 had a positive median closer to 2. Four periods showed outliers: Periods 1, 4, 5, and 6. Period 4 showed the highest number of negative outliers and Period 6 (2010 – 2018) showed the highest number of positive outliers. The only period showing a symmetric or normal distribution was Period 5 (1990 – 2010), which had a negative outlier in the positive range.

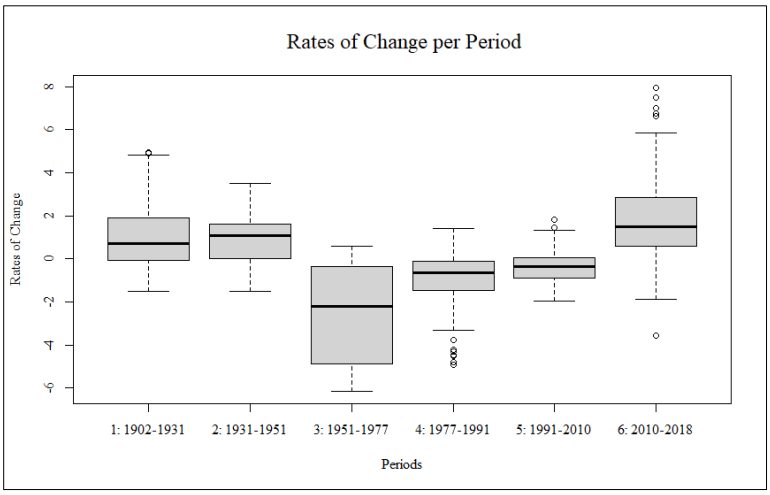

Figure 2.46: Boxplot Showing Rates of Change per Period

Periods 1and 6 showed a right-skewed distribution (positive), whereas the rest showed a left-skewed distribution (tendency to negative), except for Period 5, which was symmetric. The period with most left distribution (negative tendency) was Period 3, followed by Periods 2 and 4, suggesting that these periods have overall erosion rates rather than accretion rates.

The boxplots of both forecasted periods (Periods 8 and 9) showed negative medians (Figure 2.47). Period 8 showed a left-skewed distribution and Period 9 showed a right-skewed distribution. Both periods showed outliers: Period 8 had 27 and Period 9 had 16.

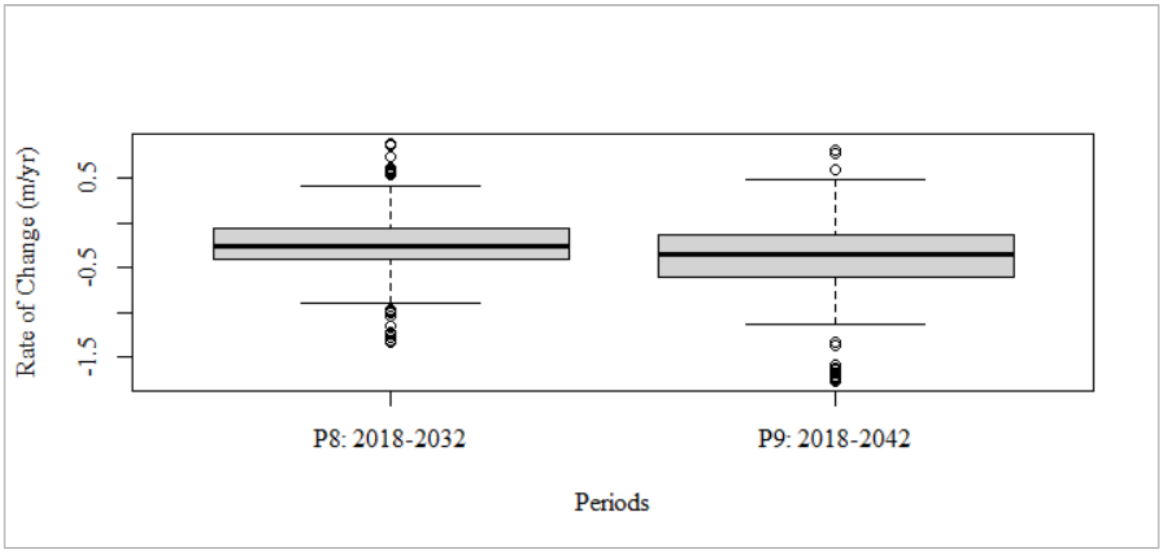

Figure 2.47: Boxplot Showing Rates of Change for Two Forecasted Periods: 2018 to 2032 and 2018 to 2042

After analyzing the boxplots, I determined that the data did not follow a normal distribution and those outliers could alter the results of pair comparisons and t-tests. Hence, both parametric and non-parametric versions were run for each period—a t-test and a Wilcoxon one-pair analysis to determine if erosion or accretion dominated a period. Afterward, I compared the statistical differences among means and medians using the pairwise t-test (mean) and the Wilcoxon test (median), to establish if accretion or erosion rates dominated the sites in statistically significant ways.

The results of testing if accretion rates dominated a period are shown in Table 2.22. This test was run for Periods 1, 2, and 6. All three periods showed significance—in both tests—indicating that overall, the three periods were dominated by accretion rates.

Table 2.22: T-Test and Wilcoxon Test Results for the Periods 1902 – 1931 (P1), 1931 – 1951 (P2), and 2010 – 2018 (P6)

H_0 **Null Hypothesis**	H_A **Alternative Hypothesis**	**Period**	***df***	**T-Test p-value**	**Wilcoxon p-value**	**Conclusion**
$d \leq 0$ True mean/median difference is less than zero	$d > 0$ True mean is more than zero. Therefore, either the first period has higher accretion rates, or second period has higher erosion rates	P1: 1902-1931	213	2.20E-16	2.20E-16	H_0 can be rejected. The period has significant overall accretion values.
		P2: 1931-1951	142	2.20E-16	3.04E-14	
		P6: 2010-2018	253	2.20E-16	2.23E-16	

The results of testing if erosion rates dominated Periods 3, 4, and 5 are shown in Table 2.3. The t-test and the Wilcoxon test showed statistical significance, indicating that these periods were, overall, dominated by erosion rates, in contrast to Periods 1, 2, and 6.

Table 2.23: T-Test and Wilcoxon Test Results for the Periods 1951 – 1977 (P3), 1977 – 1990 (P4), and 1990 – 2010 (P5)

H_0 **Null Hypothesis**	H_A **Alternative Hypothesis**	**Period**	***df***	**T-Test p-value**	**Wilcoxon p-value**	**Conclusion**
$\mu > 0$ $\eta > 0$ True mean/median is more than zero	$\mu < 0$ $\eta < 0$ True mean/median is less than zero. Therefore, the period has overall erosion.	P3: 1951-1977	81	2.20E-16	2.64E-13	can be rejected. The H_0 period has significant overall erosion values.
		P4: 1977-1991	70	6.36E-08	1.46E-08	
		P5: 1990-2010	81	6.97E-05	2.46E-05	

2.4.5.3 Two-Sample Tests: Paired T-Test and Wilcoxon Test

After analyzing each period individually, I compared pairs in chronological order. A pair comparison t-test and Wilcoxon test were run simultaneously for each pair of periods, running one-tailed and two-tailed analyses for both tests. I used the one-tailed tests to determine if the first period had higher accretion rates or the second had higher erosion

rates, and the two-tailed tests to determine if there was a statistical difference between each pair of periods.

The results of the one-tailed tests for each pair of time periods are shown in Table 2.24. The first question was: Which period presents higher accretion or erosion rates? Thus, the alternative hypothesis was that the first period had higher accretion rates than the second period, or the second had higher erosion rates than the first period. This alternative hypothesis was only accepted when comparing Periods 2 and 3. For the remaining comparisons, the null hypothesis was not rejected. The results of the paired t-tests and the Wilcoxon tests yielded the same conclusions.

Table 2.24: Results of Paired T-Tests and Wilcoxon Tests (One-tailed) Comparing Pairs of Time Periods

H_0 **Null Hypothesis**	H_A **Alternative Hypothesis**	**Period 1 (P1)**	**Period 2 (P2)**	***df***	**Pair T-Test p-value**	**Wilcoxon p-value**	**Conclusion**
$d \leq 0$	$d > 0$	P1: 1902-1931	P2: 1931-1951	142	0.58	0.74	H_0 can't be rejected. Between 1902-1931 &1931-1951, there is no statistical significance to determine that the P1 has higher accretion rates or that P2 has higher erosion rates.
True mean/median is less than zero	True mean/median difference is more than zero. Therefore, either the first period has higher accretion rates, or second period has higher erosion rates	P2: 1931-1951	P3: 1951-1977	74	6.57E-14	3.13E-10	H_0 can be rejected. Between 1931-1951 & 1951-1977, we have statistical significance to determine that P2 has higher accretion rates or P3 has higher erosion
		P3: 1951-1977	P4: 1977-1991	48	0.80	0.60	H_0 can't be rejected. Between 1951-1977 & 1977-1991, there is no statistical significance to
		P4: 1977-1991	P5: 1990-2010	56	0.99	0.99	H_0 can't be rejected. Between 1977-1991 & 1991-2010, there is no
		P5: 1990-2010	P6: 2010-2018	73	1.00	1.00	H_0 can't be rejected. Between 1991-2010 & 2010-2018, there is no

The results of the two-tailed analysis to determine whether there were statistical differences between pairs of periods are shown in Table 2.25. Periods 2 and 3, Periods 4

and 5, and Periods 5 and 6 were statistically different, but the null hypothesis could not be rejected for the comparisons between Period 1 and 2, and Period 3 and 4.

In general, if the one-tailed analysis (Table 2.24) yielded a *p-value* < 0, the two-tailed analysis (Table 2.25) also yielded a *p-value* < 0, with two exceptions in the latest periods. The one-tailed comparison between Periods 4 and 5 did not significantly determine which period had higher accretion or erosion, but it did detect that there was a statistically significant difference between the two periods. The same pattern was observed between Periods 5 and 6.

Table 2.25: Results of Paired T-Tests and Wilcoxon Tests (Two-Tailed) Comparing Pairs of Time Periods

H_0 **Null Hypothesis**	H_A **Alternative Hypothesis**	**Period 1 (P1)**	**Period 2 (P2)**	***df***	**Pair T-Test p-value**	**Wilcoxon p-value**	**Conclusion**
$d = 0$	$d \neq 0$	P1: 1902-1931	P2: 1931-1951	142	0.83	0.52	H_0 can't be rejected. Between 1902-1931 & 1931-1951, there is no statistical significance to determine there were statitically different.
Two mean/median are equal	Two mean/median are not equal. Therefore, there are statistically different.	P2: 1931-1951	P3: 1951-1977	74	1.31E-13	6.27E-10	H_0 can be rejected. Between 1931-1951 & 1951-1977, there is statitical difference.
		P3: 1951-1977	P4: 1977-1991	48	0.40	0.80	H_0 can't be rejected. Between 1951-1977 & 1977-1990, there is no statistical significance to determine there were statitically different.
		P4: 1977-1991	P5: 1991-2010	56	0.002816	0.008949	H_0 can be rejected. Between 1977-1991 & 1990-2010, there is statitical difference.
		P5: 1990-2010	P6: 2010-2018	73	6.20E-12	4.87E-10	H_0 can be rejected. Between 1990-2010 & 2010-2018, there is statitical difference.

2.5 Discussion

This work aimed to contribute to the evaluation of both short- and long-term shoreline change analyses for most of the shorelines at Loíza, Puerto Rico. Digital Shoreline Analysis System (DSAS) and other statistics integration made possible the analysis of specific patterns by areas and general trends. Furthermore, this research can contribute to present studies to address the already known physical and social vulnerability (Ruiz Vélez, 2014). The SCA in Loíza showed different erosion and accretion patterns. An increase in erosion rates was observed, especially for the period 1951 – 1977. In the most recent period (2010 – 2018), however, accretion rates were also observed in some areas.

Punta Uvero showed consistent erosion rates until 1990 – 2010, when a few accretion rates were observed in the sandpit. Between 2010 and 2018, erosion rates were present north of the sandpit, and accretion, stable, and high erosion categories were observed in the east section. The overall pattern observed, however, was erosion from east to west in the sandpit.

The sand extraction documented in Loíza since 1965 (El Mundo, 1965; Rojas Daporta, 1965; Sánchez Cappa, 1968) could explain the rates from 1951 – 1977. Historical photography from 1971 showed evidence of extraction near the Río Grande de Loíza mouth (El Mundo, 1971) and the communities' protests against these practices (El Mundo, 1973). For example, the results for Parcelas Suárez (erosion lagoons) showed accretion until this period, which was then dominated by very high erosion. The accretion in that area in previous periods (1902 – 1931 and 1931 – 1951) could explain why companies and people collected sand there.

I also observed a recovery in the erosional lagoons, however, as very high erosion rates decreased to high erosion, moderate erosion, and accretion. The recovery could be the effect of (1) wave activity in this area, which breaks at an angle, moving the sediment along the shore (Bird, 2008) from Punta Iglesias to Río Grande de Loíza; or (2) the discharge sediments input from the Río Grande de Loíza. Future studies should further analyze waves and sediment transport in the area.

The Río Grande de Loíza area also showed an abrupt switch from accretion to erosion in 1951 – 1977. One of the possible reasons for this is that the droughts documented in 1957, 1964, 1967, and 1973 – 1976 could have reduced the river discharge (EcoExploratorio, 2020). Another possible reason is the construction of a dam in 1953 at Barrio Carraízo (Ortiz Zayas et al., 2004), which limited the river discharge. Any combination of these factors could have caused less discharge and, hence, less sediment added to the shoreline. Further analysis of river discharge should be addressed to measure how these two scenarios and the sand extraction may have affected sediment availability along the Río Grande de Loíza's shoreline.

In addition, for the period 1951 – 1977, I observed the highest erosion rates in the Punta Uvero area. Areas between rocky areas or sandpits, such as Vacía Talega and the beach between Parcelas Suárez and Vieques, showed mostly accretion rates. During 1931 – 1951, however, Vacía Talega showed erosion rates, which decreased to high erosion and then mostly accretion in 2010 – 2018. La Pocita showed accretion in the first period, but erosion rates were measured for 1977 – 1990 and 1990 – 2010. In the last period (2010 – 2018), however, accretion was observed in all the transects.

The linear regressions (LRR and WLR) showed a practical approach to understanding shoreline patterns and trends, rather than only observing specific periods. For example, the LRR showed that the tendency in Punta Uvero is from moderate to high erosion. In contrast, the area of the beach of Parcelas Suárez and Vieques exhibited overall accretion. Thus, despite observing high or low rates in some specific periods, the LRR and WLR give an overall pattern. Policymakers can use these overall patterns for management purposes. For example, mitigation efforts can be focused on areas where erosion rates are concentrated. I suggest, however, that further LRR and WLR analyses should be conducted without considering the outliers (accretional or erosional) periods triggered by specific scenarios such as sand extraction, droughts, or mitigation infrastructure on the coast. Furthermore, LRR and WLR are pure mathematical computations where other factors such as wind, wave height, and currents are not considered, but the uncertainty and SST analysis can ease this concern by strengthening the SCA. For example, in Punta Uvero, the LRR showed that 17 transects were erosional. To add to this, 65% of the rates were SSTs, offering more confidence and statistical significance to establish that Punta Uvero had overall erosion rates.

The forecasting showed that accretion would decrease, and erosion would increase in 2018 – 2032. A switch may be observed from 2018 – 2042, however, with more accretion and less erosion. Again, these projections should be validated with simulation modeling (Manno et al., 2017). In addition, simulations and traditional models, such as Brunn's Model (Le Cozannet et al., 2014), should be compared to continue understanding the integration of other variables, such as sediment movement (Bagheri et al., 2019). The

forecasting tool is essential for managers, as it gives a general idea of possible future scenarios for which to prepare.

By running both parametric (t-test; Ruggiero et al., 2013) and non-parametric (Wilcoxon) tests, I was able to determine general trends for some periods and test how much these trends differed between periods. It was established that statistical significance did not vary in relation to the test used, indicating that large samples allowed the data to have a normal distribution. All the tests showed the same conclusions: that the two earliest periods and the latest period were dominated significantly by accretion rates, whereas the three periods in the middle were significantly dominated by erosion.

The more recent periods being dominated by erosion could suggest that accretional rates have decreased over time, at least until Hurricane Maria deposited more sand in some areas. According to Barreto-Orta et al. (2019), sand was deposited along several shorelines. They found that erosion rates were observed in areas where erosion rates were documented in the past, but beaches in the northeast and southwest with natural protections (coral reefs and mangroves)—such as Loíza— showed accretion rates (Barreto-Orta et al., 2019). In addition, the influence of Río Grande de Loíza and the possible increase in discharge could also explain the high accretion rates.

In conclusion, SCA is vital for understanding sea-level rise and other climate change threats (Le Cozannet et al., 2019). Before satellite data were available, SCA using long-term data was especially valuable because scientists could extract the shoreline from aerial images and topographic maps. We should therefore continue finding ways to extract different proxies to calculate SCA. Further analysis of differences between shoreline proxies should be addressed. Additionally, I recommend conducting further

analyses integrating simulation modeling with bathymetry, wind, and water-level data (Robinet et al., 2016) to understand if the abrupt changes in shorelines were human-induced or natural.

2.6 Conclusions

Shoreline change analysis in Loíza, Puerto Rico, showed variability in erosional and accretional patterns during the analyzed periods. Overall, according to statistical tests, the first two periods (1902 – 1931, 1931 – 1977) and the latest (2010 – 2018) were dominated by accretion rates, whereas erosion rates dominated the three middle periods (1951 – 1977, 1977 – 1990, 1990 – 2010). This suggests that, as expected, erosion rates increased over time. The higher accretion rates in the latest period could be related to extreme events such as Hurricane Maria in 2018, which produced high accretion. Overall, the accretion rates decreased while erosion rates increased, except for in the latest period, 2010 – 2018. Moreover, two of these periods showed the highest percentage of statistically significant rates: 1977 – 1990 (58%) and 1990 – 2010 (56%).

This investigation was able to measure the possible effect of sand extraction, droughts, and dam construction reflected in 1951 – 1977, which showed the highest percentage of erosion rates. Moreover, when it was compared with the previous period (1931 – 1951), that test was the only one that showed statistically significant support that: (1) the first period (1931 – 1951) had higher accretion rates or (2) the second period (1951 – 1977) had higher erosion rates. Overall, a higher number of statistically significant rates were measured for accretion than for erosion.

The rates did not show a normal distribution and presented outliers, but both parametric and non-parametric tests showed similar results and p-values. Because the data regarding rates of shoreline change had outliers, data for most of the periods did not have a normal distribution. Plotting boxplots for the rates also offered brand new data by

showing the tendency (skewness) for each period's rates toward being erosional (negative) or accretional (positive).

Sandpits showed mostly erosion rates. Punta Iglesias started showing erosion rates in the first period (1902 – 1931) and then recovered with accretion in the second period (1931 – 1951). However, in the long-term analysis, Punta Iglesias showed higher erosion rates than accretion rates. All periods showed erosion rates (albeit with small samples), except for the latest period, 2010 – 2018.

This research contributes to the long-term and short-term shoreline analysis in Puerto Rico using 116 years of shoreline changes. It also incorporated tools provided by DSAS (e.g., forecasting tools and division per area) that have not been used in Loíza. Moreover, it tested parametric and non-parametric to show general patterns in the shoreline change rates in Loíza.

Chapter 3 –ANALYZING COASTAL SEDIMENT TRANSPORT PATTERNS USING NUMERICAL MODELING AT LOÍZA, PUERTO RICO

3.1 Abstract

The scientific community recognizes the complexity of coastal ecosystems. This complexity may be associated with diverse coastal types, nearshore environments, and oceanographic regimes at sites. In the case of the current study site, the coastal area is mainly covered by a diverse sandy beach, rocky coastal type, river mouth, and mangrove forests. Due to this complexity, I ran numerical modeling to understand the sediment transport along the coastal areas and their hydrodynamics. This information is essential for identifying the physical variables affecting coastal changes (erosion/accretion rates).

The coupled Coastal Modeling Systems Wave and Flow were applied to estimate bottom morphological change in the nearshore/insular platform for 2018 in Loíza, Puerto Rico. Data used to run the model were obtained from the San Juan buoy from 2018. Results showed changes in bottom morphology produced by waves and currents in the nearshore/coastal insular platform. Significant morphological changes were identified after Day 89 and Day 211. Morphological changes were identified near natural barriers, such as linear coral reef areas and hardground bottom types, which may trap sediment, depending on the physical conditions at the site. An accretion event was identified along the Rio Grande de Loíza river channel. Punta Uvero in Parcelas Vieques, which had shown higher erosion rates in previous shoreline change analysis, also showed erosion in the morphological change analysis. Oceanside, however, it showed accretion. This information contributes to understanding hydrodynamics and morphological change, and

their possible effect on the erosion scenario in Loíza. These data can improve management plans to protect the communities and archaeological heritage in these areas.

3.2 Introduction

According to the United Nations Atlas of the Ocean (2016; 2017), approximately 40 – 44% of the world's population lives between 100 and 150 meters from the coast. Global population patterns along the coast have been a concern in relation to climate change threats (Osborne, 2000; Jana et al., 2013). A recent study analyzed population pattern distributions along coastlines in 1990, 2000, and 2014, and concluded that most human settlements are within 500 km of the coast (Ye & Ma, 2021). This reality endangers coastal ecosystems and processes through different changes such as coastal armoring, river channelization, and land use. Other activities on the ocean bottom (e.g., cables for internet) can also impact ecosystems on the bottom of the coast and ocean (Bartlett & Celliers, 2017). This pattern of population concentration in coastal areas is seen worldwide, including in Puerto Rico.

In Puerto Rico, according to CoRePI-PR, 13% of the population lives in the coastal zone, which comprises 44 coastal municipalities (2021). These populations are physically and economically vulnerable to coastal hazards (Santiago et al., 2021), and implicit anthropogenic activities can affect salt marshes, mangrove forests, seagrass beds, coral reefs, and other natural resource processes on the coast (He & Silliman, 2019). Another way anthropogenic changes in the environment can affect coastal ecosystems is by sediment transport.

For the current research, numerical modeling was applied to understand the sediment transport patterns and hydrodynamics at Loíza, part of the northern coast of Puerto Rico. Coastal Modeling System (CMS) Flow and CMS-Wave (United States Corps of Engineers [USACE], 2020) were used together to understand local coastal sediment transport hydrodynamics. The previous version of these coupled models was applied in Loíza by Bunch and Dortch (2000), but in the canal areas, and Chardón (2013) applied these models in Rincón, Puerto Rico. Recently, Rivera-Casillas (2020) also used an open-source numerical model, Deft3D, to understand the coastal dynamics and storm-induced changes at Rincón (2020). CMS has also been applied in other parts of the world, including Hawaii, Samoa, Alaska, and several coastal states in the United States (Coastal Inlets Research Program [CIRP], 2020).

Understanding Loíza's hydrodynamics will help us better understand the sediment transport patterns along this coast. Loíza's coast is a mosaic of different environments, such as coral reefs, sandy beaches, and rocky coasts. For example, analyzing the hydrodynamics could help us understand the role of the largest river in Puerto Rico, Río Grande de Loíza, which is part of the most extensive watershed (Quiñones & Torres, 2005). Additionally, Loíza is near the deepest trench of the Atlantic Ocean, the Bunce Fault (ten Brink, 2004). Finally, a recent study categorized Loíza as one of the most vulnerable municipalities due to physical and social erosion and economic factors (Santiago et al., 2021). Thus, by analyzing the coastal hydrodynamics, a course of action could be suggested for the Loíza coast to protect its communities, cultural heritage, and ecosystems. The main questions my research aimed to answer were:

1. Which areas show nearshore/insular platform morphological change along the Loíza coast? Which sites show erosion or accretion?
2. What type of wave-current regime is identified along the Loíza coast?

Puerto Rico's topography varies greatly, and the coast reflects these variations. Indeed, the variation in topography, soils, vegetation, and climate is greatly responsible for Puerto Rico's diversity. Puerto Rico's coastal topographies have been shaped by sea-level rise, strong storms, and drier or wetter climates. Higher energy waves characterize Puerto Rico's north coast, whereas lower-energy waves are observed in the south. The United States Department of Interior undertook a survey of shoreline geomorphology (Kaye, 1959b). In that report, the coast of Puerto Rico was described as rocky islets, reefs, shoreline areas, sand beaches, bay areas, lagoons, marshes, coastal plains, and uplands.

Coastal types do not occur homogeneously on each coast, so sediment transport patterns are also not homogenous. The north coast of Puerto Rico is generally formed by limestones, karst formations, and alluvial plains, whereas the south coast is characterized by a large alluvial fan in the eastern part, intrusive igneous, and limestone toward the north. The east and west coasts are generally formed by limestone, volcanic rock, and alluvial deposits (J. Morelock et al., 2003). The capital of San Juan, in the north, has a combination of juvenile formations and older rock formations. This area has hilly and low-lying rock types with dunes and cemented dunes (eolinate). Moving toward the south, alluvial sediments can be observed. Reef areas are present as rocky barriers on the ocean bottom near the shoreline. The shoreline is also formed of beaches or beach rocks

in intertidal waves. A combination of cliff areas can be observed in the south of old San Juan, along with isles and marshland (Kaye, 1959a).

A recent study by Takesue et al. (2021) investigated how runoff and other sediment sources affected the coral reefs in the south of Puerto Rico after Hurricane María in 2017. The researchers were able to observe how extreme events such as hurricanes can affect the sediment received by reefs. The United States Geological Survey (USGS; Cheriton et al., 2019) published a study regarding how suspended sediment transport in the south of Puerto Rico caused more stress to coral reefs. Previously, Torres and Morelock (2002) and (Acevedo et al., 1989)focused on studying interactions between sediment patterns and coral reef species in southern Puerto Rico. Torres and Morelock (2002) concluded that sediment-stressed reefs could survive a high input of sediments in the short term. A common aspect of these studies is that all used sediment sample collection methods to compare particle amounts, types, and grain sizes.

The following section will describe sediment transport, anthropogenic activities, and previous research on this topic.

3.2.1 Sediment Transport and Hydrodynamics

Sediment transport studies are essential because these processes can vary along with coastal and nearshore environments, which may shape the shoreline and nearshore bottom morphology based on variability in climatic and oceanographic conditions. Major morphological changes may occur when extreme events and/or events associated with climate change are identified. In addition, anthropogenic activities can also alter sediment sources and transport, causing significant morphological changes that can alter shoreline stability. For example, according to McGranahan et al. (2007), agricultural activities, urbanization, river channeling, deforestation, and coast armoring can alter sediment transportation patterns and sources on the coast. Bedrock erosion, soil, river discharge, and decomposition of plants and animals are examples of natural sediment sources in coastal areas (United Nations, 2022), but other contaminants can also be added as sediment to the coastal ecosystems, such as sediments from agricultural and other urban activities (Takesue et al., 2021).

Coastal hydrodynamics are responsible for sediment transport along the coast. Wave regimes, bathymetry, wind, and tides, among other physical variables, are all considered parts of coastal hydrodynamics (Kankara et al., 2013). Moreover, offshore and nearshore environments interact differently with each wave characteristic, causing the oscillation to vary along the coast (Davidson-Arnott, 2010). These wave conditions and other features can thereby affect sediment structure and sediment transport in coastal areas.

A conceptual model developed for the Oz Coast by the Queensland/Australian Government (2003) is shown in Figure 3.1. This conceptual model shows different stressors, such as the construction of canals, urbanization, farming, and sand extraction

on the coast, as well as showing natural factors such as mangroves, seagrass, and coral areas. As parts of the model, all these characteristics may influence and affect wave energy distribution, wave and wind direction, and the local bathymetry of the coast. For example, waves interacting with fixed structures such as sea walls can provoke erosion. The interactions among all these variables are often referred to as coastal hydrodynamics.

.

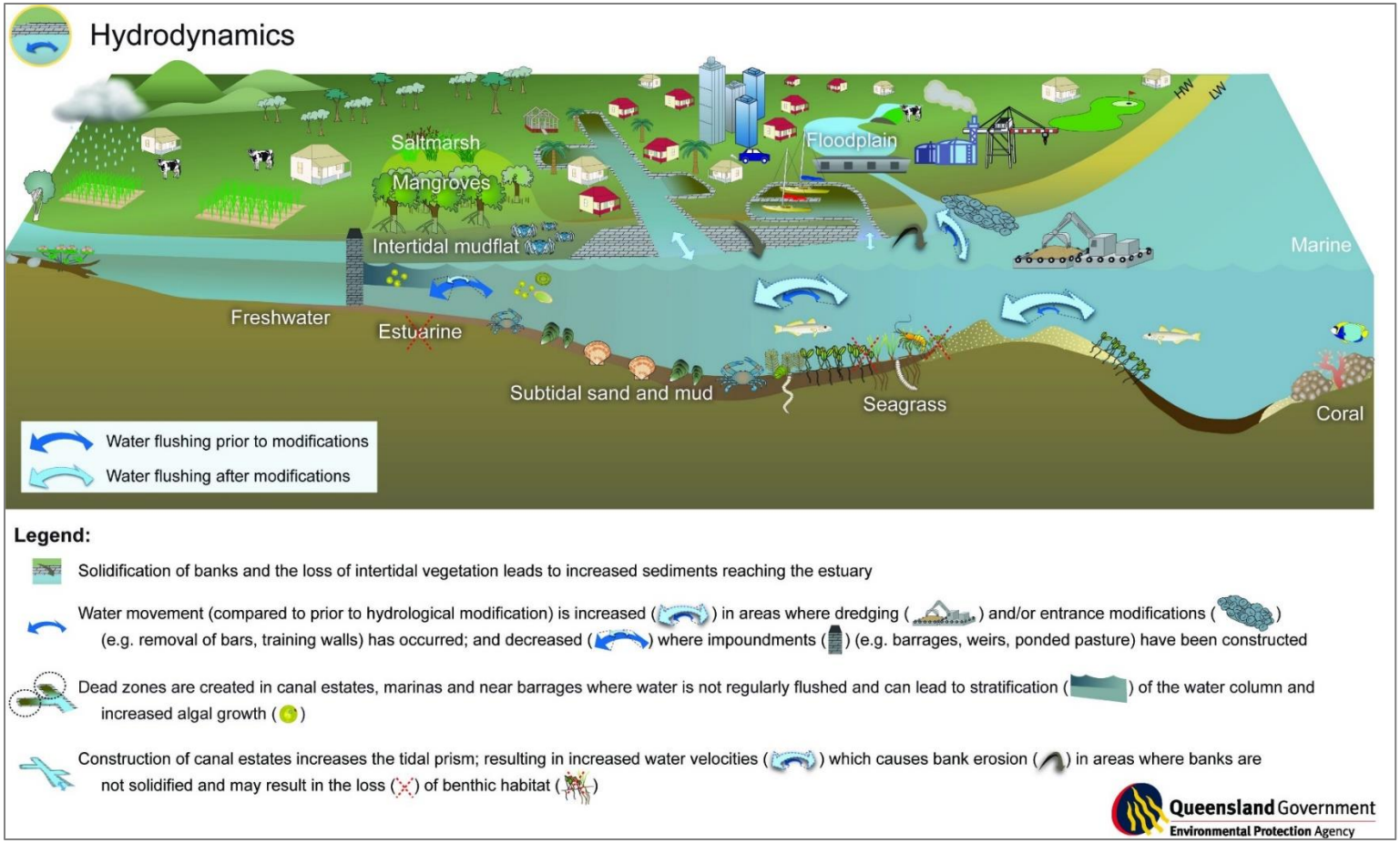

Figure 3.1. Hydrodynamic Conceptual Model Developed by the Queensland Government, Environmental Protection Agency (2003)

Coastal hydrodynamics have been studied for different coast types using several approaches, from physical models (Seabergh et al., 2005) to numerical models. These methods help us understand the complexity of coastal areas, as coastal types and features can vary greatly. Different investigations have analyzed sediment transport while focusing on a specific ecosystem. For example, Bainbridge et al. (2016) studied sediment inputs in coral reefs in the Great Barrier region in Australia by comparing the particle sizes of sediment samples between a tributary and a river mouth.

In Colombia, Devis-Morales et al. (2021) used Langragian numerical modeling to analyze sediment transportation patterns in several rivers in the Colombian basin. This model identified particles based on size (from coarse to very fine sediments). Restrepo et al. (2017) also used numerical modeling to analyze suspended sediments in Colombia, using the Continuous Wavelet Transform model to analyze the different wave signals and suspended sediments loads. In the United States, different sediment transportation scenarios cause by nourishment berms were addressed by Johnson et al. (2021). Passeri et al. (2018) applied similar methods in Alabama, where they used numerical modeling to understand sediment patterns and increasing sea-level rise in the navigation channels at Mobile Harbor

3.3 Study Area

Assessments of sediment transport and hydrodynamics were conducted in the nearshore and insular platform waters northward of the Loíza coastal municipality, specifically related to the eastern region of the Loíza coastline. The section chosen was the area from Vacía Talega to Río Herrera (Figure 3.2). The assessments of sediment transport and

hydrodynamics were conducted at two sites along the Loíza coastline, covering from the shoreline to the insular platform, up to 3 kilometers.

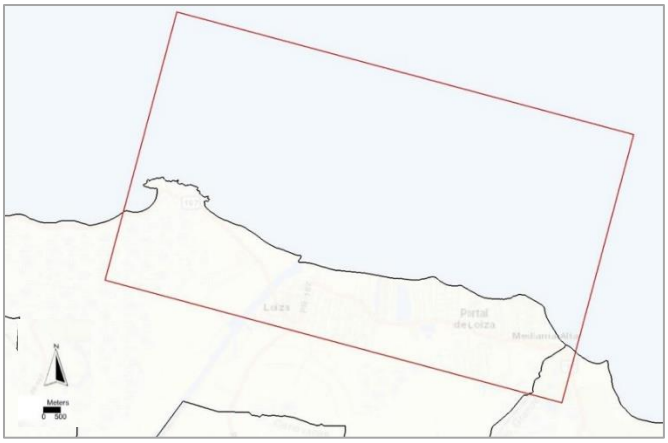

Figure 3.2 Study Area at Loíza, Puerto Rico, With Smaller Grid Selected for Model Application

Historically, Loíza was the site of preceramic cultures, sugar mill activities, an English fleet attack in 1797, and more (Picó, 2008). Even today, Loíza represents some of the Puerto Rican people's most important cultural heritage (García Lebrón, 2016). The municipality of Loíza has also been a center of social injustices. According to the latest population estimations, Loíza has 23,412 citizens and 50.4% live below the poverty level (United States Census Bureau, 2021). The murder of Adolfina Villanueva (Adams, 2021) and the tenth massacre in Puerto Rico in 2021 (Rivera, 2021) also occurred in Loíza. Furthermore, Loíza is a municipality that is vulnerable to coastal processes such as erosion, flooding, sea-level rise, and tsunami (Ruiz Vélez, 2014), exposing it to unquestionable natural and socioeconomic vulnerabilities, especially after Hurricanes Irma and María.

Many authors and agencies have focused on evaluating hazards and creating mitigation plans to protect these communities (Martínez Martínez, 2008; Jervis, 2017;

MARES, 2018; Diaz-Torres, 2019). Recently, a project was undertaken to minimize erosion in Punta Iglesias by applying hard stabilization methods in Parcelas Suárez (U.S. House of Representatives, 2020). In summary, the Loíza coast exhibits unique characteristics.

For example, its insular area is part of the deepest trench in the Atlantic Ocean, and its coast receives discharge from the most abundant river in Puerto Rico, Río Grande de Loíza. This river has straightened over time (Kaye, 1959b), which was previously suggested to be due to channelization by pre-Columbian cultures but was disregarded by Monroe (1980).

The Loíza coast also has scattered reefs, mostly in shallow areas and east of Río Grande de Loíza. For example, Elkhorn Coral and Staghorn Coral, classified as endangered species, function as critical habitats for highly migratory animal species, such as the Caribbean lemon shark and the blue marlin (Bureau of Ocean Energy Management [BOEM], National Oceanic and Atmospheric Administration [NOAA], 2021).

3.3.1 Current and Wave Regime

Ocean currents are complex and are dominated by tides, wind, and water densities due to the heat and salinity of the waters (NOAA, 2021b). The north coast of Puerto Rico is part of the North Atlantic Ocean, with circling currents or Atlantic gyre (NOAA, 2022c). This gyre starts along the Gulf Stream and flows to Europe, northwestern Africa, and the Caribbean. Hence, Loíza has an ocean current from the east (average from 1992 to 2012; Figure 3.3).

Local superficial currents show a westward flow produced by the trade winds approaching from the east (NOAA, 2022b). Significant wave direction averages were

from the north-northeast and northeast between 1980 and 2009, with average wave height varying from 0.79 to 1.45 m, and average wave period ranging from 5 to 9 seconds during that period. In 2018, major significant wave heights were observed to be 0.59 – 6.19 m (Station 41043). For 30 years, Loíza has been exposed to hurricane winds of 30 knots, followed by 50 and 64 knots (BOEM, NOAA, 2021). Puerto Rico has a semi-diurnal cycle in the north and a primarily diurnal in the south (Kaye, 1959b).

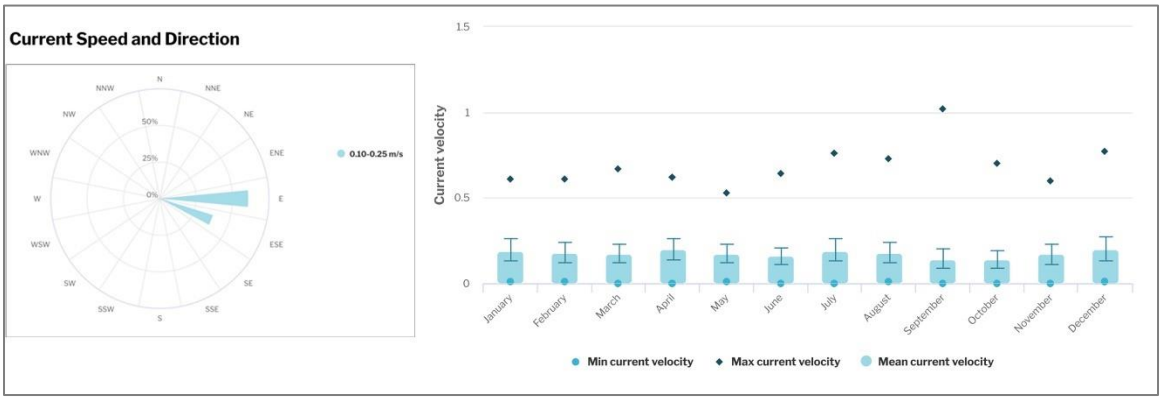

Figure 3.3: Trends in Ocean Current Velocities in Loíza, Puerto Rico, Taken from NOAA and BOEM Marine Cadaster (2021)

An example of the wave height and direction regime in Loíza (-65.8083, 18.446) is shown in Figure 3.4. Most wave heights range from 0 to 5 feet (1.5 m), with heights of 7 – 9 feet (2.1 – 2.7 m) occurring less frequently.

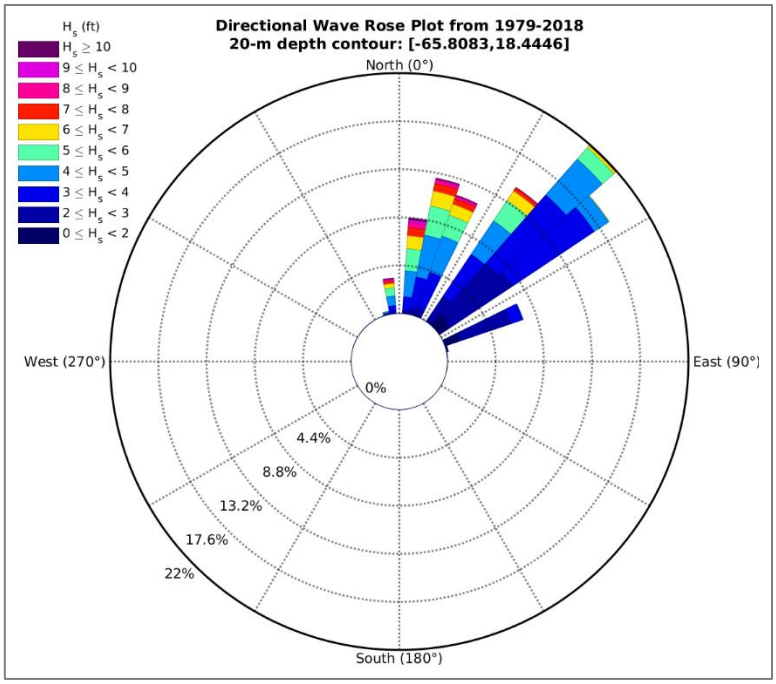

Figure 3.4: Directional Wave Rose Plot from January 1979 to December 31, 2018, at Loíza (-65.8083, 18.446); Obtained from Center for Applied Ocean Science and Engineering (2018)

3.3.2 Beach and Bottom Sediments

Geologically, Loíza is part of the northern lowlands and is surrounded by beach deposits, swamp deposits, alluvium, and the Aymamon Limestone (Bawiec, 2001). The western area has two lagoons, Laguna Torrecilla and Laguna Piñones. As part of the northern lowlands, it has longitudinal dunes, and the old dune formations exhibit eolinate formations in Boca de Cangrejos and Vacía Talega (Monroe, 1977).

Bottom sediment facies and geology are very diverse, along with the insular platform of Loíza (Figure 3.5). Fine calcareous sand is found on the eastern side. Moving to the ocean, medium to coarse continues, followed by calcareous sand and hardground, eolinate, or rock outcrops. Near the Río Grande de Loíza, the geology is classified as terrigenous (Rodríguez et al., 1998), whereas at Punta Vacía Talega, the eastern site is a combination of sand and the western site contains calcareous sand. Mixed sand is found

between Punta Maldonado and Punta Boca de Cangrejos. Seaward, bottom sediment facies showed sandy to gravelly mud (Rodríguez et al., 1993).

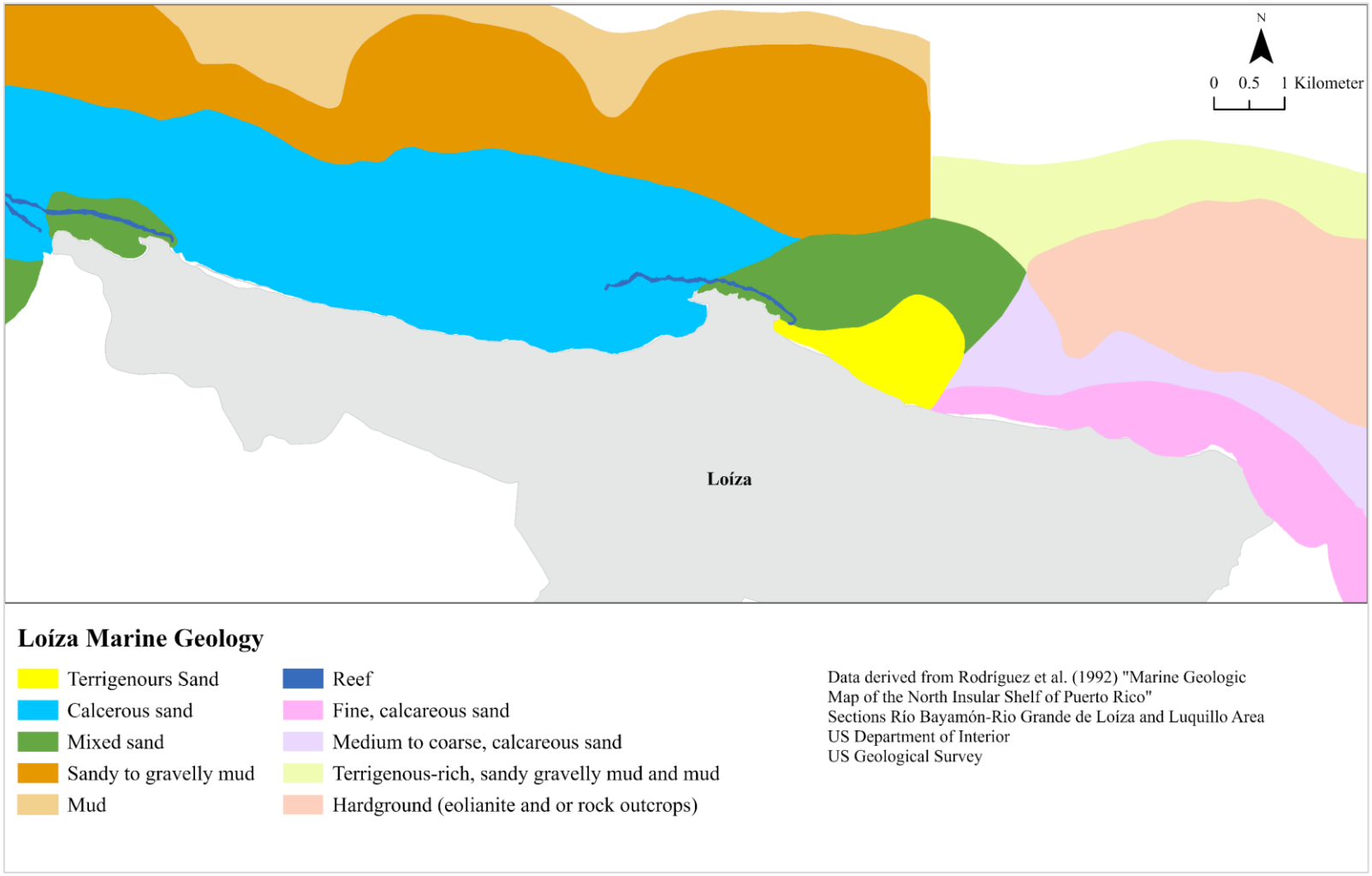

Figure 3.5: Marine Geology at Loíza, Puerto Rico, from Rodríguez et al. (1993)

Based on USGS studies, submarine canyons are located along with the insular platform and slope of the main island. Around 30 to 40 kilometers from the coast, studies have shown the largest amphitheater-shaped trench along the north coast, Loíza Amphitheater (ten Brink et al., 2006). The insular platform also showed trenches formed either by rivers or sediment erosion in the same area (Figure 3.6).

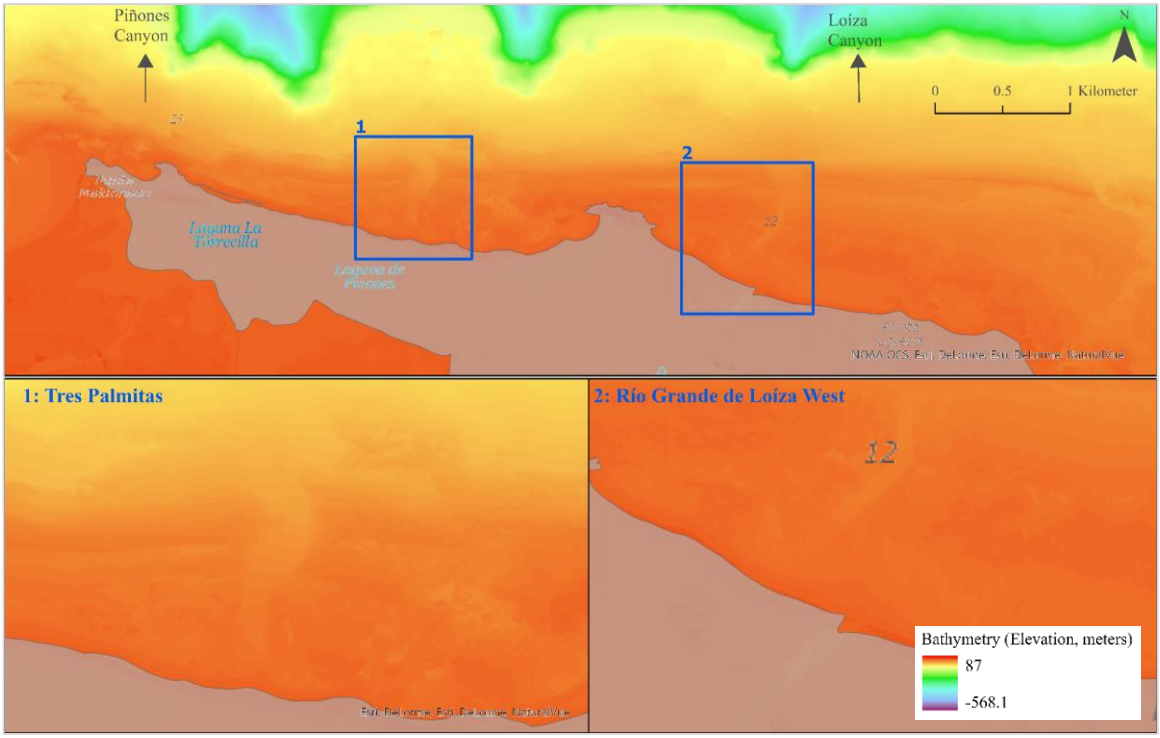

Figure 3.6: Loíza's submarine canyons and trenches. The map shows the deeper bathymetric contour at Piñones and Loíza Canyons. The blue squares indicate two small submarine canyons present in the east (Tres Palmitas) and west (Río Grande de Loíza).

3.4 Methodology

This section will describe the CMS-Wave and CMS-Flow models used in this study to simulate local hydrodynamic parameters (wave and currents) and changes in bottom morphology. This section includes the main boundary conditions and data inputs used for running the model. Finally, the setup for the models will be illustrated.

3.4.1 Coastal Modeling System (CMS) Flow and Wave

The CMS-Flow and CMS-Wave models were used to evaluate the hydrodynamics and sediment movement along Loíza's coast. CMS-Wave and CMS-Flow were coupled to simulate interactions among the measured data (wave, tides, bathymetry) for the selected period (January to December 2018). A diagram showing how these parameters interact with each other to calculate the simulation using an inline steering process is presented in Figure 3.7. CMS-Flow calculates the hydrodynamics and sediment transport (Sánchez et al., 2012). The two models are run inside the Surface Water Modeling Systems (SMS) software (Aquaveo, 2022).

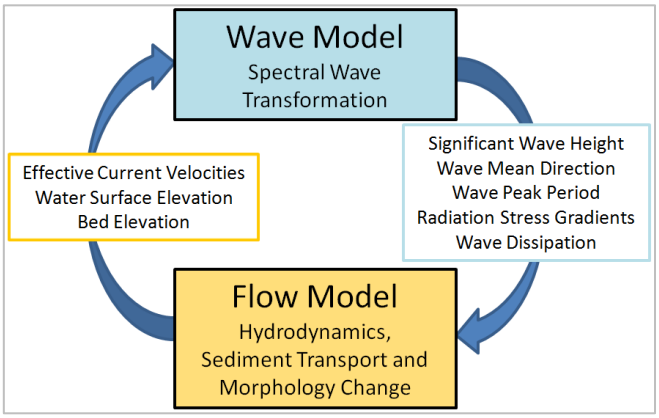

Figure 3.7: Coupling process of Coastal Modeling System (CMS) Flow and CMS Wave. Obtained from CMS User Guide (Sánchez et al., 2012).

CMS-Wave calculates wave balance equations using spectral wave information. Both models are described as "an integrated suite of numerical models for simulating flow, waves, sediment transport, and morphology change in coastal areas" (Coastal Inlets Research Program, 2018). Li et al. (2019) explained in detail the different equations used in these models. These two models can be coupled to calculate changes in nearshore/insular platform bottom morphology using wave parameter information.

The CMS-Wave model involves wave spectrum (meters squared/hertz/radian), wave direction (degree), wave height (m), and wave run-up using a “wave-action balance equation diffraction” model transformation. For this model, a Cartesian Grid can be refined in size. The CMS-Flow model requires several inputs such as bathymetry, sediment grain size (mm) present in the grid, bed friction coefficient, and wind direction (m/sec).

3.4.2 Model Data Input

Local bathymetry, shoreline, tide heights, river discharge, wave heights and spectra, sediment grain size, water temperature, and salinity were inserted into the model (see Table 3.1). The data were collected between January 1 and December 31, 2018, a period that was chosen because it preceded the impacts of Hurricanes María and Irma on Puerto Rico. Additionally, the latest shoreline change analysis data were derived using a 2018 shoreline, as this period was identified as an extreme event produced by a winter storm (Storm Riley).

Table 3.1: Summary of Data Sources

Data	Source	Data	Source
Bathymetry	Continuously Updated Digital Elevation Model, National Centers for Environmental Information, Data Viewer, National Oceanic Atmospheric Agency (NOAA)	**Wave Information**	National Buoy Center, Wave Net Portal, USACE
River Discharge	United States Geological Survey (USGS)	**Sediment Grain Size**	Insular Maps, USGS
Tides	Tides and Currents, NOAA, Wave Net Portal, United States Corps of Engineers (USACE)	**Manning's Coefficients**	National Centers for Coastal Ocean Science, Benítez & Mercado (2015)
General Temperature and Salinity	Marine Cadaster, Bureau of Ocean Energy Management, and NOAA		

The bathymetry used in this project was taken from the Continuously Updated Digital Elevation Model (CUDEM), funded by the National Centers for Environmental Information. The dataset was downloaded from the NOAA Data Viewer (Office for Coastal Management, 2019). According to the report that created this dataset, for Puerto Rico, there 12 primary bathymetry sources were used, ranging from 1900 to 2018 (Sutherland et al., 2019). This dataset was chosen because there are no other datasets, especially in the oceanside areas. It did, however, use the latest topo-bathy information from the 2018 dataset available at the time of the investigation.

Using the CUDEM, I calculated the tidal range to create the activity classification dataset required by CMS. This dataset possessed active and inactive cells that instructed the model to calculate or not calculate the hydrodynamics in specific cells. Landward cells were inactive and ocean cells were active, with the shoreline area serving as a boundary between the active and inactive cells. I calculated the tidal range to improve the measurements along this boundary, which controls the area where coastal waves interact (Gupta, 2011).

During 2018, tide ranges varied at Puntilla Station (NOAA, 2018) from 0.54 m (maximum) to -0.39 m (minimum), resulting in a tidal range of 0.93 m. This number was rounded to 1 and used to derive the contour line using the Contour Tool in ArcGIS Pro (ESRI, n.d.-b). The CUDEM dataset and the tidal range drawn to establish the limit between active and inactive cells are shown in Figure 3.8.

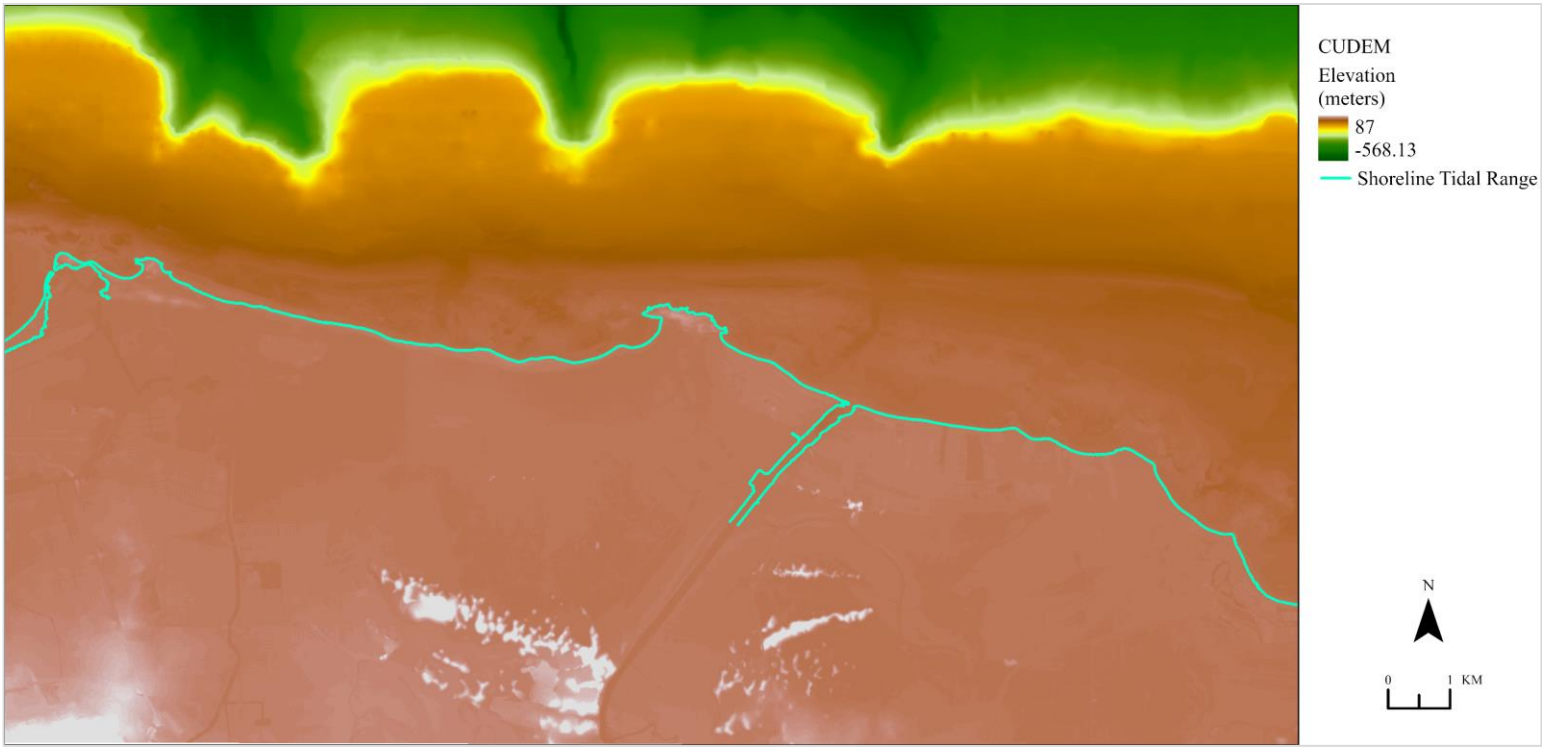

Figure 3.8: Continuously Updated Digital Elevation Model (CUDEM), with tidal change drawn to establish the limits in the activity classification dataset (active and inactive cells) in the Coastal Modeling System

Tides were collected from the Tides and Currents (NOAA, n.d.-b) and Wave Net & Tide Portal (CIRP, 2021) websites for Station 975537. Six constituents were used: M2, S2, N2, K1, M4, and O1. The characteristics and descriptions for each constituent are shown in Table 3.2. This information was used as water surface forcing in the CMS-Flow boundary parameters. Tide heights were used to calculate the tidal range to then calculate the activity classification.

Table 3.2: Tidal Constituents from Station 9755371, San Juan, La Puntilla, San Juan Bay, Puerto Rico

ID	Constituent	Amplitude (m)	Phase (deg)	Description
1	M2	0.154	264.3	Principal lunar semidiurnal constituent
2	S2	0.02	2893.3	Principal solar semidiurnal constituent
3	N2	0.037	244.5	Larger lunar elliptic semidiurnal constituent
4	K1	0.087	167.5	Lunar diurnal constituent
5	M4	0.002	19.0	Shallow water overrides of principal lunar constituent
6	O1	0.076	170.6	Lunar diurnal constituent

The boundary conditions inserted into the models based on the data collected are summarized in Table 3.3. I also added wave information and river discharge as boundary conditions. Wave heights, wave temperatures, and wind information from Station 40143 of the National Buoy Center (NOAA, n.d.-a) were used for the CMS-Wave forcing. The wave spectra were obtained with the help of the Coastal and Hydraulics Laboratory from the Tide and Wave Net Portal. Finally, the river discharge information from the Río Grande de Loíza was obtained from the National Water Dashboard developed by USGS (2018).

Table 3.3: Boundary Conditions

Simulated Period	Tidal Constituents	Wave Forcing	Riverine Forcing
January 1, 2018 [544 days]	NOAA Station 9755371, La Puntilla, San Juan Bay, Puerto Rico	Station 41043 NDBC Steering 1 hour	Rio Grande de Loíza Damsite Station 50059050

I used the multiple grain size option provided by CMS-Flow, as the model can simulate the interaction between the bed and the mixing layers (for a detailed explanation of each equation see Li et al., 2015). I obtained the data from two "Insular Shelf Maps" created by Rodríguez et al. (1993, 1998). After importing the sizes documented in the map, I determined the greatest proportion of particles to be 0.75 mm, between coarse sand and very coarse sand (Figure 3.9), although very fine sand was also documented 14% of the time. The percentiles (D10, D16, D50, D90) were extracted using the cumulative distribution of sediment grain size.

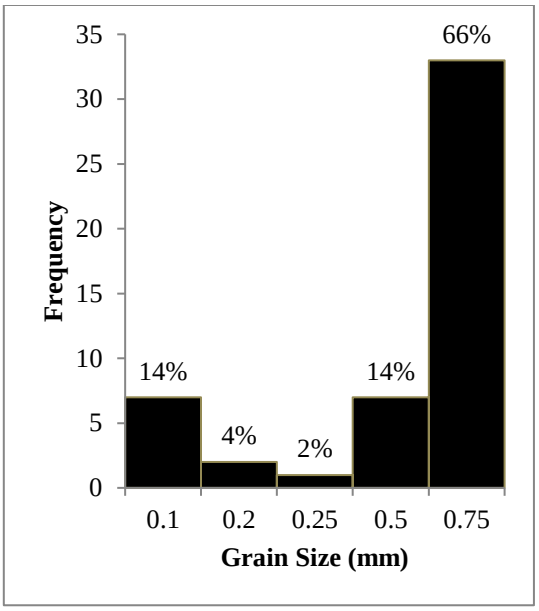

Figure 3.9: Distribution of Grain Sizes among Bottom Sediments in Loíza (Rodríguez et al., 1993, 1998)

A Manning's coefficient was assigned to each benthic area type identified at the site. The coefficients were obtained from a report by Benitéz and Mercado (2015) while the benthic area dataset was collected from the National Centers for Coastal Ocean Science (2001). I converted data into a shapefile to be inserted into SMS. shows the benthic area descriptions and Manning's coefficients are presented in Figure 3.10.

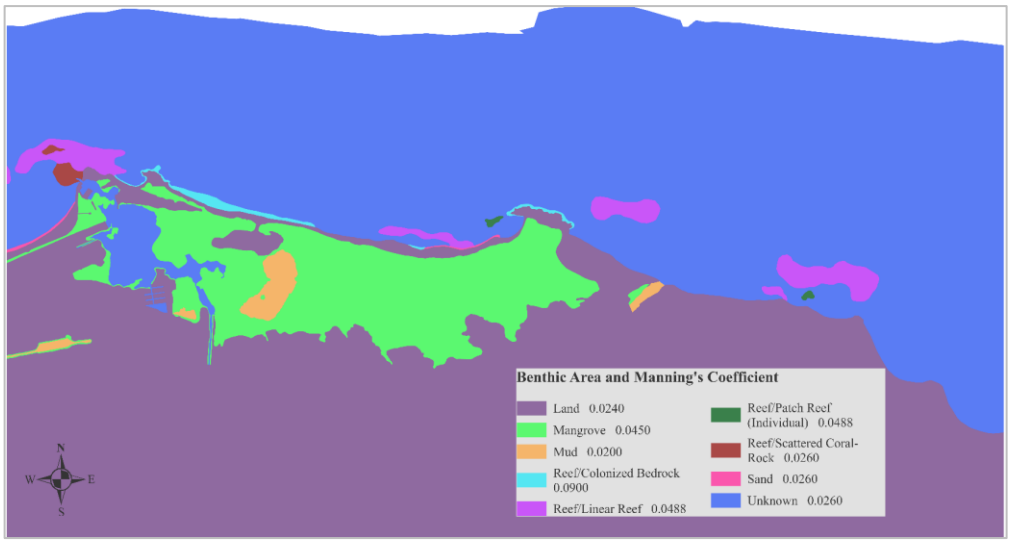

Figure 3.10: Manning's Coefficients for Land and Ocean Bottom Benthic Areas

3.4.3 Model Setup and Parameters: CMS-Wave and CMS-Flow

CMS models provide the capability to create nonuniform grids. The cartesian grid created by CMS-Wave is shown in Figure 3.11. For this wave grid, several different points were used to increase the resolution in the center of the grid. For the model setup, the boundary condition was wave height, and the wave spectra data were inserted in. eng format.

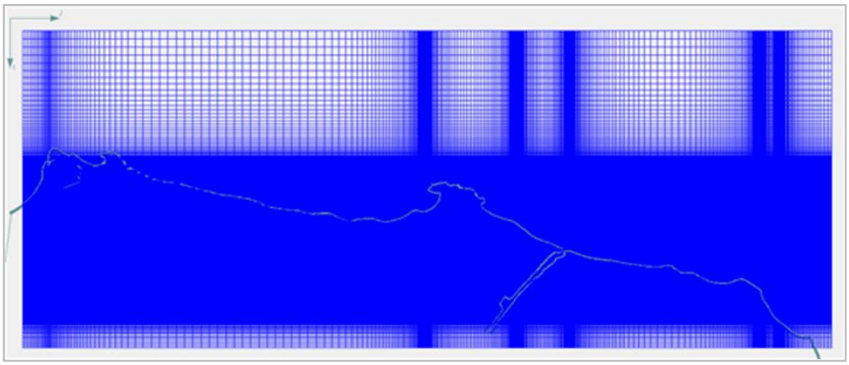

Figure 3.11: CMS Wave Cartesian Grid

The final telescoping grid created in CMS-Flow is shown in Figure 3.12: . Different resolutions were assigned along the grid, with higher resolutions assigned along the shoreline and river area. The minimum and maximum resolutions were 5 m and 160 m, respectively.

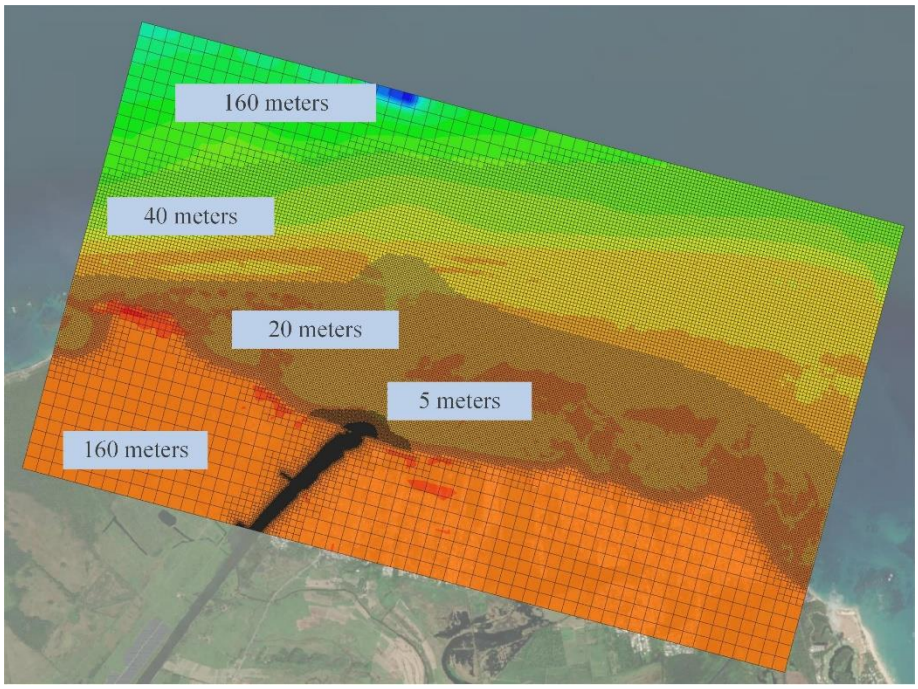

Figure 3.12: Telescoping Grid Resolutions Created in the Coastal Modeling System Flow

The parameters inserted into CMS-Flow are summarized in Table 3.4. The model has the following windows: General, Flow, Sediment Transport, Salinity/Temperature, Wave, Wind, and Output. In the Flow tab, bed roughness, turbulence parameters, and hydrodynamic timesteps are specified. Also in this menu, the user specifies the timestep for the flow calculation, selects a transport formula, and assigns the sediment classes, bed composition, and hardbottom depth.

Table 3.4: Coastal Modeling System Flow Model Parameters

Run Time	13056 hours	**Bed Layer Thickness**	0.05 meters *
Time Steps	600 seconds	**Bed Composition**	D10, D16, D50, D95
Sediment Transport	Lund-CIRP	**Hardbottom**	Reef areas, hardground areas depth
Suspended/Bedload Scaling Factor	0.2 *	**Water density**	1025.0*
Bed Slope Coefficient	0.1 *	**Constant Water Temperature**	27.0°C
Adaptation Length	10 m	**Wave**	CMS Wave sim
Multiple Grain Size	0.1 mm, 0.2 mm, 0.25 mm, 0.5 mm, 0.75 mm	**Wind**	Spatially Constant Data: Station 41043, NDBC Steering 1 hour Anemometer Height: 4.1 m

3.5 Results

Results showed nearshore/insular platform morphological change, local wave-induced current patterns, and wave height distributions based on the simulations from January 1 to December 31, 2018. The results are shown for four different periods/dates: 31 days (January 31), 89 days (March 31), 211 days (July 31), and 364 days (December 31). In this way, patterns could be observed after one month, in the middle of spring, during summer, and in the winter.

3.5.1 Nearshore/Insular Platform Coastal Morphological Change

The morphological changes that had occurred by each of the above-mentioned dates are shown in Figure 3.13. After 31 days, both sediment deposition and minor loss of sediment were observed around the nearshore site in the Vacía Talega area (west). Loss of sediment was identified north of Punta Uvero, while some sediment deposition was observed in the south and southwest of that site. Sediment deposition was also observed near coral. Minor sediment deposition was observed in deeper areas, at Vacía Talega, and along the shoreline.

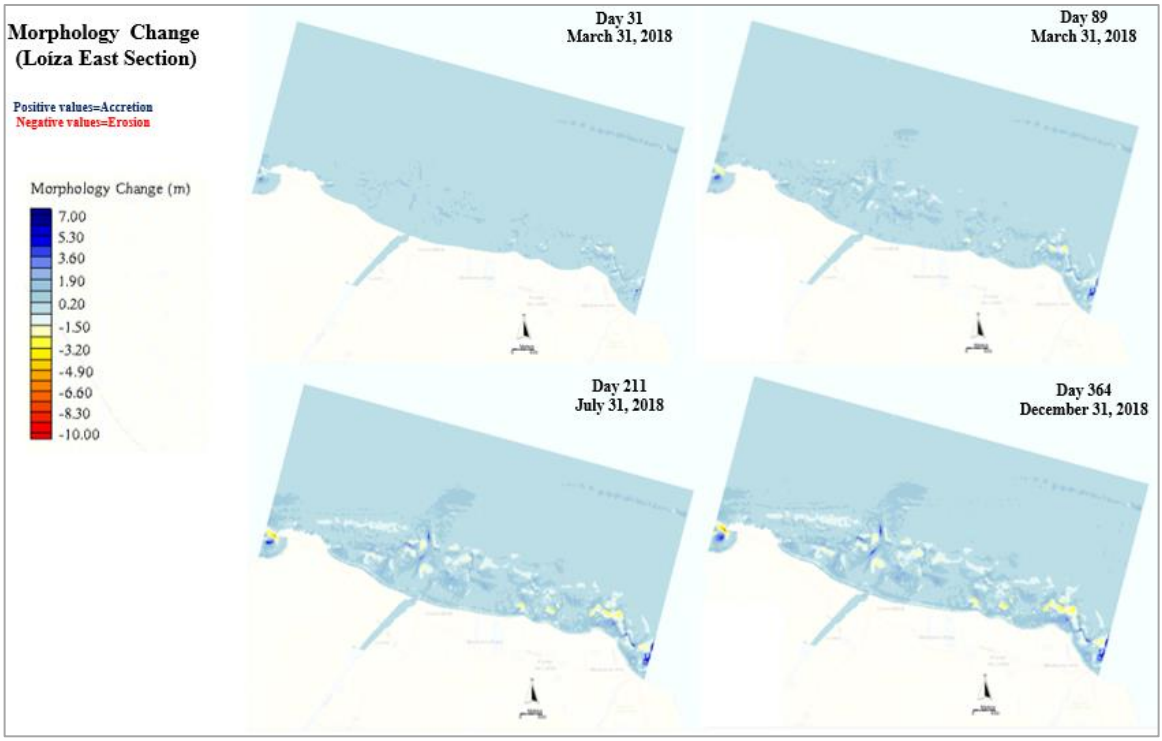

Figure 3.13: Coastal Morphology Change along the Loíza Coast: Day 31 (February 1, 2018), Day 89 (March 31), Day 211 (July 31), and Day 364 (December 31).

For the 89-day scenario (March 31), both an increase of sediment deposition and a loss of sediment were observed at sites seaward from Vacía Talega. Sediment deposition was identified around the Río Grande de Loíza river mouth, whereas new erosion sites were observed in the nearshore area north of Punta Iglesias and Parcelas Suárez.

For the 211-day period (July 31), a significant loss of sand was observed seaward from Vacía Talega. Along with the Río Grande de Loíza river mouth, higher sediment deposition was observed through submarine channels possibly associated with submarine canyons. Punta Uvero's western area showed erosion in the nearshore region, while a mix of accretion and erosion was observed on the eastern side. Along the shoreline, accretion were detected from Parcelas Suárez to Vacía Talega. In contrast, sediment depositions

were observed along the Río Grande de Loíza river channels, Vacía Talega, and eastward from Parcelas Vieques.

After 364 days, the same patterns were observed, and most of the same erosion areas remained. In Vacía Talega and the submarine canyons, more accretion was observed. At Punta Uvero, previous areas of erosion remained, with accretion and erosion occurring oceanside.

3.5.2 Local Wave-induced Current Patterns

The wave-induced current velocities for the four different periods are shown in Figure 3.14. On Day 31, most of the current pattern moved from west to east without major influences from the Río Grande de Loíza. In some areas near Punta Uvero, wave velocities increased on the west side. In the western area of Punta Vacía Talega, higher velocities were observed on this date.

On Day 89, the highest wave current velocities were observed west of Punta Uvero, near the Río Grande de Loíza mouth, and in the eastern area of Vacía Talega. At the mouth of the Río Grande de Loíza, there was a cross-shore movement from the river flow with higher velocities. At Punta Uvero, eddy currents were observed along the north, changing the direction of the currents to the west and east of Punta Uvero.

Between Day 89 and Day 211, the Río Grande de Loíza's influence on currents was observed when most of the flow was directed oceanside, with the highest velocity. The nearshore area between Parcelas Suárez and Punt Uvero, and west of Punta Uvero, also showed high wave velocities.

On Day 364, the currents showed an east-west pattern, with higher velocities than on Day 31. At Punta Uvero, sediment deposits appeared to redirect the currents seaward and

return them to the east at Parcelas Suárez. At the mouth of the Río Grande de Loíza, current velocities decreased, and I observed a direction switch inside the river flow. At Vacía Talega, there was a decrease in velocity and the pattern of movement was from west to east.

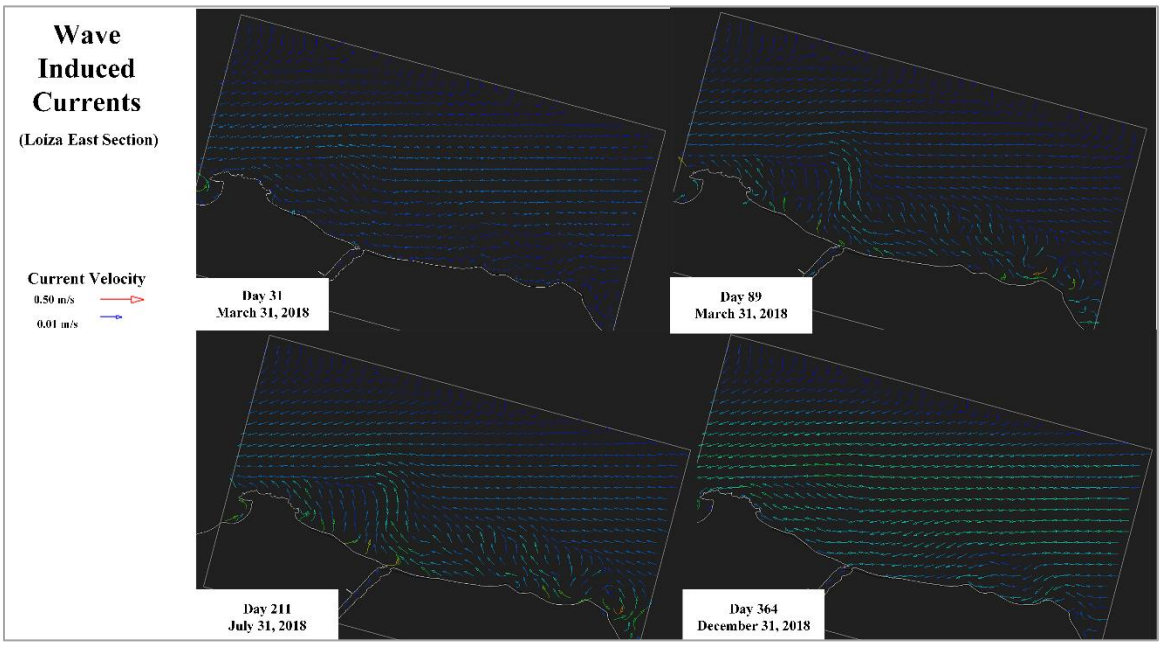

Figure 3.14: Velocities of Wave-induced Currents: Day 31 (February 1, 2018), Day 89 (March 31), Day 211 (July 31), and Day 364 (December 31).

3.5.3 Wave Heights

Wave heights and directions along the nearshore and insular platform along Loíza are shown in Figure 3.15. Lower wave heights were observed on Day 31 and Day 364. Day 89 showed the highest waves among these dates, followed by Day 211. For Day 89, higher wave heights were observed at the mouth of the Río Grande Loíza, the eastern area of Vacía Talega, Parcelas Suárez, and Punta Uvero. On Day 211, wave height increased along the grid and decreased in the submarine canyon. At Punta Uvero, a decrease in wave height was identified in the north.

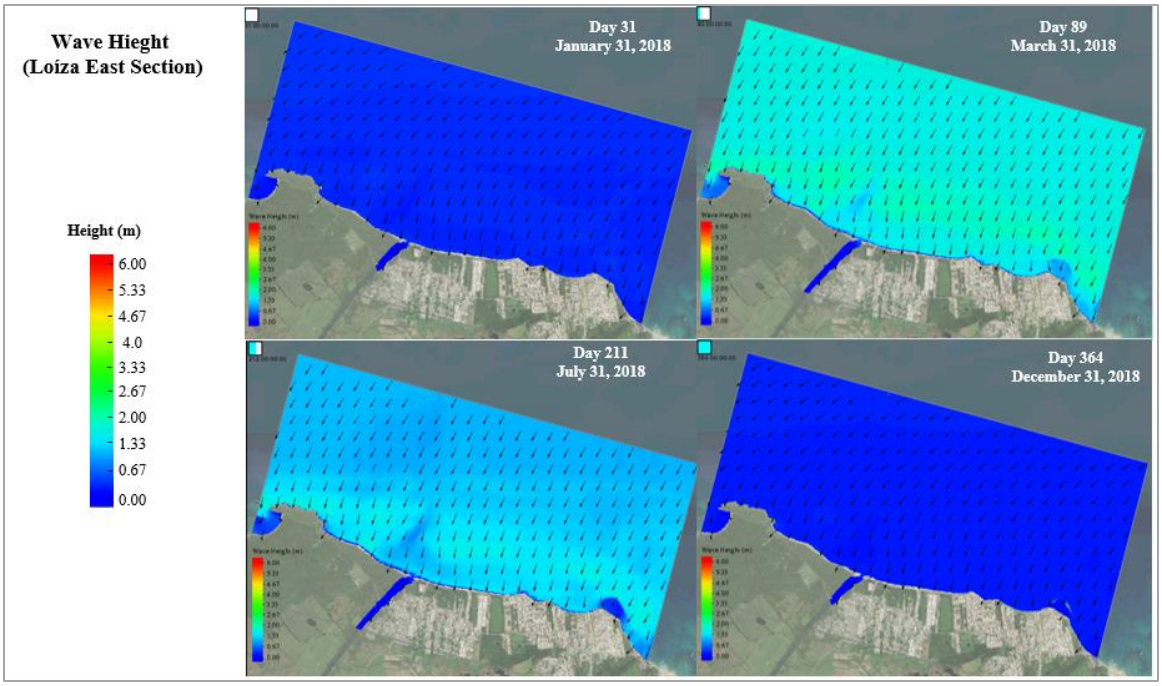

Figure 3.15: Wave Heights (m) along the Eastern Part of Loíza's Coast, with Arrows Showing Wave Direction

3.5.4 Winter Storm Riley Storm Surges

Puerto Rico received Winter Storm Riley's northeast storm surges between March 1 and March 12, 2018 (Rodríguez, 2018). These storm surges created dangerous waves, even more dangerous than those created by Hurricane María, which had impacted Puerto Rico in September 2017. According to Canals et al. (2019), Riley and other events have created the highest waves in Puerto Rico. The highest measured water levels provoked by storm surges occurred on March 5, 2018 (Figure 3.16), an event that was also reflected in my simulation results.

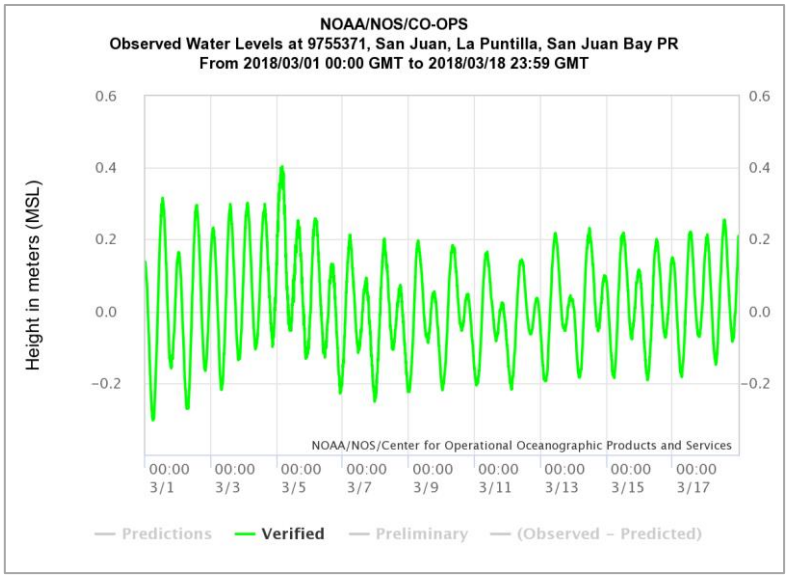

Figure 3.16. Graph of Observed Water Levels from March 1 to March 18, 2018, at Station 9755371, La Puntilla, San Juan Bay, Puerto Rico (from Tides and Currents Portal, NOAA, 2018)

Specific simulation results for the dates during Winter Storm Riley, Day 58 to Day 65 (February 28 to March 7), are presented in Figure 3.17. On these dates, storm surges created higher water levels along Loíza's coast. On February 28, wave height began to increase. On March 1, wave height grew to 3 m across most of the grid. On March 3, wave heights decreased to nearly 2 m, but on March 5 (the highest level recorded by the buoy) they increased again. Wave heights decreased and then increased again between March 6 and March 7. After these dates, wave heights overall continued to decrease. Additionally, wave heights were observed to diminish as long they touched the coast's belt reef areas.

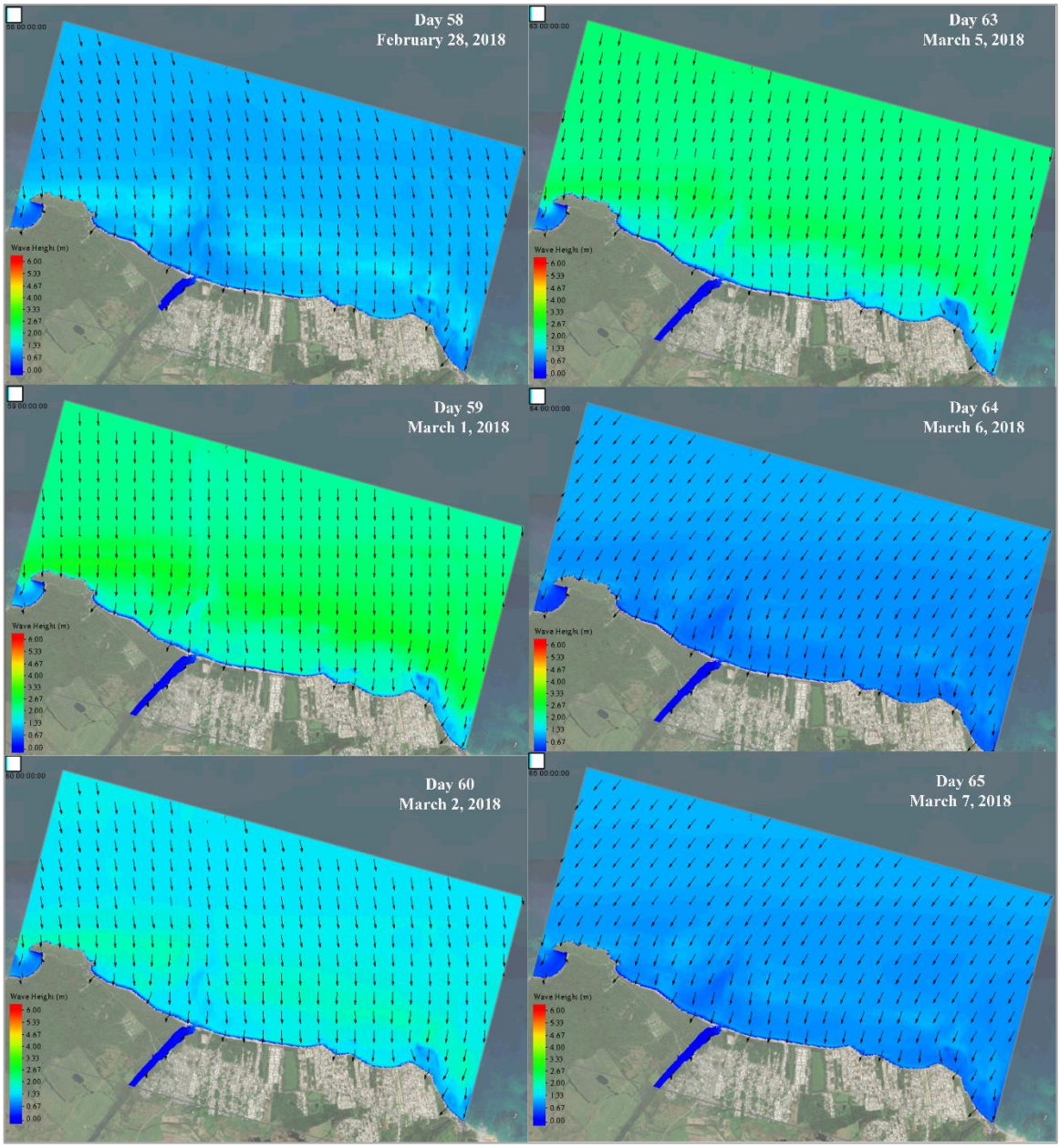

Figure 3.17: Simulation Results Showing Wave Heights at Loíza on Dates Corresponding to Storm Surges from Winter Storm Riley

3.5.5 Areas of Interest

Three areas of interest were selected to create more detailed nearshore and insular platform profiles of the bottom morphological changes. Three random transects were drawn in the areas of interest to obtain the profiles. At the Río Grande de Loíza, the transects were drawn at the mouth and channel, whereas at Punta Iglesias and Punta Uvero, the transects were drawn from land to the ocean to the east, west, and north of each sandpit.

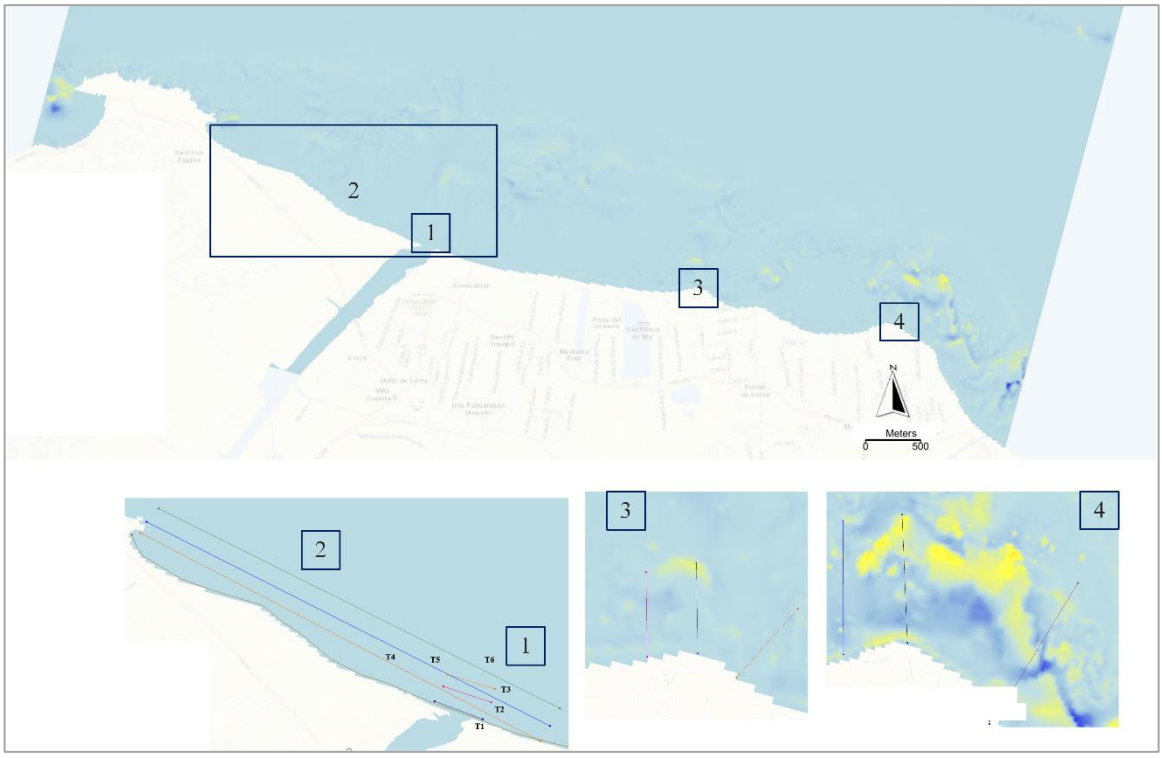

Figure 3.18 Areas of Interest and Profile Transects

3.5.5.1 Río Grande de Loíza River Mouth

The morphological changes in three transects drawn at the mouth of the Río Grande de Loíza are shown in Figure 3.19. Transect 1 is landward, Transect 2 is at the center, and

Transect 3 is oceanside. The graphs show the total morphology change per day and the distances from the east (0 m) and west (300 m).

Transect 1 showed accretion changes after Day 89 (70 m) and Day 364 (230 m). A change towards erosion in the profile was observed on Day 211 (80 m) and Day 364 (100 m). More minor changes were observed between Day 31 and Day 89 (150 to 250 m). On Day 364, I observed an up and down pattern in the eastern area. From 0 m, accretion values began to decrease continuously, but after 80 m, accretion began again, reaching the highest accretion of 2.6 m. At 240 m out from the river mouth, morphological change began to be erosional again, with a further slight increase in erosion at 260 meters.

Transect 2 showed homogenous morphological change in the first 40 m, except between Day 31 and Day 89. At 120 m from the river mouth, a divergence in morphological changes was observed for Day 31 and Day 89. At 250 m out, an abrupt change towards erosion was observed from Day 89 to Day 211. Day 31 showed higher accretional than Day 89, except at 270 m from the river mouth. Day 89 and 211 mainly showed the same pattern, except at 280 m.

Transect 3 showed a similar pattern beyond 150 m from the river mouth. Day 31 and Day 89 showed similar morphological changes in the first meters, but Day 89 was slightly more accretional. At 179 m from the river mouth, differences between these two dates began to be observed, with Day 89 exhibiting erosion. At the same distance, Day 211 and Day 364 also showed an abrupt change in erosion patterns, although both profiles were similar.

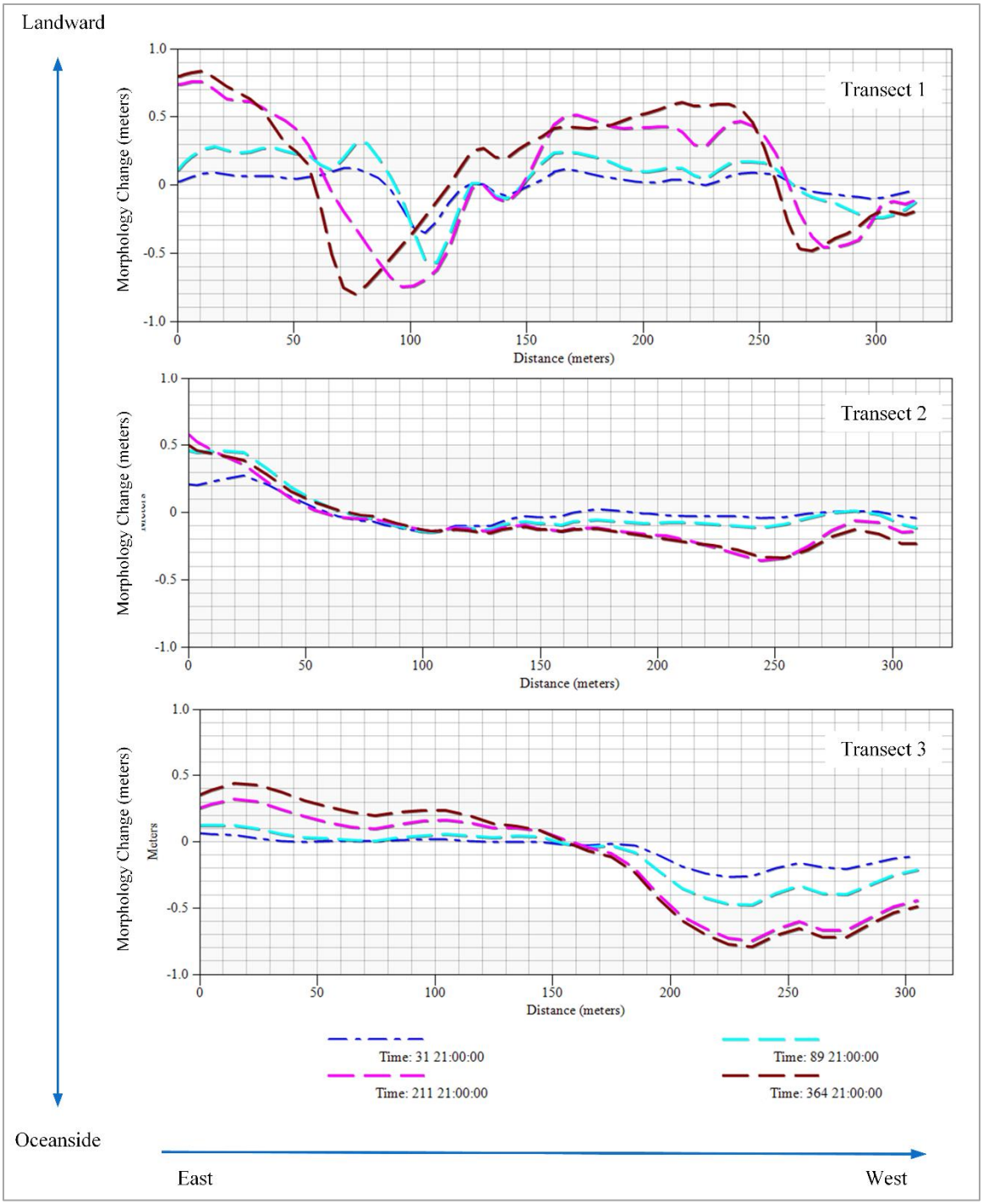

Figure 3.19: Transect Profiles Showing Morphological Changes at Different Distances from the Mouth of the Río Grande de Loíza

The other transects (4, 5, and 6) captured the submarine canyon area and the changes in morphology that occurred there Figure 3.20. The channel was observed approximately

1,500 m away from the river mouth. The profiles from Transect 4 and Transect 5 showed the most significant variation in the first 50 m. All three transects showed the highest accretion during Day 364.

Transect 4 showed an erosion pattern on the last day within the first 500 m from the river mouth, followed by accretion until 1,600 m. Near 2,000 meters, erosion was measured, followed by accretion in the last meters. Transect 5 showed a switching pattern in the first 500 m, higher accretion in the later days, and erosion between 500 and 800 m from the river mouth. A similar pattern was observed after the canyon, at 2,000 m. Transect 6 showed no abrupt changes among the dates, except from 400 m to 2,000 m. The most significant change was observed on Day 364, where accretion at 1,5000 meters is compensated for erosion at 1,900 meters. After this distance, accretion is observed at 2,100 meters All transects showed accretion from 1,000 to 1,600 meters in the submarine canyon area on Day 211 and Day 364.

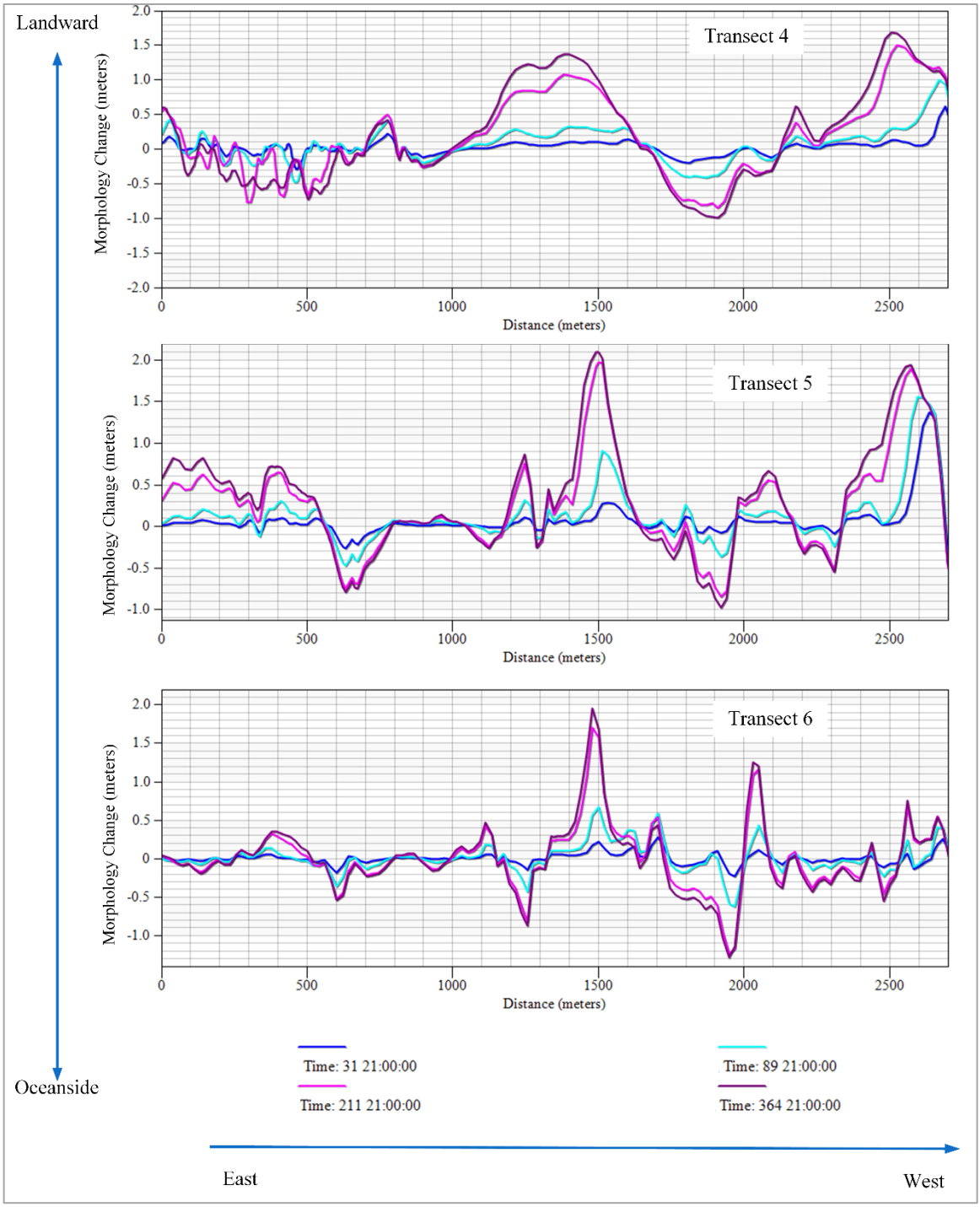

Figure 3.20: Transect Profiles Showing Morphological Changes along the Río Grande de Loíza Area and Submarine Channels

3.5.5.2 Punta Iglesias Sandpit

Transect profiles drawn to the east, north, and west of the Punta Iglesias sandpit are shown in Figure 3.21. The maximum distance from the land to the ocean was 250 m. Transect 1 shows the west area, Transect 2 shows the north, and Transect 3 shows the east area. Each graph illustrates transect profiles for the four different days chosen.

Transect 1 showed an increase in accretion patterns. On Day 31, no change was observed along with the profile, except from 140 to 180 m. At this distance, low levels of accretion were observed. On Day 89, a slight erosion was observed in the first few meters, but after 20 m, a continuous increase was observed. At 170 m, a decrease began again until it decreased to below the Day 31 morphological change. The most evident changes were observed on Day 211 and Day 364. On Day 211, the highest accretion value occurred around 70 m, and at 170 m, there was a continuous decrease to below Day 31 and Day 89 levels. On Day 364, there was a decrease between 60 and 100 m in comparison to Day 211. From 110 m to 170 m, there were nearly identical patterns of morphological change, but they began to bifurcate at 170 m. On Day 364, the lowest values of morphological change were observed, when compared to the other days.

Transect 2 showed a pattern of erosion. On Day 31, morphological changes were minimal except after 200 m, where erosion began. On Day 211, I observed a pattern to that of Day 31, but at 130 m, Day 211 began to move gradually toward erosion, reaching lower levels than those of Day 31. On Day 211 and Day 364, nearly identical patterns were observed, although on Day 364, the changes appeared to occur closer to the land. For both dates, I first observed accretion, but after a certain distance, change decreased towards erosion. On Day 211, change began to decrease at 60 m, whereas on Day 364 the

change began closer to the land, by 45 m. On Day 364, I observed the lowest values and, hence, the highest erosion.

Transect 3 showed similar patterns on the earliest dates (Day 31 and Day 89) and the latest dates (Day 211 and Day 364). I observed no change between Day 31 and Day 89, except at 220 m, where minimal accretion was observed. For Day 211 and Day 364, I also observed a close similarity, with accretion in the first meters and then a continuous increase after 50 m, with Day 364 having the highest value. At 220 m, on both days, a decrease was observed.

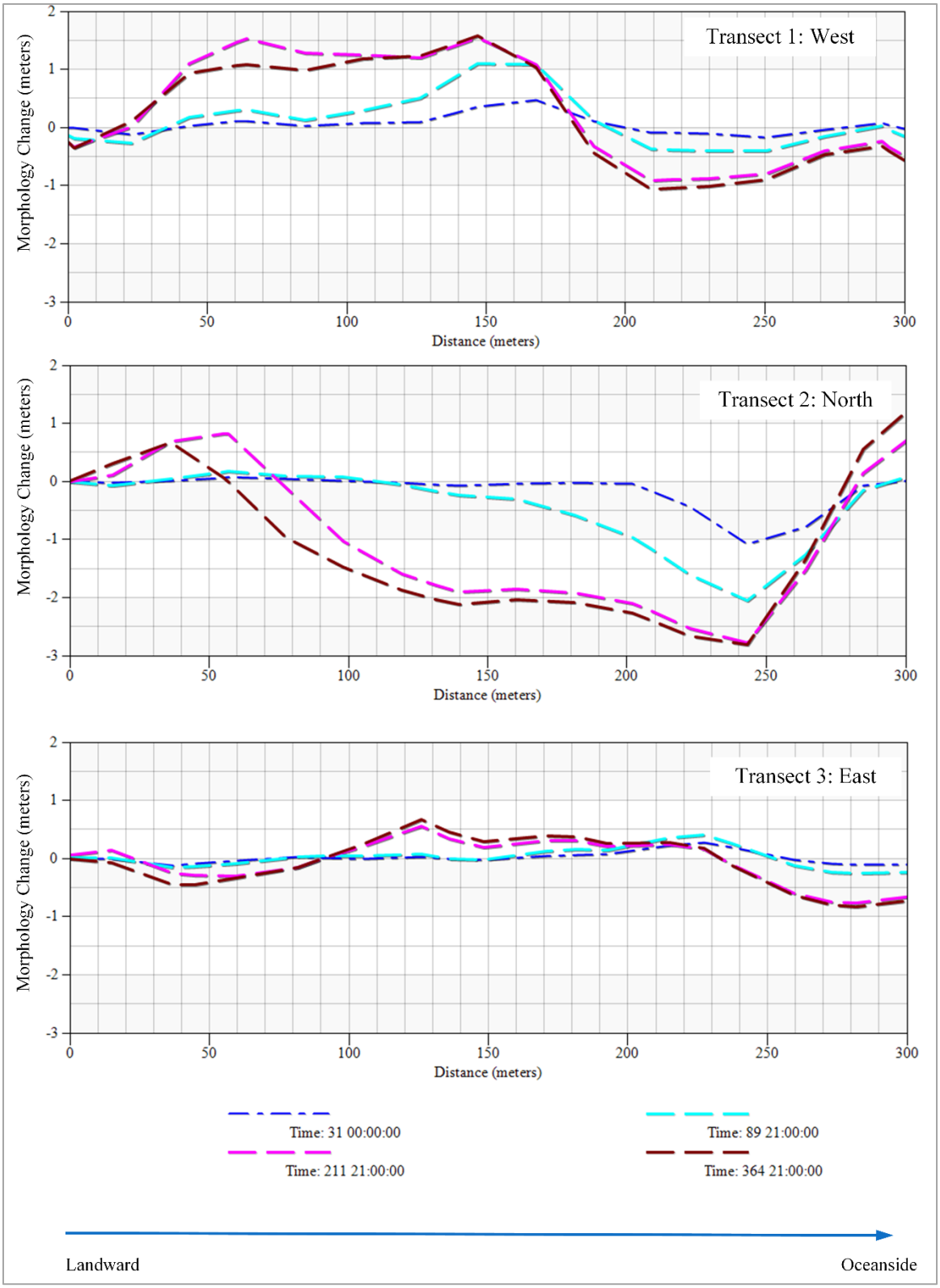

Figure 3.21: Transect Profiles Showing Morphological Changes to the West, North, and East of the Punta Iglesias Sandpit

3.5.5.3 Punta Uvero Sandpit

Transect profiles drawn to the east, north, and west of the Punta Uvero sandpit are shown in Figure 3.22. For this sandpit, Transect 1 was drawn through the west area, Transect 2 was drawn through the north area, and Transect 3 was drawn through the east area, up to a maximum of 300 m from the shoreline.

Transect 1 showed an erosional pattern. On Day 31, the most visible change was observed at 100 m from the shoreline, where some erosion was observed. On Day 89, a similar pattern to Day 31 was observed, but with higher accretion. Both Day 211 and Day 364 exhibited erosion in the first 20 m. Beyond this distance, both profiles showed an increase in accretion, although Day 364 showed the highest accretion rate.

Transect 2 showed more variation between the early days (Day 31 and Day 89) and the later days (Day 211 and Day 364). The four dates showed a rapid inclination to erosion in the first 30 m. Day 31 showed continued erosion from 60 m to 240 m, where a slight increase began. Day 89 showed a higher inclination to erosion than Day 31, and at 70 m, it surpassed Day 31 with higher accretion until 250 m. Day 211 and Day 364 showed no change from 20 to 40 m, then showed a constant increase in accretion, reaching the highest accretion around 90 m. A constant inclination toward erosion was then observed until 250 m, where change increased to accretional. Day 211 showed a rapid inclination to erosion, reaching the lowest erosion at 240 meters. At 40 m from the shoreline, values began to increase towards accretion until near 90 m.

Transect 3 showed a more negligible difference in morphological changes among the four days. Day 31 and Day 89 showed very similar changes until 60 m, beyond which

Day 89 started to show higher erosion than Day 31. Both days showed an increase at 250 m, with the highest accretion being reached on Day 364.

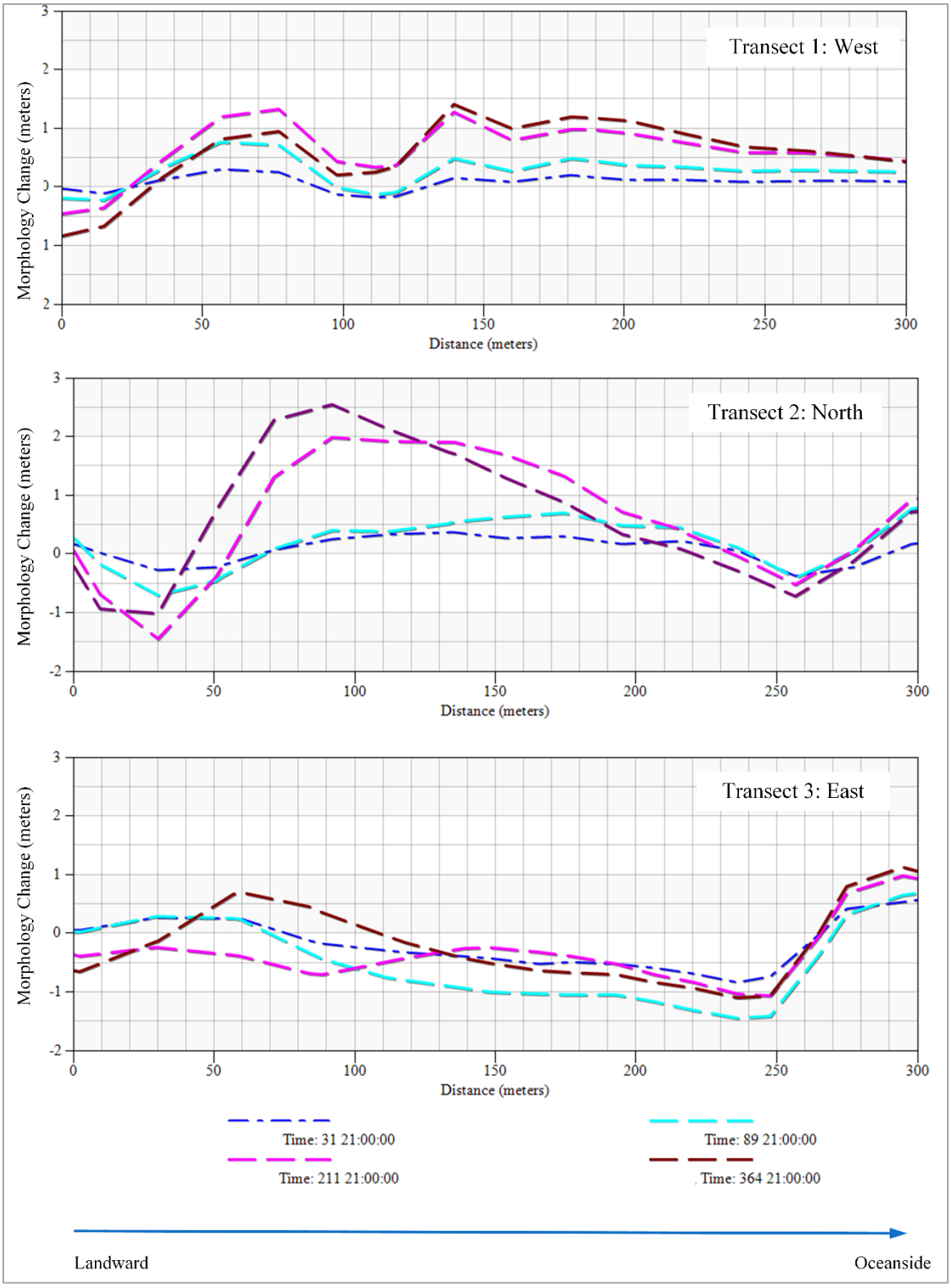

Figure 3.22: Transect Profiles Showing Morphological Changes to the West, North, and East of the Punta Uvero Sandpit

3.6 Discussion

Numerical modeling is crucial for scientists to understand what is happening in Puerto Rico when unique features such as wind, bathymetry, wave energy, and sediment sizes interact to give a unique shape of coastal features during different seasons. Before this project, a study of hydrodynamics had not addressed the entire Loíza coastline. The application of numerical modeling in Loíza, Puerto Rico, could be further validated by adding storm data parameters, as conducted by Chardón (2013), who used Hurricane Sandy parameters. Moreover, the modeling can be run using different sea-level scenarios to understand how this may affect sediment transport along the coast.

Other sources for hydrodynamics around Puerto Rico can be found online. For example, one of the primary sources for understanding hydrodynamics in Puerto Rico is the Caribbean Coastal Ocean Observing System (CARICOOS, 2022), which uses numerical modeling to project and forecast currents and wave energy along the coast of Puerto Rico. Another work that provides historical information concerning the wave atlas for Puerto Rico was developed by the Center for Applied Ocean Science and Engineering (CAOSE) from the University of Puerto Rio, Mayaguez Campus (CAOSE, n.d.)

Numerical modeling showed valuable information when compared to shoreline change results. For example, one hotspot of erosion in Loíza has been Punta Uvero in Parcelas Vieques. The morphological changes for 2018 showed erosional areas nearshore but more accretion oceanside. This change may be explained by nearshore bottom morphology to the north of Punta Uvero, which moves sediment to the east and seaward according to the current's path.

Bathymetry is a crucial dataset for this type of model; hence, the importance of having updated bathymetry for both nearshore and oceanside. In this regard, continuous data are available from the Joint Airborne Lidar Bathymetry Technical Center of Expertise (USACE, n.d.-a). Other expeditions, such as the NOAA Okeanos ship, also provide new seafloor mapping for future research (NOAA, 2022c). These explorations and future data production will narrow the gap in data for the insular platform in Puerto Rico. Moreover, it will make the application of hydrodynamic modeling even more feasible for future hard stabilization projects.

New coastal armoring projects, such as in the case of Punta Iglesia, should use numerical modeling in their approaches to decide the impacts of the revetment. For example, CMS modeling by the agency was conducted in the San Juan area in 2016 (Kelly et al., 2016), but no simulation modeling was conducted, according to the appendices for the revetment created in Punta Iglesias (USACE, 2018). According to Bush et al (2009), Loíza has been a center of "inconsistent" shoreline stabilization projects. Numerical modeling could tackle this already known situation to best protect the communities, infrastructure, and cultural heritage present on Loíza's coast.

Other research has addressed the validation of these models by comparing field data observations to the numerical model results (Chardón, 2013; Solano et al., 2018; Li et al., 2019). For the current study, this kind of approach was not conducted, although in future work, similar approaches could be undertaken by other researchers (Wang et al., 2019; Peterson, 2019).

In general, I recommend that these types of model outputs, such as morphological changes and wave-current animations, should be available for the community to

understand better these patterns, as has been done by CARICOOS. Recognizing the time and resources needed to run this kind of model, modeling could be run with systematic timeframes to understand the patterns. Moreover, as new data continue to be collected, the quality of the model projections will improve.

3.7 Conclusions

CMS-Flow and CMS-Wave modeling showed nearshore and insular platform bottom morphology changes. At the same time, by mapping currents, and wave velocities and heights, a comparison between morphological change and these variables could be addressed. Along the coastal area of Loíza, I was able to observe the seasonal pattern of currents from January to March and from September to December, with gentle variations in the wave-induced current velocities (Figure 3.14). At the same time, wave direction was primarily perpendicular to the coast, except in areas to the northeast (Figure 3.15). This suggests the possibility that most of the nearshore and insular platform bottom morphological changes are due to current movement rather than wave height changes.

Visual patterns indicated the possibility that nearshore/insular platform bottom morphological changes were associated with current patterns. On Day 31, I observed how sediment was eroded by currents coming from east to west (Figure 3.14) northward of Punta Uvero. Sediment deposition was observed westward, possibly caused by the circular movement created as wave-induced currents approached beaches. This circular motion was increased on Day 89, moving sediment to the east, and producing sediment deposition to the north. In addition, the eddies observed to the north of the Punta Uvero sandpit could be caused by the accumulation of sediment in the north area.

Morphological changes along the mouth of the Río Grande de Loíza showed more variability in the landward Transect 1 than the oceanside transects (Transects 2 and 3). This change is reflected in the precipitation and discharge information of the USGS (Station 50059050), where some of the highest values were recorded in June, July, and

November. The change in the oceanside profile could indicate that river discharge erodes the first sections of the oceanside transects, in turn suggesting that river discharge has an influence, as the current maps showed the fastest current (0.50 m/s) exiting the river, which was reflected in the abrupt change at 100 m. On the oceanside transects, erosion and accretion patterns were observed between the early days (Day 31 and Day 89) and the later days (Day 211 and Day 364). The early days' accretion patterns could indicate rain discharge from the rainy season between March and April, whereas the erosion in September could be an indication of less frequent rains, and thus fewer sediment inputs from the river.

The morphological change profiles at Punta Iglesias and Punta Uvero showed a similar pattern in the north. For example, both northern transects showed more variability than the western and eastern transects. At Punta Uvero, this transect showed higher accretion, whereas Punta Iglesias showed the highest erosion among all the transects analyzed. In contrast, on the western transects, the latest dates showed the highest accretion in both areas.

At Vacía Talega, morphological changes may be associated with wave energy and wave-induced currents, as wave-induced currents were observed to move sediment with higher current velocities on Day 89 and Day 211. Sediment accumulation was identified at the site for this period. Along with the rocky coastal type, however, sediment loss was observed. At the mouth of the Río Grande de Loíza, sediment deposition was identified along the channels, as currents from east to west moved sediment to this area from Day 89 to Day 364.

The results from the CMS model also provided other information about the area's hydrodynamics (e.g., wave period, current magnitude) that were outside the scope of my research. For this research, I was interested in observing morphological changes and current patterns along the nearshore and bottom insular area of Loíza. Further research can be conducted to analyze the additional variables provided in the models.

Chapter 4 – ASSESSMENT OF PHYSICAL VULNERABILITY OF ARCHAEOLOGICAL SITES AND PRIORITIZATION RANKING FOR MANAGEMENT IN LOÍZA, PUERTO RICO IN RESPONSE TO THREATS OF CLIMATE CHANGE ACCELERATION

4.1 Abstract

This study evaluated the physical vulnerability of archaeological sites in Loíza, Puerto Rico to climate change acceleration threats. I used the physical vulnerability and the archaeological significance documented for each site to assign a prioritization ranking value for management purposes. To do so, I combined GIS, remote sensing, statistics, and fieldwork methods to modify the Scottish Coastal Archaeology and the Problem of Erosion (SCAPE) model to include coastal erosion, shoreline recession, and flooding due to storm surges, tsunami, high tide levels, and sea-level rise risks.

First, the archaeological database was homogenized, including the chronological period, and significance was evaluated using previous archaeological reports. Next, the physical vulnerability was calculated using several variables. Shoreline change analysis was conducted in Loíza using seven historical shoreline positions (1902, 1931, 1951, 1977, 1990, 2010, 2018) and the Digital Shoreline Analysis System. Trends in rates of change (linear regression rates, LRR) per area evaluated physical vulnerability to erosional rates. Moreover, using the LRR, I estimated when archaeological sites could be impacted by shoreline recession. Additionally, a composite flooding map from the National Oceanic Atmospheric Agency was used to analyze which sites were vulnerable

to specific flooding events (FEMA Zones, sea-level rise, high tides, storm surges, and tsunami).

Results showed that most of the sites should be given high priority (45%), followed by medium priority (40%), with fewer sites showing low prioritization values (15%). Separately, most of the sites had a medium significance (44%), followed by low significance (28%), and high significance (27%). For physical vulnerability, most sites showed low vulnerability (55%), followed by medium (28%), and high (17%). In summary, this research expanded on the previous coastal approach by integrating the SCAPE model to evaluate possible prioritizations for archaeological sites in Loíza, Puerto Rico, based on each site's archaeological importance and physical vulnerability.

4.2 Introduction

This investigation aims to evaluate physical vulnerability and archaeological significance to establish a prioritization rank for the archaeological sites in Loíza. The prioritization intends to illustrate to management agencies which sites should be given the most importance. The following hazards were considered to evaluate physical vulnerability: (1) shoreline changes (erosion rates), (2) future shoreline recession, (3) proximity to the shoreline, and (4) flooding events such as storm surges, sea-level rise (SLR), tsunami, and high tide flooding. The total number of hazards per each archaeological site was used as the physical vulnerability value, whereas the archaeological significance was obtained from previous archeological reports.

The physical vulnerability and archaeological significance values were summed to obtain a prioritization value. This was accomplished by modifying the Scottish Coastal

Archaeology and the Problem of Erosion (SCAPE) model (Dawson, 2013). To do this, different sources and methodologies were combined: remote sensing, geographic information systems (GIS), statistical analysis, and fieldwork.

After conducting the prioritization assessment, I used a novel approach involving numerical modeling to analyze the morphological change around an archaeological site near the shoreline. A similar approach was applied by Dempwolff et al. (2020) at the Colonia Ulpia archaeological site located on the Rhine river, but no further research was found when I searched using the key words “morphology change”, “hydrodynamics”, and “archaeology”. I drew transects oceanside from the archaeological site’s location and then used the transects to evaluate the change in morphology (erosion or accretion) near the archaeological site, providing information that could be used further for management purposes.

The main questions to be answered in this research are listed below.

1. Which archaeological sites have higher physical vulnerability values?
2. Which sites show greater archaeological significance values?
3. Which sites show high, medium, and low priority rankings for management purposes? In which areas are these priorities concentrated?
4. Are any of the sites near areas of morphological change?

Archaeological sites have constantly been exposed to natural and anthropogenic impacts, but climate change acceleration has worsened this reality. The United Nations Educational Scientific and Cultural Organization (UNESCO) has published reports regarding climate change impacts on cultural properties, including those with archaeological value (UNESCO, 2007). These reports document how changes in

temperatures, water in soils, and SLR could affect the integrity of archaeological sites, including sites near the coast.

In the current climate change scenario, there have been three main approaches in archaeology to assessing climate change impacts: (1) interpreting how past societies survived and adapted to different climate change events (Cooper & Peros, 2010; Abbott et al., 2012; Ezcurra & Rivera-Collazo, 2018) ; (2) evaluating how climate change is impacting the integrity of archaeological sites at present (Dawson et al., 2017; Andreou, 2018); and (3) combining the first two approaches to evaluate the resilience of past societies and propose mitigation and protection plans for archaeological sites (Ezcurra & Rivera-Collazo, 2018; Hofman et al., 2021)

Impacts of climate change on cultural heritage, including archaeological sites, have been addressed in previous studies, as documented in a review by Sesana et al. (2021). For example, Anderson et al. (2017) evaluated the destruction of an archaeological site due to SLR projections in the southeastern United States, from Louisiana to Maryland. They used the Digital Index of North America Archaeology to document 8,637 sites within 200 km of the coast that SLR could impact. Reimann et al. (2018) evaluated how SLR-related flooding and erosion could impact 49 World Heritage Sites and concluded that 37 of the sites will be flooded in 100 years. In Puerto Rico, Ezcurra and Rivera-Collazo (2018) evaluated SLR impacts on archeological sites using SLR projections from NOAA. Threats to archeological sites caused by climate change acceleration is a topic that, through the years, has been gaining popularity among researchers. Past studies have used SLR projections or models to evaluate which sites could be impacted and concluded that SLR threatens the integrity of archaeological sites.

In combination with other coastal processes such as erosion, flooding, and storm surges, however, SLR could worsen climate change impacts on archaeological sites. Moreover, anthropogenic practices combined with these processes can provoke, for example, coastal erosion acceleration (Reimann et al., 2018). Shoreline change analysis (SCA) is one of the most common methods of measuring erosion or accretion rates in coastal areas. For example, Andreou (2018) used this method in Cyprus in the Middle East, and Hofman et al. (2021) used the same approach for the island of St. Kitts in the Antilles. Both investigations used the Digital Shoreline Analysis System (DSAS; Himmelstoss et al., 2018) to calculate the rate of change of the shoreline positions and total movement over the years (net shoreline movement), but Andreou (2018) used medieval maps, archaeological surveys, and aerial photos, whereas Hofman et al. (2021) used satellite images to reconstruct the historic shoreline.

Sathiyamoorthyg et al. (2020) evaluated erosion impacts east of the Bengal Bay using DSAS. The two archeological sites evaluated, Arikamedu and Sembiyankandiyur, were in Andhra Pradesh and Tamil Nadu. Similarly, Hil (2020) applied these methods in New Zealand, combining SLR projections and using aerial photography to evaluate the impact of archaeological sites in Blueskin Bay. Robinson et al. (2010) also took a similar approach, but they used an unpublished tool called SCARP! to calculate shoreline movement rates, along with using aerial photos and topographic sheets to extract the shoreline.

Other works have focused on how coastal erosion may affect archaeological sites and proposed management strategies. Tom Dawson (2010) focused his work on the coastline erosion process and published several papers concerning the management of

sites, using the case of Scotland. His work created the SCAPE model (2013), which he used to publish "Public Archaeology and Climate Change" (2017), gathering different investigations worldwide, including from Scotland, England, Ireland, Argentina, and France.

In addition to evaluating erosion in the coastal context, other studies have covered erosion processes in inland contexts, such as agricultural activities or natural processes like landslides affecting archaeological integrity. For example, Wainwright (1994) reported how soil erosion processes deposited sediments onto archaeological sites by applying a slope and runoff model to evaluate differences in deposition processes due to the slope level. In 2008, the conference "The Archaeology of Erosion, the Erosion of Archaeology" (Meylemans et al., 2014) presented investigations of how erosion processes have affected archaeological sites through plowing and landslides. The conference also included discussions on how GIS and remote sensing could help evaluate possible risks to archaeological data.

The Caribbean is vulnerable to climate change because of its geographic location (Abbott et al., 2012), and Puerto Rico is no exception. Although environmental hazards have been studied in Puerto Rico, their effects on archaeological sites have not been studied in detail with integrative approaches. In Puerto Rico, few researchers have focused on evaluating how climate change processes, especially SLR and shoreline erosion, can affect archaeological sites. Díaz Díaz et al. (2015) presented an assessment of the impacts of coastal erosion and loss of archaeological contexts at the II Congress of Natural Protected Areas in Puerto Rico, but unfortunately, their presentation contained no data, and a further literature review revealed no related publications.

Isabel Rivera-Collazo is the main researcher who has addressed this topic in greater detail in Puerto Rico. In her research with Ezcurra (2018), they used SLR models developed by NOAA to evaluate how archaeological sites may be impacted. This research evaluated the management of archaeological sites, coupled with two models established to evaluate a preservation priority. She focused on coastal landscapes for her dissertation thesis (Rivera-Collazo, 2011), in which she evaluated the Theory of Adaptive Changes to analyze the vulnerability of specific ecosystems and identified significant consequences of climate change: changes in boundary limits, biodiversity in the ecosystem, and knowledge. In later work, Rivera-Collazo focused on analyzing cave formations to evaluate adaptation strategies such as settlement relocation and micro-landscape modifications (Rivera-Collazo et al., 2015). Recently, Rivera-Collazo (2019) applied a desk-based approach to assessing the vulnerability of and threat to archaeological sites near the coast using aspects of the SCAPE model and the Reeder-Myers approach (2015). Finally, the national press covered Rivera-Collazo's current research as a unique work in this field of study (Figueroa Cancel, 2021a).

Before Rivera-Collazo began her investigations, Jesús Vega's doctoral dissertation (1990) was one of the pioneering studies on this topic in Puerto Rico. Vega's doctoral dissertation, entitled "The archaeology of coastal change, Puerto Rico", did not focus on the impacts of shoreline change on archaeological sites, but rather on archaeological sites that are now submerged due to changes in sea level. The main goals of his research were: "(1) to develop a maritime perspective on the Caribbean prehistoric migrations, (2) to search for intertidal and submerged sites in Puerto Rico as a case of study, and (3) to integrate the field data into a regional model of Caribbean coastal geoarchaeology" (p.4).

Vega recognized the impacts of SLR on archaeological sites but argued that there is worldwide evidence that sites could be protected by immersion, as the sea could provide protection because of its anaerobic conditions. Furthermore, he established that immersion might protect archaeological sites from anthropogenic activities such as sand extraction and looting. He also introduced the Model of Caribbean Submergence, which he defined as "a predictive and an interpretive model for the archaeological reconstruction of sea levels and coastal change."

In summary, the scientific community has recognized the possible impacts of climate change acceleration and natural processes on archaeological sites, which are a type of cultural heritage. In this current study, I evaluated the physical vulnerability of archaeological sites using a unique combination of variables. The following section describes the study area and my research questions. This research aimed to expand and refine my previously published results (Bracero Marrero, 2019).

4.3 Study Area and Scope

This study evaluated how vulnerable archaeological sites are to shoreline change, SLR, and flooding events in Loíza, Puerto Rico (Figure 4.1). Loíza, a cornerstone of Puerto Rican culture, is a place of traditions, music, festivals, tourism, and more (Bofill Calero, 2014). Much previous archaeological research has been conducted in Loíza, as it is a district with high archaeological potential (Meléndez Maíz, 1997), but processes such as dune destruction, sand extraction, vehicle transit, and human settlement have endangered the archaeological integrity of the region.

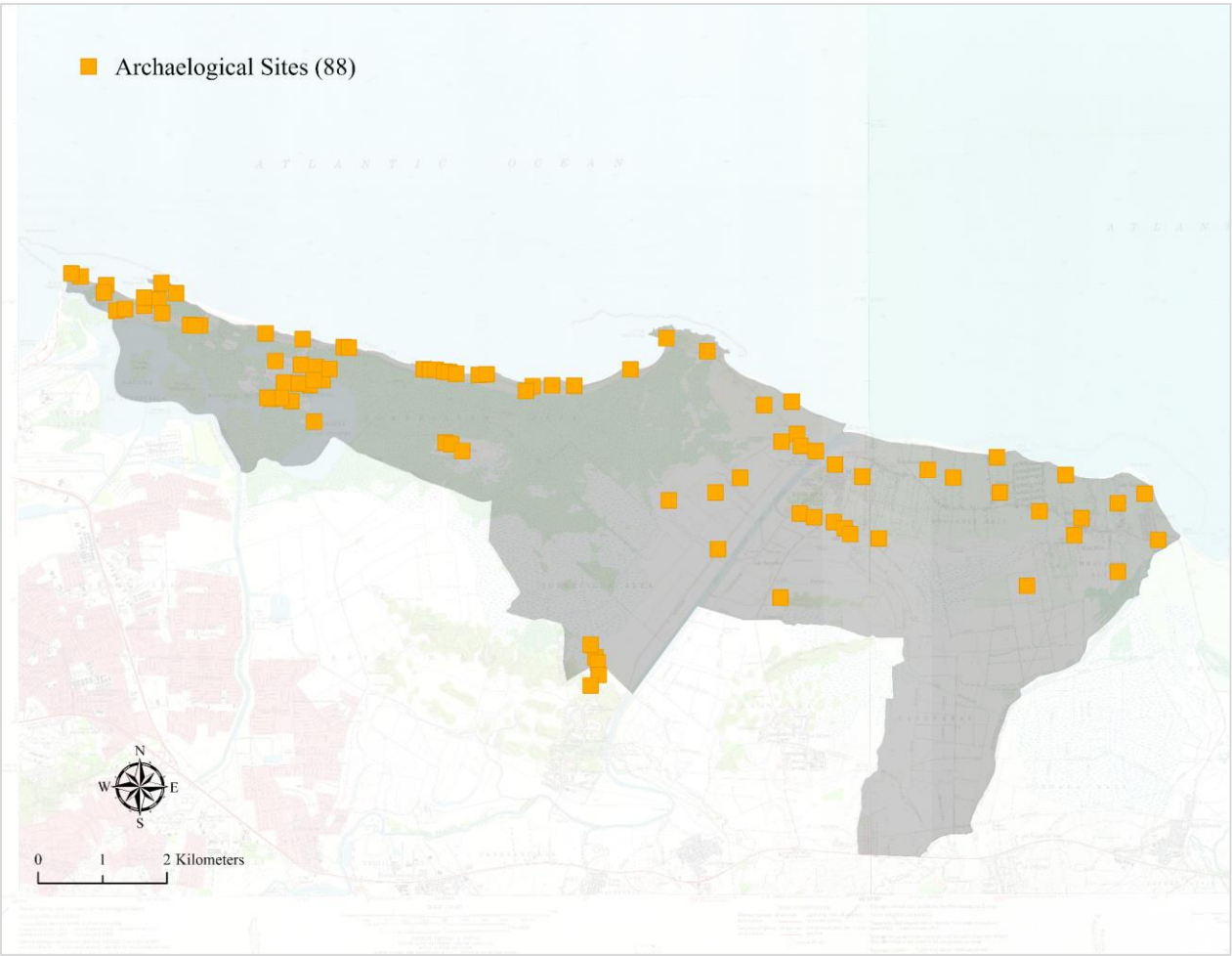

Figure 4.1: Study Area and Archaeological Site Locations (n = 88; orange squares) in Loíza, Puerto Rico. Map shows the total number of sites after merging several sources (see Section 4.4.1).

4.4 Methodology

4.4.1 Archaeological Site Data

The locations and descriptions of archaeological sites were generated from several sources. I obtained most of the archaeological data as points in GIS format, in a dataset received from the Council for the Protection of the Terrestrial Archaeological Patrimony of Puerto Rico (CAT) in 2015. I also used archaeological data presented in the archeological report "Área para la Planificación Especial de Piñones", submitted by Vélez (1990). In that report, topographic maps with site locations were included. These maps were geometrically corrected to approximate the location of the archaeological sites, pits, and residuaries, documenting 122 sites, including sites in adjacent municipalities. In addition, for each site, the historical periods, integrity, and concentration rates of archeological artifacts were recorded. Finally, the archaeological findings were divided into two different categories: sites and isolated findings. In my project, I used all the findings identified as sites.

I also visited the State Historic Preservation Office (SHPO) in Puerto Rico to consult their web map database and archaeological site inventory report of Loíza, which is available online (SHPO, 2018). The main report that I consulted was the archaeological inventory created by Meléndez Maíz and Rodríguez Ramos (1998), which included archaeological site conditions, recommendations, chronological periods, and other information for each site. I considered the location points as individual sites despite recognizing that archaeological sites are more extensive than the location point, or a cluster of points could indicate the same site.

Other publications for specific sites in Loíza were also consulted. For example, Rouse and Alegria's report (1990) focused on excavations of two of the most important sites in Loíza: María de la Cruz and Hacienda Grande. A report by Grossman and Associates Inc. (1990) was also used for additional archaeological locations. I used this information to create a new point layer in my database. Finally, the different sources mentioned were analyzed and depurated by eliminating repeated sites or adding missing sites. The final number of sites collected for Loíza was 88. The different sources used to collect the archaeological locations and descriptions are summarized in Table 4.1.

Table 4.1: Archaeological Site Sources

Source	**Total sites documented per source**
Vélez (1990)	60
GIS Point Layer CAT (2015)	44
SHPO Site Inventory	72
Maíz & Rodríguez (1998)	32

The different archaeological sources used to collect site descriptions used different terms to establish the chronological periods, but I homogenized the archaeological sites using Rouse's model (Rouse, 1992; see Rodriguez Ramos, 2010 for a critical discussion of this model). The way in which I homogenized the different classifications inside Rouse's model is depicted in Table 4.2 (see the column "Miscellaneous Classifications"). The sub-series and style were collected if available, but the "Series" attribute was given to all the sites. For those sites classified with the general term "pre-Columbian," I

assigned them to one of the corresponding three series—Ostionoid, Saladoid, or Ortoroid—and identified them with an * in the final tables in the results section.

Table 4.2: Chronological Period Homogenization Using Rouse's (1992) Model

<table>
<tr><th rowspan="2">Historic Age</th><th rowspan="2">Series</th><th colspan="2">Style</th><th rowspan="2">Miscellaneous Classifications</th></tr>
<tr><th>West</th><th>East</th></tr>
<tr><td rowspan="5">Ceramic</td><td rowspan="3">Ostionoid
600 – 1500 CE</td><td>Capá</td><td>Esperanza</td><td rowspan="2">Taíno
Chicoide</td></tr>
<tr><td colspan="2">Subseries
Chican Ostionoid</td></tr>
<tr><td>Ostiones Modified
Subseries
Ostionan-Ostionoid</td><td>Santa Elena
Subseries
Elenan-Ostionoid</td><td rowspan="2">Pre taíno
Ostionoide</td></tr>
<tr><td>Ostiones Pure
Subseries
Ostionan-Ostionoid</td><td>Monserrate
Subseries
Elenan-Ostionoid</td></tr>
<tr><td rowspan="3">Saladoid
250 BCE – 600 CE</td><td>Cuevas</td><td>Cuevas</td><td rowspan="2">Igneri
Saladoid</td></tr>
<tr><td colspan="2">Hacienda Grande</td></tr>
<tr><td colspan="2">Subseries
Cedrosan Saladoid</td><td></td></tr>
<tr><td>Archaic</td><td>Ortoiroid
1000 – 250 BCE</td><td colspan="2">Coroso
Subseries
Corosan-Ortoiroid</td><td>Arcaico
Pre-ceramic
Pre-agropotter</td></tr>
</table>

The main periods used to classify the sites using the timeframe of Rouse's model are summarized in Table 4.3. The colonial periods (PIV, PV) are classified as such because of the invasions by Spain and then the United States (Picó, 2013).

Table 4.3: Final Chronological Periods Used

ID	Value	Name	Timeframe
1	PI	Ortoiroid	1000 – 250 BCE
2	PII	Saladoid	250 BCE – 600 CE
3	PIII	Ostionoid	600 – 1500 CE
4	PIV	Colonial Spanish	1500 – 1898
5	PV	Colonial United States	1890 – 1950

4.4.2 Fieldwork

The fieldwork captured a glimpse of the archaeological sites' status and locations. I used the application Survey 123 Connect for Android to record my visits (Figure 4.2), as that tool allowed me to gather photos, voice comments, and locations. The comments gathered during these fieldwork visits were included in the final table for the archaeological sites (see Appendix.)

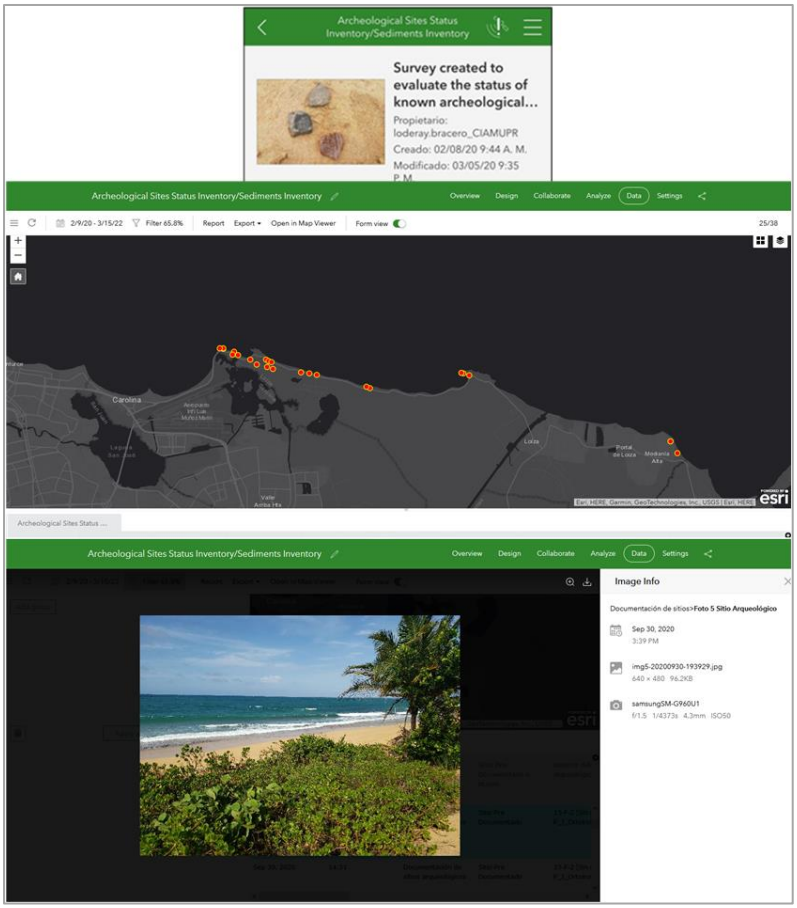

Figure 4.2: An Example of a Survey Created in Survey 123, with a Sample of Collected Data and a Fieldwork Photo. Red dots represent recorded visits.

4.4.3 Shoreline Data Sources

Several shorelines were digitized in polylinear format inside GIS to calculate erosion due to shoreline changes. I covered 116 years by collecting seven shoreline positions: 1902, 1931, 1951, 1977, 1990, 2010, and 2018. The high water line (HWL) was used as an indicator (Pajak & Leatherman, 2002) to digitize the shoreline from several sources: topographic sheets, aerial photos, and orthophotos.

Due to the image quality of these sources, the HWL could not be identified in some areas. The 1930s aerial photos were from the first flight attempt in Puerto Rico by the

United States Marines in 1930 – 1931, a project that was not completed due to funding (Sepúlveda Rivera, 2004). The aerial photos were later scanned and published in the digital journal "Revista TP" (Vélez, 2019). Sixteen aerial images were collected and used to digitize the 1931 shoreline for my project. For shorelines in 1931 and 1951, a small section (Punta Maldonado) was extracted from the raster mosaics created by López Marrero et al. (2017).

All aerial images were rectified, except for those from 1951 and 1977. Images from these years were provided by the Spatial Analysis Laboratory of the Environmental Sciences Department, UPR-RP, and I geometrically corrected them in ArcGIS 10.6.1 (ESRI, 2016) and ArcGIS Pro (ESRI, 2021). All other images were rectified with an RMSE of less than 5 m and transformed using the first polynomial transformation.

Subsequently, the HWL was digitized using a Wacom Bamboo tablet (2015), at scales from 1:300 to 1:1500, depending on the source quality. The shorelines for 2010 and 2018 were provided by the Geomorphological Laboratory, Graduate School of Planning, UPR-RP, but the shoreline for 2010 was corrected to the HWL because it initially used the wet/dry line as an indicator.

The digitized shorelines were merged into a single feature class in a personal geodatabase (.mdb), as required by DSAS. Each shoreline's data and uncertainty attributes were inserted in this feature class. Moreover, to improve the quality of the digitization, ArcGIS Topology Rules were applied: Must Not Have Dangles, Must Not Self-Overlap, Must Not Overlap, Must Be Single Part, and Must Not Intersect or Touch Interior with Errors.

4.4.4 Digital Shoreline Analysis System Add-In Tool and Statistics

DSAS Version 5.0 (Himmelstoss et al., 2018) was run in ArcMap 10.6.1 to calculate the shoreline change rate. DSAS calculates distance along time using transects and a baseline. Shoreline distances from the baseline are then calculated at a specific transect. DSAS draws the transects from a baseline created by the user to calculate statistics such as the total distance or the net shoreline movement and the rates of change. For this research, the baseline was drawn manually along the shoreline, and the transects were created every 50 m. A total of 362 transect samples were used.

I used the linear regression rate (LRR) statistic (Figure 4.3), which gives an overall trend of shoreline rates. The LRR statistics calculate the least-squares regression lines for all shorelines using each shoreline's total distance from the baseline "with respect to time (years)." Finally, for these calculations, DSAS uses all available shorelines per transect.

The LRR statistic was chosen because the differences between the other statistics, such as weighted linear regression (WLR) and the endpoint rate (EPR), were insignificant from 1902 to 2018, except for two cases. In addition, the LRR and WLR indicate trends using all shorelines, whereas the EPR uses only two shorelines (1902 and 2018). Finally, I observed that the LRR had a higher R^2 value, meaning that the transects contributed more to the rate projection.

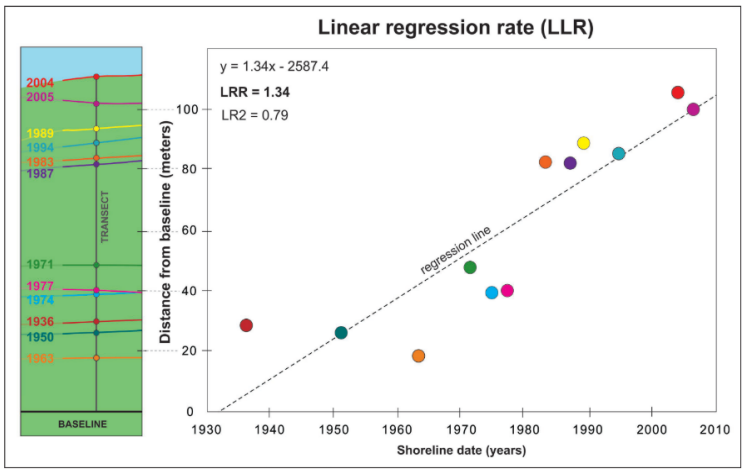

Figure 4.3: Linear Regression Rate, as Described by the Digital Shoreline Analysis System. Figure Taken from DSAS User Guide Version 5 (Himmelstoss et al., 2018, p.49)

4.4.5 Evaluation of Archaeological Significance

To evaluate each site's significance (Step 1), I used Velez's (1990) scheme (Table 4.4), as that report documented most sites. This value was edited if the sites were evaluated afterward by one of the sources I used. Two sites were assigned values of 1 due to Velez's classification in the report as "Not Apply". The significance of each context was primarily based on its conservation. Consequently, the status of the site and the possibility of future investigations were determined by its integrity, density of archaeological materials, number of cultural components, and size.

A site's integrity is based on how impacted the archaeological site has been. The density is the concentration of archaeological materials found at the site. The cultural components are the total number of time periods found on the site. Finally, the size is the approximate extension of the site, in meters. It is worth mentioning that there are various approaches to evaluating archeological significance, often referred to as "importance". All of these approaches, however, consider similar variables: cultural values, physical context, and historical context (Demas, 2000; USACE, 2014).

Table 4.4: Archaeological Significance Parameters (Vélez, 1990)

Value	Integrity	Density	Cultural Components	Size (meters)
1	Destroyed	Low	1	1 – 10
2	Severely impacted	Medium	2	10 – 25
3	Moderately Impacted	High	3	25 – 60
4	Slightly Impacted	--	4	60 – 100
5	Excellent	--	5	>100

Based on the aforementioned criteria, an archaeological significance value was determined for each site. This information was already available for the sites gathered by Vélez (1990), from Boca de Cangrejos to the west of Río Grande de Loíza. Meléndez and Rodríguez's report (1998) was used to assign a desk-based value to a site documented by SHPO. For the CAT sites and SHPO sites without significance values, I assigned a medium value of 3 for Integrity and Size, and a value of 2 for density. In addition, sites destructed by urban constructions were assigned a value of 1. Finally, each site's significance category values ranged from 1 to 18 (Step 1).

4.4.6 Physical Vulnerability to Erosion Rates

I evaluated each archaeological site's physical vulnerability to erosion rates. To establish if a rate was erosional—rather than evaluating more than 0 as accretion or less than zero as erosion—I used Stewart and Pope's classification (1993), in which a rate is considered to fit into one of five erosional categories if less than -0.3 m/year of change occurs: low, moderate, high, very high, and severe. Thus, all rates less than or equal to -0.3 m/year were considered erosional, based on the confidence interval.

The confidence interval (LCI) was calculated per transect by multiplying the user confidence percentage (95.5%) and the standard error of the slope. DSAS reported all

transects that had statistically significant erosion, and then the LCI was subtracted and summed with the LRR (LRR± LCI) to establish if a rate was significant. The rate was considered significantly erosional if it also had a completely negative LCI range (see Figure 4.4). First, I established if a rate was erosional (less than -0.3 m/yr). For example, a mean LRR of -0.49 m/yr was considered an erosional rate. The calculated LCI for this transect was 0.31 m/yr, indicating that the rate could range between -0.18 and -0.80 m/yr, both of which are negative rates.

An archaeological site with erosional rates (LRR) and both ends of the LCI range being negative was assigned a value of 1. Conversely, a site with a LRR of -0.46 m/yr and a LCI of 2.48 m/yr would be expected to exhibit rates ranging between 2.01 m/yr and -2.95 m/yr. Because one end of the range was positive, this was not considered a significant erosion rate.

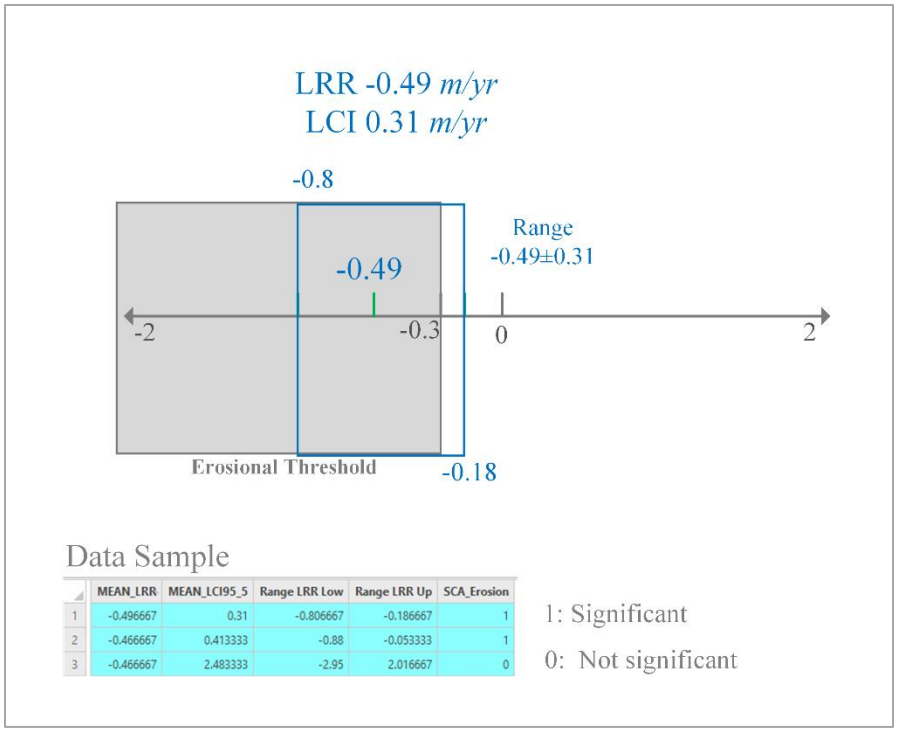

Figure 4.4: Physical Vulnerability to Significant Erosion Rates. The parameters determining whether an erosion rate was considered significant (Value of 1) or not significant (Value 0) are illustrated at the bottom of the figure.

4.4.7 Physical Vulnerability to Shoreline Recession

The LRR calculations per transect were used to estimate shoreline recession (see Figure 4.5). First, a Spatial Join (one to many) at 200 m (ESRI, n.d.-h) was applied to merge the transect attributes to the archaeological site points. Next, I chose the nearest three transects per site and calculated the average LRR, and then calculated the site's distance to the shoreline position in 2018 using the Near Distance Tool in ArcGIS Pro (ESRI, n.d.-g). Finally, I assigned the distance of each site to the shoreline and obtained the feature class of the archaeological sites and transects per archaeological site (points).

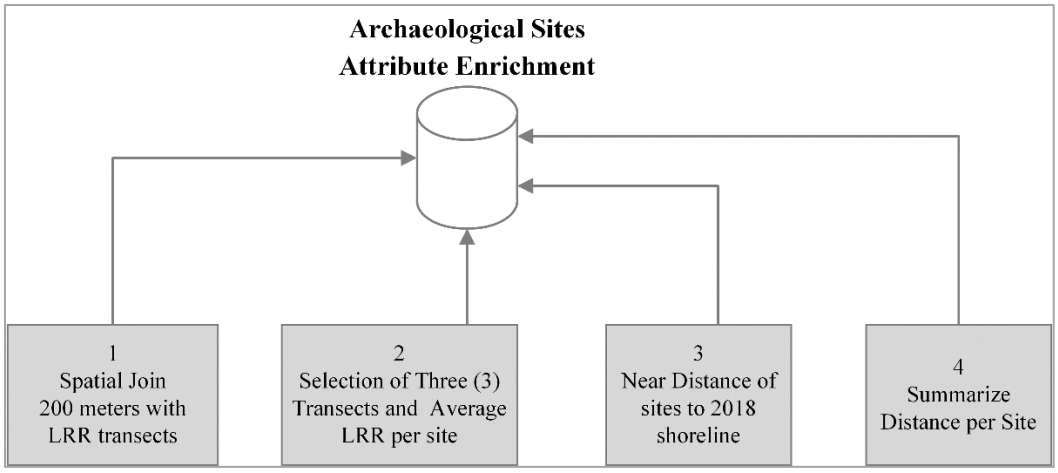

Figure 4.5: Archaeological Site Attribute Enrichment. Two attributes were assigned to each archaeological site: (1) average linear regression rates (LRR) and (2) distance to the shoreline of 2018.

Shoreline recession was considered to have occurred when, based on the LRR, the shoreline moved to the current position of the archaeological sites. For this reason, I evaluated how many years it would take for the shoreline to move to the same position as the locations of the archaeological sites.

First, I will describe the rate of change calculation to understand this approach. Equation 4.1 shows how the rate of change, or EPR, is calculated. For the EPR, the distance between two shorelines is calculated and divided by the time elapsed per transect. For example, if we used 1902 and 2018 shorelines, the time elapsed is 116 years, and the distance will vary according to the transect position.

Equation 4.1: End Point Rate, Rate of Change or Shoreline Change Rate

$$\boldsymbol{Rate\ of\ Change} = \frac{\boldsymbol{distance}\ (\boldsymbol{meters})}{\boldsymbol{time\ elapsed}\ (\boldsymbol{years})}$$

We can then calculate the time by isolating the time variable and knowing each site's distance to the shoreline (2018) and the rate of change (LRR). We can therefore estimate

how many years it will be until the shoreline recession will impact the archaeological sites. Equation 4.2 shows how the shoreline recession was estimated.

Equation 4.2: Shoreline Recession Time

$$t' = \frac{d}{\mu_{LRR}}$$

where t' is the time estimation (years) to shoreline recession impacting archaeological sites, d is the distance (meters) from each archaeological site to the shoreline (2018), and μ is the mean LRR.

4.4.8 Physical Vulnerability to Flooding Hazards: Rising Sea Levels, Storm Surges, and Tsunami

The dataset "Coastal Flood Hazard Composite," (NOAA, 2021a) published by to facilitate management decisions, was used to evaluate which flooding hazards archaeological sites were vulnerable to (Figure 4.6). The NOAA web map showed vulnerability to:

(1) high-tide flooding or nuisance flooding (U.S. Climate Resilience Toolkit, 2021)
(2) high-risk flooding (FEMA)
(3) storm surges (hurricanes, Category 1 to 3)
(4) SLR (1, 2, and 3 feet)
(5) tsunami

The data presented on the web map were requested in vector format for this research. The polygon vector data received had the "HAZ_NUM" variable, representing the total hazards per area or count. The hazards description field ("DESCRPTN") listed the types

of hazards. For example, a polygon with a total of four hazards could include the following hazards:

(1) V Zone (1% annual chance of flooding, or 100-year floodplain)

(2) A zone (1% annual chance of flooding, or 100-year floodplain)

(3) A zone (0.2% annual chance)

(4) Tsunami Run Up Zone

The hazard zones and dataset are shown in Figure 4.6. The Intersect Tool (ESRI, n.d.-f) was used to evaluate which archaeological sites fell under these hazards. Consequently, this information (hazard totals and the descriptions) was assigned to each archaeological site.

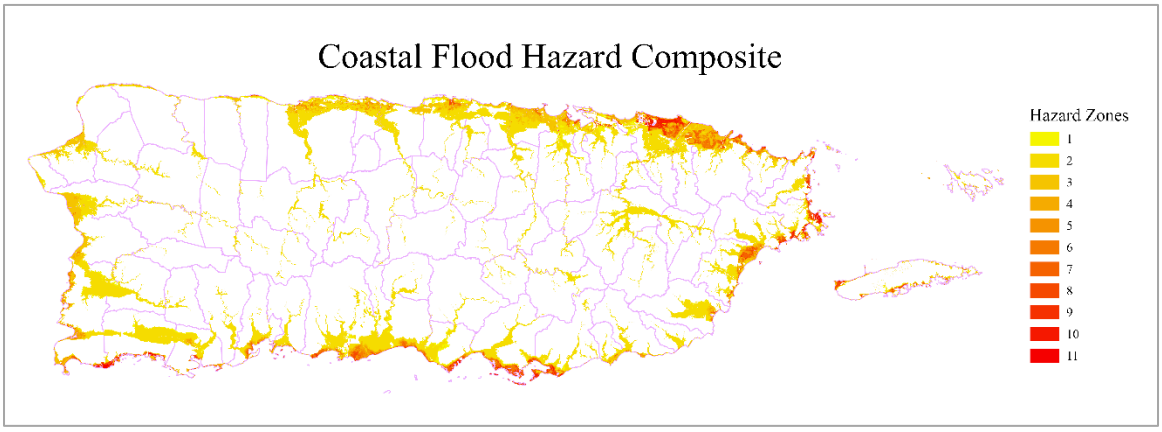

Figure 4.6 Coastal Flooding Hazards (Sea-level Rise, Tsunami, FEMA Zones, Storm Surges, and Flooding). The legend represents hazard zones: 1 to 11 hazards per area.

To estimate how different SLR scenarios could impact the archaeological sites in future years, the Assessment Flood Risks Web App Tool (Office for Coastal Management 2022b, 2002c, 2022d) was used for Loíza, Puerto Rico. This tool applied the newest 2022 projections presented in the latest report of the Intergovernmental Panel for Climate Change (IPCC, 2022). As described in "Global and Regional Sea Level Rise

Scenarios for the United States" (Sweet et al., 2022), the SLR projections were divided into five global mean sea level scenarios. The uncertainties due to processes (e.g., ice sheet melting) and emissions (e.g., greenhouse gases) were combined to generate these scenarios. The mean higher high-water line was the vertical datum used.

4.4.9 Priority Ranking Based on Physical Vulnerability and Archaeological Significance

The priority ranking for each site resulted from the physical vulnerability and the archaeological significance. After evaluating the priority for each site, I analyzed the distribution of high, medium, and low priority archaeological sites using kernel density analysis (Baxter et al., 2006). I modified the SCAPE model (Dawson, 2013) to assign these priority ranking values (Table 4.5). This model has nine stages that comprise the digitization process of archaeological data, depuration, vulnerability, and prioritization evaluation.

Table 4.5: Stages of Prioritization Using the Scottish Coastal Archaeology and the Problem of Erosion (SCAPE) Model. SCAPE Diagram Adapted from Dawson (2013, p.81) [1]

Prioritization	Action	Description
Stage 1	Create database	Digitize all records and add to database
Stage 2	Standardize records	Ensure all records carry similar information
Stage 3	Remove records without recommendation	Query database and remove all records that carry a recommendation to do 'Nil'
Stage 4	Assign sites to a class	Examine site type and description, and assign site to a class of sites
Stage 5	Assign classes to a group	Assign class of sites to a group
Review Stage 1		
Stage 6	Determine Vulnerability class	Examine condition and recommendation fields and GIS to determine erosion threat to sites
Stage 7	Remove records of non-threatened sites	Query the database and remove all sites not threatened by coastal processes
Review Stage 2		
Stage 8	Recommend action	Examine remaining records and recommend action after taking all factors into account
Stage 9	Assign priority	Assign a priority score to each site

[1] Permission to publish diagram adaptation granted by the Tom Dawson, March 4, 2022, via email.

The steps by which I applied three of the SCAPE stages are illustrated in Figure 4.7. Step 1 (Stage 5) evaluated the archaeological significance, and Step 2 (Stage 6) evaluated the physical vulnerability to erosion rates and additional variables such as flooding, proximity to erosion, and shoreline recession. For each step, the total possible value was described. For example, for Step 1, the maximum value possible for each site was 18. For physical vulnerability, the maximum was 15. Finally, the prioritization rankings ranged from 1 to 33.

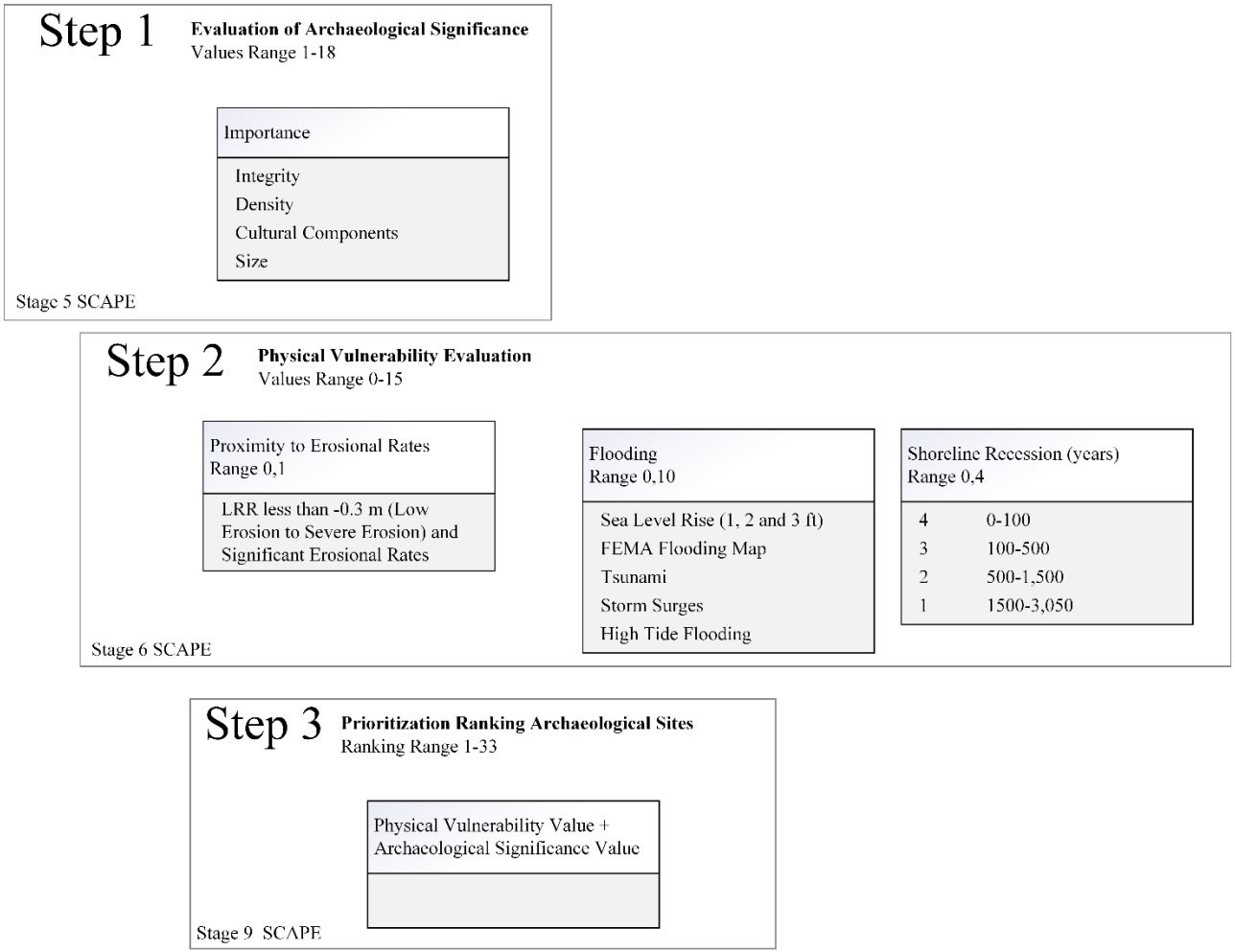

Figure 4.7: Order of Steps in which the SCAPE Model's Stages 5 and 6 Were Applied. The diagram shows the total values for each variable and the final priority ranking value.

Step 1 evaluated the archaeological significance, as described in Section 4.4.5. Four components were considered to evaluate the vulnerability to coastal processes and flooding (Step 2): (1) proximity to erosion, (2) proximity to the 2018 shoreline, (3) years until being impacted by shoreline recession, and (4) flooding events (SLR, high-tide flooding, and tsunami). I used LRR with a LCI of 95.5% to determine the proximity to erosion. Binary values were used to classify sites as not near erosion (Value 0) or close to erosion (Value 1).

The second parameter used for evaluating vulnerability was flooding hazards. I established a count of possible flooding hazards (high-tide flooding, FEMA flooding, tsunami, storm surges, and SLR), ranging from 0 to 10. The third parameter was shoreline recession. Based on the data distribution, I created four categories: 100 years, 100 – 500 years, 500 – 1,500 years, and 1,500 – 3,050 years. The values for this parameter ranged from 0 to 16.

Finally, a priority value was given to each site in Step 3. This value was obtained by adding the significance and physical vulnerability values, as calculated by Dawson (2013). The higher the value, the higher the priority for management purposes that should be given to an archaeological site. Since the range for significance was 1 – 18, and the vulnerability was 0 – 15, the range for the priority ranking was 0 – 33.

In summary, the first four SCAPE stages were applied by homogenizing and merging different data sources (Section 4.4.1), but I did not include them as part of the prioritization process. Additionally, Stages 7 and 8 were not conducted. Stage 7 was not used in this research because I evaluated all sites in Loíza, Puerto Rico, rather than only those proximate to coastal zones. Stage 8, which was intended to help archaeologist

experts propose visits, surveys, excavations, mitigation, or management plans, was not conducted because of time constraints.

4.4.10 Morphological Changes Near Archaeological Sites Using Coastal Modeling Systems

Numerical modeling was applied to analyze if these sites were near areas where morphological changes were occurring on the ocean bottom. To measure the morphological changes, I used CMS-Flow and CMS-Wave (CIRP, 2018). These models are coupled and analyze how hydrodynamics move sediment along the coast. The forcing conditions that I used to model 2018 hydrodynamics (wave currents) and morphological changes are presented in Table 4.6.

Table 4.6: Boundary Conditions for the Coastal Modeling System

Simulated Period	Tidal Constituents	Wave Forcing	Riverine Forcing
January 1, 2018 [544 days]	NOAA Station 9755371, La Puntilla, San Juan Bay, Puerto Rico	Station 41043 NDBC Steering 1 hour	Rio Grande de Loíza Damsite Station 50059050

After obtaining the results, the morphological change at one site, LO-27 Playa Berwind, at Punta Uvero near the coast, was evaluated because the site had a high priority value. I used the same three transects chosen in Section 4.4.6 and elongated them oceanside to obtain a profile showing change in the proximity of this archaeological site.

4.5 Results

The results of archaeological database depuration, evaluation of physical vulnerability, and establishment of priority values will be presented in this section. Tables and graphs were created to illustrate information regarding archaeological attributes after depuration. Additionally, maps will show the vulnerability to each physical variable and the final vulnerability value for each archaeological site. These maps were created on a smaller scale to protect the sites' locations. When needed, the results were divided into low, medium, and high values using the Jenks natural breaks classification method (ESRI, n.d.-c). Moreover, the final prioritization maps showing the Kernel densities by each priority level are also presented. The Kernel Density tool calculates the number of points in a specific area (ESRI, n.d.-d). My project ran this toll separately to establish the concentration of low, medium, and high priority values among archaeological sites in the Loíza municipality.

4.5.1 Archaeological Database

The first stages focused on polishing the archaeological data in the SCAPE model. In my project, I conducted these stages using several databases, reports, and books, as well as visiting several of the archaeological sites. The pertinent archaeological information after the depuration process is shown in Table A.1. I kept all the data source codes because, in some cases, the agencies consolidated several sites from the Vélez report into one archaeological site point. I added comments from the different sources in the "Description" field, as well as including the type of archaeological site (cave, residuary, structure), and the location used (e.g., "LOCATION CAT" or "LOCATION SHPO"). If

the location was not specified, I used the location specified in Velez's report. The "Fieldwork Comments" field showed my comments when visiting the sites, using the Survey 123 app. Finally, the "Chronological Period" showed the periods associated with each site. I assigned each site with a general dating of "pre-Columbian" to one of three periods: PI - Ortoiroid, P2 - Saladoid, or P3 - Ostionoid. I added an asterisk (*) in this field to identify these sites.

4.5.1.1 Chronological Periods of Archeological Sites

The archaeological sites in Loíza varied in their chronological distribution (Figure 4.8). Overall, amongst the sites, there were 14 unique combinations of chronological periods. The greatest proportion of the sites appeared to be from the Ostionoid period (26 sites, 30%), with the next highest proportion being from the Spanish Colonial (12 sites, 14%) period. The third highest frequency of sites dated from the Ortoiroid chronological period (11 sites, 13%). Five combinations of periods were observed at only one site each.

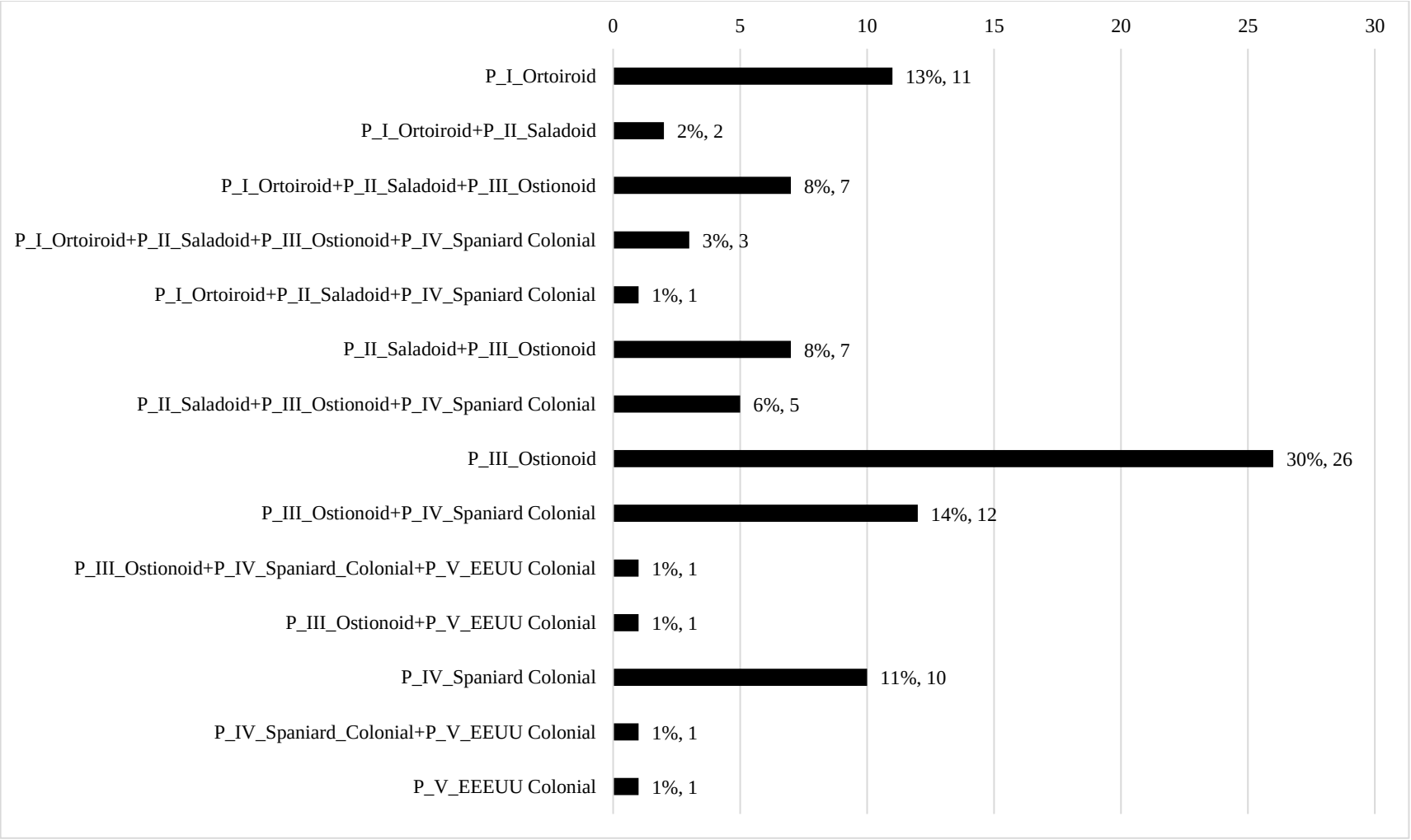

Figure 4.8: Combinations of Chronological Periods Evidenced at Archeological Sites in Loíza, Puerto Rico. Percentages and counts are shown for each category.

I also analyzed sites that only exhibited pre-Columbian, colonial, or multicomponent periods. First, I counted the archaeological sites that were only pre-Columbian (PI, PII, PIII), colonial (PIV, PV), or multicomponent (more than one period). In addition, I divided the multicomponent into sites that had: (1) more than one pre-Columbian period (PI/PII/PIII), (2) at least one pre-Columbian and one colonial period (PI/PII/PIII and PIV/PV), and (3) more than one colonial period (PIV+PV). The chronological periods I obtained by dividing the results into these categories are summarized in Figure 4.9.

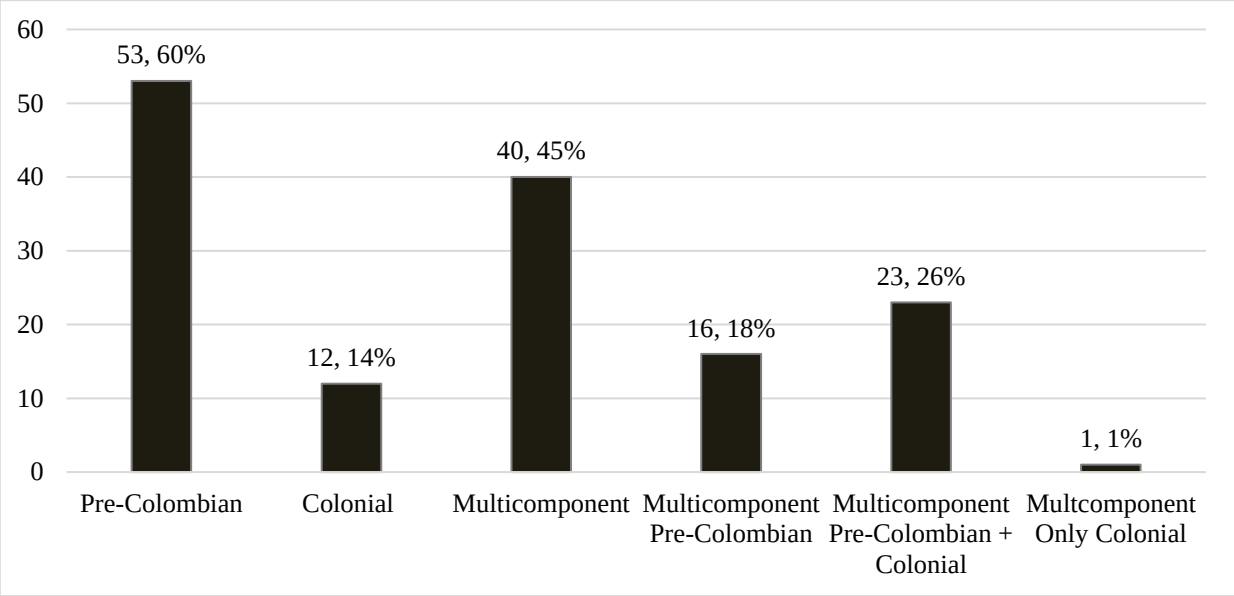

Figure 4.9: Distribution of Chronological Periods Observed at Archaeological Sites in Loíza, Puerto Rico

This analysis showed that most of the sites in Loíza, Puerto Rico are uniquely from pre-Colombian periods (60%), whereas 14% of the sites are uniquely colonial. Hence, Loíza has more archaeological sites from the pre-Colombian than the colonial period. Moreover, 45% of the archeological sites were multicomponent, the majority of which were a mix of pre-Columbian and colonial periods (26%). Finally, pre-Columbian multicomponent sites surpassed colonial multicomponent sites, comprising 18% and 1%, respectively.

4.5.2 Step 1: Significance Values of Archaeological Sites

The frequency of archaeological significance values assigned to each site are shown in Figure 4.10. Significance values of 11 were observed with the highest frequency, at 14 sites (16%), followed by values of 10 at 13 sites (15%). Significance values of 12 were observed at the third highest frequency, at nine sites (10%), followed by eight sites (9%) each with values of 6 and 13. The other remaining values were present at less than 8% of sites.

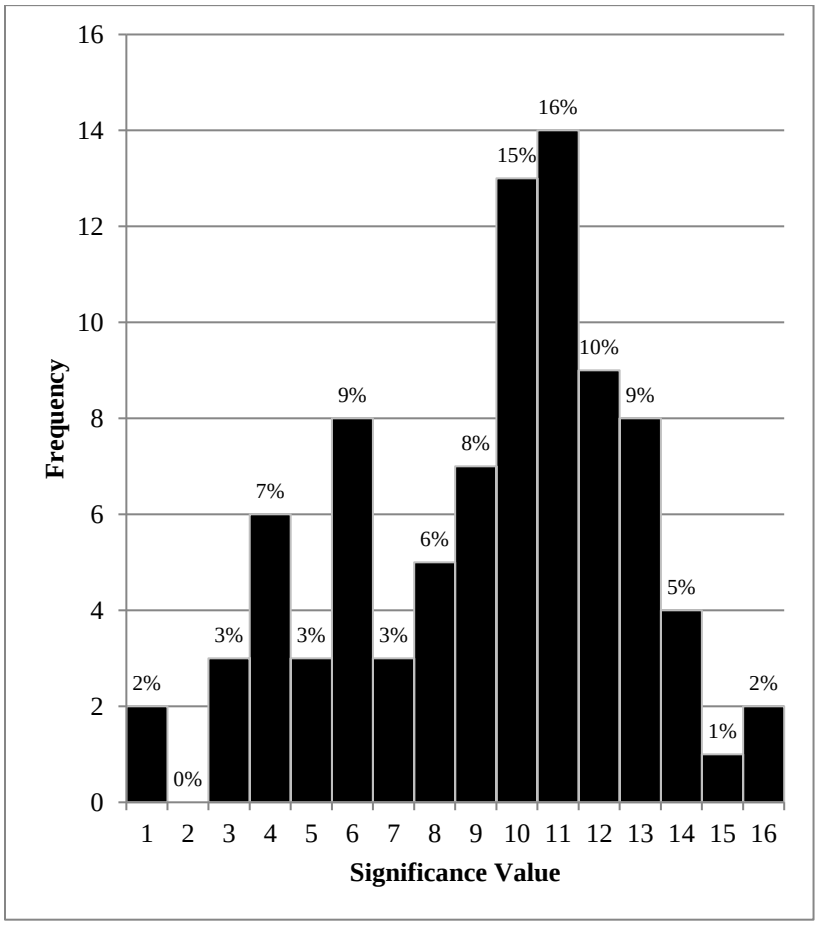

Figure 4.10: Frequencies of Archaeological Significance Values for Archaeological Sites in Loíza, Puerto Rico

Site significance values were divided into low, medium, and high significance categories using the Jenks natural breaks classification method (Figure 4.11). I observed 24 sites (27%) in the high significance category near the sandy coast and rocky land. Most sites fell into the medium category (n = 39, 44%), followed by the low category (n = 30, 34%).

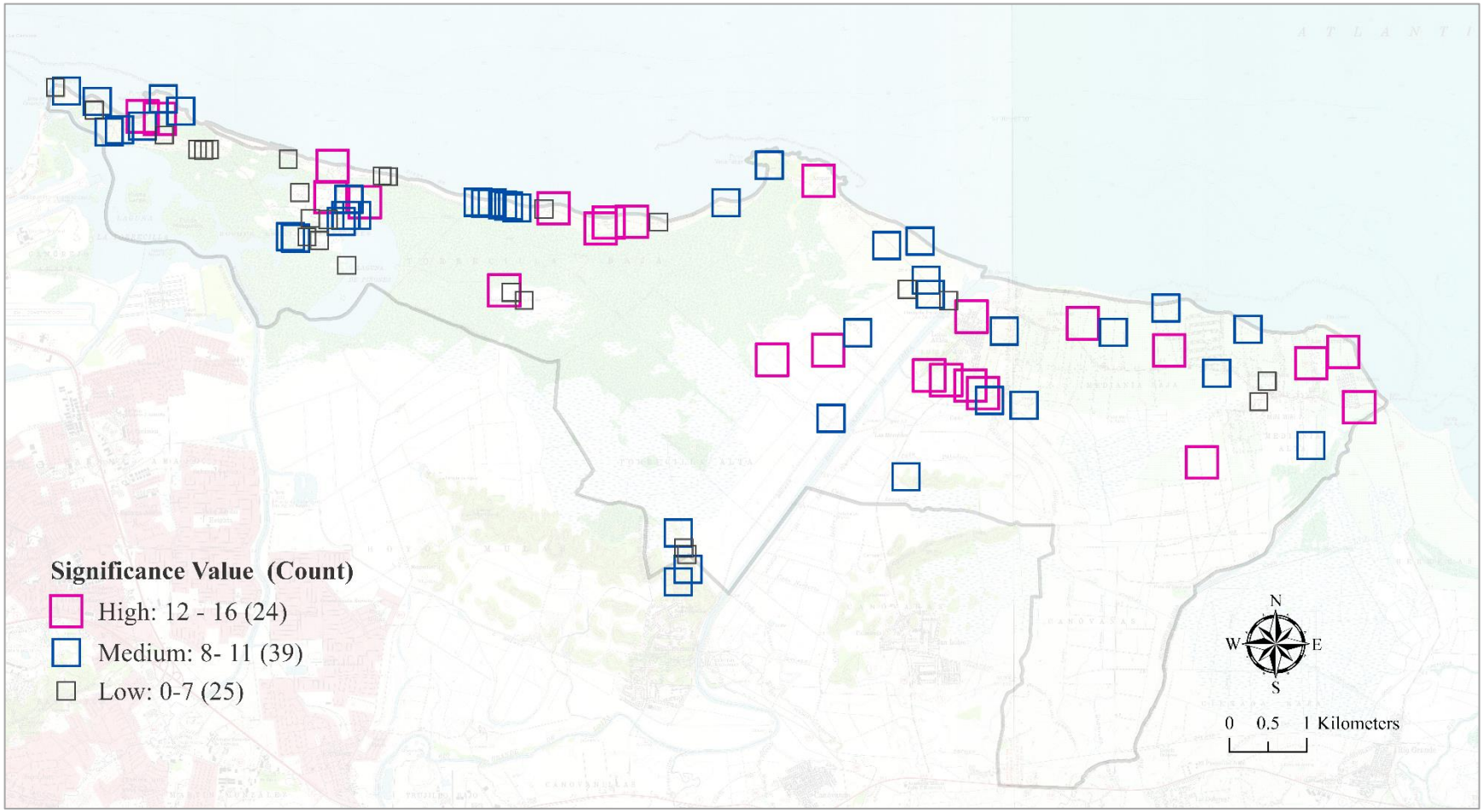

Figure 4.11 Categories of Archaeological Significance of Archaeological Sites in Loíza, Puerto Rico. Classification was conducted using the Jenks natural breaks method.

4.5.3 Step 2: Physical Vulnerability Ranking of Archaeological Sites

4.5.3.1 Vulnerability of Archaeological Sites to Significant Erosion Rates

A total of 83 archaeological sites showed a vulnerability value of 0 (86%), meaning that either the erosional LRR measured was insignificant or there was no LRR value (Figure 4.12). Only five sites showed proximity to significant erosion rates (14%).

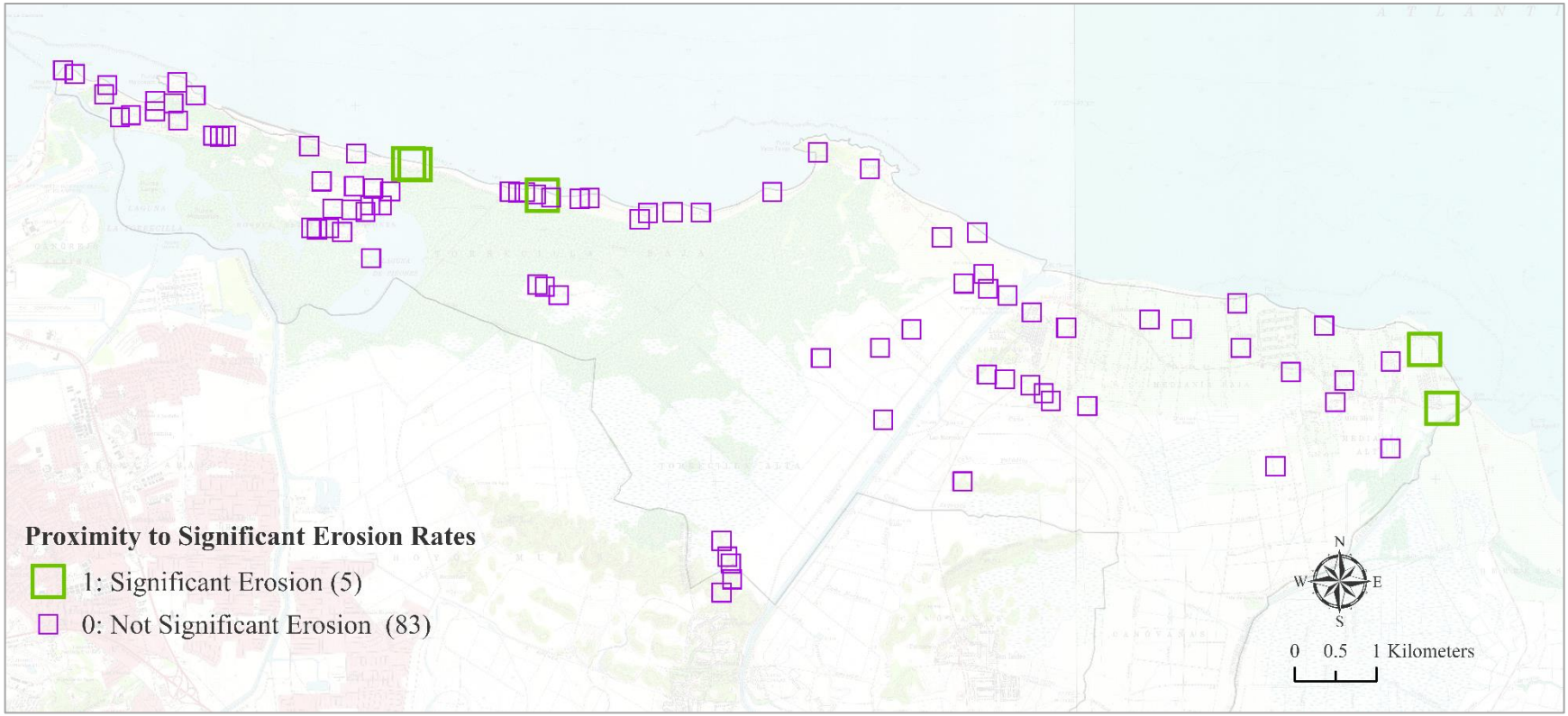

Figure 4.12: Proximity of Archaeological Sites in Loíza, Puerto Rico to Erosion Rates: Green squares represent sites with significant erosion rates, and smaller violet squares indicate no significant erosion rates or no rate data

4.5.3.2 Vulnerability of Archaeological Sites to Shoreline Recession

Using the LRR and the distance from archaeological sites to the shoreline, I estimated how many years it would be until shoreline recession affected the archaeological sites (Figure 4.13). In 100 years (Value 4), eight archaeological sites will be impacted by shoreline recession. Within 100 to 500 years, 15 sites could be impacted. For the majority of sites (n = 56), no impacts were forecasted, or no data were present.

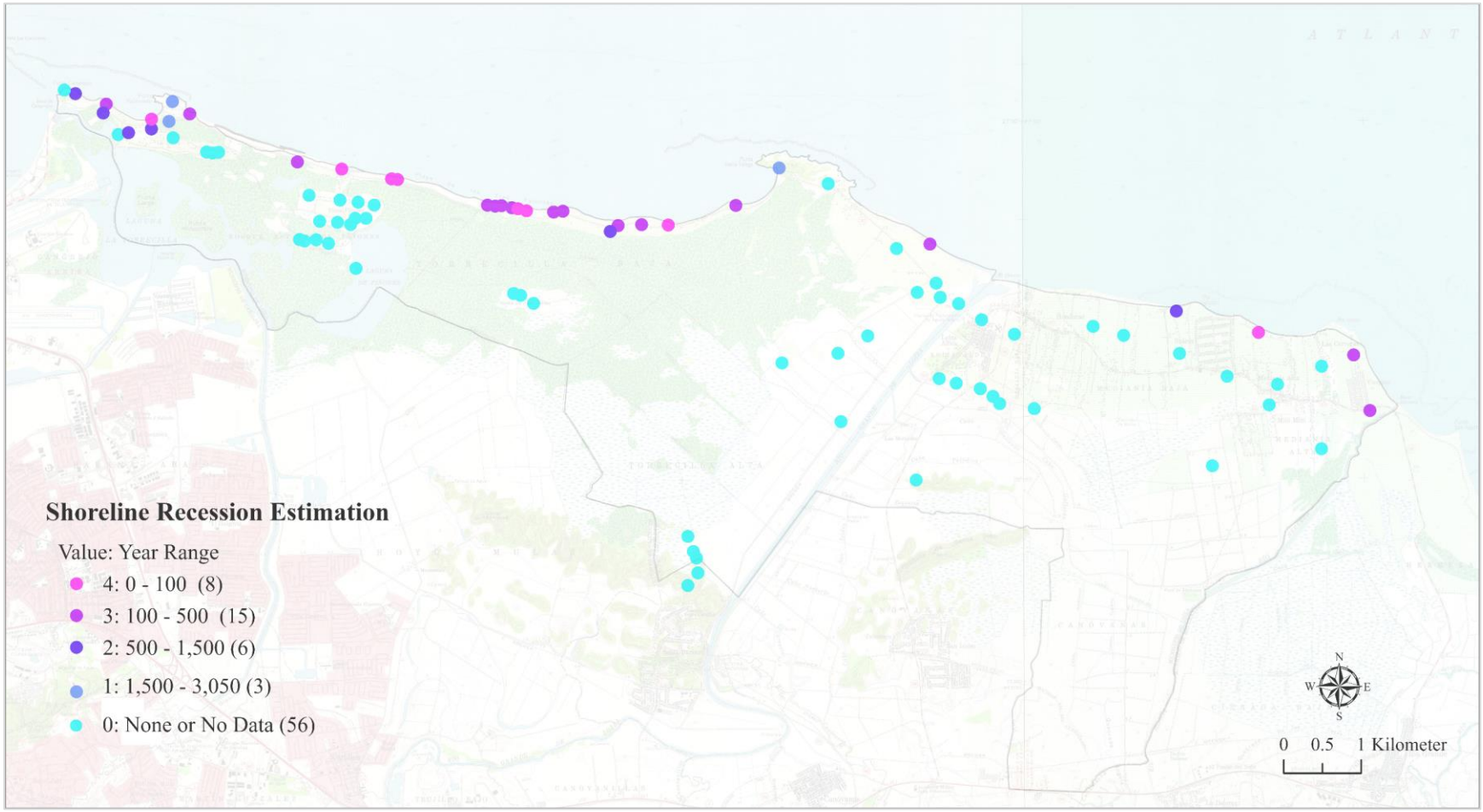

Figure 4.13: Vulnerability of Archaeological Sites in Loíza, Puerto Rico to Shoreline Recession. This figure shows when archaeological sites will be impacted according to the documented rates of change and proximity to the newest shoreline in 2018 (see Equation 4.2, Section 4.4.7).

4.5.3.3 Vulnerability of Archaeological Sites to Coastal Flooding Events: FEMA Zones, Sea-level Rise, Storm Surges, High Tides, and Tsunami

When the vulnerability of archeological sites to different flooding events was investigated using coastal flooding composite data, a total of 21 unique combinations of hazards were observed (Figure 4.14). The total number of hazards per combination ranged from 0 to 10, with a set of seven hazards being the most common combination size.

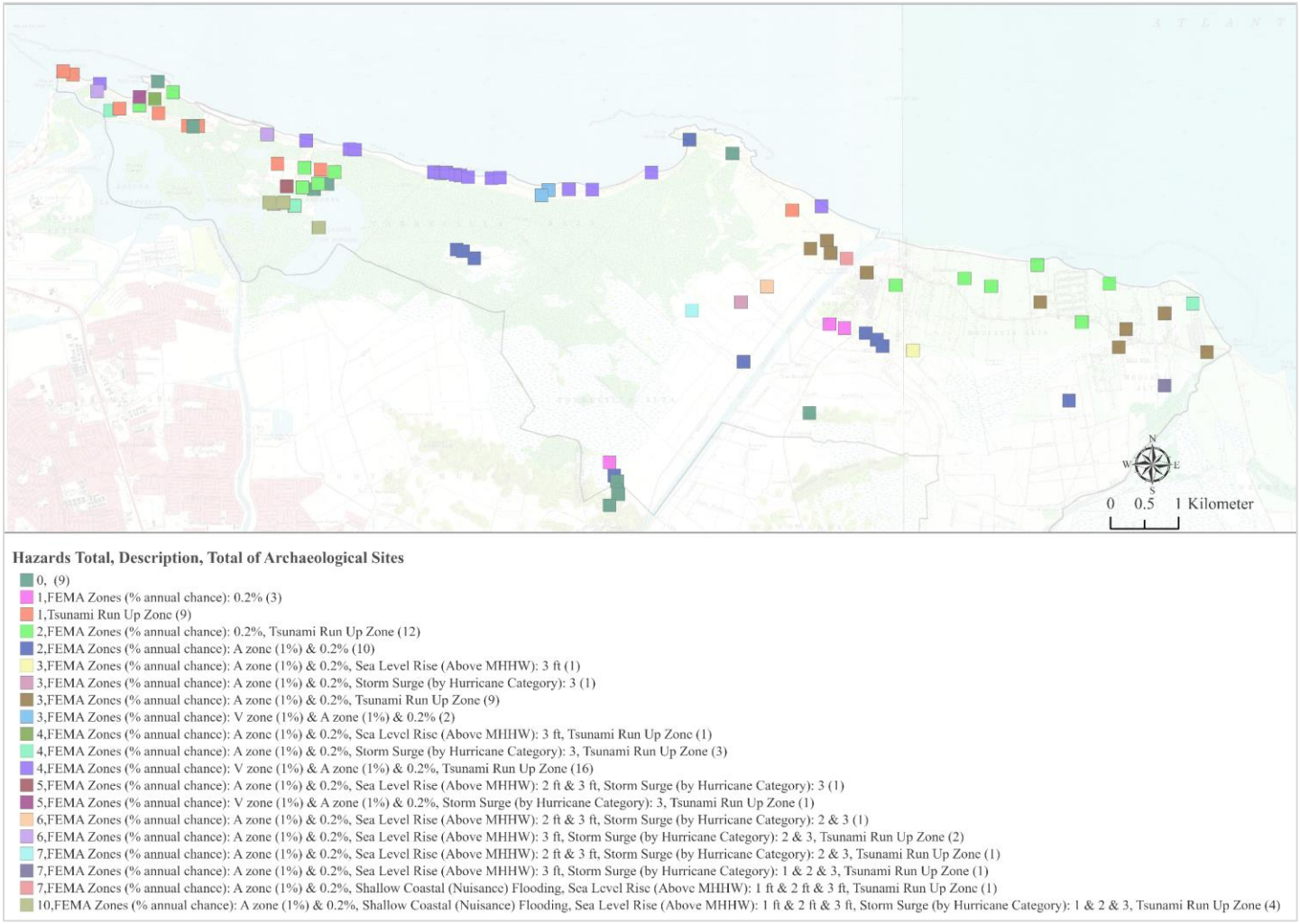

Figure 4.14: Vulnerability of Archaeological Sites in Loíza, Puerto Rico to Flooding Events. The map shows which sites could be impacted by unique combinations of flooding hazards.

The unique hazard combinations mapped in Figure 4.14 are summarized in Table 4.7. Sixteen sites had the same four hazards. Conversely, 12 sites faced the same two hazards, while another 10 sites faced a combination of two different hazards. Moreover, four sites presented the largest combination of hazards, 10 in total, and nine sites showed 0 possible hazards.

Table 4.7: Total number of archaeological sites in Loíza, Puerto Rico that are vulnerable to different unique combinations of flooding hazards

Total Number of Sites	Hazard Total	Combination of Hazards
16	4	FEMA Zones (% annual chance): V zone (1%) & A zone (1%) & 0.2%, Tsunami Run Up Zone
12	2	FEMA Zones (% annual chance): 0.2%, Tsunami Run Up Zone
10	2	FEMA Zones (% annual chance): A zone (1%) & 0.2%
9	3	FEMA Zones (% annual chance): A zone (1%) & 0.2%, Tsunami Run Up Zone
9	1	Tsunami Run Up Zone
9	0	None
4	10	FEMA Zones (% annual chance): A zone (1%) & 0.2%, Shallow Coastal (Nuisance) Flooding, Sea Level Rise (Above MHHW): 1 ft & 2 ft & 3 ft, Storm Surge (by Hurricane Category): 1 & 2 & 3, Tsunami Run Up Zone
3	4	FEMA Zones (% annual chance): A zone (1%) & 0.2%, Storm Surge (by Hurricane Category): 3, Tsunami Run Up Zone
3	1	FEMA Zones (% annual chance): 0.2%
2	6	FEMA Zones (% annual chance): A zone (1%) & 0.2%, Sea Level Rise (Above MHHW): 3 ft, Storm Surge (by Hurricane Category): 2 & 3, Tsunami Run Up Zone
2	3	FEMA Zones (% annual chance): V zone (1%) & A zone (1%) & 0.2%
1	7	FEMA Zones (% annual chance): A zone (1%) & 0.2%, Shallow Coastal (Nuisance) Flooding, Sea Level Rise (Above MHHW): 1 ft & 2 ft & 3 ft, Tsunami Run Up Zone
1	7	FEMA Zones (% annual chance): A zone (1%) & 0.2%, Sea Level Rise (Above MHHW): 3 ft, Storm Surge (by Hurricane Category): 1 & 2 & 3, Tsunami Run Up Zone
1	7	FEMA Zones (% annual chance): A zone (1%) & 0.2%, Sea Level Rise (Above MHHW): 2 ft & 3 ft, Storm Surge (by Hurricane Category): 2 & 3, Tsunami Run Up Zone
1	6	FEMA Zones (% annual chance): A zone (1%) & 0.2%, Sea Level Rise (Above MHHW): 2 ft & 3 ft, Storm Surge (by Hurricane Category): 2 & 3
1	5	FEMA Zones (% annual chance): V zone (1%) & A zone (1%) & 0.2%, Storm Surge (by Hurricane Category): 3, Tsunami Run Up Zone
1	5	FEMA Zones (% annual chance): A zone (1%) & 0.2%, Sea Level Rise (Above MHHW): 2 ft & 3 ft, Storm Surge (by Hurricane Category): 3
1	4	FEMA Zones (% annual chance): A zone (1%) & 0.2%, Sea Level Rise (Above MHHW): 3 ft, Tsunami Run Up Zone
1	3	FEMA Zones (% annual chance): A zone (1%) & 0.2%, Storm Surge (by Hurricane Category): 3
1	3	FEMA Zones (% annual chance): A zone (1%) & 0.2%, Sea Level Rise (Above MHHW): 3 ft

The total number of sites that were vulnerable to a certain number of hazards are summarized in Figure 4.15. For example, 22 archaeological sites were vulnerable to two hazards, 20 sites were vulnerable to four hazards, and 12 were vulnerable to three. Nine archaeological sites were not vulnerable to any of the flooding hazards presented in the composite map.

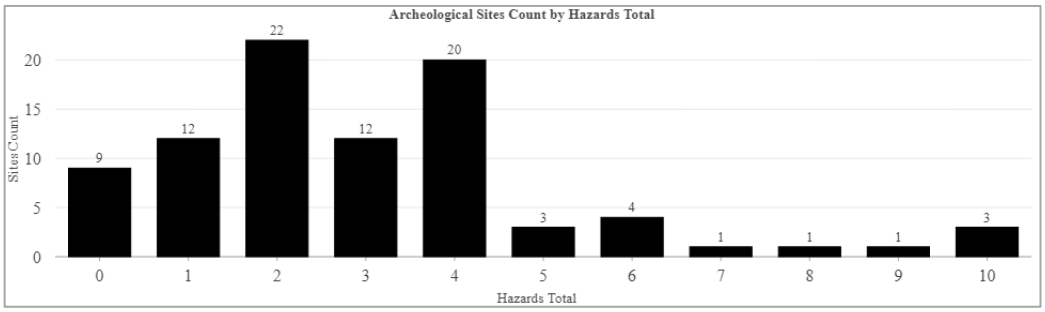

Figure 4.15: Total numbers of archaeological sites vulnerable to a certain number of hazards.

A total of 13 archaeological sites (15%) were shown to be vulnerable to SLR flooding scenarios of 1 ft (0.30 m), 2 ft (0.61 m), and 3 ft (0.91 m; Figure 4.16). Using the Intermediate scenario (see Table 4.7), four sites could be affected by a 1-ft SLR by 2050. A 2-ft SLR could impact 10 sites by 2070. Lastly, nine sites could be impacted by a 3-ft SLR by 2090.

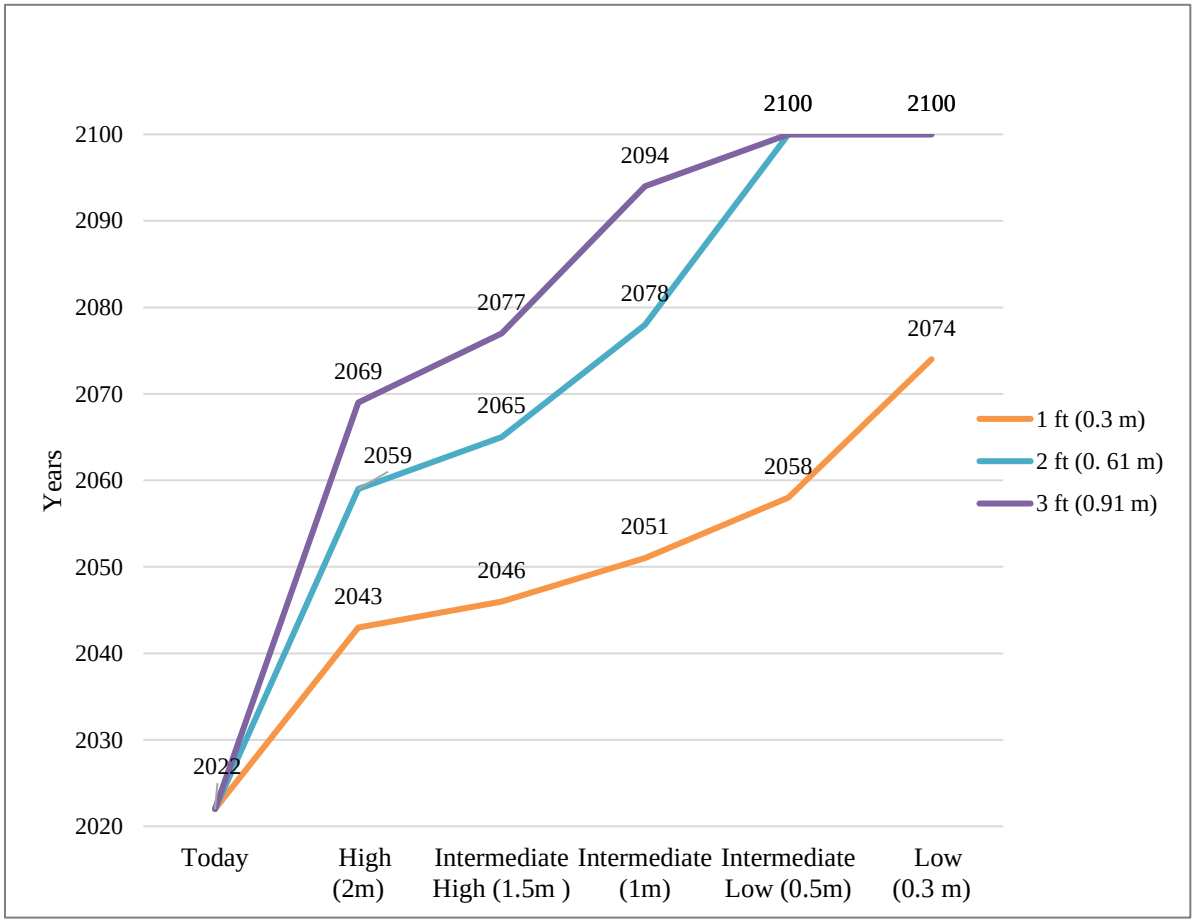

Figure 4.16: Sea-level Rise Flooding Scenarios: 1 ft, 2 ft, and 3 ft. The 2-ft and 3-ft scenarios have been projected to occur after 2100 CE.

The archaeological sites that are vulnerable to SLR scenarios are summarized in Table 4.8. Most of these sites are located to the west of Río Grande de Loíza, Piñones, Punta Maldonado, and Boca de Cangrejos.

Table 4.8: Physical Vulnerability of Archaeological Sites in Loíza, Puerto Rico to Sea-level Rise Flooding

Site Unique ID	Code Vélez	SHPO Code	TAG SHPO	SHPO Key	CAT Code	Common Name	Chronological Period	Hazard Total	Combination of Hazards
7	45-E-10	LO-7	LZ0100007	7	LO-7	Cueva Punta Maldonado or Cueva de los Indios	PI Ortoiroid+PII Saladoid+PIII Ostionoid	5	FEMA Zones (% annual chance): A zone (1%) & 0.2%, Sea Level Rise (Above MHHW): 2 ft & 3 ft, Tsunami Run Up Zone
17	None	LO-24	LZ0100024	24	None	Melilla	PIII Ostionoid	8	FEMA Zones (% annual chance): A zone (1%) & 0.2%, Sea Level Rise (Above MHHW): 2 ft & 3 ft, Storm Surge (by Hurricane Category): 1 & 2 & 3, Tsunami Run Up Zone
24	None	LO-21	LZ0100021	21	None	Cueva La Cantera	PI Ortoiroid+PII Saladoid	4	FEMA Zones (% annual chance): A zone (1%) & 0.2%, Sea Level Rise (Above MHHW): 2 ft & 3 ft
34	45-E-55	H9/45-E-55	LZ0100041	41	None	El Ancón	PIV Spanish Colonial+PV United States Colonial	7	FEMA Zones (% annual chance): A zone (1%) & 0.2%, Shallow Coastal (Nuisance) Flooding, Sea Level Rise (Above MHHW): 1 ft & 2 ft & 3 ft, Tsunami Run Up Zone

Table 4.8: Physical Vulnerability of Archaeological Sites in Loíza, Puerto Rico to Sea-level Rise Flooding (Continued)

Site Unique ID	Code Vélez	SHPO Code	TAG SHPO	SHPO Key	CAT Code	Common Name	Chronological Period	Hazard Total	Combination of Hazards
38	LO-32b	45-E-4	LZ0100045	45	LO-32b	45-E-4	PI Ortoiroid+PII Saladoid+PIII Ostionoid	6	FEMA Zones (% annual chance): A zone (1%) & 0.2%, Sea Level Rise (Above MHHW): 3 ft, Storm Surge (by Hurricane Category): 2 & 3, Tsunami Run Up Zone
41	45-E-16	45-E-16	LZ0100051	51	None	45-E-16	PIII Ostionoid	6	FEMA Zones (% annual chance): A zone (1%) & 0.2%, Sea Level Rise (Above MHHW): 3 ft, Storm Surge (by Hurricane Category): 2 & 3, Tsunami Run Up Zone
61	45-E-52	None	None	None	None	45-E-52	PII Saladoid+PIII Ostionoid	6	FEMA Zones (% annual chance): A zone (1%) & 0.2%, Sea Level Rise (Above MHHW): 2 ft & 3 ft, Storm Surge (by Hurricane Category): 2 & 3
62	None	LO-15	LZ0100015	15	LO-15	La Virginia	PI Ortoiroid+PII Saladoid+PIII Ostionoid	6	FEMA Zones (% annual chance): A zone (1%) & 0.2%, Sea Level Rise (Above MHHW): 3 ft, Storm Surge (by Hurricane Category): 2 & 3, Tsunami Run Up Zone

Table 4.8: Physical Vulnerability of Archaeological Sites in Loíza, Puerto Rico to Sea-level Rise Flooding (Continued)

Site Unique ID	Code Vélez	SHPO Code	TAG SHPO	SHPO Key	CAT Code	Common Name	Chronological Period	Hazard Total	Combination of Hazards
68	45-E-18	45-E-18	LZ0100052	52	LO-34a	45-E-18	PIII Ostionoid	5	FEMA Zones (% annual chance): A zone (1%) & 0.2%, Sea Level Rise (Above MHHW): 2 ft & 3 ft, Storm Surge (by Hurricane Category): 3
70	45-E-19	45-E-19	LZ0100053	53	None	45-E-19	PIII Ostionoid	10	FEMA Zones (% annual chance): A zone (1%) & 0.2%, Shallow Coastal (Nuisance) Flooding, Sea Level Rise (Above MHHW): 1 ft & 2 ft & 3 ft, Storm Surge (by Hurricane Category): 1 & 2 & 3, Tsunami Run Up Zone
71	45-E-26	45-E-26	LZ0100057	57	None	45-E-26	PIII Ostionoid	10	FEMA Zones (% annual chance): A zone (1%) & 0.2%, Shallow Coastal (Nuisance) Flooding, Sea Level Rise (Above MHHW): 1 ft & 2 ft & 3 ft, Storm Surge (by Hurricane Category): 1 & 2 & 3, Tsunami Run Up Zone

Table 4.8: Physical Vulnerability of Archaeological Sites in Loíza, Puerto Rico to Sea-level Rise Flooding (Continued)

Site Unique ID	Code Vélez	SHPO Code	TAG SHPO	SHPO Key	CAT Code	Common Name	Chronological Period	Hazard Total	Combination of Hazards
76	45-E-20	45-E-20	LZ0100054	54	None	45-E-20	PIII Ostionoid	9	FEMA Zones (% annual chance): A zone (1%) & 0.2%, Shallow Coastal (Nuisance) Flooding, Sea Level Rise (Above MHHW): 2 ft & 3 ft, Storm Surge (by Hurricane Category): 1 & 2 & 3, Tsunami Run Up Zone
77	None	LO-28	LZ0100028	28	None	LO-28/45-E-19	PIII Ostionoid	10	FEMA Zones (% annual chance): A zone (1%) & 0.2%, Shallow Coastal (Nuisance) Flooding, Sea Level Rise (Above MHHW): 1 ft & 2 ft & 3 ft, Storm Surge (by Hurricane Category): 1 & 2 & 3, Tsunami Run Up Zone

4.5.3.4 Total Physical Vulnerability of Archaeological Sites

When vulnerabilities to all three previously mentioned hazards were combined, most sites had a total physical vulnerability value of 1 (n = 19, 22%; Figure 4.17). The second most common value was 2 (n = 17, 19%) and the third most common was 3 (n = 12, 14%).

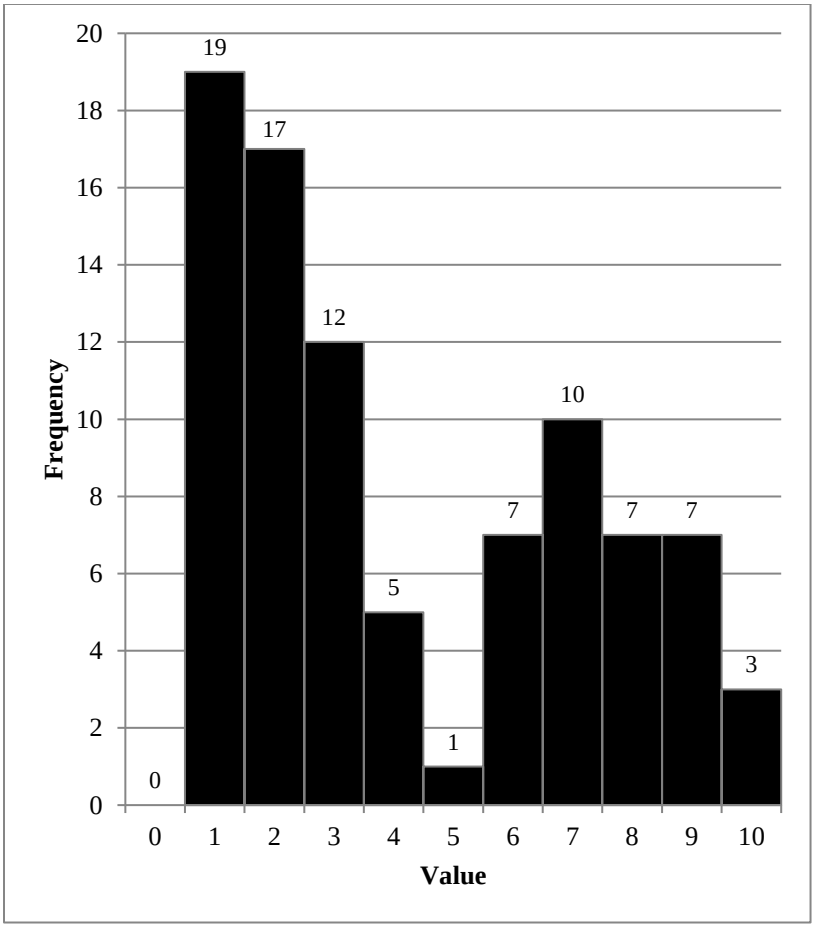

Figure 4.17: Frequencies of Total Physical Vulnerability Values for Archaeological Sites in Loíza, Puerto Rico

A map showing the vulnerabilities of archaeological sites is presented in Figure 4.18. Most of the sites were considered low vulnerability (n = 48, 55%), followed by medium vulnerability (n = 25, 28%), and then high vulnerability (n = 15, 17%). A concentration

of high and medium vulnerability was observed along the shoreline at Piñones, Torrecilla, and Vacía Talega. Sites near rocky land showed low vulnerability (Boca de Cangrejos, Punta Maldonado, and Vacía Talega), as did most of the sites to the east of Vacía Talega, with the exception of sites near Parcelas Vieques and Parcelas Suárez.

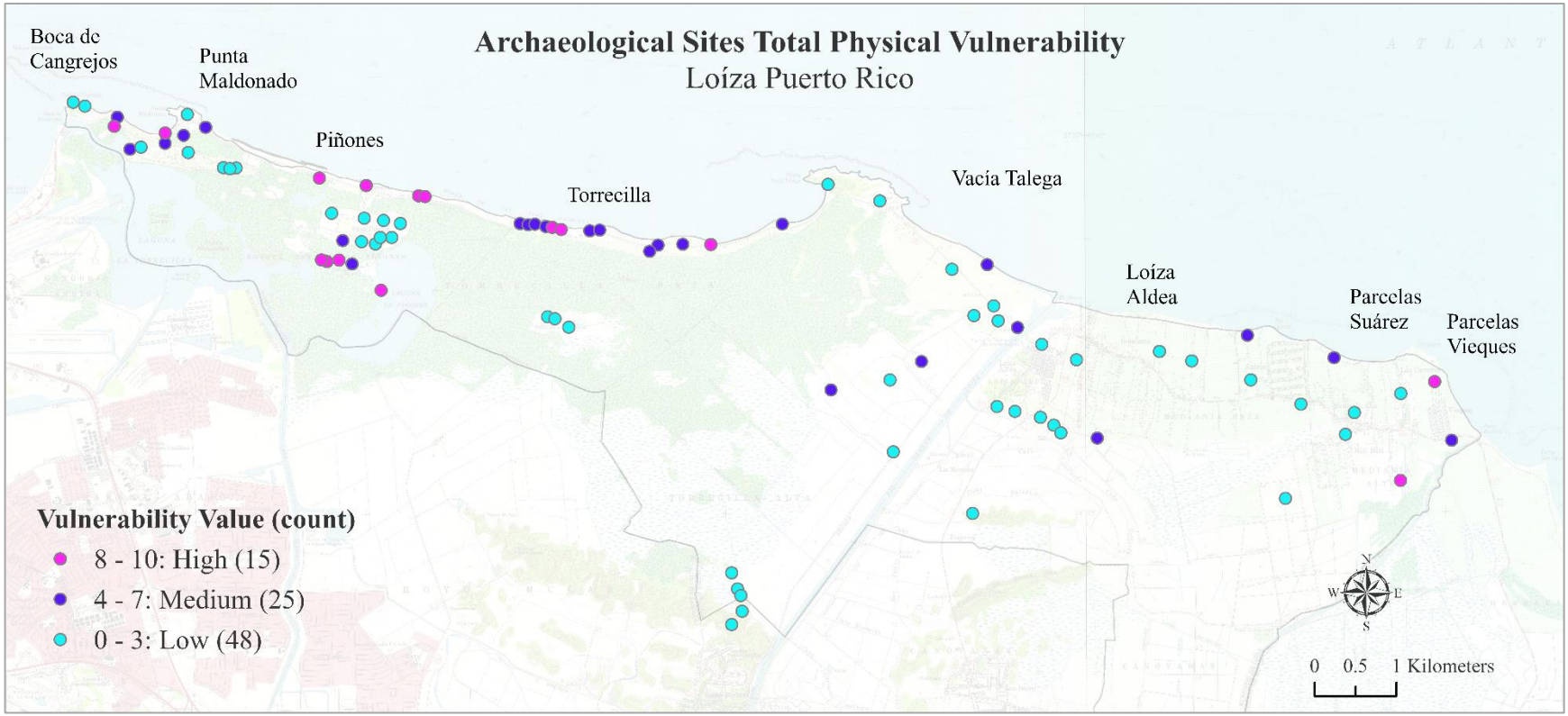

Figure 4.18: Map showing three categories of total physical vulnerability for each archaeological site in Loíza, Puerto Rico: high, medium, and low physical vulnerability

4.5.4 Step 3: Prioritization Ranking of Archaeological Sites

The prioritization ranking of the archeological sites involved summing the results of the archaeological significance and the total vulnerability. The highest frequency was observed for priority rank 13 (15%), followed by ranks 15 and 18 (9% each; Figure 4.19).

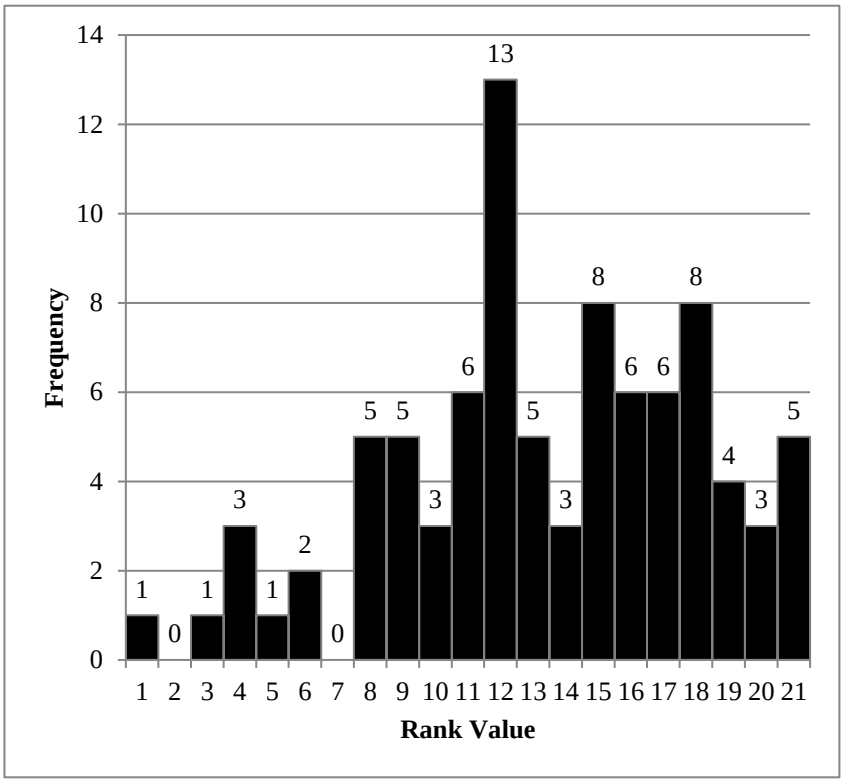

Figure 4.19: Prioritization Ranking of Archaeological Sites in Loíza, Puerto Rico

A map showing the prioritization ranking of the archaeological sites is presented in Figure 4.20. Forty of the sites (45%) were ranked high priority, followed by 35 sites (40%) that were ranked medium priority, and 13 sites (15%) that were ranked low priority. To the east of Vacía Talega, several high-priority sites clustered at Punta Maldonado, Piñones, and Torrecilla. To the west, the sites with high priority were more dispersed, except for the cave sites near Loíza Aldea. Medium-priority sites were

concentrated around la Finca Piñones and to the west of Río Grande Loíza, whereas low-priority sites were concentrated around La Torre and south of Punta Maldonado.

The following sections present results for the high, medium, and low priority rankings, including Kernel density maps and separate tables for each site.

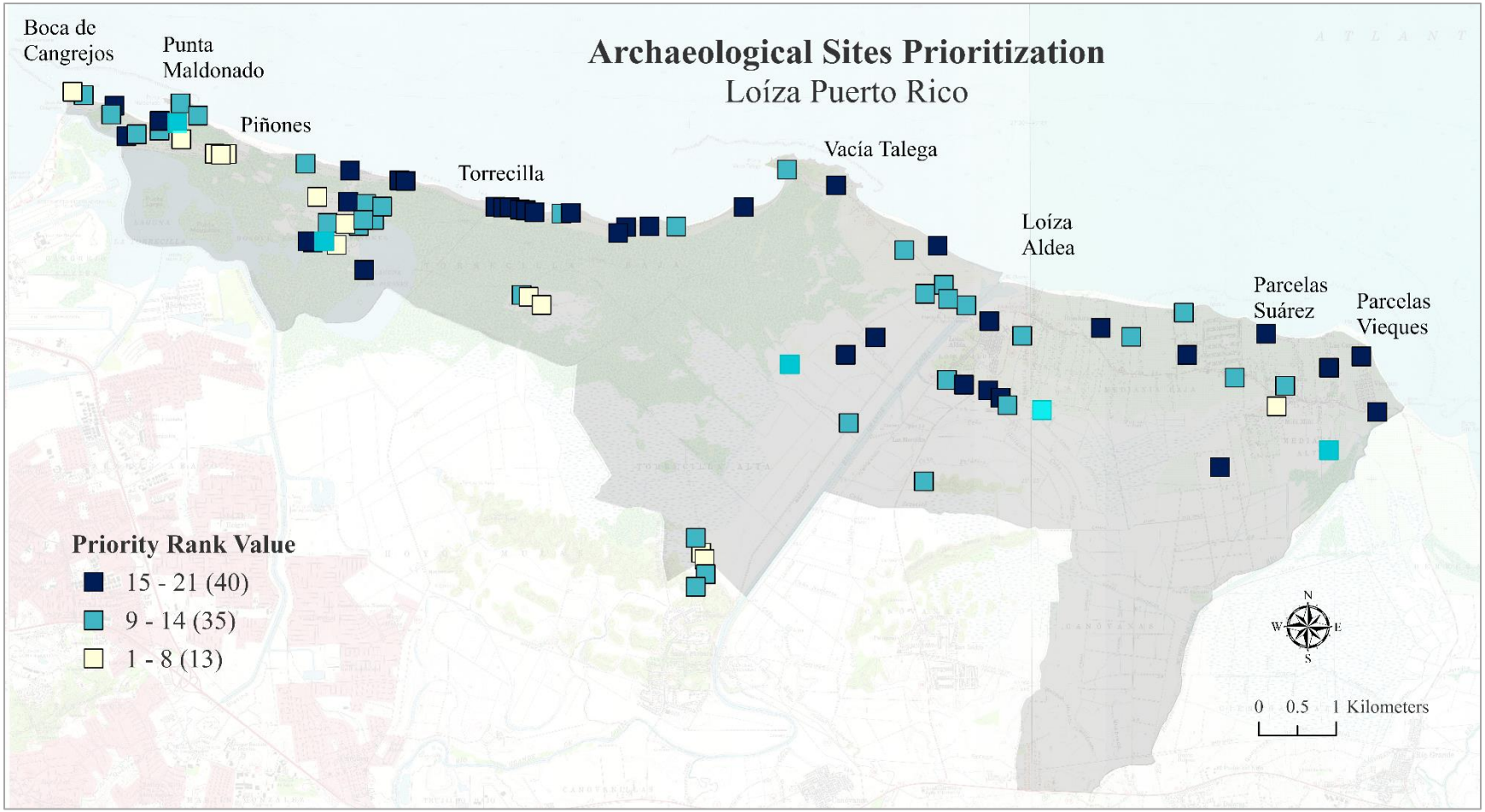

Figure 4.20: Map Showing Prioritization Rankings of Archeological Sites in Loíza, Puerto Rico

4.5.4.1 Archaeological Sites with High Priority

Four sites had the highest priority value within the high priority category, which was 21 (Table 4.9). Punta Maldonado I (ID:75), which Meléndez and Rodríguez (1998) established with high archaeological potential, was also a high priority site. The second-highest ranked sites were 45-E-35 (ID:53, 54) and Finca de Piñones (ID:48).

After conducting a Kernel Density analysis (Figure 4.21), a higher density of archaeological sites with high priority was observed from the Piñones area to Torrecilla. At Punta Maldonado and to the west of Río Grande de Loíza, some areas also showed high density.

Table 4.9: Archaeological Sites with High Priority Values

Site Unique ID	Code Vélez	SHPO Code	TAG SHPO	SHPO Key	CAT Code	Common Name	Chronological Period	Priority Ranking
16	None	LO-23	LZ0100023	23	None	Parcelas Vieques	PIII Ostionoid+PIV Spanish Colonial	21
18	None	None	None	None	LO-27	Playa Berwind	PIII Ostionoid	21
70	45-E-19	45-E-19	LZ0100053	53	None	45-E-19	PIII Ostionoid	21
75	45-E-8	LO-8	LZ1000009	9	None	Punta Maldonado I	PII Saladoid+PIII Ostionoid	21
77	None	LO-28	LZ0100028	28	None	LO-28/45-E-19	PIII Ostionoid	21
82	None	LO-29	LZ0100029	29	None	Monte Grande I	PIII Ostionoid	21
48	45-E-25	LO-20	LZ0100020	20	LO-20b	Finca Piñones 3	PI Ortoiroid+PII Saladoid+PIII Ostionoid	20
53	45-E-35	45-E-35	LZ0100060	60	LO-22c	45-E-35	PI Ortoiroid	20
54	45-E-35	45-E-35	LZ0100060	60	LO-22c	45-E-35	PI Ortoiroid	20
55	45-E-40	LO-10	LZ0100010	10	LO-10	La Vaquería, 45-E-40	PIII Ostionoid+PIV Spanish Colonial	19
62	None	LO-15	LZ0100015	15	LO-15	La Virginia	PI Ortoiroid+PII Saladoid+PIII Ostionoid	18
80	45-E-42	LO-30	LZ0100030	30	LO-30	45-E-42	PIII Ostionoid	19
7	45-E-10	LO-7	LZ0100007	7	LO-7	Cueva Punta Maldonado or Cueva de los Indios	PI Ortoiroid+PII Saladoid+PIII Ostionoid	19
12	45-E-44	LZ0100012	LZ0100012	12	LO-12	La Cocaleca	PII Saladoid+PIII Ostionoid+PIV Spanish Colonial	18
17	None	LO-24	LZ0100024	24	None	Melilla	PIII Ostionoid	19
22	None	LO-2	LZ0100002	2	LO-2	Hacienda Grande	PII Saladoid+PIII Ostionoid+PIV Spanish Colonial	18

Table 4.9: Archaeological Sites with High Priority Values (Continued)

Site Unique ID	Code Vélez	SHPO Code	TAG SHPO	SHPO Key	CAT Code	Common Name	Chronologial Period	Priority Rankin
30	None	Sitio G	LZ0100033	33	None	Sitio G/Santillana	PIII Ostionoid+PIV Spanish Colonial+PV United States Colonial	18
37	LO-32a	45-E-3	LZ0100044	44	LO-32a	45-E-3	PIII Ostionoid	18
49	45-E-35	45-E-35	LZ0100060	60	LO-22c	45-E-35	PI Ortoiroid	18
50	45-E-35	45-E-35	LZ0100060	60	LO-22c	45-E-35	PI Ortoiroid	18
51	45-E-35	45-E-35	LZ0100060	60	LO-22c	45-E-35	PI Ortoiroid	18
52	45-E-35	45-E-35	LZ0100060	60	LO-22c	45-E-35	PI Ortoiroid	18
56	45-E-41	45-E-41	LZ0100064	64	LO-37	45-E-41	PI Ortoiroid	18
15	None	LO-22	LZ0100022	22	None	Las Carreras	PII Saladoid+PIII Ostionoid	17
59	45-E-47	45-E-47	LZ0100065	65	LO-38	Playa Bonita	PIII Ostionoid+PIV Spanish Colonial	17
61	45-E-52	None	None	None	None	45-E-52	PII Saladoid+PIII Ostionoid	17
13	45-E-46	LO-14	LZ0100014	14	LO-14	Punta Vacía Talega or Arenas	PII Saladoid+PIII Ostionoid+PIV Spanish Colonial	16
21	None	Cueva Dolores	LZ0100032	32	None	Cueva Dolores	PI Ortoiroid+PII Saladoid+PIII Ostionoid	16
29	None	Sitio K	LZ0100034	34	LO-43	Sitio K	PIII Ostionoid	16
63	45-E-53	45-E-53	LZ0100069	69	None	45-E-53	PI Ortoiroid+PII Saladoid+PIII Ostionoid	16
71	45-E-26	45-E-26	LZ0100057	57	None	45-E-26	PIII Ostionoid	16
76	45-E-20	45-E-20	LZ0100054	54	None	45-E-20	PIII Ostionoid	15
4	45-E-5	LO-5	LZ0100005	5	LO-5	45-E-5	PIII Ostionoid+PIV Spanish Colonial	15
10	45-E-24	LO-4	LZ0100004	4	LO-4	Finca Piñones I	PIII Ostionoid+PIV Spanish Colonial	15

Table 4.9: Archaeological Sites with High Priority Values (Continued)

Site Unique ID	Code Vélez	SHPO Code	TAG SHPO	SHPO Key	CAT Code	Common Name	Chronologial Period	Priority
20	None	LO-1	LZ0100001	1	LO-1	Cueva María de la Cruz	PI Ortoiroid+PII Saladoid+PIII Ostionoid	15
26	None	LO-25	LZ0100025	25	LO-25	Miñi-Miñi	PII Saladoid+PIII Ostionoid+PIV Spanish Colonial	15
27	None	None	None	None	LO-41	Ocean Terrace	PI Ortoiroid+PII Saladoid+PIII Ostionoid+PIV Spanish Colonial	15
40	45-E-12	45-E-12	LZ0100048	48	LO-7b	45-E-12	PIII Ostionoid	15
46	45-E-33	45-E-33	LZ0100058	58	LO-22b	45-E-33	PIII Ostionoid	15
47	45-E-34	45-E-34	LZ0100059	59	LO-22b	45-E-34	PIII Ostionoid	15
88	None	NRHP	NRHP	NRHP	None	Parroquia Espiritu Santo y San Patricio	PIV Spanish Colonial	15

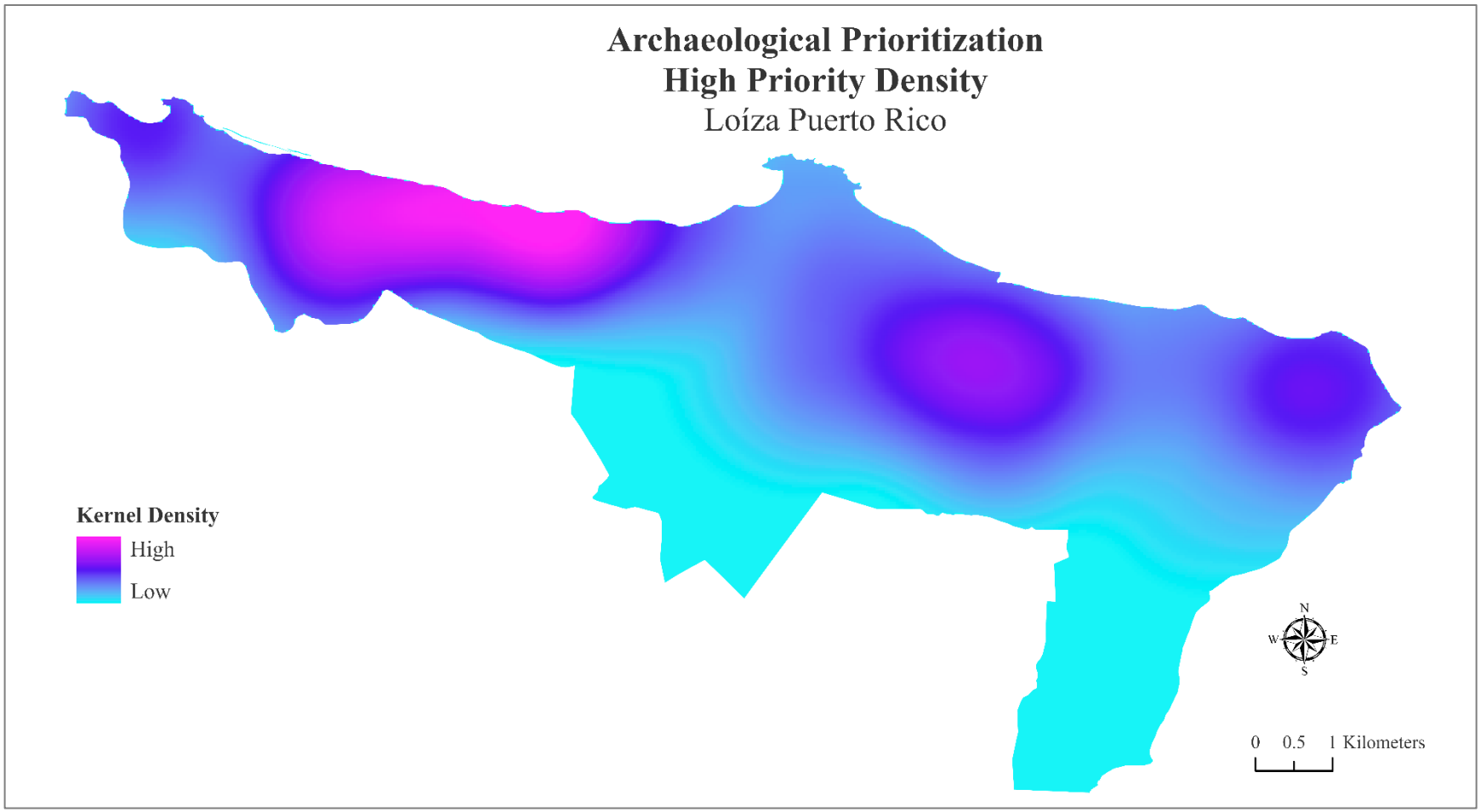

Figure 4.21: Kernel density map showing the concentrations of archaeological sites with a high priority ranking.

4.5.4.2 Archaeological Sites with Medium Priority

Thirty-four sites were included in the medium priority category, with prioritization values ranging from 9 to 14 (Table 4.10). The archaeological site 45-E-32 (ID:45) had the highest value, followed by LO-11 (ID:66). The most common prioritization value was 12 in this category, including sites such as LO-31 Punta de Cangrejos (ID:3), LO-33b (ID: 6), and Punta Maldonado II (ID:39). Sites that have been impacted by current constructions, such as Malibú Villages (ID:31) and Vistas del Océano (ID:28), were also in this category, as were Islote Piñones and Finca Piñones. The remaining sites showed lower values. At Tres Palmitas and Vacía Talega, most sites near the shoreline showed higher prioritization values.

Table 4.10: Archaeological Sites with Medium Priority Values

Site Unique ID	Code Vélez	SHPO Code	TAG SHPO	SHPO Key	CAT Code	Common Name	Chronologial Period	Priority Ranking
45	45-E-32	LO-3/45-E-32, 27,28,29,30	LZ0100003	3	LO-3	Finca Piñones II (El Alto)	PII Saladoid+PIII Ostionoid	14
66	45-E-36	LO-11	LZ0100036	36	LO-11	Juan Pérez I	PI Ortoiroid	14
5	45-E-6	LO-5	LZ0100005	5	None	45-E-6	PIV Spanish Colonial	13
19	None	LO-18	LZ0100018	18	None	Cueva Bulón	PI Ortoiroid+PII Saladoid	13
24	None	LO-21	LZ0100021	21	None	Cueva La Cantera	PI Ortoiroid+PII Saladoid	14
38	LO-32b	<Null>	LZ0100045	45	LO-32b	45-E-4	PI Ortoiroid+PII Saladoid+PIII Ostionoid	13
57	45-E-43	LO-30/45-E-42, 43	LZ0100030	30	LO-30	Monte Grande II	PIII Ostionoid	13
64	45-E-50	45-E-50	LZ0100067	67	LO-39	45-E-50	PIII Ostionoid+PIV Spanish Colonial	13
3	45-E-2	45-E-2	LZ0100042	42	LO-31: Punta Cangrejos (45-E-1, 45-E-2)	El Bunker	PV United States Colonial	12
6	45-E-7	45-E-7	LZ0100046	46	LO-33b	45-E-7	PIII Ostionoid+PIV Spanish Colonial	12
25	None	LO-26	LZ0100026	26	None	La Gallera	PIII Ostionoid	12
28	None	LO-27	LZ0100027	27	LO-18	Vistas del Océano	PIII Ostionoid+PIV Spanish Colonial	12
31	None	None	None	None	LO-44	Malibú Villages	PIII Ostionoid	12
33	None	None	None	None	LO-46	Escuela Intermedia Jesus Vizcarrondo	PI Ortoiroid+PII Saladoid+PIII Ostionoid+PIV Spanish Colonial	12
39	45-E-11	LO-8	LZ0100008	8	LO-8	Punta Maldonado II	PIII Ostionoid+PV United States Colonial	12

Table 4.10: Archaeological Sites with Medium Priority Values (Continued)

Site Unique ID	Code Vélez	SHPO Code	TAG SHPO	SHPO Key	CAT Code	Common Name	Chronologial Period	Priority Ranking
41	45-E-16	45-E-16	LZ0100051	51	None	45-E-16	PIII Ostionoid	12
44	45-E-30	LO-3	LZ0100003	3	LO-28	Isleta Piñones, 45-E-30	PIII Ostionoid	12
65	45-E-51	45-E-51	LZ0100068	68	LO-41	45-E-51	PIII Ostionoid	12
68	45-E-18	45-E-18	LZ0100052	52	LO-34a	45-E-18	PIII Ostionoid	12
78	45-E-28	LO-3	LZ0100003	3	LO-23	45-E-28	PIII Ostionoid	12
34	45-E-55	H9/45-E-55	LZ0100041	41	None	El Ancón	PIV Spanisj Colonial+PV United States Colonial	11
36	15-F-2	15-F-2/M-3-3	LZ0100036	36	CN-6	15-F-2	PI Ortoiroid	11
42	45-E-27	LO-3	LZ0100003	3	LO-21	Islote Piñones	PIII Ostionoid	11
58	45-E-45	LO-13	LZ0100013	13	LO-13	Punta Vacía Talega	PIII Ostionoid+PIV Spanish Colonial	11
81	45-E-39	45-E-39	LZ0100063	63	None	45-E-39	PIII Ostionoid	11
83	45-E-48	45-E-48	LZ0100066	66	None	45-E-48	PIV Spanish Colonial	11
14	45-E-54	45-E-54	LZ0100070	70	None	45-E-54	PIV Spanish Colonial	10
23	None	Cueva Mela	LZ0100031	31	None	Cueva Mela	PI Ortoiroid+PII Saladoid+PIV Spanish Colonial	10
60	45-E-49	LO-19	LZ0100019	19	LO-19	La Planta	PIII Ostionoid+PIV Spanish Colonial	10
43	45-E-29	LO-3	LZ0100003	3	LO-23	45-E-29	PIII Ostionoid	9
84	15-F-3	15-F-3	LZ0100072	72	CN-8	Cueva del Pueblo del Indio	PI Ortoiroid+PII Saladoid+PIII Ostionoid+PIV Spanish Colonial	9

Table 4.10: Archaeological Sites with Medium Priority Values (Continued)

Site Unique ID	Code Vélez	SHPO Code	TAG SHPO	SHPO Key	CAT Code	Common Name	Chronologial Period	Priority Ranking
85	15-F-1	15-F-1/ M3-4	LZ0100035	35	CN-24	Usubal	PIV Spanish Colonial	9
86	None	H1	LZ0100040	40	None	Molino de azúcar	PIV Spanish Colonial	9
87	None	LO-39	LZ0100039	39	None	Colobó/Sitio I?	PII Saladoid+P III Ostionoid+PIV Spanish Colonial	9

The Kernel density analysis (Figure 4.22) showed that sites in the medium priority category were concentrated around Piñones and to the east of Vacía Talega. A small density of medium priority sites was observed along Boca de Cangrejos and Punta Maldonado.

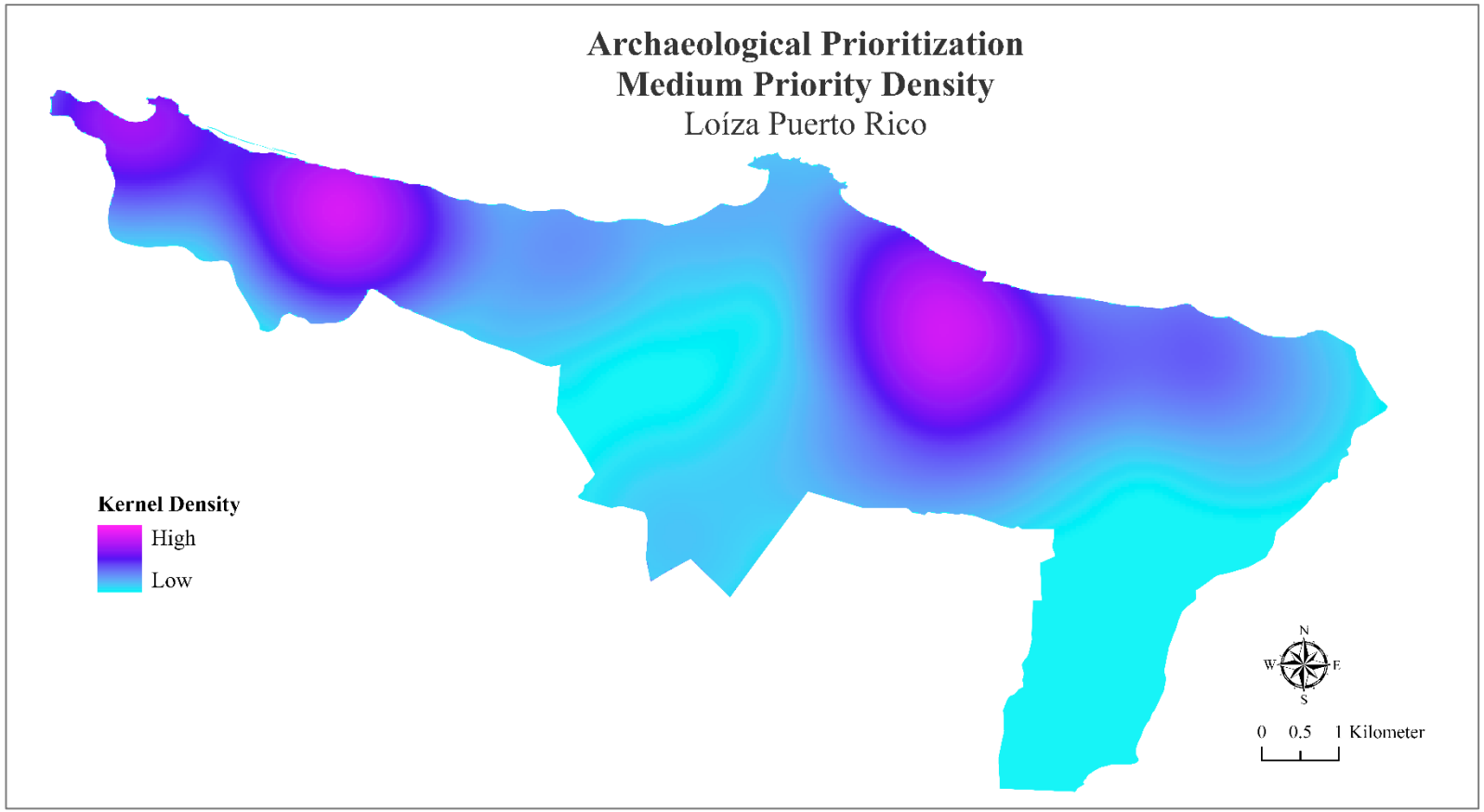

Figure 4.22: Kernel density map showing the concentrations of archaeological sites with medium priority rankings

4.5.4.3 Archaeological Sites with Low Priority

Sites in the low priority category were distributed throughout the municipality of Loíza (Table 4.11). At the same time, some sites were surrounded by sites with higher values, such as LO-31 La Torre (ID:73). There was a concentration of low-priority sites mostly between the limits of Canóvanas and Loíza, such as Cueva Camona (ID:72).

Table 4.11: Archaeological Sites with Low Priority Values

Site Unique ID	Code Vélez	SHPO Code	TAG SHPO	SHPO Key	CAT Code	Common Name	Chronologial Period	Priority Ranking
2	45-E-13	LO-6	LZ0100006	6	LO-6	45-E-13	PIII Ostionoid+PIV Spanish Colonial	8
32	None	None	None	None	None	Sitio J	PIII Ostionoid	8
67	45-E-37	45-E-37	LZ0100061	61	None	45-E-37	PI Ortoiroid	8
69	45-E-22	45-E-22	LZ100056	56	LO-34b	45-E-22	PIII Ostionoid	8
79	45-E-38	45-E-38	LZ0100062	62	None	45-E-38	PI Ortoiroid	8
11	45-E-17	45-E-17	LZ0100071	71	LO-29	Islote Piñones	PIII Ostionoid+PIV Spanish Colonial	6
35	15-F-4	15-F-4	LZ0100037	37	None	Grúas	PIV Spanish Colonial	6
73	45-E-1	<Null>	LZ0100043	43	LO-31: Punta Cangrejos (45-E-1, 45-E-2)	La Torre	PIV Spanish Colonial	5
1	45-E-15	45-E-15	LZ0100050	50	LO-33b	45-E-15	PII Saladoid+PIII Ostionoid	4
9	45-E-21	45-E-21	LZ0100055	55	None	45-E-21	PIV Spanish Colonial	4
72	15-F-5	Cueva Carmona	LZ0100017	17	CN-7	Cave.	PII Saladoid+PIII Ostionoid	4
74	45-E-14	45-E-14	LZ0100049	49	None	45-E-14	PII Saladoid+PIII Ostionoid	3
8	45-E-10	45-E-10	LZ0100047	47	None	45-E-10	PIV Spanish Colonial	1

The Kernel density analysis (Figure 4.23) showed a higher density of low-priority sites between Boca de Cangrejos and Piñones. A low-density concentration was also observed at the edge of Canóvanas and Loíza.

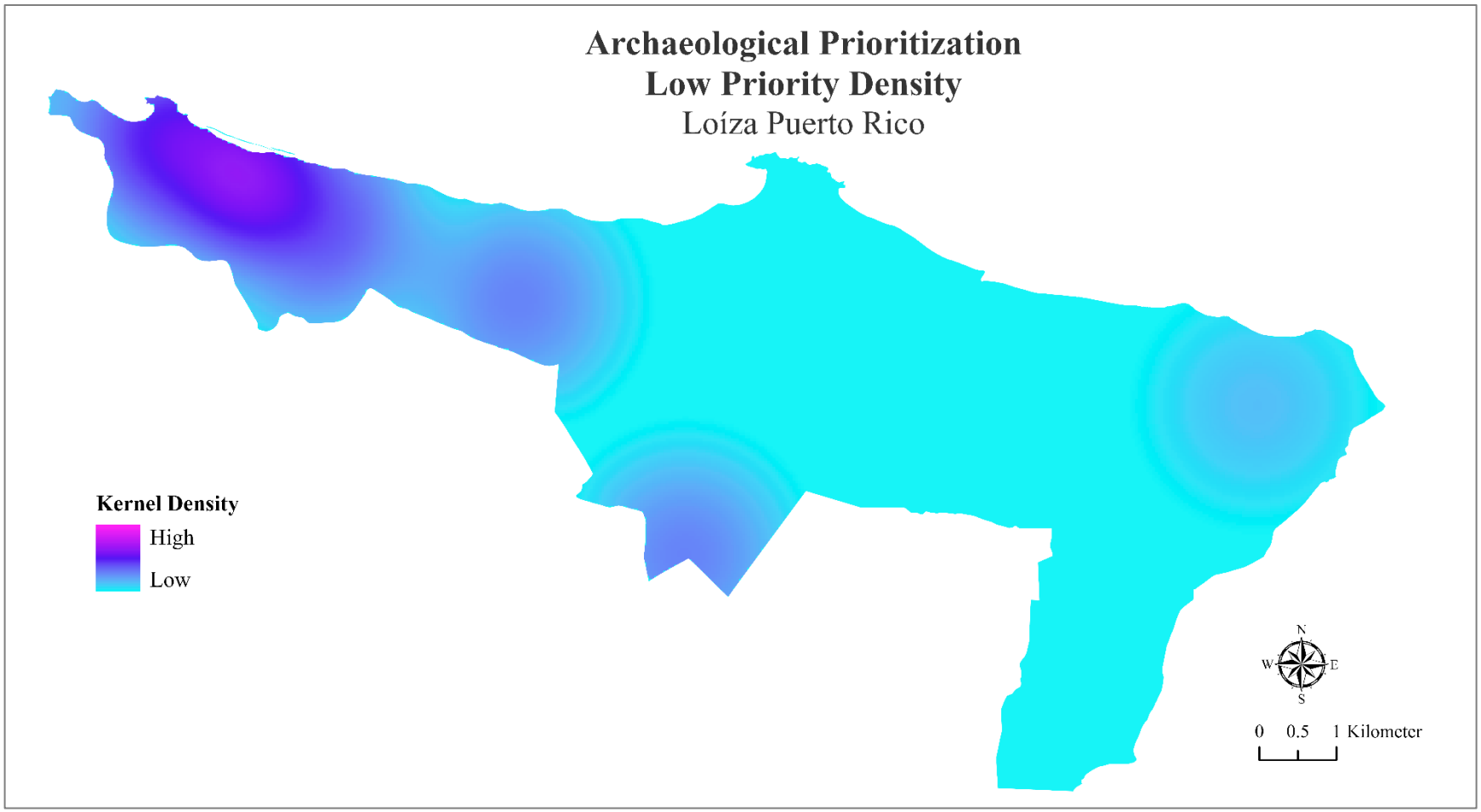

Figure 4.23: Kernel density map showing the concentrations of archaeological sites with a low priority ranking.

4.5.5 Morphological Change at Selected Sites

4.5.5.1 LO-27 Playa Berwind

In this section, I would like to illustrate the results of the morphological change near the archaeological site LO-27 Playa Berwind. This site was categorized as high priority (value of 16), so I drew transects to obtain a profile of the next 130 meters (Figure 4.24). Profiles were calculated for four different dates throughout the year (Day 31, Day 89, Day 211, and Day 364), with transects representing northern (Transect 1: T1), central (Transect 2: T2), and southern (Transect 3: T3) areas.

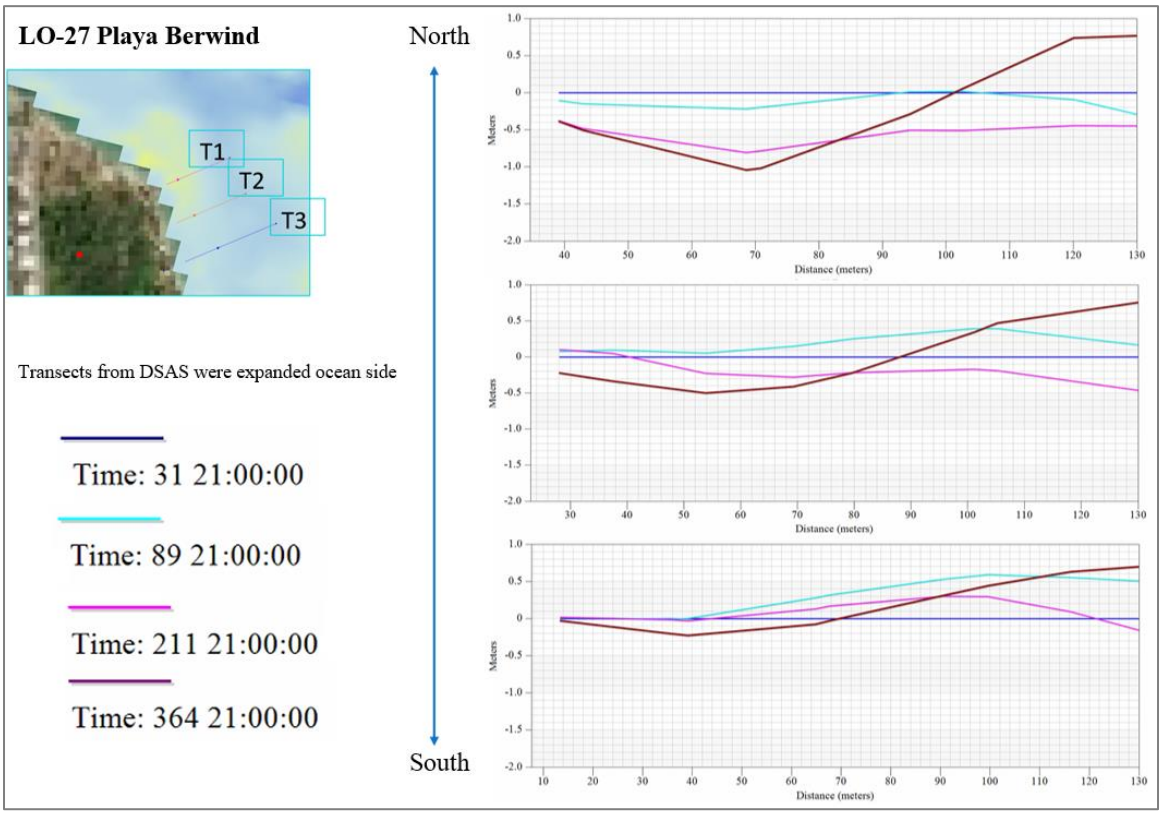

Figure 4.24: Morphological Change (Erosion and Accretion) of Ocean Bottom Near LO-27 Playa Berwind

The profiles showed higher erosion levels in the northern section at 70 meters. The T1 profile at LO-26 showed higher erosion, especially on Day 211 and Day 364. At T2

and T3, despite observing accretion on Day 89, erosion was observed on both transects on Day 211 and Day 364. Moving toward the ocean, all three transects showed accretion on Day 364. The transect that showed the greatest difference in morphology over the dates investigated was T1, followed by T2. T3 showed a pattern of accretion, erosion, and accretion, especially after 90 meters. After approximately 120 meters, all the transects showed accretion.

4.5.6 Fieldwork Visits

Several visits were conducted to record the status of the archaeological sites (Figure 4.25). Twenty-five visits were recorded in the fieldwork. The dates and the areas recorded were the following:

- February 9, 2020: Punta Vacía Talega and Parcelas Vieques
- February 16 – 17, 2020: Boca de Cangrejos and the Torrecilla Baja (Torre)
- September 30, 2020: Piñones and Tres Palmitas

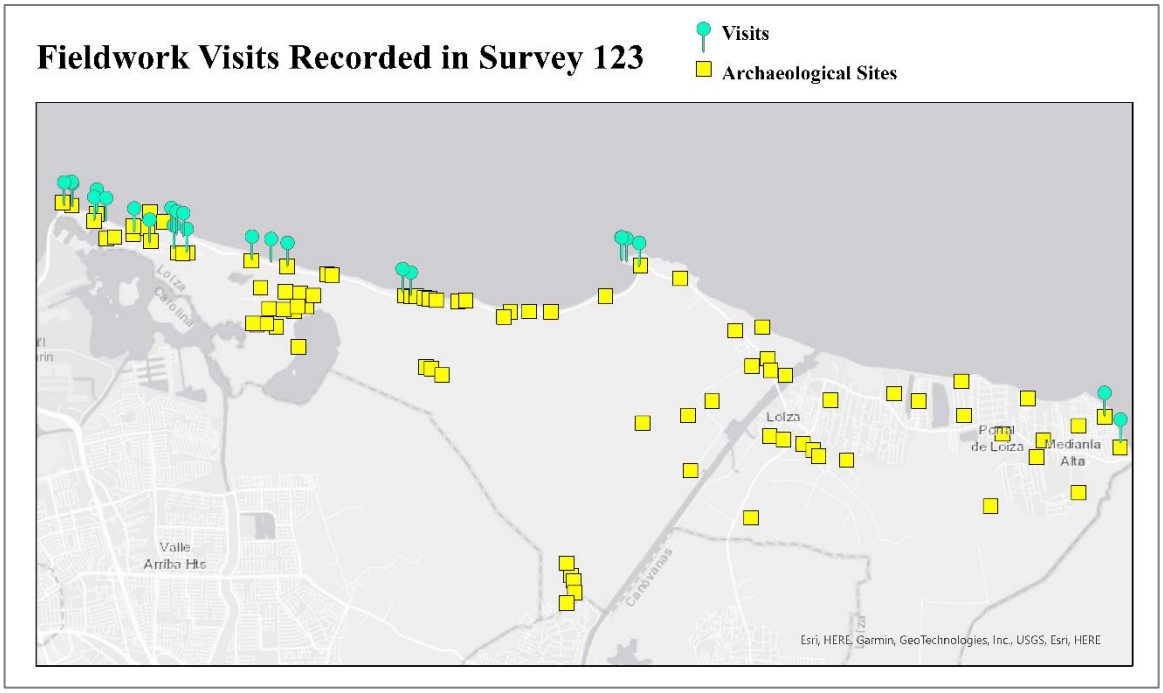

Figure 4.25: Fieldwork Visits to Archaeological Sites, Recorded on Several Dates

During these visits, four points were classified as possessing archaeological materials (Boca de Cangrejos and Punta Vacía Talega). At Punta Boca de Cangrejos (Figure 4.26). I were able to identify the Bunker (45-E-2, Clave SHPO 42, CAT LO-31), which was located near the shoreline area and covered by vegetation. According to Vélez (1990), this was a U.S. Military structure, suggested to have been constructed after the destruction of the previous site, "La Torre". The point was located at the commercial area in the CAT database, where a fieldwork visit was recorded, but no material was found in the business area and parking areas surrounding it. In the southeast area of the Bunker location, a contemporary cement structure was found, as well as some historic ceramics (hand-painted, whiteware).

Figure 4.26: Fieldwork in the Boca de Cangrejos area: The Bunker site and other exposed historical materials were found. The blue square shows some of the material found.

At Punta Vacía Talega, four points were collected: one on the beach, one on the trail, and two close to the edge of the rock area (Figure 4.27). In the beach area of Vacía Talega, exposed pre-Columbian ceramic was found for the second time since the first reconnaissance visits in 2018. Afterward, ceramic and shell materials were observed on the trail to the top of the rocky area. More materials were found at the top of the rocky area, where no vegetation was observed. Currently, this area is generally used for fishing and recreation activities, so the material found on the trail could have been eroded from the top of the area.

Figure 4.27: Fieldwork findings at Vacía Talega. Blue squares show the materials found.

In the other visited areas, materials were not found to indicate the presence of archaeological sites (Figure 4.28). Residence and commercial areas, constructions or dunes were found where archaeological sites have previously been documented. For example, at Tres Palmitas, no materials were found. The dunes have highly recovered this area, so sites could be buried beneath them. A new commercial area has been established near the Finca de Piñones site, and no archaeological materials were found. The La Torre area mainly comprises residential areas now, with no access to the exact locations of previously documented sites. In this area, several constructions and mounds of construction materials were observed.

Other sites, such as Playa Bergwind, Punta Uvero, and Parcelas Vieques, were visited using the UAS. In this regard, no materials were found, and no further information could be extracted from the aerial images taken by the drone. The images revealed the dirt roads that are present and connect the Río Herrera area with Parcelas Vieques.

Figure 4.28: Fieldwork visits where no archaeological materials were found

4.6 Discussion

4.6.1 Archaeological Prioritization at Loíza

The prioritization of specific archaeological sites represents a tool for managing resources that show high archaeological significance but are threatened due to their high vulnerability. Although every finding and archaeological site could have valuable information from a scientific perspective, some contexts should be provided a higher priority, as in the cases of Punta Maldonado I (Boca de Cangrejos) and Monte Grande I (Tres Palmitas). According to Vélez (1990) and Meléndez and Rodríguez (1998), these sites show a high quantity and diversity of archaeological material and a deep stratigraphy. In contrast, other sites such as 45-E-10 at La Torre present low priority, thus exhibiting a lesser need for intervention for their preservation.

Furthermore, sites located in what are now residence complexes, such as Malibú Villages, Vistas del Océano, and Costa Mar Village, received high priority values (17, 17, and 21, respectively). Despite these being classified as destructed (Value 1), their extent and the material present gave them a high priority value in combination with their vulnerability values (9, 4, and 11, respectively), placing them in high priority levels. These values indicate that these areas in residence complexes should perhaps have been protected or studied further.

Overall, I observed that 45% of the sites had high priority values, 40% had medium priority, and 15% had low priority values. The current prioritization analysis of archaeological sites in Loíza established that new approaches and research are needed in this municipality. Agencies such as CAT and SHPO could use this type of analysis to understand and request further information for sites vulnerable to these new hazards due

to climate change acceleration patterns. Ideally, from a scientific view, all the sites with a higher prioritization rank could motivate future archaeological investigations.

The results of this project expanded other analyses focused only on SLR impacts and general classification (low or very high) of vulnerability values (Ezcurra & Rivera-Collazo, 2018). I expanded SCAPE's model beyond coastal areas and assigned values to determine vulnerability and prioritization. A limitation of my study, however, was that the archaeological recommendation (Stage 8 Dawson) for each site was not conducted due to time constraints. In future work, the results of these prioritization levels for archeological sites in Loíza can be shared with archaeologists to collect their recommendations. Additionally, prioritization categories could guide management agencies like SHPO and CAT in choosing possible future interventions for archaeological sites, such as monitoring or excavations.

The recent work of Hofman et al. (2021) applied a robust analysis by conducting excavations based on the results of SCA at archaeological sites on St. Kitts. Their analysis, however, was limited to seven shorelines over a 30-year period (1986, 1989, 1999, 2003, 2006, 2013, and 2015), whereas in my analysis of shoreline changes, I covered a total period of 116 years (1902, 1931, 1951, 1977, 1991, 2010, and 2018), providing short- and long-term results in a much more robust diachronic framework. Consequently, this allowed me to project erosional trends with linear regression analysis, rather than just analyzing shoreline change rates in specific periods.

The flooding composite map data used to analyze physical vulnerability is freely available on the NOAA website (2021a). The composite map allows management agencies or archaeologists to streamline each archaeological site's physical vulnerability

analysis to multiple hazards using one dataset. Nevertheless, this type of data, especially SLR scenarios, is constantly changing. For example, I first used the flood composite map with 2017 SLR scenarios, but new SLR projections were released in February 2022 (Office for Coastal Management, NOAA, 2022a), hence, I updated the SLR hazard variable in the flood composite assigned for each archaeological site. One of the major differences between this projections is that long-term scenarios were eliminated for 2022.

For this reason, it should be noted that the analysis presented in this research could continue to change due to changes in climate hazard models and mapping. Additionally, other recent publications involving SCA make it more feasible to conduct SCA to obtain quantitative data to establish if archaeological sites are close to erosional change. For example, this analysis could be accomplished with recent data published by the Woods Hole Coastal and Marine Science Center (Henderson et al., 2021).

4.6.2 Challenges and Future Work

The research hereby conducted presented several limitations. First, the archaeological parameters (integrity, density, size, and cultural components) were not available for all sites, especially those not included in Velez's (1990) report. Using a desk-based approach, I applied these same parameters using Meléndez and Rodríguez's (1998) report and the descriptions available in the SHPO written inventory of the sites. Velez's scheme should be applied to further archaeological reports to describe archaeological sites.

The variation in chronological terminology given to each site in the database was another limitation. To mitigate this issue, as previously explained, I homogenized each of the records using Rouse's model and kept some terminology in the description. I would recommend homogenizing archaeological descriptions using Rouse's model and the

scheme presented in this research (Table 4.2). Further edits and schemes can be applied, as this research will be presented to the Puerto Rican and international archaeological community.

Lastly, the conglomeration of different databases was also a limitation for the locations of the archaeological sites and other attributes. The locations of the sites from the SHPO inventory provided the best resolution, organization, and accurate information. The CAT point layers also proved to be helpful for the spatial analysis in this research. The maps provided by SHPO, and the GIS data provided by CAT were beneficial because Velez's report had poor quality maps, as it was a digitized document. Because these sites were mainly in the SHPO written inventory, on web maps (with coordinates), and in Meléndez and Rodriguez's report, I was able to check the locations and add new ones. It is critical to update the list of archaeological site locations to improve the models developed in this project. In conclusion, the methods used to record the status of the sites could be used to update future archaeological site inventories.

Commonly, I observed that SHPO or CAT conglomerated sites were documented as separate sites when found by Vélez and, in some cases, the code used was different. I therefore kept all SHPO, Vélez, and CAT codes to track the sources. If one of the sources did not consider a specific site, I classified it as "None." I propose that all sources (codes and reports) should be retained in the conglomeration process to maintain a whole profile for each archaeological site throughout the homogenization process.

4.6.3 Collaboration and Current Investigations

This project integrated several technologies and approaches from different disciplines to reach the final product of a prioritization ranking of archaeological sites in Loíza based

on climate change hazards, which highlights the importance of collaboration in conducting these types of studies. Physical vulnerability analysis and prioritization of management require the integration of several scientific experts in different fields to accomplish the protection of archaeological sites.

Currently, interest in the topic of climate change and its impact on archaeological records has been increasing. The book *Public Archaeology and Climate Change*, edited by Dawson et al. (2017), is an example of how investigations into the topic have been raised, and how different contributions might serve as a basis for designing strategies for the protection of our archaeological heritage in the future, as such sites are facing, and will continue to face, the constant threat of climate change acceleration.

Recently, Sesana et al. (2021) reviewed all publications on this topic and Hofman et al. (2021) focused on the resilient and future sustainability of protecting archaeological sites. In Puerto Rico, Isabel Rivera-Collazo continues to develop and apply methodologies to protect archaeological sites on the coast, while collecting new archaeological information. Her investigations aim to gather the social components and values of archaeological heritage in Puerto Rican communities (Figueroa Cancel, 2021a), and to create a coastal vulnerability index for archaeological sites.

4.7 Conclusions

This project followed a systematic methodology to assign prioritization values based on archaeological significance and physical vulnerability in response to rapid climate change. The variables used to calculate physical vulnerability were broadly available online from U.S. federal agencies, except for the current research's long-term SCA. Determining the archaeological significance was the most time-consuming task, as it was highly intertwined with the database homogenization. For this task, several reports and sources were used, including fieldwork.

I was able to apply and adapt the SCAPE model (n.d.) to answer my research questions. By adding quantitative shoreline erosion rates and shoreline recession estimation, I added quantitative data and analysis in terms of the proximity of the archaeological site to the shoreline. Additionally, flooding hazards (SLR, FEMA Zones, storm surges, tsunami, and high-tide flooding) were added as new variables to evaluate other climate change hazards, rather than just the proximity of archaeological sites. I evaluated new hazards by coupling these coast and landward variables to calculate archaeological vulnerability. By adding these variables, my model approached the complexity of the present coastal hazards. Moreover, the morphological change near Playa Berwind showed bottom patterns that have not been analyzed in previous research in Puerto Rico. The morphological change profiles near LO-27 Berwind showed that the first 70 meters were dominated by erosion, especially toward the north. This information could be used to better understand how sites may been impacted by the effects of different hydrodynamics in the area. Because the results showed that erosion is occurring

near the archaeological site, this could indicate that this site could be affected by erosion in the future.

Another implicit contribution of this research is the homogenization of chronological periods and database design of archaeological sites in Puerto Rico using Rouse's model. Data depuration permitted me to establish which chronological periods were more frequently represented at archaeological sites along the municipality of Loíza. The chronological data homogenization used in this project and Velez's criteria for evaluating archaeological sites' significance (integrity, size, components, and density) can be used or required in archaeological reports by agencies such as CAT and SHPO.

Data entry of archaeological records is vital for further analyzing the spatial patterns of archaeological sites in Puerto Rico. SHPO and CAT can use the chronological scheme proposed in this project (Table 4.2) to homogenize their databases. For example, they could add this scheme as a new requirement for future archaeological reports. If the data has the same format and chronological information, future chronological reclassification could be conducted. However. these agencies, especially CAT, have been affected by budget cuts, however, which will likely affect their ability to update their archaeological inventory for Puerto Rico.

Prioritization values can provide an idea of the type-specific evaluations that should be conducted at each archaeological site. For example, a mitigation process could be conducted if previous excavations have received high priority values. Stage 8 of the SCAPE model can provide this type of analysis and provide specific recommendations for future work. Moreover, sorting the archaeological sites by priority value could guide governmental agencies such as CAT and SHPO to evaluate if additional documentation

should be required for specific projects. For example, if an area with a high-priority site only has historical reports, sampling requirements could be required by the proponents.

As another example, suppose projects are proposed in areas near LO-8, where extensive material has been found in previous years and which was given a priority ranking of 26 (high). In this case, the agencies in charge could request other levels of archaeological investigations based on the archaeological significance and physical vulnerability. Moreover, suppose further projects are proposed near LO-14 (priority value 16, high) and LO-13 (priority value 13, medium). In that case, the agencies in charge can request further archaeological information, such as Phase 3 or mitigation procedures, as established in current regulations (CAT, 1992).

Future work could focus on analyzing the status of archaeological sites and the possibility of investigating archaeological sites that have not been studied. The integration of fieldwork data using Survey 123, ArcGIS Suite software, and remote sensing can enhance the analysis process. These methods could be implemented to collect location information for each site in Puerto Rico, reducing uncertainty.

Loíza is a key cultural heritage location in Puerto Rico (Bofill Calero, 2014). Most of the archaeological sites in Loíza are from the lesser known and more extended history of Puerto Rico: pre-Columbian history. For this reason, the municipality's land should be protected to protect its archeological sites. Similar approaches to the protected area of Bosque Estatal de Piñones (Castro Prieto et al., 2019) should be addressed to protect the archaeological patrimony of Loíza. In addition, Loíza has two sites, LO-7 (Cueva de los Indios or Punta Maldonado) and the Parroquia Espíritu Santo, that are included in the National Register of Historic Sites (SHPO, 2010). Due to the combination of critical

habitats, protected areas, and archaeological potential, the municipality should be considered an archaeologically sensitive area, protected from further constructions, especially near the coast.

Chapter 5 – SUMMARY

Overall, this research aimed to answer the following question: How can coastal processes impact archaeological sites in Loíza, Puerto Rico? To this end, Chapter 2 began by conducting long-term and short-term shoreline change analysis (SCA) in Loíza by using statistical tests to analyze trends and differences over the years. I used historical data going back to 1902 to carry out a long-term analysis of 116 years, which has not been done in Loíza, Puerto Rico. This analysis showed areas that have continuously been eroded. In contrast, short-term SCA allowed me to estimate how random events, such as dam construction in Río Grande de Loíza and sand extraction, could have impacted the shoreline, provoking more erosion. Linear regression models can aid in understanding trends in shoreline changes rather than changes in only specific periods. Moreover, adding other statistical analyses proved a feasible approach to withdrawing more important information about shoreline change rates. For example, which types of change (erosional or accretional) dominated specific periods? How many outliers were observed in the data that could suggest random events?

For this chapter, two limitations were the visibility of the shoreline in some years and the use of statistically significant transects with a 95.5% CI. The former could be mitigated by adding aerial photos with better visibility from other years, as well as expanding the analysis using satellite data for future work. Further analysis of the different proxy-data used as shoreline for this approach should also be addressed. Regarding the second limitation, the CI could be reduced in the future to 90%. This could increase SST values because, for management purposes, estimation of possible damage could be sufficient.

Chapter 3 showed the importance of understanding what is happening below water and its relationship with shoreline shaping. I was able to model how a small channel along the Río Grande de Loíza is trapping sediments that travel with currents from east to west and west to east, provoking accretion in that area. Moreover, morphological change analysis showed how areas that are already known to be erosional, such as Punta Uvero, have also been eroded near water. Additionally, I observed how eddy currents were placed along the eastern sides of the shoreline in Parcelas Suárez and Parcelas Vieques, suggesting a reason for the higher erosion rates observed in those areas. A limitation of the study was validating the model with new data. Future research could add other sediment traps or on-site profilers to improve the validation. Additionally, due to time constraints, the whole shoreline was not addressed.

Chapter 4 investigated how archaeological sites could be impacted by shoreline changes and other flooding events that are projected to be enhanced by climate change. First, I designed a database that allows the user to insert all the available chronological information of an archaeological series using Rouse's model, with which I was able to homogenize different archaeological record sources. Using the previous SCA linear regression, I then estimated how many years would pass before archaeological sites could be impacted by shoreline recession, assuming the constant rate of the linear regression rates. Data that were freely available from federal agencies were used to conduct spatial analysis to understand which sites could be impacted by sea-level rise, storm surges, tsunami, high-tide flooding, and flooding by FEMA Zones. I successfully expanded the variables and applied the SCAPE model to determine which archaeological sites should be prioritized for management purposes. The increase in data availability supports this

kind of analysis being conducted on geospatial communities in archaeology. One of the limitations was the lack of archaeological recommendations for the archaeological sites according to their vulnerability, which can be addressed in future work.

In summary, the research presented in this dissertation contributed to the field in these four ways:

(1) provided 116 years of long-term and short-term SCA, which was not previously available for Loíza, Puerto Rico

(2) provided statistical analysis applications to analyze trends in shoreline change rates in Loíza

(3) analyzed the prioritization model for archaeological sites in Loíza, adding climate change variables

(4) provided a view of ocean morphological change and movement of currents along the coast of Loíza using numerical modeling.

The combination of disciplines and methods used in this research highlights the importance of an interdisciplinary approach to answering scientific questions.

Literature Cited

Abbott, D., Anderies, J. M., Cooper, J., Dugmore, A., Fitzhugh, B., Hegmon, M., Ingram, S., Kintigh, K., Kinzig, A., Kohler, T., Kulow, S., McClung, E., McGovern, T., Meegan, C., Nelson, B., Nelson, M., Paulette, T., Peeples, M., Quilter, J., … Vésteinsson, O. (2012). *Surviving Sudden Environmental Change: Answers From Archaeology* (J. S. Payson & Cooper (Eds.)). University Press of Colorado. http://www.upcolorado.com/excerpts/9781607321682.pdf

Acevedo, R., Morelock, J., & Olivieri, R. A. (1989). Modification of Coral Reef Zonation by Terrigenous Sediment Stress. In *PALAIOS* (Vol. 4, Issue 1). https://doi.org/10.2307/3514736

Adams, J. (2021). Dispatches from the Edge of Empire. *Women, Gender, and Families of Color*, *9*(1), 61–82. https://www.jstor.org/stable/10.5406/womgenfamcol.9.1.0061

Addo, K. A., Walkden, M., & Mills, J. P. (2008). Detection, measurement and prediction of shoreline recession in Accra, Ghana. *ISPRS Journal of Photogrammetry & Remote Sensing*, *63*, 543–558. https://doi.org/10.1016/j.isprsjprs.2008.04.001

Agency for Cultural Resource Management (ACRM), & Leap Sustainable Development. (2016). *Archaeological Impact Assessment: Proposed Sand Mine on the Farm Brakke Kuyl No. 38 and No. 39 Blouberg Western Cape.* https://sahris.sahra.org.za/sites/default/files/heritagereports/Report CKR Brakuil Sand Mining - AIA_0.pdf

Anders, F., & Byrnes, M. (1991). Accuracy of Shoreline Change Rates as Determined from Maps and Aerial Photographs. *Shore and Beach*, *59*(1), 17–26.

Anderson, D. G., Bissett, T. G., Yerka, S. J., Wells, J. J., Kansa, E. C., Kansa, S. W., Myers, K. N., DeMuth, R. C., & White, D. A. (2017). Sea-level rise and archaeological site destruction: An example from the southeastern United States using DINAA (Digital Index of North American Archaeology). *PLOS ONE*, *12*(11), 1–25. https://doi.org/10.1371/journal.pone.0188142

Andreou, G. M. (2018). Monitoring the impact of coastal erosion on archaeological sites: the Cyprus Ancient Shoreline Project. *Antiquity*, *92*(361), 1–6. https://doi.org/10.15184/aqy.2018.1

Aquaveo. (2022). *Surface-Water Modeling System (SMS) (Version S 13.0.14) [Computer Software]*. http://www.aquaveo.com

Bagheri, M., Zaiton Ibrahim, Z., Bin Mansor, S., Abd Manaf, L., Badarulzaman, N., & Vaghefi, N. (2019). Shoreline change analysis and erosion prediction using historical data of Kuala Terengganu, Malaysia. *Environmental Earth Sciences*, *78*, 477. https://doi.org/10.1007/s12665-019-8459-x

Bainbridge, Z., Lewis, S., Smithers, S., Wilkinson, S., Douglas, G., Hillier, S., & Brodie, J. (2016). Clay mineral source tracing and characterisation of Burdekin River (NE Australia) and flood plume fine sediment. *Journal of Soils and Sediments*, *16*(2), 687–706. https://doi.org/10.1007/S11368-015-1282-4

Barker, A. W. (2018). Looting, the Antiquities Trade, and Competing Valuations of the Past. *Annual Review of Anthropology*, *47*, 455–474. https://doi.org/10.1146/annurev-anthro-102116

Barone, F. (2021). *Archaeology, absolute, archaeomagnetic, argon, dating methods,*

dendrochronology, fission-track, fluorine, magnetic, paleomagnetic, potassium, radioactive, radiocarbon, relative, seriation, stratigraphy, thermoluminescence. Teaching EHRAF, Yale University. https://hraf.yale.edu/teach-ehraf/relative-and-absolute-dating-methods-in-archaeology/

Barreto-Orta, M.; Marti, L., Santaella, O., Cabrera, N., Gladik, T., Alvira, Z., Silva, L., & Reyes, A. (2017). *Assessment of beach morphology at Puerto Rico Island*. http://drna.pr.gov/wp-content/uploads/2017/05/Geomorphic-Assessment-of-Puerto-Rico-1977-to-2016.pdf

Barreto-Orta, M.; Méndez Tejeda, R.; Rodríguez, E.; Cabrera, N.; Díaz, E.; and Pérez, K. (2019). (PDF) The state of the beaches at Puerto Rico after Maria. *Shore & Beach, 89*(1), 16–23. https://www.researchgate.net/publication/332061474_The_state_of_the_beaches_at_Puerto_Rico_after_Maria

Barreto-Orta, M. (1997). *Shoreline Changes in Puerto Rico (1936-1993)* [Doctoral Dissertation, University of Puerto Rico, Mayagüez Campus]. ProQuest. https://www.proquest.com/docview/304430432

Bartlett, D., & Celliers, L. (Eds.). (2017). *Geoinformatics for Marine and Coastal Management*. CRC Press: Taylor & Francis Group.

Bawiec, W. J. (2001). U . S Geological Survey Open-File Report 98-38 Geology , Geochemistry , Geophysics , Mineral Occurrences and Mineral Resource Assessment for the Commonwealth of Puerto Rico. *US Geological Survey 98-38*, 1–337.

Baxter, M. J., Beardah, C. C., & Wright, R. V. S. (2006). Some Archaeological Applications of Kernel Density Estimates. *Journal of Archaeological Science*, *24*(1997), 347–354.

Beck, T. M. (2019). *Tracking Sediment Bypassing, Geomorphological Analysis, and Regional Sediment Management at Tidal Inlets* [Doctoral Dissertation, University of South Florida]. ProQuest https://www.proquest.com/docview/2281202155/25E6456566014338PQ/1

Benitéz, J., & Mercado Irizarry, A. (2015). *Storm Surge Modeling in Puerto Rico in Support of Emergency Response, Risk Assessment, Coastal Planning and Climate Change Analysis*.

Berggren, Å. (2009). The relevance of stratigraphy. *Archaeological Dialogues*, *16*(1), 22–25. https://doi.org/10.1017/S138020380900275X

Bird, E. (2008). *Coastal Geomorphology: An Introduction* (2nd ed.). Wiley. https://doi.org/10.1029/01eo00219

Bishop-Taylor, R., Nanson, R., Sagar, S., & Lymburner, L. (2021). Mapping Australia's dynamic coastline at mean sea level using three decades of Landsat imagery. *Remote Sensing of Environment*, *267*(112734). https://doi.org/10.1016/j.rse.2021.112734

Boak, E. H, Turner, I. L. (2005). Shoreline Definition and Detection : A Review. *Journal of Coastal Research*, *21*(4), 688–703. https://doi.org/10.2112/03-0071.1

Boas, I., D., R., & Wrathall, D. (2020). Grounding Big Data on Climate-Induced Human Mobility. *Geographical Review*, *110*, 195–209. https://doi.org/10.1111/gere.12355

Bofill Calero, J. O. (2014). Bomba, danza, calipso y merengue: Creación del espacio

social en las fiestas de Santiago Apóstol de Loíza. *Latin American Music Review*, *35*(1), 115–138. https://doi.org/10.7560/LAMR35105

Bracero Marrero, L. I. . (2019). Using Airborne and Uas Aerial Images to Evaluate Coastal Change and Impacts to Archaeological Sites Along Loiza ’s Coast , Puerto Rico. *IEEE International Geoscience and Remote Sensing Society (IGARSS) Symposium 2019*, 9149–9152. https://ieeexplore.ieee.org/abstract/document/8899100

Brooks, S. M., & Spencer, T. (2012). Shoreline retreat and sediment release in response to accelerating sea level rise: Measuring and modelling cliffline dynamics on the Suffolk Coast, UK. *Global and Planetary Change*, *80–81*, 165–179. https://doi.org/10.1016/j.gloplacha.2011.10.008

Bunch, B. W., Cerco, C. F., & Dortch, M. (2000). *Hydrodynamic and Water Quality Model Study of San Juan Bay Estuary*. https://www.researchgate.net/publication/235186152

Bureau of Ocean Energy Management (BOEM) ; National Oceanic and Atmospheric Administration (NOAA). (2021). *Ocean Report for Custom Area near Suarez , PR [Marine Cadastre]*. https://marinecadastre.gov/oceanreports/@-7339550.338342372,2089301.0672614009/13/eyJ0IjoiYm8iLCJiIjoiIiwiZiI6MCwicyI6MCwiYSI6IjM2ODJkNGQwNTRhZmFjYTJmNzQ4NGFhMWU0ODY4MzZjIiwibCI6WzAsNzBdfQ==

Bush, D. M., Neal, W. J., & Jackson, C. W. (2009). Summary of Puerto Rico’s vulnerability to coastal hazards: Risk, mitigation, and management with examples.

Special Paper of the Geological Society of America, *460*(January 2009), 149–165. https://doi.org/10.1130/2009.2460(11)

Byrnes, M.R.; Mcbride, R.A., Hiland, M. W. (1991). Accuracy standards and development of a national shoreline change database. *Coastal Sediments*, 1027–1042. https://cedb.asce.org/CEDBsearch/record.jsp?dockey=0071729

Canals, M., Ernesto, D., Evans, C., Haibo, X., Patricia, C., Morell, J., Aponte, L., Chaparro, Hernández, E., Cuevas, E., Rodríguez, S., González, A., & Team, C. (2019). *Puerto Rico's Wave Climate: Hurricanes, Winter Swells and Coral Reef [Power Point Slides]*. http://www.pr-ccc.org/wp-content/uploads/2019/12/2-Dr.-Miguel-Canals_El-Clima-del-Oleaje-en-PR.pdf

Caribbean Coastal Ocean Observing System (CARICOOS). (2022). *Wave Model Cariccos*. https://www.caricoos.org/map/nearshore-breaker-model?locale=es

Carter, R. (1988). Sea Level Changes. In *Coastal Environments: An introduction to the Physical, Ecological and Cultural Systems of Coastline* (pp. 245–279). Academic Press.

Castro Prieto, J., Gould, W., Ortiz Maldonado, C., Soto Bayó, S., Llerandi Román, I., Gaztambide-Arandes, S., Quiñones, M., Cañon, M., & Jacobs, K. (2019). *Inventario detallado de áreas protegidas y otros mecanismos para la conservación de terrenos en Puerto Rico*.

Center for Applied Ocean Science and Engineering (CAOSE). (n.d.). *PR Wave Climate Atlas — UPRM Center for Applied Ocean Science and Engineering*. Retrieved May 24, 2022, from http://www.canalsresearch.com/wave-climate-atlas

Center for Applied Ocean Science and Engineering (CAOSE). (2018). *Wave Climate Atlas-Point Output*. http://www.canalsresearch.com/wave-climate-atlas-point-output

Chardón, P. (2013). *Field observations and numerical simulations of storm-induced nearshore morphology change in Rincón , Puerto Rico* [Master's Thesis, University of Puerto Rico, Mayagüez Campus]. Coastal Inlets Research Program Website http://cirp.usace.army.mil/pubs/theses.php

Cheriton, O. M., Storlazzi, C. D., Rosenberger, K. J., & Sherman, C. (2019). Controls on sediment transport over coral reefs off southwest Puerto Rico: Seasonal patterns and Hurricane Maria. *Coastal Sediments*, 903–915. https://doi.org/10.1142/9789811204487_0079

Church, J. a., Clark, P. U., Cazenave, a., Gregory, J. M., Jevrejeva, S., Levermann, a., Merrifield, M. a., Milne, G. a., Nerem, R. ., Nunn, P. D., Payne, a. J., Pfeffer, W. T., Stammer, D., & Unnikrishnan, a. S. (2013). Sea level change. *Climate Change 2013: The Physical Science Basis. Contribution of Working Group I to the Fifth Assessment Report of the Intergovernmental Panel on Climate Change*, 1137–1216. https://doi.org/10.1017/CB09781107415315.026

Coastal Inlets Research Program (CIRP). (2018). *Coastal Modeling System (Version 3.2) [Computer Software]*. https://cirpwiki.info/wiki/CMS#Documentation_Portal

Coastal Inlets Research Program (CIRP). (2020). *Coastal Inlets Research Program (CIRP) Publications [Web Map App]*. https://erdcchl.maps.arcgis.com/apps/webappviewer/index.html?id=3117c376e3f9420d93c397de902b5956

Coastal Inlets Research Program (CIRP). (2021). *Wavenet and Tidenet*. https://cirp.usace.army.mil/products/metocean.php

Coastal Research and Planning Institute of Puerto Rico (CoRePI-PR). (2021). *Radiografía de la Costa [Story Map]*. El Estado de Costa En Puerto Rico. https://storymaps.arcgis.com/stories/bc4b7c14ec904571a47175129f6baba8

Consejo para la Protección del Patrimonio Arqueológico Terrestre de Puerto Rico. (2015). *Archaeological Cultural Resources [GIS Shapefile Point Layer]*. Consejo para la Protección del Patrimonio Arqueológicos Terrestre.

Consejo para la Protección del Patrimonio Arqueológicos Terrestre. (1992). *Procedimiento para la Radicación y Evaluación de Proyectos de Construcción y Desarrollo*. http://app.estado.gobierno.pr/ReglamentosOnLine/Reglamentos/4643.pdf

Cooper, J., & Peros, M. (2010). The archaeology of climate change in the Caribbean. *Journal of Archaeological Science*, *37*(6), 1226–1232. https://doi.org/10.1016/j.jas.2009.12.022

Crespo Jones, H. (2013). *Shoreline Changes during the last 60 years in Arecibo, Puerto Rico* [Undergraduate Research, University of Puerto Rico, Mayaguez Campus]. http://gers.uprm.edu/pdfs/topico_hector1.pdf

Crowell, M., Leatherman, S. P., & Buckley, M. K. (1991). *Historical shoreline change : error analysis and mapping accuracy Historical Shoreline Change : Error Analysis and Mapping Accuracy * The United States Federal Emergency Man-*. https://www.researchgate.net/profile/Mark_Crowell2/publication/279557852_Histor

ical_shoreline_change_error_analysis_and_mapping_accuracy/links/56e997b608ae95bddc29f78f/Historical-shoreline-change-error-analysis-and-mapping-accuracy.pdf?origin=publication_

Davidson-Arnott, R. (2010). Introduction to Coastal Processes & Geomorphology. In *Journal of Coastal Research* (Vol. 226). https://doi.org/10.2112/1551-5036(2006)22[1589:BR]2.0.CO;2

Dawson, T. (2010). A system for prioritising action at archaeological sites recorded in the Coastal Zone: Assessment surveys. *Historic Scotland*. https://risweb.st-andrews.ac.uk/portal/en/researchoutput/a-system-for-prioritising-action-at-archaeological-sites-recorded-in-the-coastal-zone-assessment-surveys(deb3b2c7-69a4-43d4-92fc-0d96fd5609a4).html

Dawson, T. (2013). *Erosion and Coastal Archaeology: Evaluating the Threat and Prioritizing Action*. https://research-repository.st-andrews.ac.uk/bitstream/handle/10023/4183/Dawson2013BAR_Homer_Erosion.pdf?sequence=1&isAllowed=y

Dawson, T. (2017). *Public Archaeology and Climate Change* (M.-Y. Dawson, Tom; Numura, Courtney; López-Romero, Elías; Daire (Ed.)). https://ebookcentral-proquest-com.uprrp.idm.oclc.org/lib/uprrp-ebooks/reader.action?docID=5185069

Demas, M. (2000). Planning for Conservation and Management of Archeological Sites: A Values-Based Approach. In *Management Planning for Archaeological Sites: An International Workshop Organized by the Getty Conservation Institute and Loyola Marymount University* (pp. 27–54). The Getty Conservation Institute.

Dempwolff, L. C., Lojek, O., Selke, V., Goseberg, N., & Gerlach, R. (2020). Hydrodynamic cross-scale archaeology at a roman river harbour. *Water*, *12*(3365). https://doi.org/10.3390/W12123365

Devis-Morales, A., Rodríguez-Rubio, E., Montoya-Sánchez, R. A., Devis-Morales, A., Rodríguez-Rubio, E., & Montoya-Sánchez, R. A. (2021). Modelling the transport of sediment discharged by Colombian rivers to the southern Caribbean Sea. *Ocean Dynamics*, *71*, 251–277. https://doi.org/10.1007/S10236-020-01431-Y

Díaz Torres, E. (2019). *Plan de acción para reducir la vulnerabilidad física y social ante eventos extremos (marejadas, huracanes, erosión e inundación costera) en tres comunidades costeras del municipio de Loíza.* [Master's Thesis] University of Puerto Rico Río Piedras Campus.

Díaz, E.L.; Gould, W. A. ., Álvarez-Berríos, N., Aponte-Gonzalez, F., Archibald, W., Bowden, J. H. ., Carrubba, L., Crespo, W., Fain, S. J. ., González, G., Goulbourne, A., Harmsen, E., Khalyani, A. H., Holupchinski, E., Kossin, J. P. ., Leinberger, A. J. ., Marrero-Santiago, V. I. ., Martinez-Sanchez, O., McGinley, K., Oyola, M. M., … Torres-Gonzalez, S. (2018). *Chapter 20 : US Caribbean. Impacts, Risks, and Adaptation in the United States: The Fourth National Climate Assessment, Volume II*. https://doi.org/10.7930/NCA4.2018.CH20

Díaz Díaz, M., Rivera Collazo, I., & Barreto-Orta, M. (2015). La erosión costera como agente de cambio geomorfológico y pérdida de contexto arqueológico [Power Point Slides]. *Society for American Archeology 80th Annual Meeting*. https://www.academia.edu/28948962/LA_EROSIÓN_COSTERA_COMO_AGENTE_DE_CAMBIO_GEOMORFOLÓGICO_Y_PÉRDIDA_DE_CONTEXTO_ARQU

EOLÓGICO

Do, A. T. K., De Vries, S., & Stive, M. J. F. (2019). The Estimation and Evaluation of Shoreline Locations, Shoreline-Change Rates, and Coastal Volume Changes Derived from Landsat Images. *Journal of Coastal Research*, *35*(1), 56–71. https://doi.org/10.2112/JCOASTRES-D-18-00021.1

Donadio, C., Vigliotti, M., Valente, R., Stanislao, C., Ivaldi, R., & Ruberti, D. (2018). Anthropic vs. natural shoreline changes along the northern Campania coast, Italy. *Journal of Coastal Conservation*, *22*(5), 939–955. https://doi.org/10.1007/s11852-017-0563-z

EcoExploratorio. (2020). *Sequías en Puerto Rico*. https://ecoexploratorio.org/amenazas-naturales/sequias/sequias-en-puerto-rico/

El Mundo. (1965, September 25). *Puerto Rico Ilustrado: Suplemento Sabatino*. 12.

El Mundo. (1971, October 10). *Photography: Folder No. 4707*. https://upr.contentdm.oclc.org/

El Mundo. (1973, January 1). *Photography: Folder No. 4707*.

Enevold, R., Rasmussen, P., Løvschal, M., Olsen, J., & Odgaard, B. V. (2019). Circumstantial evidence of non-pollen palynomorph palaeoecology: a 5,500 year NPP record from forest hollow sediments compared to pollen and macrofossil inferred palaeoenvironments. *Vegetation History and Archaeobotany*, *28*, 105–121. https://doi.org/10.1007/s00334-018-0687-6

Environmental Systems Research Institute (ESRI). (n.d.-a). *ArcGIS Pro Documentation Geodatabase topology rules and fixes for polyline features*. Retrieved August 18,

2021, from https://pro.arcgis.com/en/pro-app/latest/help/editing/geodatabase-topology-rules-for-polyline-features.htm

Environmental Systems Research Institute (ESRI). (n.d.-b). *Contour (3D Analyst)—ArcGIS Pro*. Retrieved December 8, 2021, from https://pro.arcgis.com/en/pro-app/latest/tool-reference/3d-analyst/contour.htm

Environmental Systems Research Institute (ESRI). (n.d.-c). *Data classification methods—ArcGIS Pro*. Retrieved March 20, 2022, from https://pro.arcgis.com/en/pro-app/2.8/help/mapping/layer-properties/data-classification-methods.htm

Environmental Systems Research Institute (ESRI). (n.d.-d). *How Kernel Density works—ArcGIS Pro*. Retrieved March 20, 2022, from https://pro.arcgis.com/en/pro-app/latest/tool-reference/spatial-analyst/how-kernel-density-works.htm

Environmental Systems Research Institute (ESRI). (n.d.-e). *Imagery appearance—ArcGIS Pro*. Retrieved May 17, 2021, from https://pro.arcgis.com/en/pro-app/latest/help/data/imagery/raster-display-ribbon.htm

Environmental Systems Research Institute (ESRI). (n.d.-f). *Intersect (Analysis)—ArcGIS Pro*. Retrieved October 20, 2021, from https://pro.arcgis.com/en/pro-app/latest/tool-reference/analysis/intersect.htm

Environmental Systems Research Institute (ESRI). (n.d.-g). *Near (Analysis)—ArcGIS Pro*. Retrieved October 24, 2021, from https://pro.arcgis.com/en/pro-app/latest/tool-reference/analysis/near.htm

Environmental Systems Research Institute (ESRI). (n.d.-h). *Spatial Join (Analysis) Tool:*

(ArcGIS Pro 2.8.2). https://pro.arcgis.com/en/pro-app/tool-reference/analysis/spatial-join.htm

Environmental Systems Research Institute (ESRI). (n.d.-i). *Survey 123 App Field*.

Environmental Systems Research Institute (ESRI). (2016). *ArcGIS 10.5 [Computer Software]*. https://www.esri.com/en-us/home

Environmental Systems Research Institute (ESRI). (2019). *Survey 123 Connect 3.3.26*.

Environmental Systems Research Institute (ESRI). (2021). *ArcGIS Pro [Computer Software]* (2.0-2.5). Environmental Systems Research Institute.

Erlandson, J. M. (2012). As the world warms: Rising seas, coastal archaeology, and the erosion of maritime history. *Journal of Coastal Conservation*, *16*(2), 137–142. https://doi.org/10.1007/s11852-010-0104-5

Evis, L. H., Hanson, I., & Cheetham, P. N. (2016). An experimental study of two grave excavation methods: Arbitrary Level Excavation and Stratigraphic Excavation. *Science & Technology of Archaeological Research*, *2*(2), 177–191. https://doi.org/10.1080/20548923.2016.1229916

Ezcurra, P., & Rivera-Collazo, I. C. (2018). An assessment of the impacts of climate change on Puerto Rico's Cultural Heritage with a case study on sea-level rise. *Journal of Cultural Heritage*, *32*(2017), 198–209. https://doi.org/10.1016/j.culher.2018.01.016

Fatorić, S., & Seekamp, E. (2017). A measurement framework to increase transparency in historic preservation decision-making under changing climate conditions. *Journal of Cultural Heritage*. https://doi.org/10.1016/J.CULHER.2017.08.006

Figueroa Cancel, A. (2021a, February 22). Estudian impacto del cambio climático en río Grande de Loíza | Ciencia Puerto Rico. *El Nuevo Día*. https://www.elnuevodia.com/ciencia-ambiente/cambio-climatico/notas/estudian-impacto-de-erosion-costera-en-yacimientos-arqueologicos/

Figueroa Cancel, A. (2021b, March 11). El cambio climático amenaza con desaparecer parte del patrimonio histórico en las costas de Puerto Rico. *El Nuevo Día, Ciencia Puerto Rico*. https://www.elnuevodia.com/ciencia-ambiente/cambio-climatico/notas/el-cambio-climatico-amenaza-con-desaparecer-parte-del-patrimonio-historico-en-las-costas-de-puerto-rico/

Finkl, C. W. (2004). Coastal Classification : Systematic Approaches Comprehensive Scheme. *Journal of Coastal Research*, *20*(1), 166–213. http://fau.digital.flvc.org/islandora/object/fau%3A2031

Foti, G., Barbaro, G., Bombino, G., Fiamma, V., Puntorieri, P., Minniti, F., & Pezzimenti, C. (2019). Shoreline changes near river mouth: case study of Sant'Agata River (Reggio Calabria, Italy). *European Journal of Remote Sensing*, *52*(54), 102–112. https://doi.org/10.1080/22797254.2019.1686955

Fuchs, S.; Frazier, T.; Siebeneck, L. (2018). Physical Vulnerability - Vulnerability and Resilience to Natural Hazards. In *Vulnerability and Resilience to Natural Hazards* (pp. 32–52). Cambridge University Press. https://www.cambridge.org/core/books/abs/vulnerability-and-resilience-to-natural-hazards/physical-vulnerability/6B046595CFAD855605B6B516F72F04F0

García Lebrón, D. (2016). *Loíza: historia, cultura y grandes retos*. Noticias-Universidad

de Puerto Rio Río Piedras. https://www.uprrp.edu/2016/02/loiza-historia-cultura-y-grandes-retos/

Garret, Christopher; Toulany, B. (1980). Variability of the flow through the Strait of Belle Isle. *Journal of Marine Research*, *39*(1), 163–189.

Gómez, J. F., Byrne, M. L., Hamilton, J., & Isla, F. (2017). Historical Coastal Evolution and Dune Vegetation in Isla Salamanca National Park, Colombia. *Journal of Coastal Research*, *33*(3), 632–641. https://doi.org/10.2112/JCOASTRES-D-15-00189.1

Gorman, L.; Morang, A., and LarsonN, R. (1998). Monitoring the coastal environment. Part IV. Mapping, shoreline changes, and bathymetric analysis. *Journal of Coastal Research*, *14*(1), 61–92.

Grossman & Associates Inc. (1990). *Excavation and Analysis Results of Archaeological Investigations at Mediania Alta (L-23) and Vieques (L-22) [Report]*.

Gupta, A. (2011). The Tropical Coasts. In *Tropical Geomorphology* (pp. 170–194). Cambridge University Press.

Harris, E. C. (1981). *Principles of Archaeological Stratigraphy* (2nd ed). Academic Press. https://doi.org/10.2307/3888021

He, Q., & Silliman, B. R. (2019). Climate Change, Human Impacts, and Coastal Ecosystems in the Anthropocene. *Current Biology*, *29*(19), R1021–R1035. https://doi.org/10.1016/J.CUB.2019.08.042

Henderson, R.; Helsin, J.; Himmelstoss, E. A. (2021). Puerto Rico shoreline change: A GIS compilation of shorelines, baselines, intersects, and change rates calculated

using the digital shoreline analysis system version 5.1. In *ScienceBase*. Unites States Geologial Survey (USGS). https://www.sciencebase.gov/catalog/item/61255b87d34e40dd9c03f390

Hil, G. (2020). Better Management Through Measurement: Integrating Archaeological Site Features into a GIS-Based Erosion and Sea Level Rise Impact Assessment—Blueskin Bay, New Zealand. *Journal of Island and Coastal Archaeology*, *15*(1), 104–126. https://doi.org/10.1080/15564894.2018.1531331

Himmelstoss, E. A., Henderson, R. E., Kratzmann, M. G., Farris, A. S., Henderson, R. E., & Farris, A. S. (2018). Digital Shoreline Analysis System (DSAS) version 5.0 user guide. *Open-File Report*. https://doi.org/10.3133/ofr20181179

Hofman, C. L., Stancioff, C. E., Richards, A., Auguiste, I. N., Sutherland, A., & Hoogland, M. L. P. (2021). Resilient Caribbean Communities : A Long-Term Perspective on Sustainability and Social Adaptability to Natural Hazards in the Lesser Antilles. *Sustainability*, *13*(17), 9807.

Hsu, T.W., Lin, T.-Y., & Tseng, I.-F. (2007). Human Impact on Coastal Erosion in Taiwan. *Journal of Coastal Research, 23*(4), 961–973. http://content.ebscohost.com/ContentServer.asp?T=P&P=AN&K=25963286&S=R&D=asn&EbscoContent=dGJyMNLr40SeqK44xNvgOLCmr1Cep7RSs6m4SrSWxWXS&ContentCustomer=dGJyMPGutkyyr7FPuePfgeyx44Dt6fIA

Intergovernmental Panel on Climate Change. (2021). Headline Statements from the Summary for Policymakers. *Work Group I: The Physical Science Basis*. https://www.ipcc.ch/report/ar6/wg1/resources/spm-headline-statements/

Intergovernmental Panel on Climate Change. (2022). *Sixth Assessment Report*. https://www.ipcc.ch/assessment-report/ar6/

Jana, A., Biswas, A., Maiti, S., & Bhattacharya, A. K. (2013). Shoreline changes in response to sea level rise along Digha Coast, Eastern India: an analytical approach of remote sensing, GIS and statistical techniques. *Journal of Coastal Conservation*, *18*(3), 145–155. https://doi.org/10.1007/s11852-013-0297-5

Jayanthi, M., Thirumurthy, S., Samynathan, M., Duraisamy, M., Muralidhar, M., Ashokkumar, J., & Vijayan, K. K. (2018). Shoreline change and potential sea level rise impacts in a climate hazardous location in southeast coast of India. *Environmental Monitoring and Assessment*, *190*(1). https://doi.org/10.1007/s10661-017-6426-0

Jean, M., Pajak, & Leatherman, S. (2002). The High Water Line as Shoreline Indicator. *Journal of Coastal Research*, *18*(2), 329–337.

Jensen, J. R. (2005). Geometric Correction. In J. Challice (Ed.), *Introductory Digital Image Processing: A Remote Sensing Perspective* (3rd ed., pp. 227–254). Pearson Education, Inc.

Jervis, R. (2017, September 22). Hurricane Maria aftermath: Puerto Rico battles epic flooding. *USA Today*. https://www.usatoday.com/story/news/world/2017/09/22/hurricane-maria-aftermath-puerto-rico-battles-floods/692251001/

Johnson, C. L., Mcfall, B. C., Krafft, D. R., Brown, M. E., & Coelho, B. (2021). Sediment Transport and Morphological Response to Nearshore Nourishment

Projects on Wave-Dominated Coasts. *Journal of Marine Science and Engineering*, *9*(1182). https://doi.org/10.3390/jmse9111182

Kabuth, A. K., Kroon, A., & Pedersen, J. B. T. (2014). Multidecadal Shoreline Changes in Denmark. *Journal of Coastal Research, 296*(4), 714–728. https://doi.org/10.2112/JCOASTRES-D-13-00139.1

Kankara, R. S., Mohan, R., & Venkatachalapathy. (2013). Hydrodynamic Modelling of Chennai Coast from a Coastal Zone Management Perspective. *Journal of Coastal Research, 29*(2), 347–357. https://doi.org/10.2112/JCOASTRES-D-11-00071.1

Kaye, C. A. (1959a). Geology of San Juan Metropolitan Area, Puerto Rico: Coastal Geology of Puerto Rico [Paper 317]. *Geological Survey Professional Paper*. https://pubs.usgs.gov/pp/0317a/report.pdf

Kaye, C. A. (1959b). Shoreline Features and Quaternary Shoreline Changes Puerto Rico: Coastal Geology of Puerto Rico [Paper 317-B]. *Geological Survey Bulletin 1042-I*, 49–139. https://pubs.usgs.gov/pp/0317b/report.pdf

Kelly, R., Legault, P. E., & Torruella, A. (2016). *CMS Modeling of the North Coast of Puerto Rico [Power Point Slides]*. https://rsm.usace.army.mil/pubs/pdf2/2016/2016_ASBPA_Legault_brief.pdf

Ken State University. (2021). *Paired Samples t Test - SAS Tutorials - LibGuides at Kent State University*. University Libraries. https://libguides.library.kent.edu/SAS/PairedSamplestTest

Kermani, S., Boutiba, M., Guendouz, M., Guettouche, M. S., & Khelfani, D. (2016). Detection and analysis of shoreline changes using geospatial tools and automatic

computation: Case of jijelian sandy coast (East Algeria). *Ocean and Coastal Management, 132*, 46–58. https://doi.org/10.1016/j.ocecoaman.2016.08.010

Le Cozannet, G., Bulteau, T., Castelle, B., Ranasinghe, R., Wöppelmann, G., Rohmer, J., Bernon, N., Louisor, J., & Salas-Y-Mélia, D. (2019). Quantifying uncertainties of sandy shoreline change projections as sea level rises. *Scientific Reports, 9*(42). https://doi.org/10.1038/s41598-018-37017-4

Le Cozannet, G., Garcin, M., Yates, M., Idier, D., & Meyssignac, B. (2014). Approaches to evaluate the recent impacts of sea-level rise on shoreline changes. *Earth-Science Reviews, 138*, 47–60. https://doi.org/10.1016/j.earscirev.2014.08.005

Le Cozannet, G., Oliveros, C., Castelle, B., Garcin, M., Idier, D., Pedreros, R., & Rohmer, J. (2016). Uncertainties in Sandy Shorelines Evolution under the Bruun Rule Assumption. *Frontiers in Marine Science, 3*(49). https://doi.org/10.3389/fmars.2016.00049

Li, H., Beck, T. M., Moritz, H. R., Groth, K., Puckette, T., & Marsh, J. (2019). Sediment Tracer Tracking and Numerical Modeling at Coos Bay Inlet, Oregon. *Journal of Coastal Research, 35*(1), 4. https://doi.org/10.2112/JCOASTRES-D-17-00218.1

Li, H., Lin, L., Lu, C.-C., Reed, C. W., & Shak, A. T. (2015). Modeling study of Dana Point Harbor, California: littoral sediment transport around a semi-permeable breakwater. *Journal of Ocean Engineering and Marine Energy, 1*(2), 181–192. https://doi.org/10.1007/s40722-015-0018-2

Long, J. W., & Plant, N. G. (2012). Extended Kalman Filter framework for forecasting shoreline evolution. *Geophysical Research Letters, 39*(13).

https://doi.org/10.1029/2012GL052180/FORMAT/PDF/OEBPS/PAGES/2.PAGE.XHTML

López Marrero, T; M.A. Lorenzo Perez, C.F. Rivera Lopez, A.C. Gonza lez Toro, D. Rivera Santiago, H. . N. C. and P. N. H. ndez G. (2017). *Porto Rico 1930 & 1951 Georeferenced: A Coastal Mosaic*. Interdisciplinary Center for Coastal Studies, University of Puerto Rico, Mayaguez Campus. http://www.prgeoref.org/.

Manno, G., Lo Re, C., & Ciraolo, G. (2017). Uncertainties in shoreline position analysis: The role of run-up and tide in a gentle slope beach. *Ocean Science*, *13*(5), 661–671. https://doi.org/10.5194/os-13-661-2017

Marine Awareness Research & Education Society (MARES). (2018). *Plan de Adaptación de Base Comunitaria al Cambio Climático del Municipio de Loíza*. https://www.drna.pr.gov/wp-content/uploads/2019/07/Plan-Adptc-Loiza-RVSN_9-22-18.pdf

Marques, L. (2020). *Capitalism and Environmental Destruction*. Springer. https://doi.org/10.4324/9781315265704-12

Martínez Martínez, Y. (2008). *Plan de mitigación al riesgo de erosión costera, entre la desembocadura del Río Grande de Loíza y el Río Herrera, Municipio de Loíza*. [Master's Thesis] University of Puerto Rico Río Piedras Campus.

Marzeion, B., & Levermann, A. (2014). Loss of cultural world heritage and currently inhabited places to sea-level rise. *Environmental Research Letters*, *9*(3). https://doi.org/10.1088/1748-9326/9/3/034001

Mcgranahan, G., Balk, D., & Anderson, B. (2007). The rising tide: assessing the risks of

climate change and human settlements in low elevation coastal zones. *Environment & Urbanization*, *19*(1), 17–37. https://doi.org/10.1177/0956247807076960

Meléndez Maíz, M., & Rodríguez Ramos, R. (1998). *Inventario de Recursos Arqueológicos en la franja costera entre el río Grande de Loíza y el río Herrera: Análisis Regional de Boca de Cangrejos a Punta Miquillo*.

Meléndez Maíz, M. (1997). Estudio arqueológico de Piñones-Vacía Talega, Barrio Torrecilla Baja, Loíza, Puerto Rico. *Segundo Encuentro de Investigadores: Ocho Trabajos de Investigación Arqueológica En Puerto Rico*, 31–38.

Meylemans, E., Bogemans, F., Deforce, K., Jacops, J., Perdaen, Y., Storme, A., & Verdurmen, I. (2014). The Archaeology of Erosion, the Erosion of Archaeology. *The Archaeology of Erosion, the Erosion of Archaeology*, 127–146. https://oar.onroerenderfgoed.be/publicaties/RELM/9/RELM009-001.pdf

Miller, J. K., & Dean, R. G. (2004). A simple new shoreline change model. *Coastal Engineering*, *51*(7), 531–556. https://doi.org/10.1016/j.coastaleng.2004.05.006

Monroe, W. (1977). Las divisiones geomórficas de Puerto Rico. In M. T. De Galiñanes (Ed.), *Geovisión de Puerto Rico: aportaciones recientes al estudio de la geografíá*. Editorial Universitaria, Universidad de Puerto Rico.

Monroe, W. (1980). Some Tropical Landforms of Puerto Rico [Paper 1159]. *Geological Survey Professional Paper*. https://pubs.er.usgs.gov/publication/pp1159

Moore, L. J. (2000). Shoreline mapping techniques. *Journal of Coastal Research*, *16*(1), 111–124.

Moore, L. J., Ruggiero, P., & List, J. H. (2006). Comparing mean high water and high

water line shorelines: Should prosy-datum offsets be incorporated into shoreline change analysis? *Journal of Coastal Research, 22*(4), 894–905. https://doi.org/10.2112/04-0401.1

Morelock, J. (1978). *Shoreline of Puerto Rico*. http://edicionesdigitales.info/biblioteca/costapr.pdf

Morelock, J., Ramirez, W., & Barreto Orta, M. (2003). *The Worlds's Coasts: Puerto Rico*. http://geology.uprm.edu/Morelock/GEOLOCN_/pdfdoc/wcPR.pdf

Morelock, Jack;, & Barreto, M. (2000). *An Update of Coastal Erosion in Puerto Rico*. http://geology.uprm.edu/Morelock/pdfdoc/erosion2000.pdf

Moussaid, J., Fora, A. A., Zourarah, B., Maanan, M., & Maanan, M. (2015). Using automatic computation to analyze the rate of shoreline change on the Kenitra coast, Morocco. *Ocean Engineering*, *102*, 71–77. https://doi.org/10.1016/j.oceaneng.2015.04.044

National Aeronautics and Space Administration (NASA). (2019). *The Causes of Climate Change*. Global Climate Change: Vital Signs of the Planet. https://climate.nasa.gov/causes/

National Aeronautics and Space Administration (NASA). (2022). *The Earth's Radiation Budget*. NASA Science: Share the Science. https://science.nasa.gov/ems/13_radiationbudget

National Centers for Coastal Ocean Science (NCCOS). (2001). *Puerto Rico and the U.S. Virgin Islands Benthic Areas [Dataset]*. https://products.coastalscience.noaa.gov/collections/benthic/e95usvi_pr/

National Geodetic Survey National Oceanic and Atmospheric Administration (NOAA). (2019). *Shoreline Data Explorer Topographic Sheets 2581-2582 [Datasets]*. https://www.ngs.noaa.gov/CUSP/

National Oceanic and Atmospheric Administration (NOAA); National Centers for Environmental Information; OCM Partners. (2022). *Puerto Rico 2009-10 Orthographic Imagery from 2010-06-15 to 2010-08-15*. https://www.fisheries.noaa.gov/inport/item/49483

National Oceanic and Atmospheric Administration (NOAA). (n.d.-a). *National Buoy Center*. https://www.ndbc.noaa.gov/

National Oceanic and Atmospheric Administration (NOAA). (n.d.-b). *Tides & Currents*. https://tidesandcurrents.noaa.gov/

National Oceanic and Atmospheric Administration (NOAA). (2018). San Juan, La Puntilla, San Juan Bay, PR - Station ID: 9755371. In *Tides and Currents*. https://tidesandcurrents.noaa.gov/stationhome.html?id=9755371

National Oceanic and Atmospheric Administration (NOAA). (2021a). *Coastal Flood Exposure Mapper [Web Map]*. https://coast.noaa.gov/floodexposure/#-10575352,4439107,5z

National Oceanic and Atmospheric Administration (NOAA). (2021b). *What is a current?* Ocean Facts. https://oceanservice.noaa.gov/facts/current.html

National Oceanic and Atmospheric Administration (NOAA). (2022a). *About San Juan, Puerto Rico — WebGNOME documentation*. https://gnome.orr.noaa.gov/doc/location_files/san_juan_tech.html

National Oceanic and Atmospheric Administration (NOAA). (2022b). *Boundary Currents - Currents: NOAA's National Ocean Service Education*. https://oceanservice.noaa.gov/education/tutorial_currents/04currents3.html

National Oceanic and Atmospheric Administration (NOAA). (2022c). *NOAA Ship Okeanos Explorer: 2022 Expeditions Overview: NOAA Ocean Exploration*. https://oceanexplorer.noaa.gov/okeanos/explorations/2022-overview/welcome.html

Ochoa, B., García-Diez, M., Maíllo-Fernández, J. M., Arrizabalaga, Á., & Pettitt, P. (2019). Gravettian figurative art in the Western pyrenees: Stratigraphy, cultural context, and chronology. *European Journal of Archaeology*, *22*(2), 168–184. https://doi.org/10.1017/eaa.2018.31

Office for Coastal Management; National Oceanic and Atmospheric Administration (NOAA). (2019). *NOAA: Data Access Viewer*. Digital Coast. https://coast.noaa.gov/dataviewer/#/%0Ahttps://coast.noaa.gov/dataviewer/#/lidar/search/-13624866.850632792,4547749.985311793,-13623648.635494499,4549890.222103777

Office for Coastal Management; National Oceanic and Atmospheric Administration (NOAA). (2022a). *Digital Coast Sea Level Rise Viewer: Frequent Questions*. https://coast.noaa.gov/data/digitalcoast/pdf/slr-faq.pdf

Office for Coastal Management; National Oceanic and Atmospheric Administration (NOAA). (2022b). *Quick Flood Assessment Report for Loíza, PRI (1ft)*.

Office for Coastal Management; National Oceanic and Atmospheric Administration (NOAA). (2022c). *Quick Flood Assessment Report for Loíza, PRI (2ft)*.

Office for Coastal Management; National Oceanic and Atmospheric Administration (NOAA). (2022d). *Quick Flood Assessment Report for Loíza, PRI (3ft)*. https://coast.noaa.gov/stormwater-floods/assess/

Oficina de Fotogrametría. (n.d.). *Fotos áereas [1951, 1977, 1991]*.

Oficina Estatal de Conservación Histórica. (2010). *Registro Nacional de Lugares Históricos OECH [Points Layer]*. Oficina de Gerencia y Prespuesto. http://gis.otg.pr.gov/Downloads/Metadata/RNLH.htm

Ortiz Zayas, J., Quiñones, F., Palacios, S., Vélez, Á., & Mas, H. (2004). *Características y Condición de los Embalses Principales en Puerto Rico*. https://www.recursosaguapuertorico.com/Los_Embalses_en_Puerto_Rico__2004__por_Jorge_F__Ortiz__Ferdinand_Qui__ones_y_otros.pdf

Osborne, P. L. (2000). Global Ecology: biodiversity conservation, climate change and sustainable development. In *Tropical Ecosystems and Ecological Concepts* (pp. 397–410). Cambridge University Press.

Oyedotun, T. D. T. (2014). Shoreline Geometry : DSAS as a Tool for Historical Trend Analysis. *British Society for Geomorphology*, *Chapter 3*(Sec 2.2).

Ozturk, D., & Sesli, F. A. (2015). Shoreline change analysis of the Kizilirmak Lagoon Series. *Ocean and Coastal Management*, *118*, 290–308. https://doi.org/10.1016/j.ocecoaman.2015.03.009

Pacific Coastal and Marine Science Center. (2021). *Coastal Climate Impacts*. United States Geological Survey. https://www.usgs.gov/centers/pcmsc/science/coastal-climate-impacts?qt-science_center_objects=0#qt-science_center_objects

Passeri, D.L, Long, J. W., Jenkins, R. ., & Thompson, D. M. (2018). *Effects of Proposed Navigation Channel Improvements on Sediment Transport in Mobile Harbor, Alabama Open-File Report 2018-1123*.

Passeri, Davina L., Hagen, S. C., Bilskie, M. V., & Medeiros, S. C. (2015). On the significance of incorporating shoreline changes for evaluating coastal hydrodynamics under sea level rise scenarios. *Natural Hazards*, *75*(2), 1599–1617. https://doi.org/10.1007/s11069-014-1386-y

PBC. (2021). *R Studio [Computer Software]*. https://www.rstudio.com/

Peterson, J. (2019). Coastal Ecosystems Facing Inundation: Wetlands, and Beaches. In *A New Coast: Strategies for Responding to Devastating Storms and Rising Seas* (pp. 71–80). Island Press.

Picó, F. (2008). *Historia General de Puerto Rico*. Ediciones Huracán.

Picó, F. (2013). *1898: La Guerra Después de la Guerra* (4th ed.). Ediciones Huracán.

Pirazzoli, P. A. (2005). A review of possible eustatic, isostatic and tectonic contributions in eight late-Holocene relative sea-level histories from the Mediterranean area. *Quaternary Science Reviews*, *24*. https://doi.org/10.1016/j.quascirev.2004.06.026

Prasita, V. D. (2015). Determination of Shoreline Changes from 2002 to 2014 in the Mangrove Conservation Areas of Pamurbaya Using GIS. *Procedia Earth and Planetary Science*, *14*, 25–32. https://doi.org/10.1016/j.proeps.2015.07.081

Programa de Manejo de la Zona Costanera. (2017). *El estado de la costa de puerto rico 2017* (E. L. Díaz & K. M. Hevia (Eds.)).

Puerto Rico Climate Change Council (PRCC). (2013). *Puerto Rico ' s State of the*

Climate Assessing Puerto Rico ' s Social-Ecological Vulnerabilities in a Changing Climate. http://pr-ccc.org/download/PR State of the Climate-FINAL_ENE2015.pdf

Queensland Government; Environmental Protection Agency. (2003). *Hydrodynamics (changed from natural) model*. Oz Coasts: Australian Online Coastal Information. https://ozcoasts.org.au/conceptual-diagrams/stressors/hydrodynamics_model/

Quiñones, F., & Torres, S. (2005). *Las Cuencas Principales de Puerto Rico*. *Figura 2*. http://www.recursosaguapuertorico.com/Las_Cuencas_Principales_de_PR__resumen__V.pdf.

Radio Televisón Española; Agencias EFE. (2022). *Calentamiento global erosiona sitios prehispánicos mayas en México*. https://www.rtve.es/noticias/20220206/calentamiento-global-erosiona-sitios-prehispanicos-mayas-mexico/2282840.shtml

Rapp, George, Jr.;Hill, C. L. (1998). Construction, Destruction, Preservation. In *Geoarchaeology: The Earth-Science Approach to Archaeological Interpretation* (pp. 198–222). Yale University Press.

Reeder-Myers, L. A. (2015). Cultural Heritage at Risk in the Twenty-First Century: A Vulnerability Assessment of Coastal Archaeological Sites in the United States LK -. *Journal of Island and Coastal Archaeology*, *10*(3), 436–445. https://uprrp.on.worldcat.org/oclc/7989211410

Reimann, L., Vafeidis, A. T., Brown, S., Hinkel, J., & Tol, R. S. J. J. (2018). Mediterranean UNESCO World Heritage at risk from coastal flooding and erosion due to sea-level rise. *Nature Communications*, *9*(1). https://doi.org/10.1038/s41467-

018-06645-9

Remote Sensing Techniques for Archaeology (RESEARCH). (2021). *Land-use change - Research*. https://www.re-se-arch.eu/remote-sensing-techniques-for-archaeology/project/project-presentation/land-use-change/

Renfrew, Colin; Bahn, P. (2004a). When?: Dating Methods and Chronology. In *Archeology: Theories, Methods, and Practice* (4th Editio, pp. 121–164). Thames and Hudson Ltd.

Renfrew, Colin; Bahn, P. (2004b). Where?: Survey and Excavations of Sites and Features. In *Archeology: Theories, Methods and Practice colin* (4th Editio, pp. 75–120). Thames & Hudson Inc.

Restrepo, J. C., Orejarena R, A. F., & Torregroza, A. C. (2017). Suspended sediment load in northwestern South America (Colombia): A new view on variability and fluxes into the Caribbean Sea. *Journal of South American Earth Sciences*, *80*, 340–352. https://doi.org/10.1016/J.JSAMES.2017.10.005

Richards, J., Zhao, G., Zhang, H., & Viles, H. (2019). A controlled field experiment to investigate the deterioration of earthen heritage by wind and rain. *Heritage Science*, *7*(51), 1–13. https://doi.org/10.1186/S40494-019-0293-7/FIGURES/6

Rivera-Casillas, P. (2020). *Assessment of storm-induced coastal changes on a high-energy microtidal reef-fringed coast* [Master's Thesis, University of Puerto Rico, Mayagüez Campus]. UPRM Digital Institutional Repository https://scholar.uprm.edu/handle/20.500.11801/2685?locale-attribute=es

Rivera-Collazo, I. C. (2019). Severe Weather and the Reliability of Desk-Based

Vulnerability Assessments: The Impact of Hurricane Maria to Puerto Rico's Coastal Archaeology. *Journal of Island and Coastal Archaeology*, *15*(2), 1–20. https://doi.org/10.1080/15564894.2019.1570987

Rivera Collazo, I. C. (2011). *Between land and sea in Puerto Rico: climates, coastal landscapes and human occupations in the mid-Holocene Caribbean* [Doctoral Dissertation, University College London]. UCL Discovery http://discovery.ucl.ac.uk/1331902/

Rivera Collazo, I. C., Winter, A., Scholz, D., Mangini, A., Miller, T., Kushnir, Y., & Black, D. (2015). Human adaptation strategies to abrupt climate change in Puerto Rico ca. 3.5 ka. *Holocene*, *25*(4). https://doi.org/10.1177/0959683614565951

Rivera, M. (2021, August 11). Una matanza en Loíza cobra la vida de tres jóvenes. *El Vocero*. https://www.elvocero.com/ley-y-orden/policiacas/una-matanza-en-lo-za-cobra-la-vida-de-tres-j-venes/article_967e0d26-4048-11ec-9dd9-d3654c46af16.html

Robinet, A., Castelle, B., Idier, D., Le Cozannet, G., Déqué, M., & Charles, E. (2016). Statistical modeling of interannual shoreline change driven by North Atlantic climate variability spanning 2000–2014 in the Bay of Biscay. *Geo-Marine Letters*, *36*(6), 479–490. https://doi.org/10.1007/s00367-016-0460-8

Robinson, M. H., Alexander, C. R., Jackson, C. W., McCabe, C. P., & Crass, D. (2010). Threatened archaeological, historic, and cultural resources of the Georgia coast: Identification, prioritization and management using GIS technology. *Geoarchaeology*, *25*(3), 312–326. https://doi.org/10.1002/gea.20309

Rodríguez, R.W; Schwab, William C.; Carlo, Milton; Thieler, R. (1998). *Geologic Map*

of the Norteastern Insular Shelf of Puerto Rico-Luquillo Area. US Geologial Survey. https://www.usgs.gov/maps/marine-geologic-map-northeastern-insular-shelf-puerto-rico-luquillo-area

Rodríguez, R.W; Webb, Richard M.T.; Bush, Daavid M.; Scanlon, K. M. (1993). *Marine Geologic Map of the North Insular Shelf of Puerto Rico-Río Bayamón to Río Grande de Loíza*. US Geologial Survey. https://pubs.er.usgs.gov/publication/i2207

Rodríguez, D. J. (2018, March 6). Hasta el sábado podría extenderse evento de marejada | La Isla Oeste. *La Isla Oeste*. https://laislaoeste.com/hasta-el-sabado-podria-extenderse-evento-de-marejada/

Rodriguez Ramos, R. (2010). From "Cultures" in Isolation to People in Interaction. In *Rethinking Puerto Rico Precolonial History*. The University of Alabama Press.

Rojas Daporta, M. (1965, November 4). Continúa la extracción Area Medianía y Loíza. *El Mundo*, 18.

Ross, S. M. (2010). *Introductory Statistics* (3rd ed.). ELSEVIER.

Rouse, Irving; Alegría, R. E. (1990). Excavations at María de la Cruz Cave and Hacienda Grande Village Site, Loíza Puerto Rico. In A. F. Pospisil, Leopold; Wilde (Ed.), *Yale University Publications in Anthropology* (Issue 80). Department of Anthropology and the Peabody Museum Yale University.

Ruggiero, P., Kratzmann, M. G., Himmelstoss, E. A., Reid, D., Allan, J., & Kaminsky, G. (2013). *National Assessment of Shoreline Change-Historical Shoreline Change Along the Pacific Northwest Coast: U.S. Geological Survey Open-File Report 2012-1007*. https://doi.org/http://dx.doi.org/10.3133/ofr20121007.

Ruiz Vélez, R. (2014). *Aspectos Demográficos y Vulnerabilidad Municipio de Loíza [Power Point Slides]*. http://www.prsn.uprm.edu/Spanish/tsunami/mapa/info/loiza/PerfilVulnerabilidad_Loiza.pdf

Sabour, S., Brown, S., Nicholls, R. J., Haigh, I. D., & Luijendijk, A. P. (2020). Multi-decadal shoreline change in coastal natural world heritage sites – A global assessment. *Environmental Research Letters*, *15*(10). https://doi.org/10.1088/1748-9326/ab968f

Sagan, C. (1985). *Carl Sagan testifying before Congress in 1985 on climate change*. YouTube. https://www.youtube.com/watch?v=Wp-WiNXH6hI

Sánchez, A., Beck, T., Lin, L., Demirbilek, Z., Brown, M., & Li, H. (2012). *Coastal Modeling System Draft User Manual*. https://cirpwiki.info/images/6/67/CMS_UsersManual_050912.pdf

Sánchez Cappa, L. (1968, February 15). Comprueban Daños por Extracción Arena. *El Mundo*, 19.

Santiago, L., Barreto, M., Montañez-Acuña, A., Flecha, T., Cabrera, N., Bonano, V., Bracero Marrero, L., & Díaz, E. (2021). A Coastal Vulnerability Framework to Guide Natural Infrastructure Funds Allocation in Compressed Time. *Environmental Management*, *67*(1), 67–80. https://doi.org/10.1007/S00267-020-01397-Z

Sathiyamoorthyg; Vasudevan, S., & Subhrajit, R. (2020). Digital Estimation Of Shoreline Changes in the Archaeological Sites of Tamil Nadu Coast : Arikamedu and Sembiyankandiyur. *Journal of Critical Views*, *7*(14).

https://doi.org/10.31838/jcr.07.14.754

Scottish Coastal Archaeology and the Problem of Erosion (SCAPE). (n.d.). Retrieved November 8, 2021, from https://scapetrust.org/

Seabergh, W. C., Lin, L., & Demirbilek, Z. (2005). Laboratory Study of Hydrodynamics Near Absorbing and Fully Reflecting Jetties [ERDC/CHL TR-05-8]. *United States Army Corps of Engineers*. https://erdc-library.erdc.dren.mil/jspui/bitstream/11681/7596/1/CHL-TR-05-8.pdf

Sepúlveda Rivera, A. (2004). En clave gris. In *Puerto Rico: Atlas histórico de la sociedad puertorriqueña*. Caricamar.

Sesana, E., Gagnon, A. S., Ciantelli, C., Cassar, J. A., & Hughes, J. J. (2021). Climate change impacts on cultural heritage: A literature review. *Wiley Interdisciplinary Reviews: Climate Change*, *12*(4). https://doi.org/10.1002/WCC.710

Shayegh, S., Moreno-Cruz, J., & Caldeira, K. (2021). The Shoreline Deformation in Convex Beach due to Sea Level Rise. *IOP Conference Series: Earth and Environmental Science*, *925*(1), 012050. https://doi.org/10.1088/1755-1315/925/1/012050

Shoshany, M.; Degani, A. (19992). Shoreline detection by digital image processing of aerial photography. *Journal of Coastal Research*, *8*(1), 29–34.

Society for American Archaeology. (2018). *What is Archaeology*. About Archaeology. https://www.saa.org/about-archaeology/what-is-archaeology

Solano, M., Canals, M., & Leonardi, S. (2018). Development and validation of a coastal ocean forecasting system for Puerto Rico and the U.S. virgin islands. *Journal of*

Ocean Engineering and Science, *3*(3), 223–236. https://doi.org/10.1016/j.joes.2018.08.004

State Historic Preservation Office. (2018). *Sitios Arqueológicos de Loíza*. https://www.oech.pr.gov/publications/Información Arqueológica del Municipio de Loíza.pdf#page=5&zoom=auto,-150,354

Statistics Solutions. (2021). *Paired Sample T-Test*. https://www.statisticssolutions.com/free-resources/directory-of-statistical-analyses/paired-sample-t-test/

Stewart, CJ.; Pope, J. (1993). *Erosion Processes Task Group Report*. Retrieved by request

Sutherland, M.G.; Amante, C.J.; Carignan, KS.; Love, M. R. (2019). *NOAA National Centers for Environmental Information Topo-Bathymetric Digital Elevation Modeling : Puerto Rico and US Virgin Islands*. Retrieved by request

Sweet, W.V., B.D. Hamlington, R.E. Kopp, C.P. Weaver, P.L. Barnard, D. Bekaert, W. Brooks, M. Craghan, G. Dusek, T. Frederikse, G. Garner, A.S. Genz, J.P. Krasting, E. Larour, D. Marcy, J.J. Marra, J. Obeysekera, M. Osler, M. Pendleton, D. Roman, L. Schmi, and C. Z. (2022). *Global and Regional Sea Level Rise Scenarios for the United States*. https://oceanservice.noaa.gov/hazards/sealevelrise/noaa-nos-

Taçon, P. S. C., May, S. K., Wesley, D., Jalandoni, A., Tsang, R., & Mangiru, K. (2021). History Disappearing: The Rapid Loss of Australian Contact Period Rock Art. *Journal of Field Archaeology*, *46*(2), 119–131. https://doi.org/10.1080/00934690.2020.1869470

Takesue, R. K., Sherman, C., Ramirez, N. I., Reyes, A. O., Cheriton, O. M., Ríos, R. V., & Storlazzi, C. D. (2021). Land-based sediment sources and transport to southwest Puerto Rico coral reefs after Hurricane Maria, May 2017 to June 2018. *Estuarine, Coastal and Shelf Science*, *259*, 107476. https://doi.org/10.1016/J.ECSS.2021.107476

ten Brink, Uri; Geist, Eric L.; Lynett, Patrick; Andrews, B. (2006). Submarine Slides North of Puerto Rico and their Tsunami Potential. *NSF Caribbean Tsunami Workshop*. https://doi.org/10.1142/9789812774613_0004

ten Brink, J. (2004). *The Puerto Rico Trench: Exploring the Deepest Place in the Atlantic Ocean [Film]*. Woods Hole Coastal and Marine Science Center, USGS.

Thieler, E. R., & Danforth, W. W. (1994). Historical shoreline mapping (II): application of the digital shoreline mapping and analysis systems (DSMS/DSAS) to shoreline change mapping in Puerto Rico. *Journal of Coastal Research*, *10*(3), 600–620.

Thieler, R. E., Rodríguez, R. W., & Himmelstoss, E. A. (2007). Historical Shoreline Changes at Rincón , Puerto Rico , 1936-2006. In *Open-File Report 2007-1017*. http://pubs.usgs.gov/of/2007/1017/

Tooley, M. J. (1993). Long Term changes in eustatic sea level. In T. M. . Warrick, Richard A.;Barrow, E.M.;Wigley (Ed.), *Climate Change and Sea Level Change: observations, projections and implications* (pp. 81–110). Cambridge University Press.

Torres, J.L.; Morelock, J. (2002). Effect of terrigenous sediment influx on coral cover and extension rates of three Caribbean massive coral species. *Caribbean Journal of*

Science, *38*(3–4). https://www.researchgate.net/publication/236869300_Effect_of_terrigenous_sediment_influx_on_coral_cover_and_extension_rates_of_three_Caribbean_massive_coral_species

United Nations. (2017). Factsheet: People and Oceans. *The Ocean Conference*. https://www.un.org/sustainabledevelopment/wp-content/uploads/2017/05/Ocean-fact-sheet-package.pdf

United Nations. (2022). *Sedimentation and Erosion | The Caribbean Environment Programme (CEP)*. United Nations Environment Programme. https://www.unep.org/cep/sedimentation-and-erosion

United Nations Atlas of the Oceans. (2016). *Human Settlements on the Coast: The ever more popular coasts*. UN Atlas of the Ocean. http://www.oceansatlas.org/subtopic/en/c/114/

United Nations Educational Scientific and Cultural Organization (UNESCO). (2007). Case Studies on Climate Change and World Heritage. *World Heritage Convention*. https://whc.unesco.org/en/activities/396

United States Census Bureau. (2021). *QuickFacts: Loíza, Puerto Rico*. https://www.census.gov/quickfacts/fact/table/loizamunicipiopuertorico,PR

United States Corps of Engineers (USACE). (n.d.-a). *Joint Airborne Lidar Bathymetry Technical Center of Expertise*. Retrieved May 24, 2022, from https://www.sam.usace.army.mil/Missions/Spatial-Data-Branch/JALBTCX/

United States Corps of Engineers (USACE). (n.d.-b). *Loiza, Puerto Ric: Emergency*

Streambank Protection. Jacksonville District Website. Retrieved August 17, 2021, from https://www.saj.usace.army.mil/Missions/Continuing-Authorities-Program/Section-14-Emergency-Streambank-Protection/Loiza-Puerto-Rico/

United States Corps of Engineers (USACE). (2014). *Prioritizing Archaeological Sites for Cost-Effective Long-Term Management [Public Works Technical Bulletin]*. https://www.wbdg.org/FFC/ARMYCOE/PWTB/pwtb_200_1_134.pdf

United States Corps of Engineers (USACE). (2018). *Integrated Feasibility Report and Environmental Assessment Loíza, Puerto Rico [Section 14 Study DRAFT]*. https://jp.pr.gov/Portals/0/Evaluacion Ambiental/Integrated Feasibility Report and EA.pdf?ver=2018-04-23-192232-050

United States Corps of Engineers (USACE). (2020). *Coastal Modeling System*. https://cirp.usace.army.mil/products/cms.php

United States Geological Survey (USGS). (2018). *Río Grande de Loíza, Stations 500059050 [Discharge Data]*. National Water Dashboard [Web Map]. https://dashboard.waterdata.usgs.gov/app/nwd/?region=lower48&aoi=default

US. Climate Resilience Toolkit. (2021). *High-Tide Flooding*. https://toolkit.climate.gov/topics/coastal-flood-risk/shallow-coastal-flooding-nuisance-flooding

US. House of Representatives. (2020, August 11). *Coast erosion control project starts in Loíza | Congresswoman Jenniffer González-Colón*. https://gonzalez-colon.house.gov/media/press-releases/coast-erosion-control-project-starts-lo-za

Vega, J. (1990). *The Archaeology of Coastal Change Puerto Rico* [Doctoral Dissertation,

University of Florida]. ProQuest https://search.proquest.com/docview/303859916?pq-origsite=summon

Vélez, J. (1990). *Estudio Arqueologico del Area de Planificacion Especial de Pinones, Fases I-A y I-B*. Retrieved from Consejo para la Protección del Patrimonio Arqueológico Terrestre de Puerto Rico

Vélez, L. (2019). *Welcome to the Porto Rico 1930 Aerial Image Database*. Turning Point: Advances in Geo-Spatial Technology. http://pr1930.revistatp.com/

Vicente, M. L. (1931). El mapa topográfico de Puerto Rico. *Revista de Obras Públicas de Puerto Rico*, *8*(5), 117–118. https://prgeoref.weebly.com/uploads/8/6/3/9/86396506/vicente__1931_.pdf

Vu, M. T., Lacroix, Y., & Nguyen, V. T. (2018). Investigating the effects of sea-level rise on morphodynamics in the western Giens tombolo, France. *IOP Conference Series: Earth and Environmental Science*, *167*(1), 012027. https://doi.org/10.1088/1755-1315/167/1/012027

Wacom [Apparatus]. (2015). *Wacom Intous Tablet* (https://www.wacom.com/en-us/products/pen-tablets/one-by-wacom). https://www.wacom.com/en-us/products/pen-tablets/one-by-wacom

Wainwright, J. (1994). Erosion of archaeological sites: Results and implications of a site simulation model. *Geoarchaeology*, *9*(3), 173–201. https://doi.org/10.1002/gea.3340090302

Wang, F., Tian, Y., & Xiong, L. (2019). Climate Change Scenarios and Implications for Marine System Sustainability. *Journal of Coastal Research*, *94*(spl), 55–59.

https://doi.org/10.2112/SI94-010.1

Wildesen, L. E. (1982). The Study of Impacts on Archaeological Sites. *Advances in Archaeological Method and Theory, JSTOR*, *5*, 51–96. https://www.jstor.org/stable/20210053?seq=1

Williams, A. R. (2017). Alaska's Thaw Reveals—and Threatens—a Culture's Artifacts. *National Geographic Magazine*. https://www.nationalgeographic.com/magazine/article/artifact-melt-alaska-archaeology-climate-change

Williams, J., & Corfield, M. (2013). Construction impacts on in situ preservation of archaeological sites and artefacts. *Environmental Science*, 276–279. https://www.semanticscholar.org/paper/Construction-impacts-on-in-situ-preservation-of-and-Williams-Corfield/bfed39854bf0846336269c4a7ffff7ecd517f153

World Heritage Centre. (2007). Climate Change and World Heritage: Report on predicting and managing the impacts of climate change on World Heritage and strategy to assist State Parties to implement appropriate management responses. In *World Heritage Report* (Vol. 22). https://whc.unesco.org/en/series/22/

Wu, X., Liu, C., & Wu, G. (2018). Spatial-temporal analysis and stability investigation of coastline changes: A case study in Shenzhen, China. *IEEE Journal of Selected Topics in Applied Earth Observations and Remote Sensing*, *11*(1), 45–56. https://doi.org/10.1109/JSTARS.2017.2755444

Ye, H., & Ma, T. (2021). Changes in the Geographical Distributions of Global Human

Settlements. *Journal of Resources and Ecology*, *12*(6), 829–839. https://doi.org/10.5814/j.issn.1674-764x.2021.06.011

Yu, M.; Gao, Q.; Villanueva, L.; Bracero Marrero, L. I. M. (2015). *Aerial Photos Collected and Processed by NASA Roses Project #NNX12AE98G*.

Zhurbin, I. V., Borisov, A. V., Nazmutdinova, A. I., Milich, V. N., Petrov, R. P., Ivanova, M. G., Modin, R. N., Knyazeva, L. F., Vorobieva, N. G., & Zinchuk, S. V. (2019). The Use of remote sensing, geophysical methods and soil analysis in the study of sites disturbed by agricultural activity. *Archaeology, Ethnology and Anthropology of Eurasia*, *47*(2), 103–111. https://doi.org/10.17746/1563-0110.2019.47.2.103-111

Appendix

Table A.1: Attributes of Archaeological Sites in Loíza, Puerto Rico

Site Unique ID	Vélez Code	SHPO Code	CAT Code	SHPO TAG	SHPO Key	Common Name	Chronological Period	Description	Fieldwork Comments
1	45-E-15	45-E-15	LO-33b	LZ0100050	50	45-E-15	PII Saladoid+PIII Ostionoid	Residuary. Vélez general dating "agroalfarero".	No materials were found. House in construction.
2	45-E-13	LO-6	LO-6	LZ0100006	6	45-E-13	PIII Ostionoid+PIV Spanish Colonial	Residuary. Meléndez & Rodríguez, small site of shell midden. Vélez classified as Spanish and Taino. Location used SHPO.	No materials were found, no access to the location due to housing.
3	45-E-2	45-E-2	LO-31: Punta Cangrejos (45-E-1, 45-E-2)	LZ0100042	42	El Bunker	PV_United States Colonial	SHPO: this Bunker is from the USA military. Vélez, construction may suggest the destruction of the other site "La Torre" (45-E-1). CAT: LO-31.	Survey 123: Yes. Southeast unidentified concrete block structure with a historic ceramic (hand painted: whiteware).

Table A.1: Attributes of Archaeological Sites in Loíza, Puerto Rico (Continued)

Site Unique ID	Vélez Code	SHPO Code	CAT Code	SHPO TAG	SHPO Key	Common Name	Chronological Period	Description	Fieldwork Comments
4	45-E-5	LO-5	LO-5	LZ0100005	5	45-E-5	PIII_Ostionoid+PIV_Spanish Colonial	Residuary. Meléndez & Rodríguez, high density shell and few ceramics. Conglomerated in SHPO as LO-5. Location of Vélez was used.	Not visited.
5	45-E-6	LO-5	None	LZ0100005	5	45-E-6	PIV Spanish Colonial	Residuary. Conglomerated in SHPO as LO-5. According to Vélez, it is from Period IV.	Not visited.
6	45-E-7	45-E-7	LO-33b	LZ0100046	46	45-E-7	PIII_Ostionoid+PIV_Spanish Colonial	Residuary.	No materials were found. Vélez classified it as colonial and pre-Columbian. CAT location corresponds to 45-E-10
7	45-E-10	LO-7	LO-7	LZ0100007	7	Cueva Punta Maldonado or Cueva de los Indios	PI Ortoiroid+P II Saladoid+P III Ostionoid	Cave. Vélez general chronological pre-Columbian. Location SHPO	Not visited.

Table A.1: Attributes of Archaeological Sites in Loíza, Puerto Rico (Continued)

Site Unique ID	Vélez Code	SHPO Code	CAT Code	SHPO TAG	SHPO Key	Common Name	Chronological Period	Description	Fieldwork Comments
8	45-E-10	45-E-10	None	LZ0100047	47	45-E-10	PIV Spanish Colonial	Filling. Vélez classification is Spanish. CAT location is as Lo-33b	No materials were found.
9	45-E-21	45-E-21	None	LZ0100055	55	45-E-21	PIV_Spanish_Colonial	Filling.	Not visited.
10	45-E-24	LO-4	LO-4	LZ0100004	4	Finca Piñones I	PIII_Ostionoid+PIV_Spanish Colonial	Residuary. Shell midden	Not visited.
11	45-E-17	45-E-17	LO-29	LZ0100071	71	Islote Piñones	PIII Ostionoid+PIV Spanish Colonial	Residuary	Not visited.
12	45-E-44	LZ0100012	LO-12	LZ0100012	12	La Cocaleca	P II Saladoid+PIII Ostionoid+PIV Spanish Colonial	Residuary. Meléndez, elevated dune. Some areas have integrity. Historic S.18-19	Not visited.
13	45-E-46	LO-14	LO-14	LZ0100014	14	Punta Vacía Talega or Arenas	PII_Saladoid+PIII_Ostionoid+PIV_Spanish Colonial	Residuary housing. Meléndez & Rodríguez, multicomponent, dense deposit, stratigraphy, possible center Esperanza, village of combat with Spaniards. Almost all pre-Columbian styles present. Location CAT.	Not visited.
14	45-E-54	45-E-54	None	LZ0100070	70	45-E-54	PIV Spanish Colonial	Brick structure.	Not visited.

Table A.1: Attributes of Archaeological Sites in Loíza, Puerto Rico (Continued)

Site Unique ID	Vélez Code	SHPO Code	CAT Code	SHPO TAG	SHPO Key	Common Name	Chronological Period	Description	Fieldwork Comments
15	None	LO-22	None	LZ0100022	22	Las Carreras	PII Saladoid+PIII Ostionoid	Residuary. Meléndez & Rodríguez, villa. Frequent occupations, several sites. Not present in CAT and SHPO inventories. Grossman wrongly classified this site as L-22 north of L-23 without considering Rodriguez and Walker's reports. Location SHPO & Meléndez	Not visited.
16	None	LO-23	None	LZ0100023	23	Parcelas Vieques	PIII Ostionoid+PIV Spanish Colonial	Residuary. Meléndez & Rodríguez, three stages of "Elenoide", site excavated by Grossman (company). SHPO location is different from Meléndez & Rodríguez coordinates and description in the SHPO report. Location Grossman report.	No materials were found and was covered by vegetation.

Table A.1: Attributes of Archaeological Sites in Loíza, Puerto Rico (Continued)

Site Unique ID	Vélez Code	SHPO Code	CAT Code	SHPO TAG	SHPO Key	Common Name	Chronological Period	Description	Fieldwork Comments
17	None	LO-24	None	LZ0100024	24	Melilla	PIII_Ostionoid	Residuary. Meléndez & Rodríguez, flood, need to relocate.	Not visited.
18	None	None	LO-27	None	None	Playa Berwind	PIII Ostionoid	Residuary.	No materials were found. Vegetation.
19	None	LO-18	None	LZ0100018	18	Cueva Bulón	PI Ortoiroid+PII Saladoid	Cave. Meléndez & Rodríguez, site with high investigation potential	Not visited.
20	None	LO-1	LO-1	LZ0100001	1	Cueva María de la Cruz	PI Ortoiroid+PII Saladoid+PIII Ostionoid	Cave. Meléndez & Rodríguez, housing? Multicomponent. Very important. Location CAT.	Not visited.
21	None	Cueva Dolores	None	LZ0100032	32	Cueva Dolores	PI Ortoiroid+PII Saladoid+PIII Ostionoid	Cave. Meléndez, burial, important site. General pre-Columbian.	Not visited.
22	None	LO-2	LO-2	LZ0100002	2	Hacienda Grande	PII Saladoid+PIII Ostionoid+PIV Spanish Colonial	Cave. Meléndez & Rodríguez, main site Hacienda Grande style. Important due to the presence of all pre-Columbian groups.	Not visited.

Table A.1: Attributes of Archaeological Sites in Loíza, Puerto Rico (Continued)

Site Unique ID	Vélez Code	SHPO Code	CAT Code	SHPO TAG	SHPO Key	Common Name	Chronological Period	Description	Fieldwork Comments
23	None	Cueva Mela	None	LZ0100031	31	Cueva Mela	PI Ortoiroid+PII Saladoid+PIV Spanish Colonial	Cave. Meléndez & Rodríguez, housing? Closed cave.	Not visited.
24	None	LO-21	None	LZ0100021	21	Cueva La Cantera	PI Ortoiroid+PII Saladoid	Cave. Meléndez, multicomponent. Looting. Site extends outside the cave.	Not visited.
25	None	LO-26	None	LZ0100026	26	La Gallera	PIII Ostionoid	Residuary. Meléndez & Rodríguez, apparently has integrity. Phase III pending. Location SHPO.	Not visited.
26	None	LO-25	LO-25	LZ0100025	25	Miñi-Miñi	PII_Saladoid+PIII_Ostionoid+PIV_Spanish Colonial	Villa. Meléndez & Rodríguez, site with great extension, and deep.	Not visited.
27	None	None	LO-41	None	None	Ocean Terrace	PI Ortoiroid+PII Saladoid+PIII Ostionoid+PIV Spanish Colonial*	Not specified. CAT, general dating pre-Columbian and Spanish.	Not visited.

Table A.1: Attributes of Archaeological Sites in Loíza, Puerto Rico (Continued)

Site Unique ID	Vélez Code	SHPO Code	CAT Code	SHPO TAG	SHPO Key	Common Name	Chronological Period	Description	Fieldwork Comments
28	None	LO-27	LO-18	LZ0100027	27	Vistas del Océano	PIII Ostionoid+PIV Spanish Colonial	Residuary. Constructed. Meléndez & Rodríguez, housing? Site covered by filling to construct Vista del Océano. Location CAT	Not visited.
29	None	Sitio K	LO-43	LZ0100034	34	Sitio K	PIII_Ostionoid	Residuary. Constructed. Meléndez & Rodríguez, possibly destructed. Most explore west.	Not visited.
30	None	Sitio G	None	LZ0100033	33	Sitio G/Santillana	PIII Ostionoid+PIV Spanish Colonial+PV United States Colonial	Residuary. Meléndez & Rodríguez, three areas are distinguished. No present food materials.	Not visited.
31	None	None	LO-44	None	None	Malibú Villages	PIII Ostionoid	Not specified. Constructed. CAT, "Santa Elena" pre-Columbian and colonial.	Not visited.
32	None	None	None	None	None	Sitio J	PIII Ostionoid	Site only present in Meléndez & Rodríguez inventory	Not visited.

Table A.1: Attributes of Archaeological Sites in Loíza, Puerto Rico (Continued)

Site Unique ID	Vélez Code	SHPO Code	CAT Code	SHPO TAG	SHPO Key	Common Name	Chronological Period	Description	Fieldwork Comments
33	None	None	LO-46	None	None	Escuela Intermedia Jesus Vizcarrondo	PI Ortoiroid+PII Saladoid+PIII Ostionoid+PIV Spanish Colonial*	Not specified. CAT, ceramic fragments, glass, metal, and bones. Historic and prehistoric. Phase II is recommended. General dating pre-Columbian.	Not visited
34	45-E-55	H9/45-E-55	None	LZ0100041	41	El Ancón	PIV Spanish Colonial+PV United States Colonial	Residuary	Not visited.
35	15-F-4	15-F-4	None	LZ0100037	37	Grúas	PIV Spanish Colonial	Building base bricks. Location SHPO	Not visited.
36	15-F-2	15-F-2/M-3-3	CN-6	LZ0100036	36	15-F-2	PI Ortoiroid	Shell midden.	Not visited.
37	LO-32a	45-E-3	LO-32a	LZ0100044	44	45-E-3	PIII Ostionoid	Residuary. Vélez (1990) described as pre-Columbian, "Etapa Agroalfarera", sub-Taina. Residuary.	No materials were found. It was near the boardwalk.
38	LO-32b	45-E-4	LO-32b	LZ0100045	45	45-E-4	PI Ortoiroid+PII Saladoid+PIII Ostionoid	Shell midden. Vélez described it as a pre-Columbian, non-specified chronology.	No materials were found. Houses and the street were documented.

Table A.1: Attributes of Archaeological Sites in Loíza, Puerto Rico (Continued)

Site Unique ID	Vélez Code	SHPO Code	CAT Code	SHPO TAG	SHPO Key	Common Name	Chronological Period	Description	Fieldwork Comments
39	45-E-11	LO-8	LO-8	LZ0100008	8	Punta Maldonado II	PIII Ostionoid+PV United States Colonial	Residuary. Vélez chronology, as "subtaina" and "contemporary". Meléndez & Rodríguez, small ceramic fragments.	Not visited.
40	45-E-12	45-E-12	LO-7b	LZ0100048	48	45-E-12	PIII Ostionoid	Residuary.	Not visited.
41	45-E-16	45-E-16	None	LZ0100051	51	45-E-16	PIII_Ostionoid	Residuary.	No materials were found. New constructions were being built.
42	45-E-27	LO-3	LO-21	LZ0100003	3	Islote Piñones	PIII Ostionoid	Shell midden. Location CAT. SHPO consolidated this site with LO-03 (north).	Not visited.
43	45-E-29	LO-3	LO-23	LZ0100003	3	45-E-29	PIII Ostionoid	Shell midden. CAT consolidated this point with LO-23 (45-E-28). SHPO consolidated this site with LO-03 (north).	Not visited.
44	45-E-30	LO-3	LO-28	LZ0100003	3	Isleta Piñones, 45-E-30	PIII Ostionoid	Residuary. SHPO consolidated this site with LO-03 (east) with 45-32,27,28,29.	Not visited.

Table A.1: Attributes of Archaeological Sites in Loíza, Puerto Rico (Continued)

Site Unique ID	Vélez Code	SHPO Code	CAT Code	SHPO TAG	SHPO Key	Common Name	Chronological Period	Description	Fieldwork Comments
45	45-E-32	LO-3/45-E-32, 27,28,29,30	LO-3	LZ0100003	3	Finca Piñones II (El Alto)	PII Saladoid+PIII Ostionoid	Residuary. Shell midden.	Not visited.
46	45-E-33	45-E-33	LO-22b	LZ0100058	58	45-E-33	PIII Ostionoid	Residuary.	Not visited.
47	45-E-34	45-E-34	LO-22b	LZ0100059	59	45-E-34	PIII_Ostionoid	Residuary.	Not visited.
48	45-E-25	LO-20	LO-20b	LZ0100020	20	Finca Piñones 3	PI Ortoiroid+PII Saladoid+PIII Ostionoid	Residuary. Shell midden. Vélez described three chronological periods: "arcaico", "agroalfarero", "taina". Meléndez & Rodríguez described possible preceramic component.	No materials were found. New constructions at the west of the site point.
49	45-E-35	45-E-35	LO-22c	LZ0100060	60	45-E-35	PI_Ortoiroid	Shell midden. SHPO & CAT consolidated in one point.	No materials were found.
50	45-E-35	45-E-35	LO-22c	LZ0100060	60	45-E-35	PI_Ortoiroid	Shell midden. SHPO & CAT consolidated in one point.	No materials were found.
51	45-E-35	45-E-35	LO-22c	LZ0100060	60	45-E-35	PI Ortoiroid	Shell midden. SHPO & CAT consolidated in one point.	No materials were found.
52	45-E-35	45-E-35	LO-22c	LZ0100060	60	45-E-35	PI Ortoiroid	Shell midden. SHPO & CAT consolidated in one point.	No materials were found.

Table A.1: Attributes of Archaeological Sites in Loíza, Puerto Rico (Continued)

Site Unique ID	Vélez Code	SHPO Code	CAT Code	SHPO TAG	SHPO Key	Common Name	Chronological Period	Description	Fieldwork Comments
53	45-E-35	45-E-35	LO-22c	LZ0100060	60	45-E-35	PI_Ortoiroid	Shell midden. SHPO & CAT consolidated as one point.	No materials were found.
54	45-E-35	45-E-35	LO-22c	LZ0100060	60	45-E-35	PI_Ortoiroid	Shell midden. SHPO & CAT consolidated as one point.	No materials were found.
55	45-E-40	LO-10	LO-10	LZ0100010	10	La Vaquería, 45-E-40	PIII Ostionoid+PIV Spanish Colonial	Residuary. Meléndez & Rodríguez, impacted and dune eroded.	Not visited.
56	45-E-41	45-E-41	LO-37	LZ0100064	64	45-E-41	PI_Ortoiroid	Shell midden.	Not visited.
57	45-E-43	LO-30/45-E-42, 43	LO-30	LZ0100030	30	Monte Grande II	PIII Ostionoid	Residuary. Meléndez, shell midden, a small site at the street border. SHPO consolidated 45-E-42 with 45-E-43.	Not visited.
58	45-E-45	LO-13	LO-13	LZ0100013	13	Punta Vacía Talega	PIII Ostionoid+PIV Spanish Colonial	Residuary.	Ceramic materials were found on two visits. Other materials were found inside the trail.
59	45-E-47	45-E-47	LO-38	LZ0100065	65	Playa Bonita	PIII Ostionoid+PIV Spanish Colonial	Conuco (small farm). Mounds.	Not visited.

Table A.1: Attributes of Archaeological Sites in Loíza, Puerto Rico (Continued)

Site Unique ID	Vélez Code	SHPO Code	CAT Code	SHPO TAG	SHPO Key	Common Name	Chronological Period	Description	Fieldwork Comments
60	45-E-49	LO-19	LO-19	LZ0100019	19	La Planta	PIII Ostionoid+PIV Spanish Colonial	Residuary. Meléndez, housing? Multicomponent, relative dating (1375 – 1405 CE). Location CAT.	Not visited.
61	45-E-52	None	None	None	None	45-E-52	PII_Saladoid+PIII_Ostionoid	Shell midden. Vélez, general dating pre-Columbian "agroalfarera".	Not visited.
62	None	LO-15	LO-15	LZ0100015	15	La Virginia	PI Ortoiroid+PII Saladoid+PIII Ostionoid*	Residuary. General dating CAT pre-Columbian. Location CAT.	Not visited.
63	45-E-53	45-E-53	None	LZ0100069	69	45-E-53	PI Ortoiroid+PII Saladoid+PIII Ostionoid*	Shell midden. Vélez, general dating pre-Columbian.	Not visited.
64	45-E-50	45-E-50	LO-39	LZ0100067	67	45-E-50	PIII Ostionoid+PIV Spanish Colonial	Residuary.	Not visited.
65	45-E-51	45-E-51	LO-41	LZ0100068	68	45-E-51	PIII_Ostionoid	Residuary.	Not visited.
66	45-E-36	LO-11	LO-11	LZ0100036	36	Juan Pérez I	PI Ortoiroid	Shell midden. Meléndez, no ceramic is present. Location CAT.	Not visited.
67	45-E-37	45-E-37	None	LZ0100061	61	45-E-37	PI_Ortoiroid	Shell midden.	Not visited.
68	45-E-18	45-E-18	LO-34a	LZ0100052	52	45-E-18	PIII_Ostionoid	Residuary.	Not visited.
69	45-E-22	45-E-22	LO-34b	LZ100056	56	45-E-22	PIII Ostionoid	Residuary.	Not visited.
70	45-E-19	45-E-19	None	LZ0100053	53	45-E-19	PIII Ostionoid	Residuary. Location SHPO.	Not visited.
71	45-E-26	45-E-26	None	LZ0100057	57	45-E-26	PIII_Ostionoid	Residuary.	Not visited.

Table A.1: Attributes of Archaeological Sites in Loíza, Puerto Rico (Continued)

Site Unique ID	Vélez Code	SHPO Code	CAT Code	SHPO TAG	SHPO Key	Common Name	Chronological Period	Description	Fieldwork Comments
72	15-F-5	Cueva Carmona	CN-7	LZ0100017	17	Cave.	PII Saladoid+PIII Ostionoid	Cave. Location CAT.	Not visited.
73	45-E-1	45-E-1	LO-31: Punta Cangrejos (45-E-1, 45-E-2)	LZ0100043	43	La Torre	PIV Spanish Colonial	Brick structure. La Torre reflects the construction of S. SXI. Its remnant suggests that it was moved from its original position due to the construction of the Bunker (45-E-2). In CAT inventory LO-31.	No exposed materials were found.
74	45-E-14	45-E-14	None	LZ0100049	49	45-E-14	PII Saladoid+PIII Ostionoid	Residuary. Vélez general chronology "agroalfarero".	No access to point, housing. No materials were found at surrounding points.
75	45-E-8	LO-8	None	LZ1000009	9	Punta Maldonado I	PII Saladoid+PIII Ostionoid	Residuary. Vélez extensive with shell midden and Elenoid ceramic, chronology "subtaina". Meléndez & Rodríguez, epi-Saladoid, Ostionoid, and Elenoid.	Not visited. Location assigned according to previous knowledge. Described as in the "north of the Street. #187".

Table A.1: Attributes of Archaeological Sites in Loíza, Puerto Rico (Continued)

Site Unique ID	Vélez Code	SHPO Code	CAT Code	SHPO TAG	SHPO Key	Common Name	Chronological Period	Description	Fieldwork Comments
76	45-E-20	45-E-20	None	LZ0100054	54	45-E-20	PIII Ostionoid	Shell midden. Location SHPO.	Not visited.
77	None	LO-28	None	LZ0100028	28	LO-28/45-E-19	PIII Ostionoid	Shell midden. Meléndez & Rodríguez described deep shell midden. Location SHPO, not in Vélez but SHPO used again the 45-E-19 code.	Not visited.
78	45-E-28	LO-3	LO-23	LZ0100003	3	45-E-28	PIII Ostionoid	Shell midden. CAT consolidated this point with LO-23 (45-E-29). SHPO consolidated this site with LO-03 (north).	Not visited.
79	45-E-38	45-E-38	None	LZ0100062	62	45-E-38	PI Ortoiroid	Shell midden. Location SHPO.	Not visited.
80	45-E-42	LO-30	LO-30	LZ0100030	30	45-E-42	PIII Ostionoid	Residuary. SHPO and CAT consolidated in 45-E-43 (east).	Not visited.
81	45-E-39	45-E-39	None	LZ0100063	63	45-E-39	PIII Ostionoid	Residuary.	Not visited.
82	None	LO-29	None	LZ0100029	29	Monte Grande I	PIII Ostionoid	Housing. Meléndez & Rodríguez, extensive site, deep, stratigraphy, dune eroded.	Not visited.
83	45-E-48	45-E-48	None	LZ0100066	66	45-E-48	PIV_Spanish Colonial	Bricks/housing.	Not visited.

Table A.1: Attributes of Archaeological Sites in Loíza, Puerto Rico (Continued)

Site Unique ID	Vélez Code	SHPO Code	CAT Code	SHPO TAG	SHPO Key	Common Name	Chronological Period	Description	Fieldwork Comments
84	15-F-3	15-F-3	CN-8	LZ0100072	72	Cueva del Pueblo del Indio	PI Ortoiroid+PII Saladoid+PIII Ostionoid+PIV Spanish Colonial*	Cave. Vélez, general dating pre-Columbian. Location CAT.	Not visited.
85	15-F-1	15-F-1/ M3-4	CN-24	LZ0100035	35	Usubal	PIV Spanish Colonial	Farm crops. Location SHPO, CAT southwest.	Not visited.
86	None	H1	None	LZ0100040	40	Molino de azúcar	PIV Spanish Colonial	Sugar mill. SXVI.	Not visited.
87	None	LO-39	None	LZ0100039	39	Colobó/ Sitio I?	PII Saladoid+PIII Ostionoid+PIV Spanish Colonial	Residuary. SHPO, multicomponent, and historic. Location SHPO. Meléndez & Rodríguez described similar characteristics as Sitio I. Bombing station destroyed. Explore adjacent lands.	Not visited.
88	None	NRHP	None	NRHP	NRHP	Parroquia Espiritu Santo y San Patricio	PIV Spanish Colonial	Church was constructed in 1645 and extended in 1729.	Not visited.